University of Salford MANCHESTER

Development of Novel Heterocyclic Compounds as Vascular Targeting Agents

Patrick Killoran

School of Environment & Life Sciences,

University of Salford, Salford, UK

Submitted in partial fulfilment of the requirements

of the Degree of Doctor of Philosophy, July 2015

Acknowledgement

This research project would not have been possible without the support of many people. I wish to express my gratitude to my supervisor Dr John (Hadders) Hadfield for his patience and advice. A big thanks to Prof A McGown and Kidscan (Holly, Chris X 2, James, Jane and Lowri) for the funding and enthusiasm that made this happen.

I would like to thank Guillaume Mossand and Mellisa Rosell for their help with the synthesis of dibenzo(b,d)oxepines. My thanks also extend to Tiabauld Peuden and Dr Nick Hirst for their invaluable help in the development of the Ziegler-Ullman biaryl coupling methodology and Pd catalysed *o* arylation respectively. Lots of thanks also to the lovely Kamila Schmidt for her help with biological testing and her heavy metal melodies! Along with being the biggest wind-up artist in Salford, Kirit Amin is a true wizard of NMR, I would be lost without his assistance and I thank him greatly! A letter should be sent to the Vatican to get the ball rolling on Mark Parlby's sainthood, thanks for everything. I also extend my thanks to all of the technicians, who have helped and given me cake over the years, I am very grateful.

Dr Steve Rossington is a true gent and a friend. If you substitute the L.A underground for the University of Salford in the opening sequence of the A-Team, that sums up what a great guy he is. Without his wise words and encouragement I would be sorely stuck! Many thanks to thank the man, the myth, the chemist Dr Jim Wilkinson for sharing his priceless wisdom on everything from organic chemistry to the carry on movies!

An especially big thank you goes to my good pal Ryan and his lovely girlfriend Becky for taking me into their home and extending me great generosity and friendship, it saddens me greatly that there will be no more handsome haircut Fridays! Thanks to Andrew McGowsling and Natalie Barnes for the support and fun memories in lab. I pass the torch to you guys; don't hold it beside the stills! To all of the placement/project students that I have worked

with/tortured thank you and good luck! (Lewis, Amjad, Chris “Sir Donksalot” Lawson and many more!). The lovely Iustina Slabu has been and always will be my chemistry buddy, thanks for your support!

On a more serious note I have to thank my two personal physicians Dr Evin Winters and Dr Gavin Callaghan for keeping me safe through some treacherous expeditions… A tip of the hat to you both! Many thanks to my consigliere Kerill Winters for his wise (guy) words. To the members of Whiskey Dust thanks for the memories, give it a few years, someone will make an offer we can’t refuse!!

2(Dr) Alex Mastin has been a great friend and often a voice of reason, I will miss our Friday think tank! Manisha Patel is also a great pal but she messed up badly by feeding me and will have to suffer the consequences… Gemma Lace Costigan is a hip lady, thanks for all the advice! Thanks to all of the Staff who make Salford such a friendly place to work.

I fondly remember some great “extracurricular” adventures during my PhD with some lovely people. Kathrin and Tom, that rendition of “I would do anything for love” still haunts me! Dr Robert Coles is a dance champion! I never told Soran Baban this, in Gaelic his name means means “A wild man”. Firozeh…….. ? I extend a special thanks to Geoff and Cath Hide for all of the kindness they have shown over my time at Salford.

I have to thank my family for their support throughout this process, I love you all dearly in spite of the school boy jokes! Thanks to my dad, brother, Paula and Ian for all your love and support.

Thanks to my beautiful girlfriend Helen for putting up with me for so long

I love my mum, she is an inspiration to me every day, it couldn’t have been easy bringing up two bad boys on your own! I dedicate this to you.

"A scientist in his laboratory is not a mere technician: he is also a child confronting natural phenomena that impress him as though they were fairy tales."

Marie Curie

Abstract

In **chapter one** the biology of cancer is introduced along with a brief history of drug treatment and the status quo of cancer therapeutics. This includes a general overview of cancer prevalence, carcinogenesis, and biochemistry. The main targets for cancer therapeutics are introduced along with in-depth look at cancer vasculature, tubulin binding agents and their mechanisms of action.

In **chapter two** the development of the routes to the dibenzo[*c,e*]oxepine target compounds are described. The optimisation of a key biaryl precursor molecule for these analogues is described. This includes a brief overview of palladium catalysed coupling chemistry and a screen for suitable catalytic systems.

In **chapter three** the development of an intramolecular ring closing process for dibenzo[*b,d*]oxepine is described. This includes investigation into non-phenolic oxidative coupling and a screen for oxidants. Palladium/phosphine catalysed intramolecular arylation is also discussed.

In **chapter four** the synthesis of the target compounds is described along the development of routes to further analogues.

In **chapter five** the biological testing of compounds is discussed. This features an introduction to biological evaluation methods for anti cancer compounds. The results for all of the MTT and tubulin binding assays (MA) are presented, revealing a fluorinated dibenzo[*c,e*]oxepine analogue with cytotoxicity within the nanomolar range (MTT K562 - IC50 60 nm, MA - 1.2 μM). Furthermore a link has also been established between the cytotoxic activity profiles of a series of simple biaryl compounds and Combretastatin A-4.

Table of Contents

Table of Figures

Chapter 1: Introduction

What is cancer?

Understanding the genesis of cancer is an ongoing process. Extraordinary progress has been made over the past 30 years in determining the most fundamental basis of the process at a molecular level. The decoding of the human genome has led to the identification of several genetic precursors to cancer. This, along with the identification of several efficacious natural compounds, has led to research into several targets areas

"Cancer" is a generic umbrella term that covers over 150 different conditions that affect most tissues in the body. Tissues that are susceptible to malignancies (most are) can present them in various grades and types. Even though each type has unique features, the basic mechanisms in tumour formation are quite similar.

Cells in a healthy human body exist as a complex interdependent system that regulates each other's proliferation. Healthy cells only reproduce under instruction of cells in their proximity; this system of collaboration ensures the maintenance of an appropriate tissue size and structure. Cancer cells exist in stark contrast to this in that they over-proliferate, affecting tissue structure and avoiding controls on growth.

Cancer growth is determined by a set of basic principles that have been identified over the past 30 years. The cells of a tumour began as a single cell at one point, usually years before the tumours inception stimulated by inappropriate reproduction. The changes that lead to cancer occur through a build up of mutations in specific genes within the cell. The understanding of these genes is paramount to the formation and development of cancer treatments.

All eukaryotic cells contain genes; these are sequences of DNA arranged on chromosomes located in the nucleus of the cell. Each gene codes for a specific sequence of amino acids from which proteins are made. Mutations in genes can cause changes in the activity or the

quantity of the protein. Cancer is determined by two types of gene, proto oncogenes and tumour suppressor genes. These genes, when non-mutated, are important in the regulation of cell life cycle. Proto oncogenes encourage the growth of a cell before cell division, tumour suppressor genes inhibit this. Mutation of proto oncogenes can lead to excessive multiplication causing either the formation of too much protein product or an overactive version of it. Conversely, mutation in a tumour-suppressor gene inactivates its control over growth leading to uncontrolled cell proliferation.

Cancer in essence is caused by DNA mutation/damage. During the process of cell division, any damaged/mutated DNA is either repaired or destroyed by the various cellular DNA repair mechanisms. Cancer cells are neither destroyed nor repaired by these mechanisms because the repair mechanisms have been deactivated by mutation. When the DNA damage in a cell exceeds its repairing capability the mutation is passed on to the next cell. When this mutation is on a gene related to DNA repair mechanisms, further replication will increase the rate of mutation at other sites. This concept is known as the mutator phenotype (**Fig 1**) and evidence of this is shown in the fact that cancer cells show thousands of DNA mutations (Loeb. 2001).

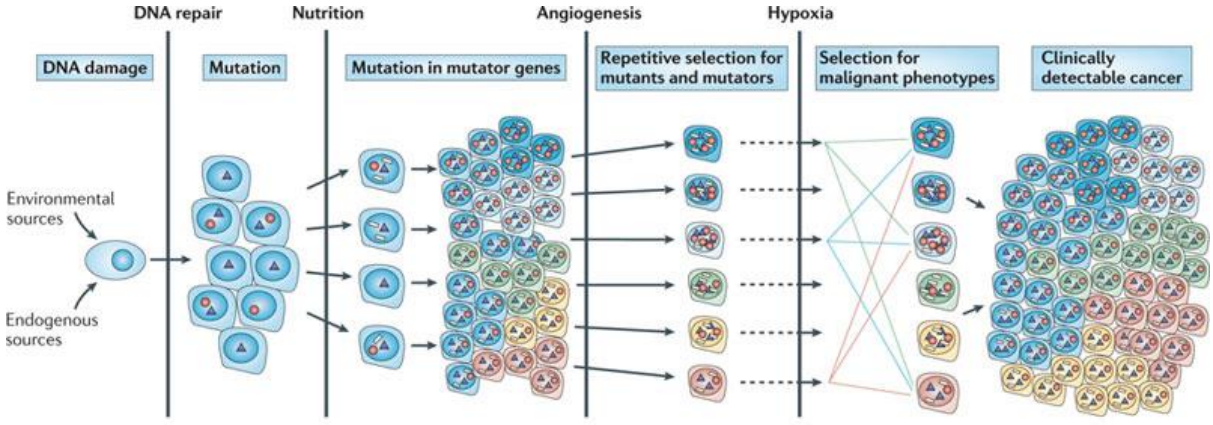

Figure 1 Diagram showing the concept of the mutator phenotype from the initial point of DNA damage to point of clinical detection (Loeb. 2001).

The causes of cancer are varied and many. Several environmental factors have been identified. These include tobacco, red meat, numerous chemicals, environmental pollutants, UV-light and radiation. Microbial infections have also been shown to cause cancers such as aflatoxin from the fungus *Aspergillus flavus* from certain nuts and the human papilloma virus which can cause cervical cancer. Genetic factors also apply to causes of cancer with approximately 10% of cancers being entirely hereditary (Gopie *et al*. 2012).

Instances of cancers differ between the sexes with men more likely to develop cancer, this increases over the age of 64. This phenomenon has been documented in a recent study on brain/central nervous system cancers over 37 years (1975-2007). Kohler's group commented that male nervous system cancers accounted for 90/100000 cases in 1990 whereas cases of female nervous system cancers was less than half of this (40/100000) in 1995 indicating a gender–specific factor for CNS cancers (Kohler *et al*. 2011).

Cancer can also be described as a disease of the elderly as cases in both sexes increase rapidly from the age of 55 (**Fig 2**), (Bassily *et al*. 2010) this is due the natural process of ageing at the cellular level and a lifetime accumulation of mutations. Treatment of the condition amongst the elderly is complicated by functional decline, low haematopoietic reserve and a high prevalence of co morbidities (Bassily *et al*. 2010).

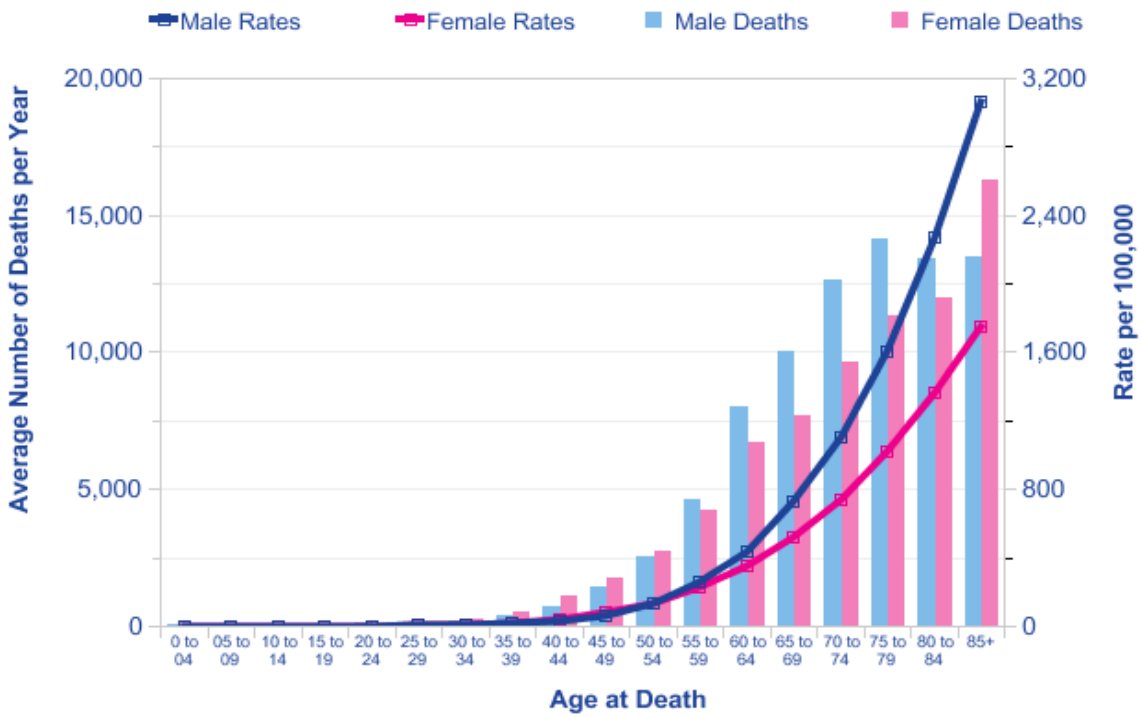

Figure 2 Graph showing cancer mortality as a function of age (Bassily *et al*. 2010).

Cancer causes and metastasis

Tumours are classed as benign, pre-malignant or malignant. Benign tumours are not classed as cancerous; they do not invade neighboring tissues, metastasize or grow abnormally. Metastasis occurs when cancerous cells break away from the primary tumour, and travel to other parts of the body through either the circulatory or lymphatic system. This process complicates treatment and is sometimes referred to as haematogenous or lymphatic spread (Lorusso & Rüegg 2012).

Metastatic or secondary tumours arise when the breakaway cancer cells arrive at a distant site, penetrate through the epithelial cells and begin to proliferate. The process of local metastasis is also possible where primary tumour cells permeate through local tissue and form secondary tumour sites within close proximity to the initial tumour (Oppenheimer 2006). Ability of cancer to metastasize is classed as one of the six hallmarks of cancer. Hanahan and Weinberg concluded in the early 2000s that all malignant cancer growth is a manifestation of six abilities of a cancer cell:

Tissue invasion and metastasis

Self-sufficiency in growth signals

Insensitivity to growth inhibitory signals

Evasion of apoptosis

Potential for unlimited replication

Angiogenesis

Ten years later the group defined the above six hallmarks, they suggested the addition of two more (Hanahan & Weinberg 2011):

Reprogramming of energy metabolism

Evading immune destruction

Growth and proliferation in normal cells are instigated by external signals, whereas cancer cells do not require these signals from surrounding tissue and proliferate uncontrolled. This is due to the production of their own hormone signals or the induction of their own internal stimulus.

Cancer cells also have the ability to ignore the signals that regulate growth allowing them to avoid the normal mechanism of growth inhibition to proliferate.

Immortality or avoidance of apoptosis is another hallmark of cancer. Cell life in normal cells is determined by repetitive nucleotide sequences at each end of the chromosomes called telomeres. In normal cells each time a cell divides, the telomeres get shorter. When the telomeres get too short the cell will cease growth, enter senescence, or begin programmed cell self-destruction (apoptosis), this depends on the cell's genetic background. Cancer cells evade the mechanisms normally in place to induce the previously mentioned consequences of ageing. Apoptosis provides space for new cells and avoidance of this allows the damaged or altered genetic information to pass to the next generation of cells.

Cancer cell cycle

The growth of cancer is not only caused by break down in the cell signaling pathways, it also causes disruption of the cell cycle. The cell cycle clock (**fig 3**), is made up of an arrangement of proteins that interact with each other in the nucleus. These proteins integrate various stimulatory and inhibitory pathway information, if the stimulatory messages are in greater numbers the cell can advance through its growth cycle. There are four stages in the cell cycle and advancement through them is driven by changing levels of cyclin proteins.

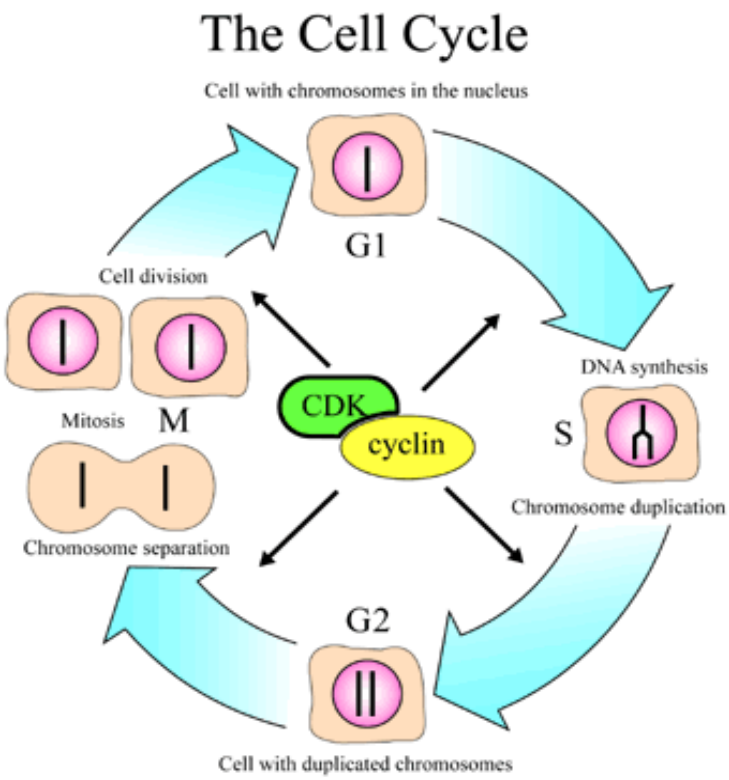

Figure 3 diagram showing the 4 phases of the cell cycle (G1, S, G2, M) and how this is regulated by cyclin (Dehay & Kennedy. 2007).

The G_1 phase is crucially important as it is this that decides if the cell will continue into the S phase. This is activated by a molecular switch.

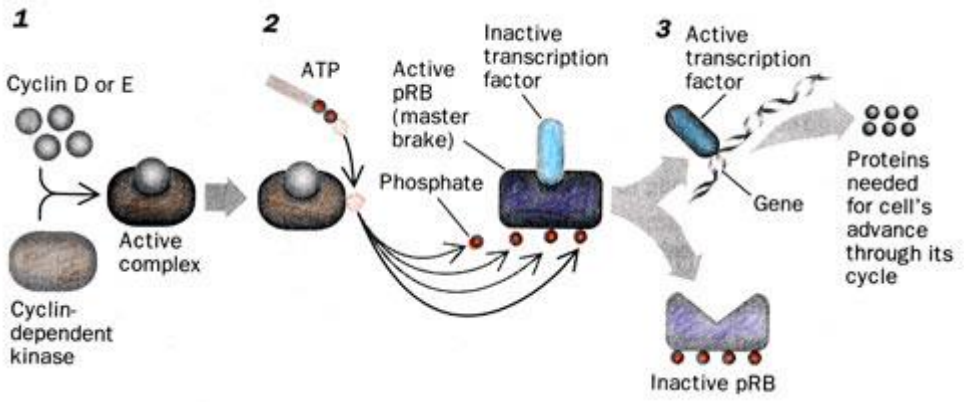

Figure 4 diagram showing advancement from G_1 to S phase via the activation of a molecular switch (Machaca. 2011).

The process (**Fig 4**) begins with a rise in the levels of cyclin D, followed by an increase in the levels of cyclin E. Combination of these proteins leads to the activation of cyclin dependent

kinase enzymes (**Fig 4, 1**). These enzymes transfer phosphate groups from ATP molecules to a pRB protein, this is also known as the master brake of the cycle. If this protein lacks phosphate groups it blocks the cycle through the sequestering of various transcription factors. The brake on cycling is removed (**Fig 4, 2**) when the pRB receives enough phosphates from the cyclin-kinase complex freeing the transcription factors to act on genes (**Fig 4, 3**). This leads to the induction of the various proteins needed for further progression through the cell cycle. The overall effect of any change in the levels of the proteins is deregulation of the cycle clock and hence excessive cell proliferation (Machaca. 2011).

Types of cancer

As mentioned there are several different types of cancer, a broad system of classification exists based either on type of cell or tissue that the cancer has come from.

Carcinoma – this is the most common type of cancer. It occurs at epithelial cells, usually in older people. Common types are breast, prostate, lung, colon and pancreas.

Lymphoma / Leukaemia – these tumour classes come from hematopoietic cell. They tend to include cancer of the lymph nodes and various tissues of the immune system.

Sarcoma – these are tumours' of the connective tissue. All sarcoma originate from mesenchymal cells from bone marrow. Susceptible tissues include cartilage, bone, muscle and fat.

Blastoma – these cancers are more common in children as they are derived from embryonic cells.

Germ line – cancers derived from sperm or ova (Pluripotent cells) from testicle or ovary.

Cancer chemotherapy

This is the use of pharmaceutical agents to kill cancer cells through several different mechanisms. The main drug target areas are interference with the cell division process and damage to the DNA of cancerous cells. The principle behind chemotherapy is to damage rapidly dividing cells, this includes both cancerous and healthy cells with the knowledge that cancerous cells cannot repair themselves against the cytotoxicity but normal cells can. This type of treatment is typically used to deal with metastasis as it affects rapidly dividing cells throughout the body.

In principle this treatment works because the cancer cells replicate quicker than most normal cells. This means that it affects mainly cancer cells and a small number of healthy cells as a lower number of healthy cells replicate before the drug is passed from the body.

Treatment is usually given in cycles, this is to give the patients time to recover from the side-effects caused by damage to normal cells. These usually include; hair loss, diarrhea, fatigue and nausea. The drugs are normally given in combinations to reduce cancer resistance.

There are several chemotherapeutic drug classes in use; treatment is usually tailored for each patient depending on type and class of malignancy.

Antimetabolites

These are compounds that mimic biochemical molecules. They usually bind to proteins (receptors or enzymes) causing inactivation of a biological response. For this to occur the compounds are usually very similar in structure to the compound they are mimicking. The main process that these drugs interfere with is the production of nucleic acids. This is done in various ways such as inhibiting the production of deoxyribonucleoside triphosphates, this is an immediate precursor in the synthesis of DNA - so failure to produce this halts replication. This usually requires a long duration of interference to cause cell death. Many anti-metabolites are so similar in structure to pyrimidine or purine bases that they can successfully substitute for them in the anabolic nucleotide pathways and compete with /inhibit the normal substrates for the enzymes. Nucleotide anti-metabolites are so similar in structure to their normal counterparts that they can be also be incorporated into DNA and RNA even with the highly selective nature of polymerases. This leads to the initiation of various DNA repair mechanisms and cell death. Five main groups of anti-metabolite are in use (**Fig 5, 1- 5**);

Pyrimidine antagonists – i.e. 5-Fluorouracil **(1)** (Mader *et al*. 1997)
Purine antagonists – i.e. 6-thioguanine **(2)** (Nelson. 1990)
Folate inhibitors – i.e. Methotrexate **(3)** (Obasaju *et al*. 1993)
Sugar modified nucleoside analogues – i.e. cytarabine **(4)** (Mehta *et al*. 2011)
Ribonucleotide reductase inhibitors – i.e. Triapine **(5)** (Sigmond *et al*. 2007)

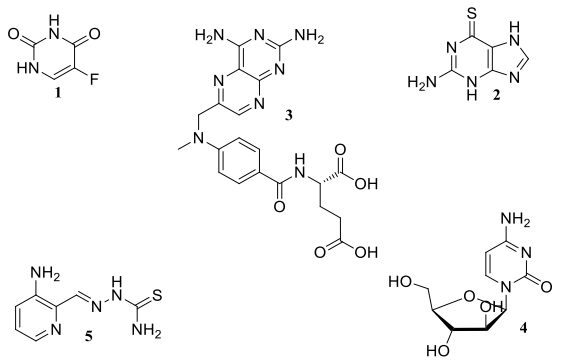

Figure 5 Common anti-metabolite cancer drugs

Alkylating agents

This is the most widely used class of anticancer drugs. These compounds are electrophiles that form covalent bonds with biological macromolecules. The most common targets are nucleophilic sites at DNA bases (NH_2, OH etc) and will usually result in the attachment of an alkyl group to DNA. The main sites for alkylation (**Fig 6**) are nitrogen atoms at guanine **(6)**, adenine **(7)** and cytosine **(8)**.

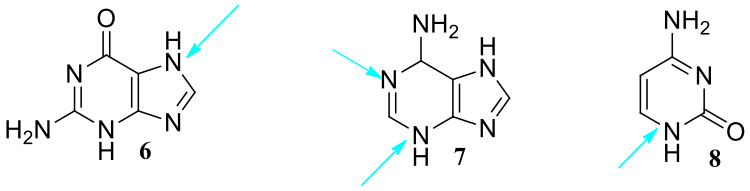

Figure 6 Main sites for alkylation on DNA base guanine (6), adenine (7) and cytosine (8).

Alkylation causes damage in various forms as the helical structure of the DNA is rendered defective. The usual disruption caused is DNA breaks or incorrect links within or between the strands of the molecule. The lethal lesions are usually caused by the interstrand link or less frequently intrastrand cross-linking as caused by e.g. cis-platin (Fuertes *et al*. 2003). Apoptosis occurs if the damage caused is not fixed by any of the various DNA repair mechanisms. Examples include (**Fig 7**).

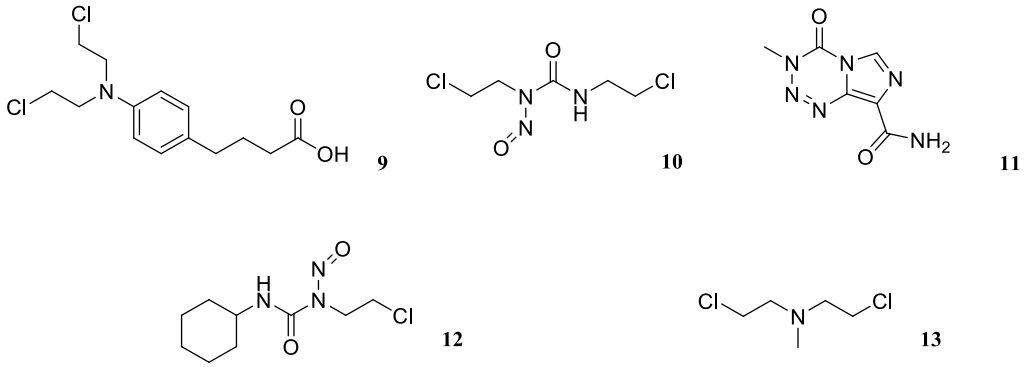

Figure 7 Structures of commonly used alkylating agents Chlorambucil (9), bischloroethylnitrosourea (BCNU) (10), temozolomide (11), lomustine (CCNU) (12) and chlormethine (13).

DNA intercalating agents

These compounds are geometrically flat or contain flat regions. They stack between paired DNA bases to form a DNA-drug interaction that is vital for cytotoxicity. The compounds bond to the DNA through Van der Waals forces and hydrogen bonding; due to this they are usually aromatipolycyclic and planar. The drug is positioned rigidly in a perpendicular fashion to the DNA helical axis.

The interaction between the drug and base is more energetically favored and so stronger than the interaction between base pairs. Intercalating agents tend to be used against fast growing cancer cells such as Hodgkin's Lymphoma, for which Daunorubicin (**Fig 8, 14**) is used in the clinic (Tulpule *et al*. 2001). The antibiotic dactinomycin (**Fig 8**, **15**) has also been used for the treatment of children's cancers such as Ewing's Sarcoma (Balamuth and Womer. 2010) and Wilm's tumour (Ehrlich *et al*. 2006).

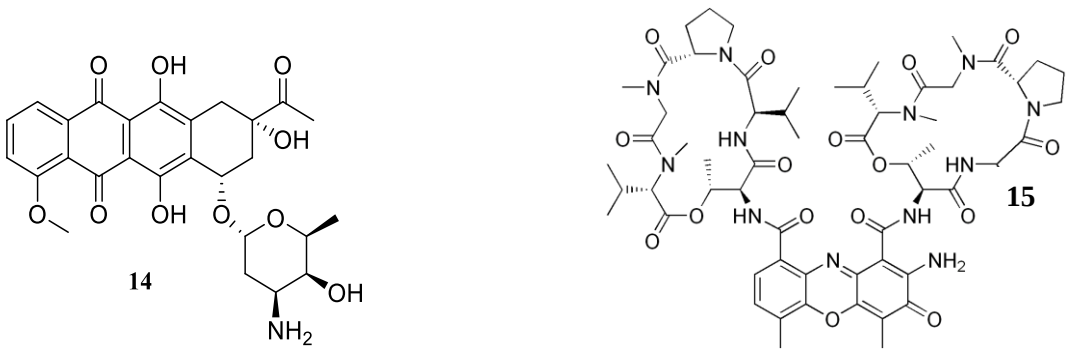

Figure 8 Daunorubicin (**14**) and dactinomycin (**15**), two commonly used DNA intercalating drugs

Angiogenesis and tumour vasculature

When a tumour grows to roughly 1-2 mm in diameter, the process of angiogenesis, formation of new blood vessels begins. At this size vasculature is required for further growth and metabolism. The supply of blood to cancer cells is essential for providing oxygen and nutrients and removing the cytotoxic waste produced.

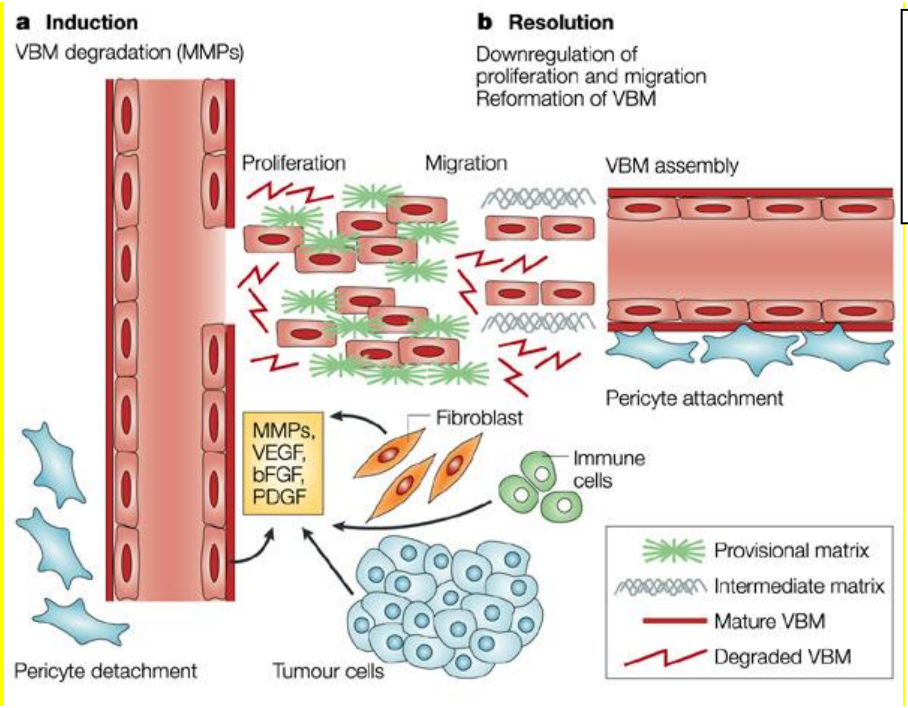

VBM – Vascular Basement Membrane

MMP – Matrix metalloproteinases

Figure 9 Diagram showing the induction (a) and resolution (b) steps for the process of angiogenesis for tumour vasculature

It has been shown that the establishment of a blood vessel network directly correlates with survival, growth and development of a tumour (Hinnen and Eskens. 2007).

This process begins (see **FIG 9**) when regular blood circulation becomes inadequate and the oxygen supply to cells is restricted. Various angiogenic proteins are activated to stimulate the production of new blood vessels. Vascular endothelial growth factor (VEGF) and fibroblast growth factors (FGF) are released by a signal cascade to instigate differentiation of the endothelial cells that constitute blood vessels In addition, further proteins are recruited to

remodel the extracellular matrix, stabilize the blood vessels and regulate the differentiation of cells to form capillaries, veins and arteries (Eskens and Verweij. 2006).

The vascular network formed in solid tumours is distinct when compared to non-cancerous tissue. This is due to a process called neovascularisation. This process involves parallel proliferation of endothelial cells that cover the inner surface of blood vessels. This process differs from angiogenesis in that angiogenesis mainly deals with the growth of sprouts and capillary buds from existing vessels (Raja *et al*. 2012).

Cancer cells have a faster rate of proliferation than normal cells. Due to this neovascularization lags behind cell growth resulting in the formation of vasculature that varies greatly from normal vessels in both structure and morphology.

The difference in cancer vasculature is different at a cellular level as tumour vessels express proteins that are either not present or at a low concentration in non-cancerous cells. Examples of these proteins are angiogenic growth factor receptors and $\alpha_v$integrins, the presence of which has been identified from human breast carcinoma xenografts on mice using an *in vivo* phage library. This phage library also allowed the identification of cancer cell specific amino acid motifs including the RGD motif (arginine, glycine and aspartic acid) which can selectively bind to the integrins $\alpha_v\beta3$ and $\alpha_v\beta5$. The group reported that the motif is expressed in several cancers including sarcoma, melanomas and carcinomas (Jussila and Alitalo. 2002).

The importance of blood supply in the development and growth of solid tumours has not been overlooked and compounds that specifically target vasculature have been developed. These compounds have been broadly classified as anti-angiogenic agents and care needs to be taken to distinguish between them. Anti-angiogenic compounds target proteins involved in the generation of new vessels preventing vasculature growth whereas vascular targeting agents actively target and cause physical damage to pre-existing blood vessels. Some agents both

prevent the formation of new vessels and cause disruption to existing vasculature. In this case the classification of said compound is based on the primary mode of action (Hinnen and Eskens. 2007).

Normal (non-cancerous) tissues in the body have a well maintained blood supply provided by an efficient and orderly vascular network (**Fig 10, a**). This is regulated by a demand driven metabolic balance between pro and anti-angiogenic factors and a complex network of lymphatic vessels that remove the subsequent metabolic waste products. The normal microvascular architecture is hierarchical with an even distribution of mature vessels to allow the appropriate transport of oxygen and nutrients to cells.

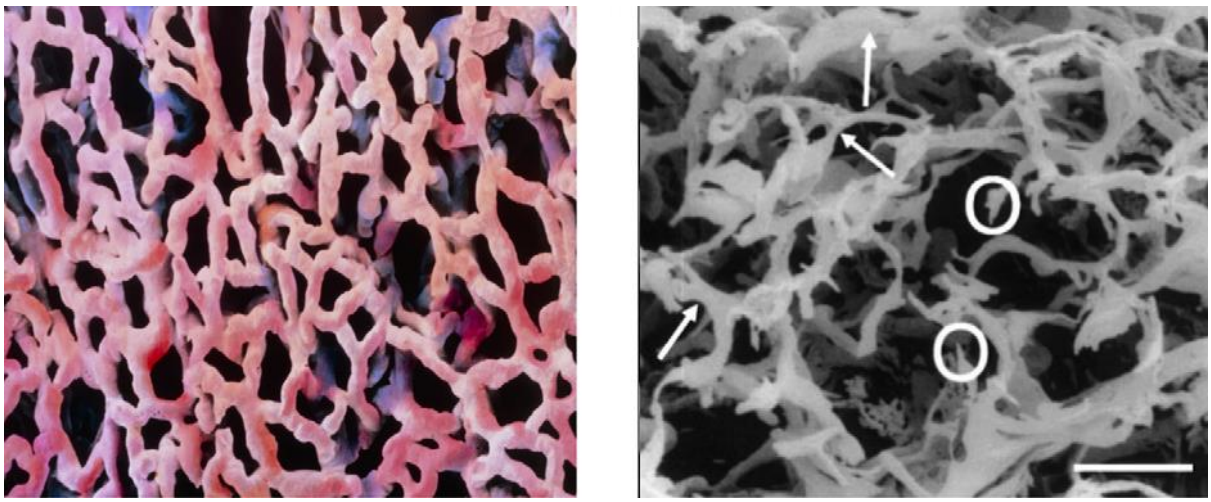

Figure 10 (a) An SEM image showing the microvascular structure of normal lung tissue. (b) An SEM image showing the microvasculature of adenocarcinoma. The arrows show abnormal structures, arrows point to blind ends.

In tumours, rapid expansion of cell population and related over expression of angiogenic factors lead to the formation of a disordered and inefficient network of blood vessels that differ drastically from healthy blood vessels (**Fig 10, b**). This vasculature is characterised as a tangled, disorganised maze of immature, permeable vessels without a hierarchy (Konerding *et al*. 2001). Tumour vasculature tends to be uneven in shape and non-uniform in diameter with dead ends. They can also have shunts between arterioles and venules. The complementary lymphatic system is equally disordered, uniform and leaky causing fluid

engorged vessels (Padera *et al*. 2002). These structural flaws massively reduce the vasculature's ability to both deliver required nutrients through the blood and remove waste through the lymph system. Compared to normal vasculature tumour vessels are much more permeable. As they are immature vessels that are lacking in smooth muscle cells leaving them with an abnormal basement membrane caused by gaps in the endothelial lining (Gee *et al*. 2003). This hyperpermeability leads to inadequate osmotic force causing a build up in interstitial pressure (Vaupel *et al*. 1987). The irregular shape of the vessels causes geometric resistance that often leads to insufficient amounts of oxygen reaching tumour cells, this is evident the presence of micro regional hypoxia (Vaupel and Hockel. 2000).

Anti-angiogenic Agents

The aim of anti-angiogenic therapies is to target and inhibit the key molecular factors in a cell that are required to develop new vessels for tumours. Without the development of sufficient vasculature to deliver oxygen and remove waste, tumour growth is limited to a few millimetres in diameter and the tumour remains benign and metastasis is avoided (van der Bilt *et al*. 2012).

The process of angiogenesis is complex (**Fig 11)** and depends heavily on regulation of biochemical signals, receptors and various cell types to manage what is known as the "Angiogenic cascade". Many signaling molecules have been identified as crucial to the process but the target deemed most important and therefore heavily investigated is the protein vascular endothelial growth factor (VEGF). This pro angiogenic factor incites the growth of vasculature as a response to certain stimuli such as hypoxia, the lack of or reduced levels of oxygen (Dibbens *et al*. 1999).

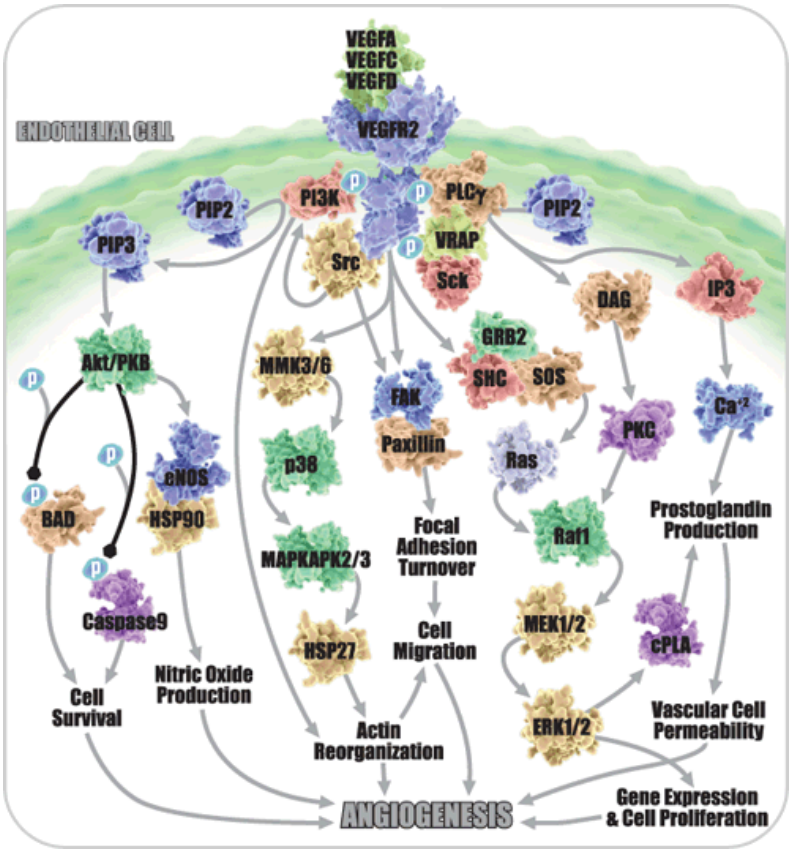

Figure 11 Diagram showing the complexity of the VEGF biochemical pathway leading to angiogenesis (Sabioscience, 2012)

VEGF is vital for the proliferation of endothelial cells and therefore new vasculature but it is also important in the regulation of vasculature transport by inducing an increase in permeability. It has also been shown that the rate of angiogenesis as a function of VEGF secretion can be affected by oncogene activation or tumour suppressor deactivation.(Lennard *et al*. 2001) Several therapeutic approaches have been developed to directly target both VEGF (Jubb *et al*. 2006) and VEGFR (VEGF receptor). Inhibition of tyrosine kinase (VEGFR) using small molecule pharmaceuticals have had promising results in the cliniespecially the use of these compounds in combination with established therapeutic agents (Madhusudan and Ganesan. 2004). Several other angiogenic factors exist and have been researched as targets (Dong *et al*. 2007). Despite the potential in the area it should be noted that several cellular angiogenic pathways exist, all with highly sophisticated regulation

mechanisms with this in mind targeting one factor is very unlikely to cause enough disruption to cease formation of vasculature.

Tubulin and microtubules

Microtubules are important proteins that make up part of the cell cytoskeleton. These compounds are long protein polymer filaments that have a tube like shape and are essential for cell division in eukaryotic cells. The main building block for microtubules is tubulin, this protein is found in almost all differentiated cells in the body (Ludueña. 1997).

Microtubules are made up of repeating units of α-tubulin and β-tubulin heterodimers, with a mass around 50,000 Daltons per dimer (**Fig 12, a**). These structures can measure up to several micrometres in length with the tubulin heterodimers maintained in an equilibrium The structures of both the α and β tubulin subunits are very similar, this is reflected by the fact that they share a 40% sequential homology (Aylett *et al*. 2011).

Microtubule arrays are used to physically separate chromosomes during cell division. As the cell divides the microtubules maintain the direction and plane of cleavage of the genetic material. These tasks require the dynamic assembly and disassembly of the microtubules especially during the process of mitosis. The presence of microtubules is also important for cell shape maintenance, movement of vesicles through the cell, cell signaling and morphogenesis (Dupuis-Williams *et al*. 1996).

The tubulin sub-units polymerize to create a robust polymer that possesses an essential resistance to bending, compression and stretching. These properties along with the various mechanical properties of transitional filaments and actin filaments give the cytoplasm its strength and shape; this in turn forms the cytoskeleton which dictates the spatial organization of the cell. The formation of these cytoskeletal polymers exist in a highly dynamic

equilibrium in which they polymerize, depolymerize and move through the cytoplasm with a timescale of seconds to minutes (Castro *et al*. 2010).

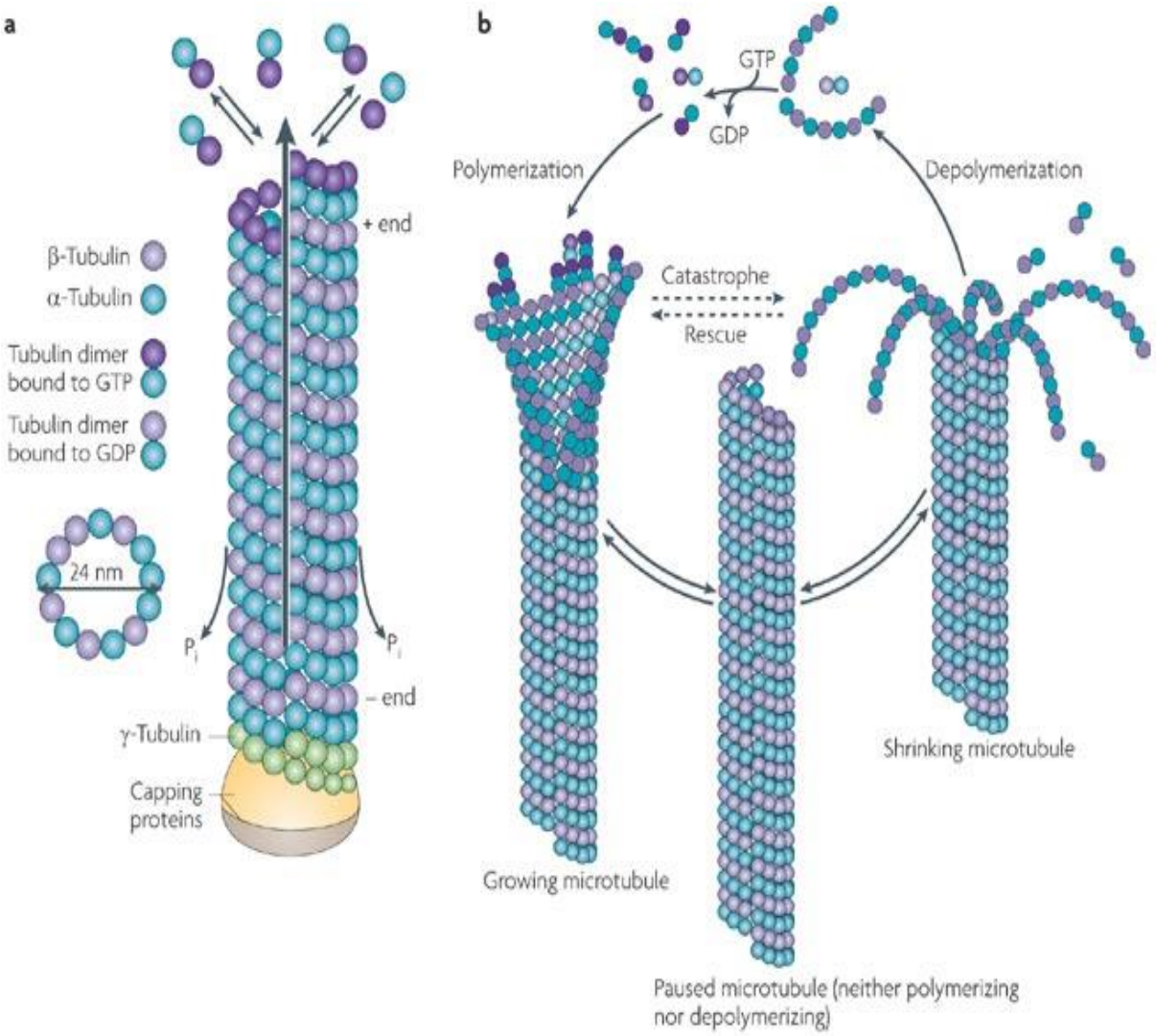

Figure 12 a - Diagram of a fully formed microtubule. b - Diagram showing the 3 stages of microtubule dynamic assembly (Conde & Caceres 2009), (http://www.nature.com/nrn/journal/v10/n5/box/nrn2631_BX1.html. 2012b)

The process begins with the gathering of the α and β tubulin subunits forming a short microtubule nucleus (**Fig 12, a**). This nucleus is then elongated at both ends resulting in the formation of a hollow cylindrical shaped structure composed of a head to tail layout of subunits arranged as 13 protofilaments. These filaments have a helical arrangement

(sometimes referred to as a super helix.) The ends of the microtubules are designated as a plus end in which a β-subunit is at the end or a minus end in which a α-subunit is at the end (Lai *et al*. 1994).

The stabilization/destabilization of microtubules is associated with the binding interactions of a group of proteins called microtubule associated proteins (MAPs). These proteins can bind to other proteins or small molecules to change dynamics classing them in a regulatory role (Brun *et al*. 2009).

The cycle of tubulin polymerization/depolymerization (**Fig 12, b**) begins with the binding of GTP at the β-subunit causing its activation. This begins the formation of a several consecutive monomers of GTP known as a "Cap" at the end of a microtubule, the presence of which is essential for growth to continue. When tubulin is polymerized, GTP irreversibly hydrolyses to GDP.

As a precautionary measure to prevent all of the GTP converting to GDP the microtubule is briefly destabilized to allow detachment of the tubulin-GDP complex. It is believed that the essential dynamic instability is driven by the competition between the attachment of GTP to tubulin and the hydrolysis of GTP (**Fig 13)**. This important property allows the interruption of slow growth periods with a rapid disassembly. With this in mind, compounds that interfere with the formation/deformation of microtubules can potentially act as chemotherapeutic agents (Nawrotek *et al*. 2011)**.**

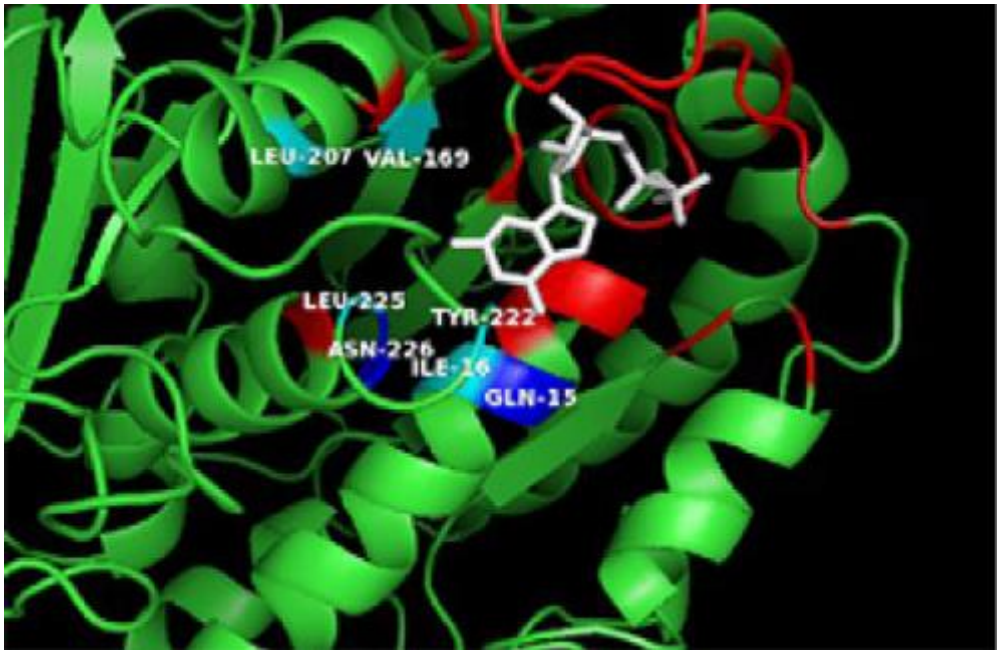

Figure 13 Image of GDP-bound tubulin (Chen *et al*. 2008).

Tubulin as a drug target

Owing to their ubiquitous nature, the presence of tubulin in the cytoskeleton is essential for eukaryotic cells and of vital importance in various cell processes, in particular mitosis. The tubulin assembles to make microtubules and in turn form the mitotic spindle that is required to pull apart the chromosomes into each subsequent daughter cell. They have key roles forming cell shape during angiogenesis, cell proliferation and migration. In the context of cancer, microtubule-motor proteins are crucial in the transport of vital onco proteins.

Microtubules are highly dynamic polymers by nature, constantly changing length during various phases of elongation/shortening. This dynamic property makes tubulin an excellent target for anti-cancer drugs.

There are two main drug classes that bind to tubulin causing microtubule inhibition. These are compounds that either stabilize (Microtubule stabilizing agents MSAs) or destabilize (Microtubule destabilizing agents MTAs) microtubules. MSAs stabilize the polymer and promote polymerization whereas MTAs prevent polymerization and promote

depolymerization. The presence of MSAs allow the polymerization of GDP- bound tubulin into microtubules, an action that doesn't happen under normal conditions. Many MAPs have been shown to act as MSAs but none of them bind as well as non-indigenous compounds allowing for a more stabilized polymer (Aylett *et al*. 2011).

The precise mechanism for MSA induced mitotic arrest and subsequent apoptosis has not been fully elucidated, however it is generally accepted that the stabilization causes interference with cellular spindle dynamics. This causes the cell to fail at mitotic check points causing an arrest at the G2/M phase. Failure at this stage of the cell cycle is a hallmark of tubulin binding agents. Microtubules also play a role in endothelial cell migration. Therefore targeting tubulin also has an inhibitory effect against angiogenesis and vascularization in tumours (Jordan and Wilson. 2004).

Both classes contain a vast range of structurally diverse molecules that vary from large complex natural products to small simple drug analogues. Compounds are classified based on their effects on tubulin polymer mass at high concentration. Both classes at low concentration cause inhibition of microtubule dynamic stability leading to mitotic arrest with little effect on overall polymer mass (Jordan *et al*. 1993).

Target selectivity comes from the fact that these drugs disrupt immature proliferating tumour endothelial cells which replicate 20 times faster than in healthy vasculature (Denekamp 1982). This occurs either through direct apoptosis or effects caused by endothelial cell reliance on a tubulin/microtubule-based cytoskeleton to maintain cellular shape. The disruption of an oxygen supply causes ischemia that induces a cascade of secondary tumour cell death (Dark *et al*. 1997).

Microtubule stabilizing agents

Microtubule stabilizing agents stop the disassembly of GDP bound tubulin forming stable polymers. These compounds bind to either the taxoid or laulimalide/peloruside sites located on the luminal and external faces of the β-subunit respectively. Activation of either site causes the stabilization of an important β-subunit loop resulting in the stabilization of the microtubule lattice. This class of compounds represents most of the clinically used treatments. Most of these compounds are large, complex structures with a massive diversity in shape.

Taxoid binding site

The taxoid binding site was first discovered over 20 years ago by Rao (Rao *et al*. 1992). The site was detected on the β-subunit by using [^{3} H] taxol to directly radiolabel tubulin. Taxol binds to the site with 1:1 stoichiometry, effecting protofiliment interaction. The site is located on the luminal face of β-tubulin, the same location on α tubulin is occupied by 8 extra amino acid residues. Most of the bonding interactions occur at the taxane ring and most MSA compounds reversibly compete with taxol. The taxol binding pocket itself consists of the S9-S10 loop and parts of the core helix of the β-subunit. When taxol is bound it sits on the N-terminus of the microtubule loop protruding from the protofiliment, this acts as a secondary structure for microtubule stabilization (Sui and Downing. 2010), (Nogales *et al*. 1995). As mentioned taxol binds to the luminal site of β –tubulin. When polymerized the molecule is facing the inside of the microtubule and the corresponding location on α-tubulin is occupied with eight extra residues. These amino acids help to stabilize the M-loop and it had been long suspected that taxol/taxanes replicate this action on the β-subunit. This loop is located between strand 7 (S7) and helix 9 (H9). It provides important lateral interactions to the taxol binding pocket. (Löwe *et al*. 2001). A recent study confirmed this through X-ray crystallography (Prota *et al*. 2013).

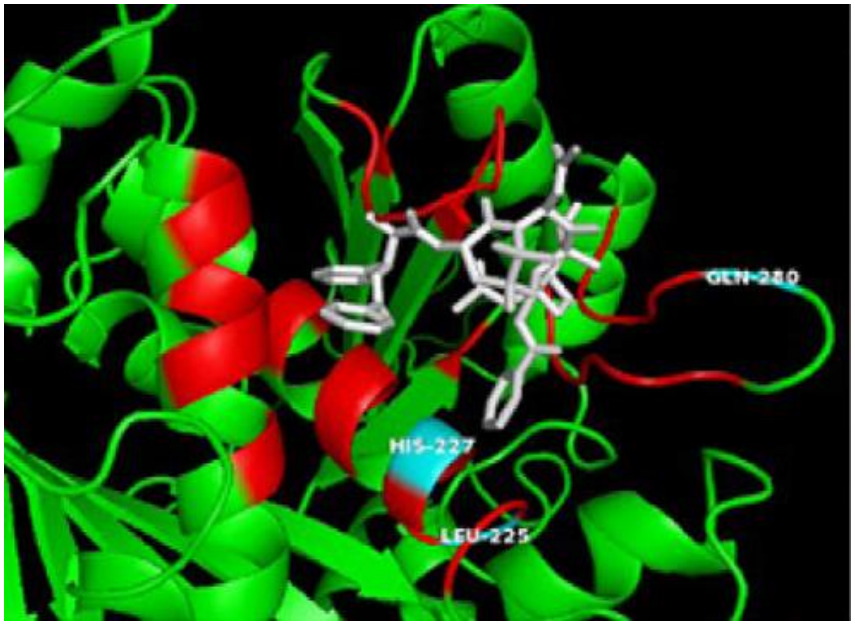

Figure 14 Image showing paclitaxel bound to the taxoid binding site on tubulin (Chen *et al*. 2008).

The binding pocket (**Fig 14)** is located inside a hydrophobic cleft and binds to taxol through hydrogen bonds and numerous hydrophobic interactions. Several amino acid residues directly interact when taxol is bound. These interactions have been further validated by Snyder (Snyder *et al*. 2001) through the use of molecular docking. A model of the taxol bioactive conformation was constructed using data from crystallographic density analysis. The model showed 3 H-bond interactions and confirmed the hydrophobic interactions.

Paclitaxel (**FIG 15, (16)**) was one of the first compounds of this class discovered and over the years along with its semi-synthetic analogue (docetaxel) paclitaxel has been heavily researched as anticancer therapeutics. Paclitaxel was first identified in 1971 (Jordan *et al*. 1993) in a US National Cancer Institute screening program for anticancer agents as an isolate from the bark of the Pacific Yew (*Taxus brevifolia*). A major problem with the compound was acquiring a supply of it as it required material from the bark of two trees to provide a dose for a single patient. Several total synthesis have been achieved (Nicolaou *et al*. 1994) but with multiple steps and low yields, other sources were required. The problem was overcome by semi-synthesis of taxol and its analogues from other natural products from yew

needles, an overall better method as needle harvesting doesn't kill the tree. Paclitaxel and its analogues have been termed taxoids and the method of action is the selective binding to β tubulin subunits. The binding of taxoids causes microtubule stabilization through the acceleration of tubulin polymerization leading to a halt in cell division (Horwitz. 1994).

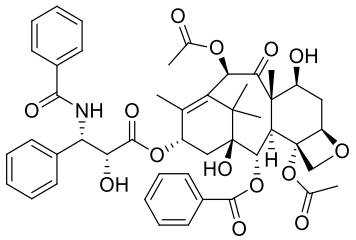

16

Figure 15 the natural product Paclitaxel **(**16)

Many changes to the "Top" face of the pharmacophore of taxol led to increased aqueous solubility and better pharmacokinetic properties leading to the development of two compounds BMS 188797 and BMS 184476. Further modifications to the taxol structure resulted in an overall effect of increasing the potency by a magnitude of 3. The more substantial changes involved changing aromatic groups with more hydrophobic moieties; this also showed a serendipitous activity against drug resistant cancer strains. Further modification to the structure has resulted in the first orally active taxol, ortataxel. The compound showed increased activity due to increased restriction to rotation in the pharmacophore.

The Laulimalide/Peloruside Binding Site

Tubulin has another binding site that induces microtubule stabilisation; the location of this site was greatly debated with evidence suggesting its presence on both α and β subunits. The binding of laulimalide (**Fig 16, (17)**) was first thought to be localised to a loop region (S9-S10) on the α subunit (Nguyen *et al*. 2010). This was supported by NMR data for peloruside

(**Fig 16, (18)**) bound to the α-subunit in its bioactive conformation, in particular the interactions at the αM-loop (Pineda *et al*. 2004). Nogales proposed a limitation to this theory in that the S9-S10 loop has 8 extra amino acid residues that would obstruct the site and strengthen the links between the α subunits and the protofilaments making the binding of a MSA unlikely (Löwe *et al*. 2001). Almost 10 years later Huzil determined that the peloruside site was in fact located on the β-subunit's exterior surface close to the subunit interface (**Fig 17)** (Nguyen *et al*. 2010). The proposed site is quite close in sequence to the taxoid binding site but structurally distant.

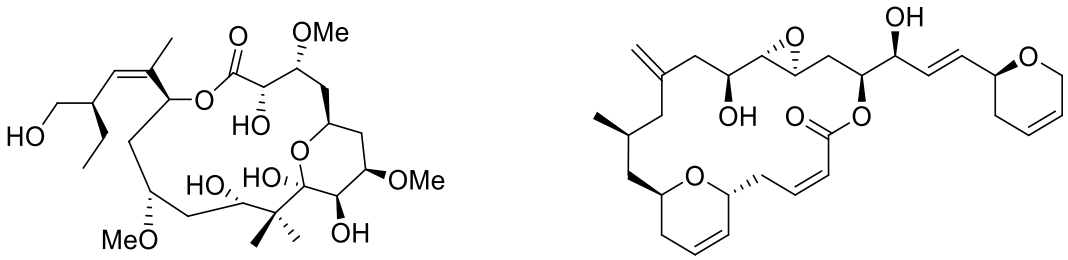

Figure 16 Image showing the structures of Laulimalide (A) and Peloruside (B)

Using a different technique, Chen identified the same region as an almost identical match. The group used digital signal processing to search for binding hot spots (Chen *et al*. 2008). The site was further supported by modelling work and radiolabelling studies that gave further insight into the structure, binding and electrostatic/hydrophobic interactions that strengthen the case for the presence of the laulimalide/peloruside site on the β subunits as opposed to the α-subunit (Nguyen *et al*. 2010). The study agreed with Huzil's location for the binding site but uncovered more complex bonding than originally proposed. This involved an intramolecular H-bond that gives peloruside a more rigid orientation allowing a hydroxyl group to interact with an arginine residue.

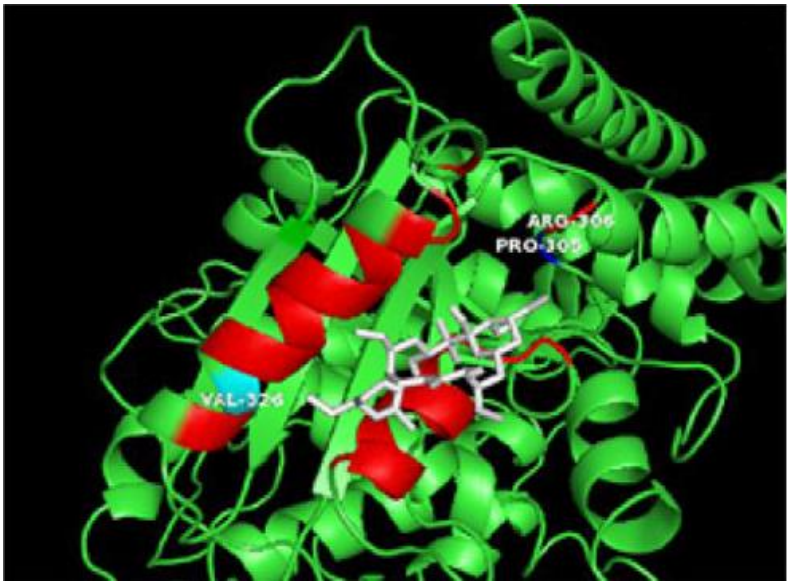

Figure 17 Image of Peroruside bound at the lau/Pel tubulin binding site (Chen *et al*. 2008)

Another study based on laulimalide used molecular docking and mass shift perturbation analysis to show that the molecule binds to the external surface of the microtubule, making the laulimalide/peloruside site unique in that all of the other known tubulin binding sites are located inside the microtubule (Bennett *et al*. 2010). As it stands there is more evidence to suggest a single site located on the β-subunit as opposed to the α subunit. Simultaneous binding at both proposed sites is possible but not supported as Pera's (Pera *et al*. 2010) studies show a 1:1 stoichiometry. An x-ray crystal structure is required to fully elucidate the structure.

Microtuble Destabalising Agents

These molecules bind to the vinca domain or the colchicine binding site, two distinct sites located at a distance from each other on tubulin. Nevertheless the actions of both classes of ligands share a common effect; they inhibit the formation of microtubules, therefore triggering disassembly.

Binding at the vinca binding region

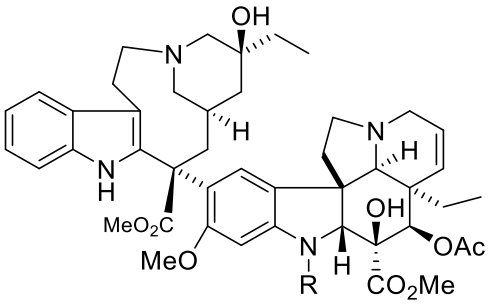

Figure 18 Structure showing Vinca alkaloid core R = CH3: (+) – Vinblastine (19), R = CHO: (+) – Vincristine (20) Drugs that target the Vinca binding domain

Several known natural products competitively bind to tubulin at the vinca binding domain. The compounds vinblastine **(19)** and vincristine **(20)** (**Figure 18**) were the first antimitotic compounds to be approved for clinical cancer therapy. Both compounds cause microtubule destabilisation. At low concentrations vinblastine inhibits mitotic progression and at high concentration causes depolymerisation of microtubules (Jordan *et al*. 1992). This leads to apoptosis and is followed by cell death. The compound binds to the β-subunit of tubulin at the positive end of microtubules - this feature is specific to vinca domain binders, **Fig 19** shows vinblastine bound to polymerised tubulin. Vincristine can bind to tubulin both in its polymerised and unpolymerised forms. Vinca domain agents bind fast and in a reversible manner, causing a conformational change to allow better contact. These drugs cause a slowing of the dynamic assembly/disassembly of microtubules. This inhibits the assembly of the mitotic spindle creating tension at the kinetochores that renders chromosomes at the spindle poles too short to reach the spindle equator blocking progression to anaphase thus causing mitotic arrest (Ehrlich *et al*. 2006).

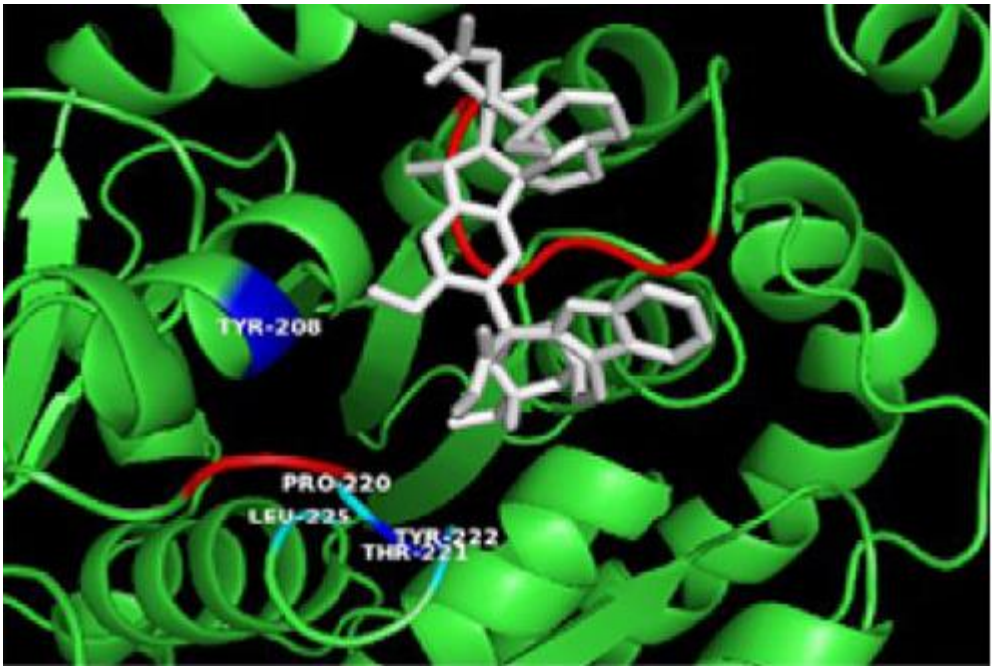

Figure 19 Image of vinblastine-bound tubulin(Chen *et al*. 2008)

Dolastatins 10 and 15 also bind to the tubulin vinca binding domain. These peptide compounds extracted from sea slugs (*Dolabella auricularia*) act as non-competitive inhibitors of tubulin with vincristine and vinblastine. Both compounds have a much higher binding affinity to tubulin than vincristine and vinblastine and this is evident from the much higher cytotoxicity exhibited. Dolatstatins are retained in the vinca binding site much longer than vinca compounds which are removed from the cells quickly (Verdier-Pinard *et al*. 2000).

Colchicine binding site

Since the original discovery that tubulin was the biological target for colchicine (**Fig 20, (21)**) in the sixties (Weisenberg *et al*. 1968), little progress was made in elucidating the ligand-protein structural relationship until a study was published by Bai 30 years later (Bai *et al*. 2000). The study attempted to identify the colchicinoid binding site location in tubulin using both molecular modelling and biochemical techniques. The group also showed that the site of interaction for podophyllotoxin (another MTA) overlapped partially with that of colchicine. The location of site was finally validated by X-ray crystallography (Ravelli *et al*. 2004). This study showed the structure of tubulin complexed with a colchicine analogue (DAMA-colchicine) and the stathmin like domain of the RB3 protein. Another tubulin crystal structure was subsequently reported featuring a double tubulin heterodimer complexed to the stathmin-like domain of the RB3 protein; the structure was free from any ligands.

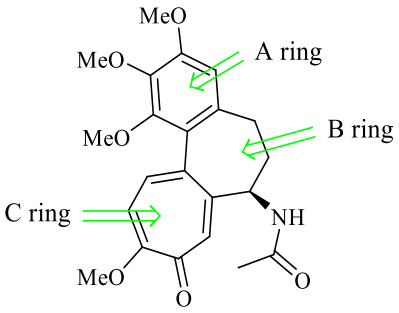

21

Figure 20 Diagram showing the structure of colchicine and its ring naming system

Several other crystal structures of tubulin complexed MTAs have since been published suggesting a slightly different mode of action, causing a change in the microtubule structure from linear to curved (Dorléans *et al*. 2009).

The colchicine binding site is located in a deep pocket at the interface between the tubulin heterodimers. Due to the hindered location, major conformational changes need to occur to allow inhibitors to enter the site. The binding region should be referred to as a "Domain" instead if a site due to its complexity.

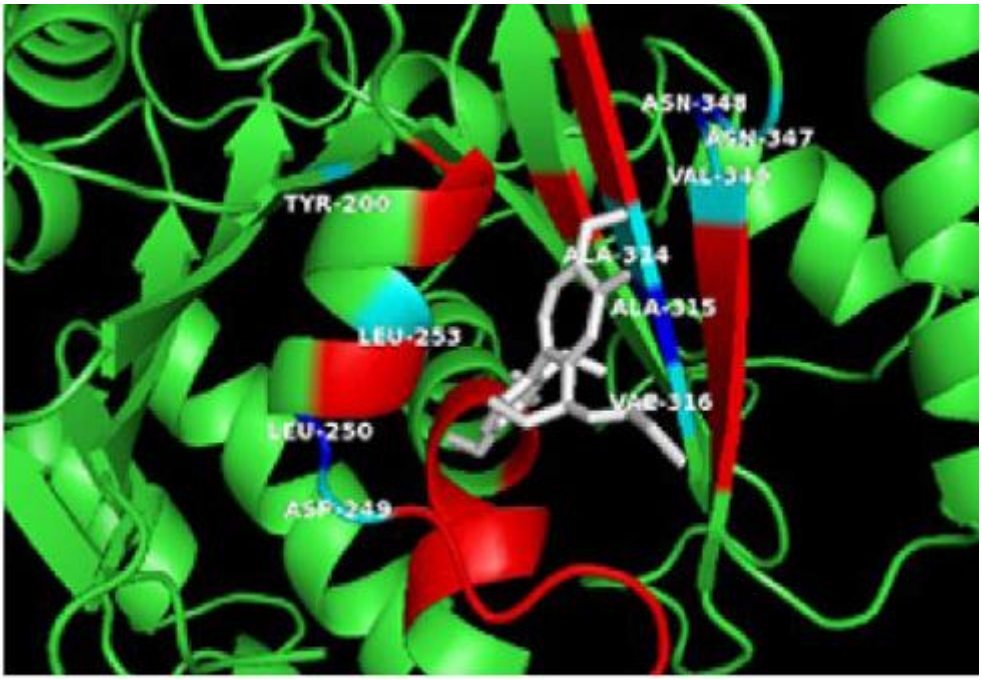

Figure 21 Image of Colchicine-bound tubulin**(Chen *et al*. 2008)**

Colchicine binds to tubulin in its non-polymerised form in two steps. **Fig 21** shows a image of colchicine-bound tubulin. The MTA first forms a weak, reversible complex with tubulin. This causes a conformational change in the protein that leads to the formation of a stronger pseudo-irreversible complex (Skoufias and Wilson. 1992).

Vascular Targeting Agents

Podophyllotoxin

Podophyllotoxin (**22)** binds to the colchicine binding site on the tubulin β-subunit. The compound is a competitive inhibitor of tubulin, binding more rapidly and with more affinity in a reversible manner than colchicine. This compound has a unique mechanism of action in that it doesn't interfere with the tubulin GDP/GTP exchange; instead the compound disrupts tubulin dependant GTP hydrolysis (Cortese *et al*. 1977). Molecular docking studies on podophyllotoxin and colchicine showed that even though both compounds bind at the binding site on the tubulin β-subunit, they don't fully overlap in their bonding interactions and therefore show quite different biological binding profiles (Stanton *et al*. 2011). The full mechanism of the compounds antimitotic action hasn't fully been elucidated but it known that it interrupts microtubule dynamic instability (Jordan *et al*. 1992).

Unfortunately podophyllotoxin was unsuitable for further development into a useful clinical drug. However etopside and teniposide, two analogues of the compound were further developed into clinically used drugs to treat lung and testicular cancer respectively. Strangely both analogues show poor binding affinity to tubulin compared to the parent molecule but exhibit a strong inhibition of DNA topoisomerase-II, an enzyme used in the relaxation of super coiled DNA during cell division (Pommier *et al*. 2010).

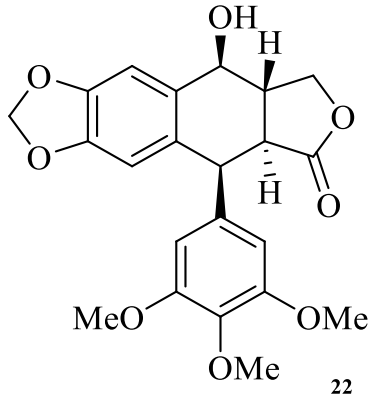

22

Figure 22 structure of Podophyllotoxin

Combretastatin A-4

More recently some small molecule vascular targeting agents have shown promise in clinical trials. Combretastatin A-4 phosphate (CA-4, **(23)**) is a prodrug salt of a natural compound found in the South African willow (*Combretum caffrum*). Many analogues of combretastatin have been tested and all have a common two ring structure bridged by an ethene unit (Gaukroger, K. *et al*. 2003a), (Galli, U. *et al*. 2015). The rings are commonly referred to as the A-ring and B-ring (**Fig 23**). The A ring in almost all of the analogues contains the characteristic 3,4,5-trimethoxy motif. The *Z*-isomer of CA-4 **(23)** is more biologically active than the *E*-isomer **(25)** as it is also cytotoxic. Changing R groups on the B-ring of combretastatin has been shown to improve anti-tumour activity (Ohsumi *et al*. 1998). CA-4 is currently in the stage 3 human cancer clinical trials.

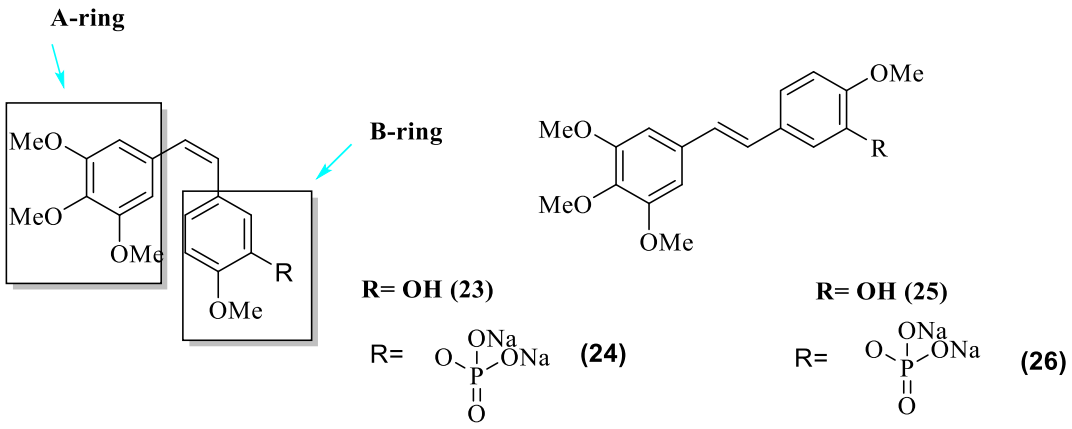

Figure 23 Diagram showing the ring labelling system of CA-4 (23), CA-4 phosphate (24) and the structure of the Trans configuration of CA-4 (25) phosphate (26).

Phenstatin (**27**) is a related vascular disrupting agent that resulted from a SAR analysis of CA-4; bearing a close structural similarity to its parent molecule - it is a potent inhibitor of mitosis. This compound and its more water soluble prodrug have almost identical biological profiles to combretastatin in terms of cytotoxicity and potency (Pettit *et al*. 1998). The compound is currently in clinical trials for human solid tumours.

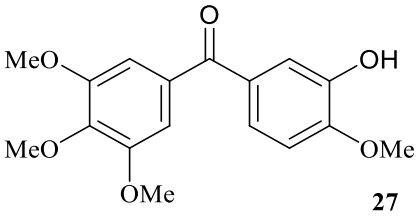

Figure 24 structure of Phenstatin

CA4 **(23)** has a close structural relationship with colchicine with which it competitively binds to the colchicine binding site with a higher binding affinity causing inhibition of microtubule formation (McGown and Fox 1989). The compound binds to tubulin in the low µM range causing it to be highly cytotoxic with typical IC_{50} values in the low nM range. Unfortunately CA-4 **(23)** has poor water solubility and the drug in its basic form wasn't developed further.

This problem was overcome in the mid 1990s by Pettit's group through the development of the CA-4 **(23)** sodium phosphate prodrug (CA-4-P **(24)**, fostrabulin™) (Pettit *et al*. 1995). The compound in its prodrug form has an improved biovailability profile but is inactive until it is converted to the active CA-4 **(23)** through the action of non-specific phosphatase enzymes *in vivo*.

Even though CA-4-P **(24)** has entered clinical trials the exact mechanism by which vascular disrupting agents work is still not fully understood. Various *in vitro* studies on several cell types have been performed. Between a concentration range of 0.1 to 1.0 μM in HUVEC cells, the drug causes complete disruption of the microtubules within 30 minutes (Galbraith *et al*. 2001) This depolymerisation of microtubules causes a rapid transformation of the cellular structure, remodelling the cytoskeleton and morphology of focal adhesions, resulting in the phosphorylation of myosin fibres causing them to interact with myosin. This leads to improved contractibility and formation of actin stress fibres. This depolymerisation was shown to be directly proportional to the sequence of phosphorylation and myosin fibre formation (Kanthou and Tozer. 2002)

Activation of ROCK (Rho kinase) through the upstream interactions of Rho A (GTPase) have been shown to regulate these alterations to cytoskeletal structure and morphology (**Fig 25**). The exact mechanism by which microtubule disruption triggers activation of RhoA has not yet been fully elucidated. It has been postulated that a set of guanidine nucleotide exchange factors (GEF) are released from the microtubule disruption activating RhoA and causing in GTPase activation (Krendel *et al*. 2002).

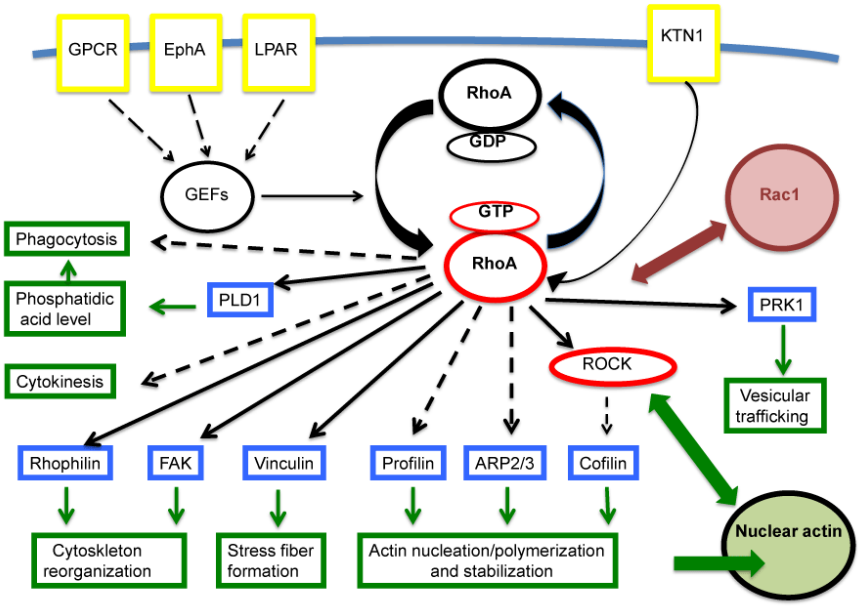

Figure 25 diagram showing the complexity of the ROCK RHOA pathway (Kloc *et al*. 2005)

Another trait of CA-4-P **(24)** treated cells is membrane blebbing. The cells become more rounded in shape as f-actin accumulates in blebs on the cell surface, forming a spherical network that engulfs the cytoplasm causing focal adhesions to appear deformed. Endothelial cells treated with CA-4-P **(24)** rapidly become more permeable to numerous macromolecules; this is due to increased contractibility and interruption of cell-cell connections. Tozer found that this increased permeability can be reduced through the inhibition of ROCK and RhoA. This points to a link between CA-4-P activated signal pathway induction and the structural and morphological changes to treated endothelial cells (Dark *et al*. 1997).

Disruption to adherens junctions also occurs when endothelial cells are treated with CA-4-P. These sites are the point where the actin cytoskeleton is linked to the cytoplasmic face. This disruption also causes increased permeability of endothelial cells (Vincent *et al*. 2005). Many factors contribute to dysfunctional cell division. Depending on the concentration and exposure to CA-4-P along with cell type, microtubule disruption can result in phase arrest at G2/M and subsequent apoptosis (Dark *et al*. 1997). It has also been found that the changes to

endothelial changes caused by CA-4-P can be reversed. Twenty-four hours after cellular drug clearance endothelial cells can rebuild cellular structure to a level similar to pre-treatment. This is unusual compared to the disruption caused by colchicine which is non-reversible. It has been postulated that differing effects may be caused by differences in binding kinetics for each molecule as CA-4-P binds faster and with a larger affinity to tubulin than colchicine. CA-4-P also dissociates over 100 times quicker (Lin *et al*. 1989).

Several animal studies have been performed to assess the selective and rapid action of the compound on tumour vasculature using both xenograft targets.(Dark *et al*. 1997), (Chaplin *et al*.), (Pedley *et al*. 2001). Initial signs of anti-vascular activity are evident from as little as 10 minutes after administration. Complete vascular shutdown occurs after 30 minutes along with a marked increase in vasculature permeability. This extensive collapse in vasculature results in haemorrhagic necrosis within an hour, which is largely located in the tumours' centre (Chaplin *et al*. 1999). This may be the reason that the viable rim can repopulate after only 1 dose (Grosios *et al*. 2000).

ZD6126

As previously mentioned, colchicine is the oldest known tubulin –binding agent. It is a secondary plant metabolite that has been used medicinally in traditional medicine for hundreds of years. The alkaloid was first isolated from the plant autumn crocus *Colchicum autumnale* in 1820. By the end of the 1930s the compound's anti-vascular properties were discovered.(Boyland and Boyland. 1937) and initial results from studies on animal and human tumours showed promise but the compound's toxicity stopped further clinical studies by 1950.(Ludford *et al*. 1948) A derivative of colchicine, ZD6126 showed almost identical

antivascular activity to that of CA-4-P on endothelial cells. The compound itself is unable to bind to tubulin; however it is converted to N-acetylcolchinol (NAC) by various serum phosphatases. NAC is an active metabolite of colchicine that binds to the colchicine binding site in a more rapid fashion and in contrast, a reversible manner (Kang *et al*. 1990). Some colchicine analogues contain an unsaturated oxepine B-ring. These compounds show the same anti-vascular and antimitotic activity *in vitro* as NAC **(29)** but this only occurs at a higher dose (Joncour *et al*. 2008).

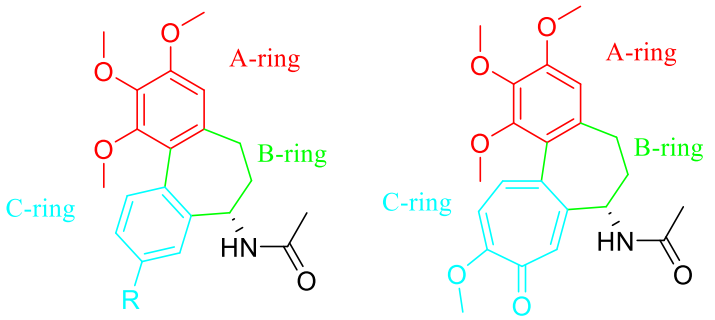

R = OPO_3Na_2 ZD6126 28
R = OH NAC 29
21

Figure 26 Diagram showing the ring labelling system and structures for colchicine (21), its metabolite NAC (29) and its analogue ZD6126 (28)

ZD6126 **(28)** is structurally similar to colchicine in that both contain a 6-membered A-ring with a trimethoxy motif and a 7 membered B-ring. The compounds differ in the C-ring in which ZD6126 **(28)** has a smaller 6 membered ring as opposed to the 7-membered ring in colchicine **(21) (Fig 26)** both compounds selectively bind to the colchicine binding site on the β-subunit of tubulin. When bound to the tubulin, the polymerization of tubulin/formation of microtubules is inhibited leading to cell cycle arrest and apoptosis. The entire mechanism for binding and inactivation at the colchicine site has yet to be fully elucidated but SAR analysis

has verified that the trimethoxy motif on the A ring in is essential to biological activity (Zefirova *et al*. 2011).

ZD6126 also exhibits a specific cytotoxic effect against tumour cells whereas colchicine does not, leading to damage of normal cells. ZD6126 was shown to cause increased hypoxia and decreased tumour volume when tested against murine xenographs (Wachsberger *et al*. 2005).

ZD6126 was able to show total disruption of microtubules in endothelial cells 40 minutes after administration. This led to the induction of actin stress fibre resulting in cellular contraction and cell blebbing (Micheletti *et al*. 2003). These morphological changes occurred selectively at a non-toxic dose and predominantly in proliferating endothelial cells as opposed to quiescent endothelial cells. Clearance of ZD6126 resulted in the endothelial cells reverting to their orginal cell shape within 3 hours implying that the effect of NAC is reversible. The *in vivo* activity of the drug was investigated through preclinical screens against various solid tumour models (mouse and human) (Davis *et al*. 2002). ZD6126 as a single administration in mice at a well tolerated dose induced retraction of endothelial cells resulting in increased permeability, platelet activation, coagulation and basement membrane exposure. This compound exhibited characteristic VDA effects resulting in stoppage of blood followed by a quick onset (within 1 hour) of tumour necrosis (Goertz *et al*. 2002).

Doubling the dosage to 100 mg/kg improved the retardation of tumour growth when administered over 5 days. The study revealed that the maximum tolerated dose of ZD6126 in mice was 400 mg/kg with significant necrotic effect shown at doses as low as 25 mg/kg. A pharmacokinetic study was also performed and revealed that, when mice received a well-tolerated single dose (61 mg/kg), the drug rapidly hydrolyses to NAC which is subsequently cleared from the plasma with an approximate half-life of 1 hour (Davis *et al*. 2002) The drug entered clinical trials in the early 2000s. The initial aim of testing was to determine dose

limitations, the maximum tolerated dose and efficiency of a single dose. All participants had advanced stage solid tumours and after a 21 day regime it was determined that the maximum tolerated dose was 112 mg/kg when given once a day for a week with a drug half-life of 1-3 hours (Beerepoot *et al*. 2006), (LoRusso *et al*. 2008).

Reported side-effects included nausea, vomiting, headache, and pain, which were thought to be dose related. At this stage there were minor signs of cardiotoxicity in the form of a reduced cardio ejection fraction (Beerepoot *et al*. 2006). Interestingly, at tolerated doses the compound didn't show any vascular damage to normal tissue in an MRI study confirming the drug's specificity to tumour vasculature (Evelhoch *et al*. 2004). The compound was entered into phase II clinical trials as three different combination therapies wih 5-fluorouracil, leucovorin and oxaliplatin. The drug failed at this stage due to the presentation of cardiotoxic side-effects resulting in a number of patients requiring the dose to be limited due to QT prolongation (Lorusso & Rüegg 2008), (Hollebecque *et al*. 2012).

Oxepines

More recent research in the area of vascular targeting agents has focused on dibenzoxepines (**Fig 27)**, whose structures are similar to NAC **(29)** with a 7- membered central heteroatom ring with an oxygen in the central [*c,e*] position. Several analogues have been made, mostly consisting of a trimethoxy containing A-ring and varied R groups on the C-ring. It is believed but still not confirmed that these targets also bind to the colchicine site on tubulin β-subunits. *In vitro* studies on these compounds have revealed that the basic pharmacophore requires the basic 3-ring structure with a trimethoxy A-ring to effect VTA activity (Colombel *et al*. 2010).

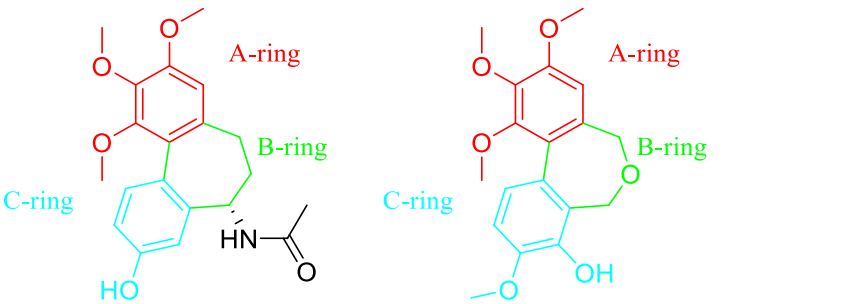

NAC

3,9,10,11-tetramethoxy-5,7 -dihydrodibenzo[c,e]oxepin-4-ol **30**

Figure 27 Structures of the VTA compounds NAC and dibenzoxepines

As previously mentioned, colchicine is too toxic to use as a VTA, but as the colchicine binding site can accommodate a number of different pharmaceutical motifs, various groups have been performing pharmacophore based design to try and produce a compound that has maximum efficacy as a VDA, excellent pharmacokinetics and reduced cardiotoxicity. Edwards *et al,* while working on the axial chirality of colchicine binding analogues, analyzed the dihedral angle of various oxepine type compounds and discovered that the degree of helicity at the biaryl core of dibenz[c,e]oxepines resembles closely that of colchicine (Edwards *et al*. 2011).

This led to the formation of several dibenzo[c,e]oxepine derivatives that had structural elements of both ZD6126 **(28)** and CA-4 **(23)**. One of the compounds 3,9,10,11-tetramethoxy-5,7-dihydrodibenzo[c,e]oxepin-4-ol **(30)** showed an excellent cytotoxic activity against K562 leukaemia cells (IC_{50}, 2.2 nM). The compounds also successfully bound to tubulin as determined by a tubulin binding assay. Similarily a number of hybrid type NAC/phenstatin like compounds have been evaluated. They all have in common the single carbon bridge of phenstatin with the conformational stability provided by a central 6 or 7 membered ring.

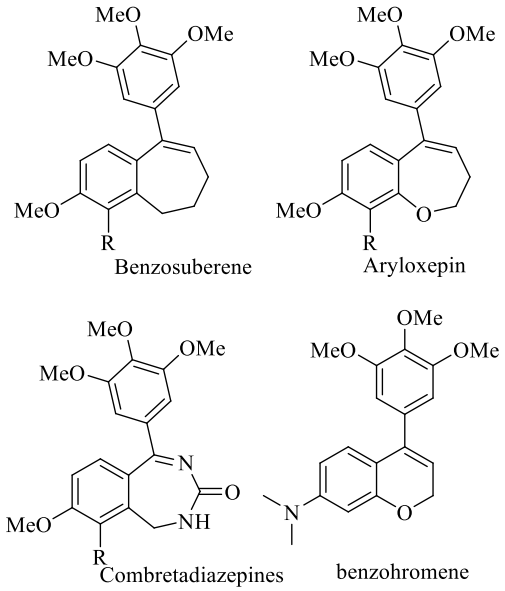

Figure 28 The structure of 4 benzosuberene type analogues

A series of potent suberene type combretastatin like analogues have been reported to show excellent inhibitory activity against cancer cell lines (Tanpure *et al*. 2013)**.** The group made a series of analogues varying the pattern of methoxy groups and functional groups (**Fig 28)**. Impressive IC_{50} values in the picomolar range were reported along with synthesis of water soluble prodrugs.Further analysis of the benzosuberene type fused ring system was reported in the synthesis of a series of combretadiazepine compounds. The series featured a 1,4-benzodiazepin-2-one fused ring system, a so called privileged structure that improves

conformational stability by locking in the Z-conformation of CA-4. The compounds show a similar biological profile to CA-4 in tubulin binding and cytotoxicity (neuroblastoma cells) with an improved pharmacokinetic profile (Galli *et al*. 2015)**.**

Project aims

The aim of this project was to further develop oxepine analgues as potential antivascular agents. Building on previous investigations (Edwards *et al*. 2011; Gaukroger *et al*. 2003b; McGown & Fox 1989) into tubulin binding, a series of dibenzoxepines was synthesised and biologically evaluated.

Design rationale

In the area of colchicine binding vascular targeting agents hundreds if not thousands of compounds have been investigated over the past 20 years. Dichotomising compounds further into combretastatin or colchicine type structures can be difficult due to the massive structural diversity of studied molecules.

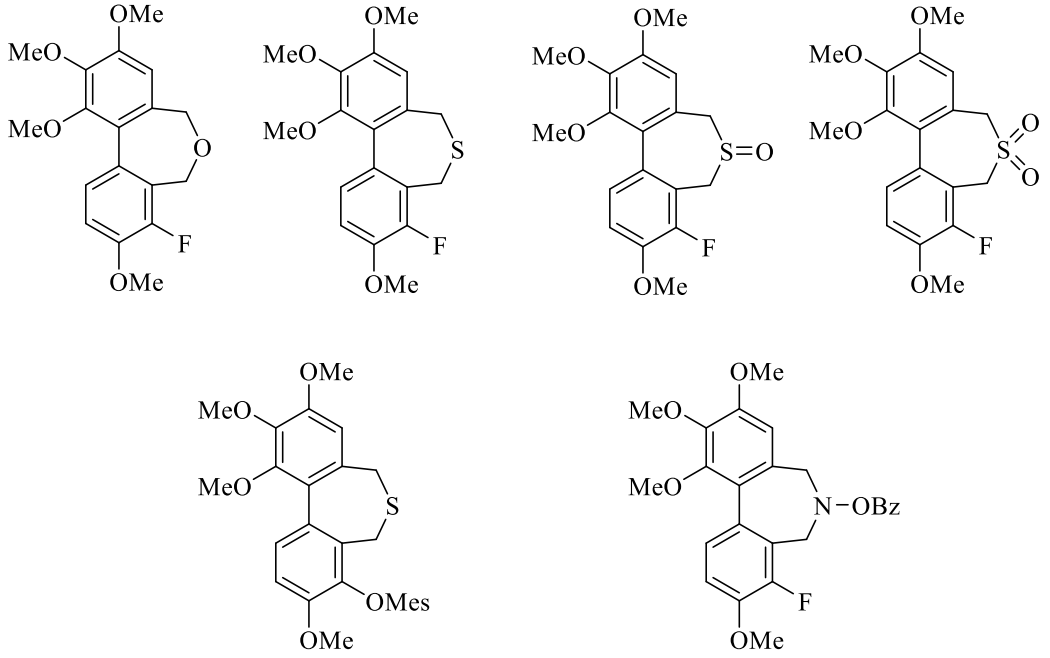

Figure 29 Diagram showing the target oxepine compounds

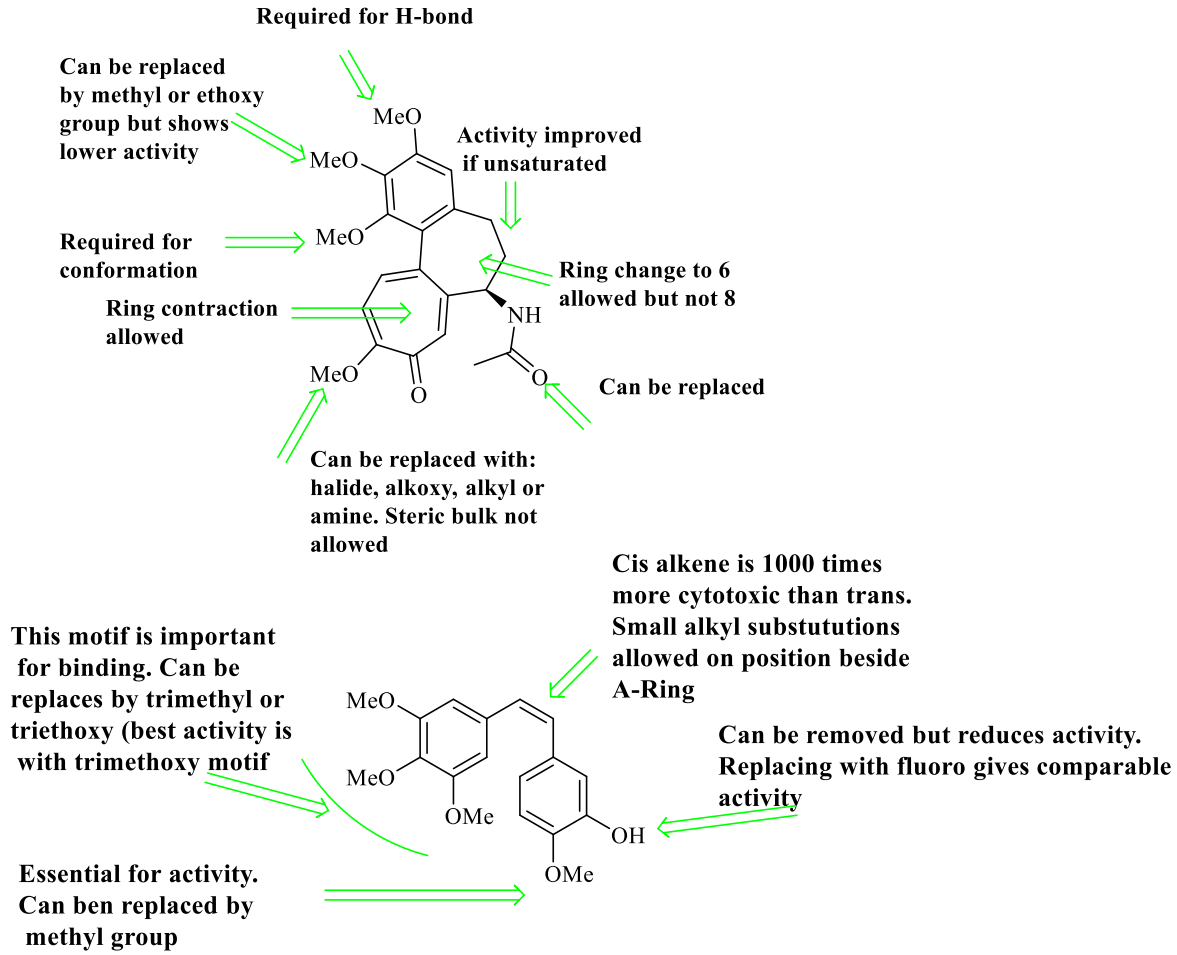

Figure 30a Diagram showing a structure activity relationship analysis on colchicine

One constant in the criteria for activity in the colchicine binding site is the presence of the trimethoxy motif will feature in all compounds.

SAR analysis of both compounds (**Fig 30a**) shows the importance of the trimethoxy moiety. What is unusual is the variation in location of the motif **(Fig 31)**. In NAC **(29)** the pattern is 2,3,4 on the A ring but in both Phenstatin **(27)** and combretastatin derivatives the pattern is 3,4,5, even though the distance between the main rings are different (**Fig 31** red lines).

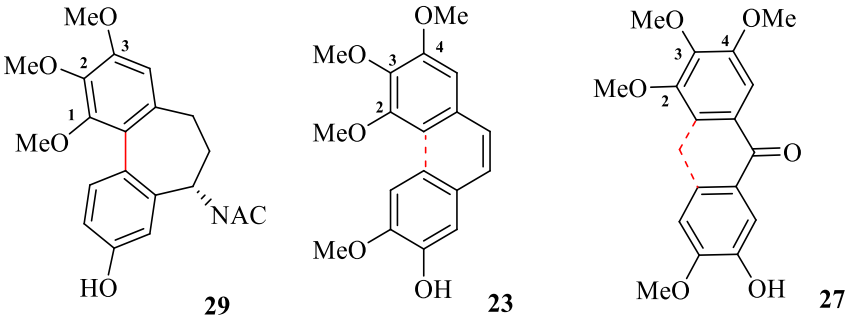

Figure 30b Diagram showing the relationship between NAC (29), CA-4 (23) and Phenstatin (27)

Analogues with an altered seven-membered rings containing sulphur and nitrogen were synthesised. The conformation of the synthesised oxepine analogues changes the angle between the two aryl rings and alters the interaction of the molecules with tubulin.

McNulty (McNulty *et al*. 2015) recently reported low µM activity from a simplified NAC/Combretastatin hybrid (**31**) with a similar methoxy substitution to the Edwards (Edwards *et al*. 2011) oxepine analogues and CA-4 **(Fig 32).**

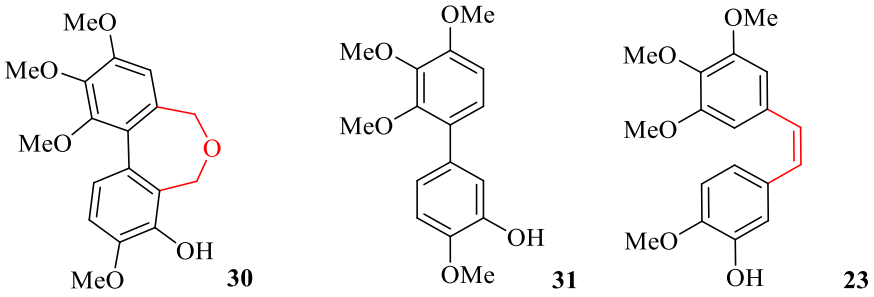

Figure 31 Diagram showing the similarities between Edwards Oxepine (30), Mc Nulty's NAC/ Combretastatin hybrid (31) and CA-4 (23)

A simplified series of biaryls without a central heterocyclic ring have also be synthesized and tested. These molecules will be analogous to dibenzoxepines, they will be tested to further explore the colchicine pharmacophore.

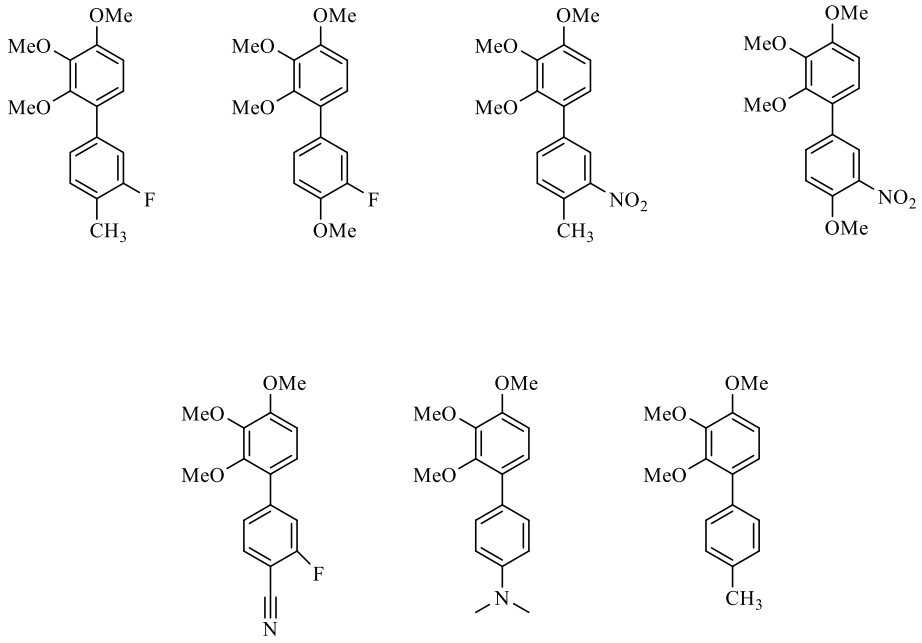

Figure 32 Diagram showing the target biaryl compounds

Chapter 2: Development of a route to the desired analogues

Introduction

The central theme for this chapter is carbon- carbon cross coupling. In a coupling reaction two molecular fragments are combined leading to the formation of a new bond. This process is often catalyzed by a transition metal (Pd, Cu, Ni). The explosion of research in this area since the 1970s has generated powerful, practical and robust methodologies that have been recognised with a Nobel prize and feature as a valuable tool throughout research from academia to industry. Previous work on dibenzo[c,e]oxepine compounds **(30)** by Edwards (Edwards *et al*. 2011) utilized Ullmann coupling to synthesise a series of compounds similar to our target molecules. Ullmann coupling is one of the earliest examples of coupling and serves as a good example of homo coupling **(Fig 33)**, in which 2 equivalents of an aromatic halide **(32)** react to form a symmetrical or homocoupled product **(33)**.

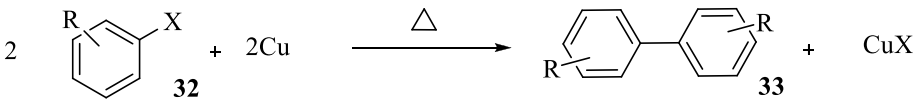

Scheme 32 shows a general reaction scheme for an Ullmann reaction involving the homocoupling of an aromatic halide in the presence of copper at high temperature to form a biaryl product.

The Ullmann reaction used by Edwards **(Fig 33)** shows that when 2 different aromatic halides (**34)** and **(35)** are used, a mixture of hetero and homo coupled products are produced. In this case the heterocoupled product (36) is the desired compound. Ullmann coupling is traditionally utilised in synthesis requiring symmetrical molecules as the major product is usually homocoupled.

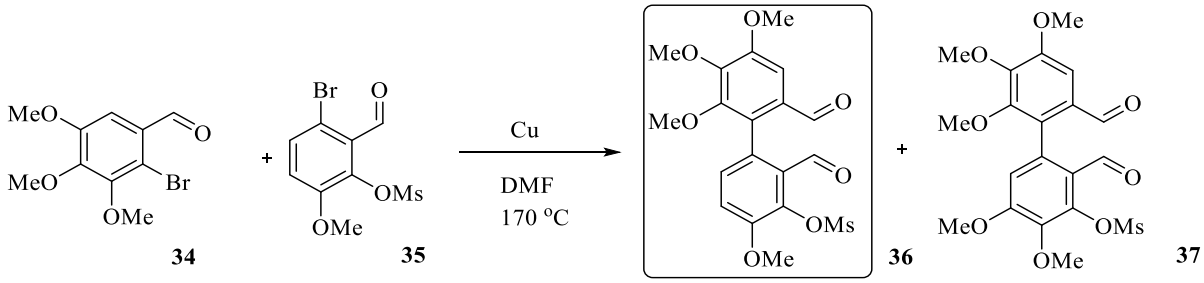

Scheme 33 Reaction scheme for an Ullmann reaction used by Edwards to form a central biaryl precursor (36) to a dibenzoxepines analogue

The mechanism for the Ullmann reaction has been has been well investigated in the literature but has yet to be fully elucidated. A thorough investigation by Paine (Paine 1987) involving several sources of copper revealed that a single copper ion (Cu(I)) species was the intermediate, ruling out the presence of a radical. The work also alluded to the large variability in yield suggesting that availability of surface copper ions and the ease at which they dissolve for homogenous catalysis was an important factor. Ullmann coupling is quite robust but lacks selectivity when cross coupling is required. In an attempt to remedy this, Ziegler (Ziegler *et al*. 1980) published a modified Ullmann procedure which has been shown to successfully cross couple sterically hindered aryl halides, including precursors for natural compounds with a similar trimethoxy motif **(Fig 35, (39))** (Stark *et al*. 2010), (Nelson & Meyers 1994). Encouragingly, this method has also been reported in the synthesis of NAC **(29)** (Broady *et al*. 2007).

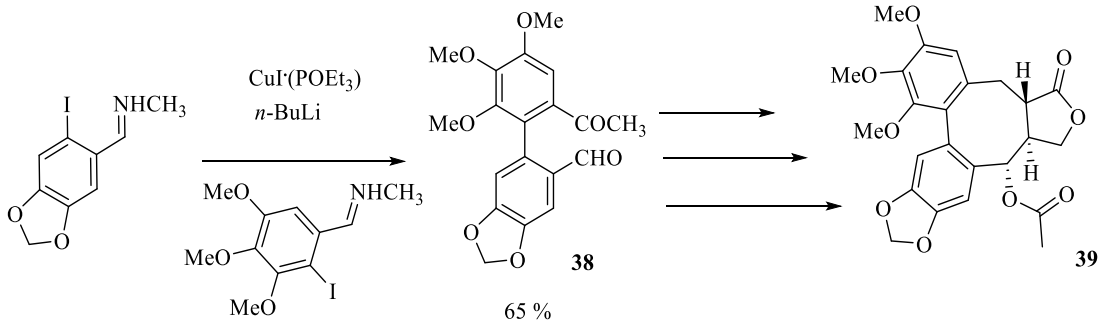

Scheme 34 Diagram showing the modified Ullmann coupling used by Ziegler to synthesise a central biaryl precursor in the synthesis of steganacin (39)

The Zeigler-Ullmann reaction works particularly well with electron rich aryl halides. The process requires the presence of directing groups (cyclohexylimine, acetal, thioacetal) groups in the position *ortho* to the halide group in each aryl coupling partner. This serves both to protect carbonyl groups from reaction with butyl lithium and to direct the oxidative insertion of copper. Ziegler proposed a mechanism **(Fig 36)** in which the electron rich ring is first lithiated **(40)** through halogen-lithium exchange and reacted with $CuI{\cdot}P(OEt)_3$ to form an organocuprate compound **(41)**, aided by the coordination effect of the nitrogen. Addition of the coupling partner **(42)** results in an oxidative addition at the copper resulting in an increase in formal oxidation state from (I) to (III) **(43 to 44)**, coordination by nitrogen ligands followed by reductive elimination to give biaryl **(45)**.

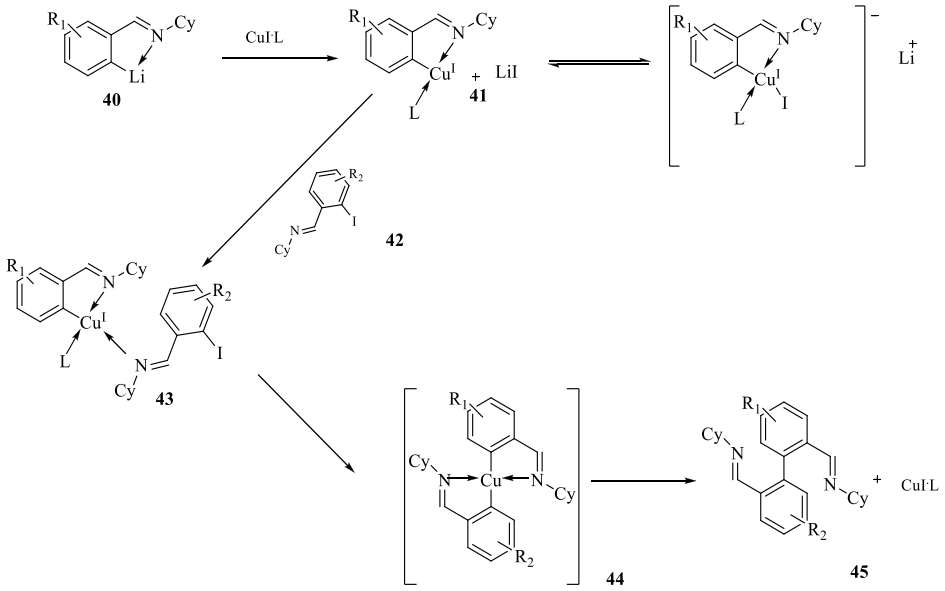

Scheme 35 Reaction scheme showing the proposed mechanism for the modified Ziegler cross coupling reaction

Palladium-catalysed cross- coupling

An obvious starting point for this was palladium catalysed cross-coupling. Since its discovery in the late 1970's (Miyaura *et al*. 1979), Suzuki–Miyaura cross-coupling has become a widely used carbon-carbon bond forming reaction. This involves the palladium catalysed coupling of an aryl/alkyl halide with an aryl/alkyl boronic acid. Numerous examples and reviews have been published reporting high yields and excellent functional group tolerance along with an ever growing selection of ligand / catalyst systems.

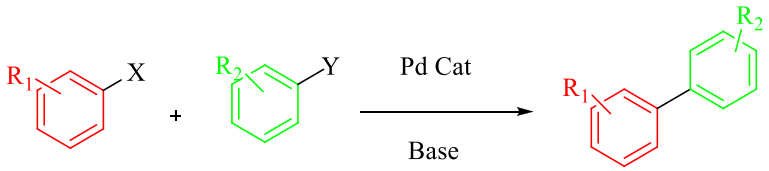

Reaction	X	Y	Reference
Kumada	I, Br,	MgX	(Tamao, Sumitani, & Kumada, 1972)
Negishi	I, Br,	ZnX	(King, Okukado, & Negishi, 1977)
Stille	I, Br, Triflate	$Sn(Alkyl)_3$	(Stille & Lau, 1977)
Suzuki	I, Br, Triflate	$B(OH)_2$, BF_3K, BPIN	(Miyaura, Yamada, & Suzuki, 1979)
Hiyama	I, Br, Triflate	$Si(OMe)_3$	(Hatanaka & Hiyama, 1988)

Figure 36 Scheme showing a general palladium catalysed cross coupling reaction between an aryl halide and a partner xdnucleophile to generate a biaryl, the table indicated the required X and Y group for commonly used name processes.

Fig 37 shows the most frequently used biaryl forming coupling reactions. The most commonly utilised reactions are Suzuki and Stille in which organic halides (or pseudo halides) are "coupled" with nucleophilic coupling partners (boronic acids and stannanes). **Fig 38** is focused on the state of palladium during carbon-carbon bond formation. The catalytic cycle is common to all C-C processes (Kumada, Negishi, and Hiyami etc) in which the halide undergoes an oxidative addition to form a $Pd^{(II)}$ species that transmetalates a coupling partner to remove the halide. This new $Pd^{(II)}$ species undergoes reductive elimination to form the coupled product and regenerate the $Pd^{(0)}$ catalyst for further cycles.

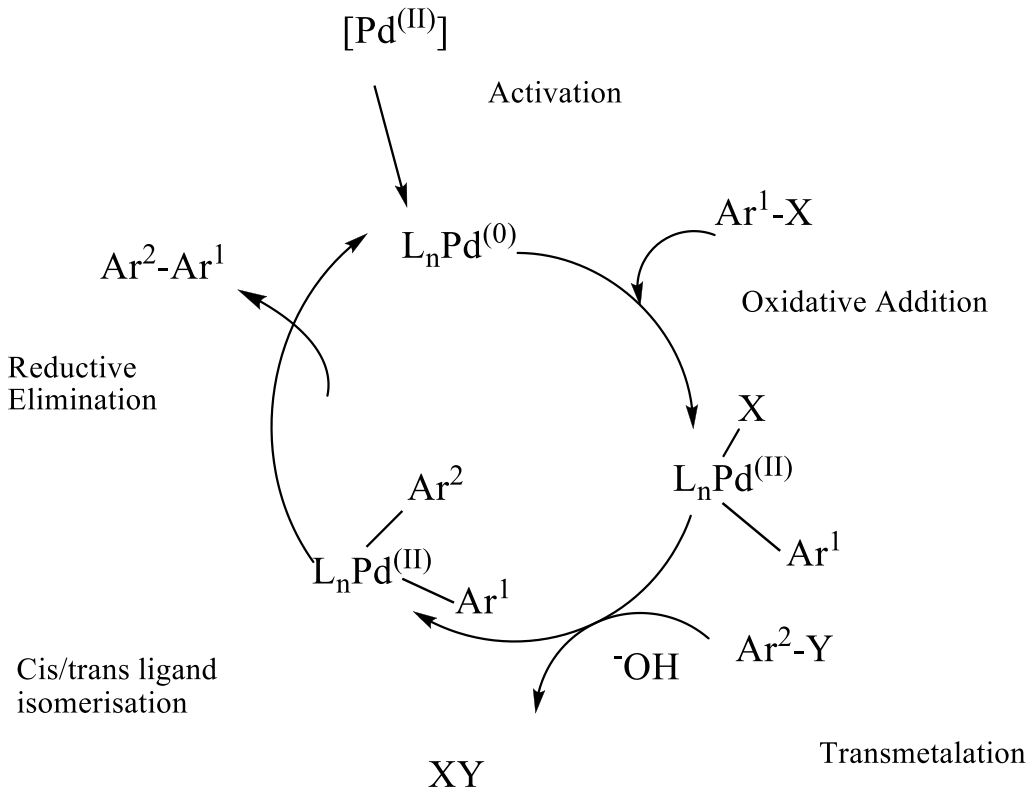

Figure 37 Shows the catalytic cycle for palladium during a Suzuki cross coupling reaction. X is a halide and Y is the nucleophilic coupling partner

The reaction mechanism for the catalytic cycle **(Fig 38)** is generally accepted and typically described around the oxidation state of palladium. This begins with the oxidative addition of the palladium catalyst to the alkyl/aryl halide forming an organopalladium complex. Palladium (0) is oxidized to Palladium (II) in the process resulting in the breaking of the carbon – halogen bond meaning that palladium is bound to both halide and ligand. This is the rate determining step for the reaction (Casado & Espinet 1998).

This is followed by a transmetallation step which involves the transfer of ligands from one organometallic species to another. This occurs during the reaction but the exact mechanism is uncertain and greatly disputed. The general consensus is that the alkyl/aryl component of the nucleophilic coupling partner is transferred to the palladium species and replaced with previously added base. Apart from Stille coupling, Pd catalysed C-C reaction doesn't occur in the absence of base and often 2-4 eq is required suggesting that the role of base is to both

activate the nucleophilic species and facilitate formation of the new palladium (II) species. (**Fig 39**) shows 2 proposed pathways (Path A and Path B) for transmetallation in Suzuki coupling (Matos and Soderquist. 1998). Both proposed pathways result in the same organopalladium transition state from which reductive elimination gives the desired carbon – carbon bond.

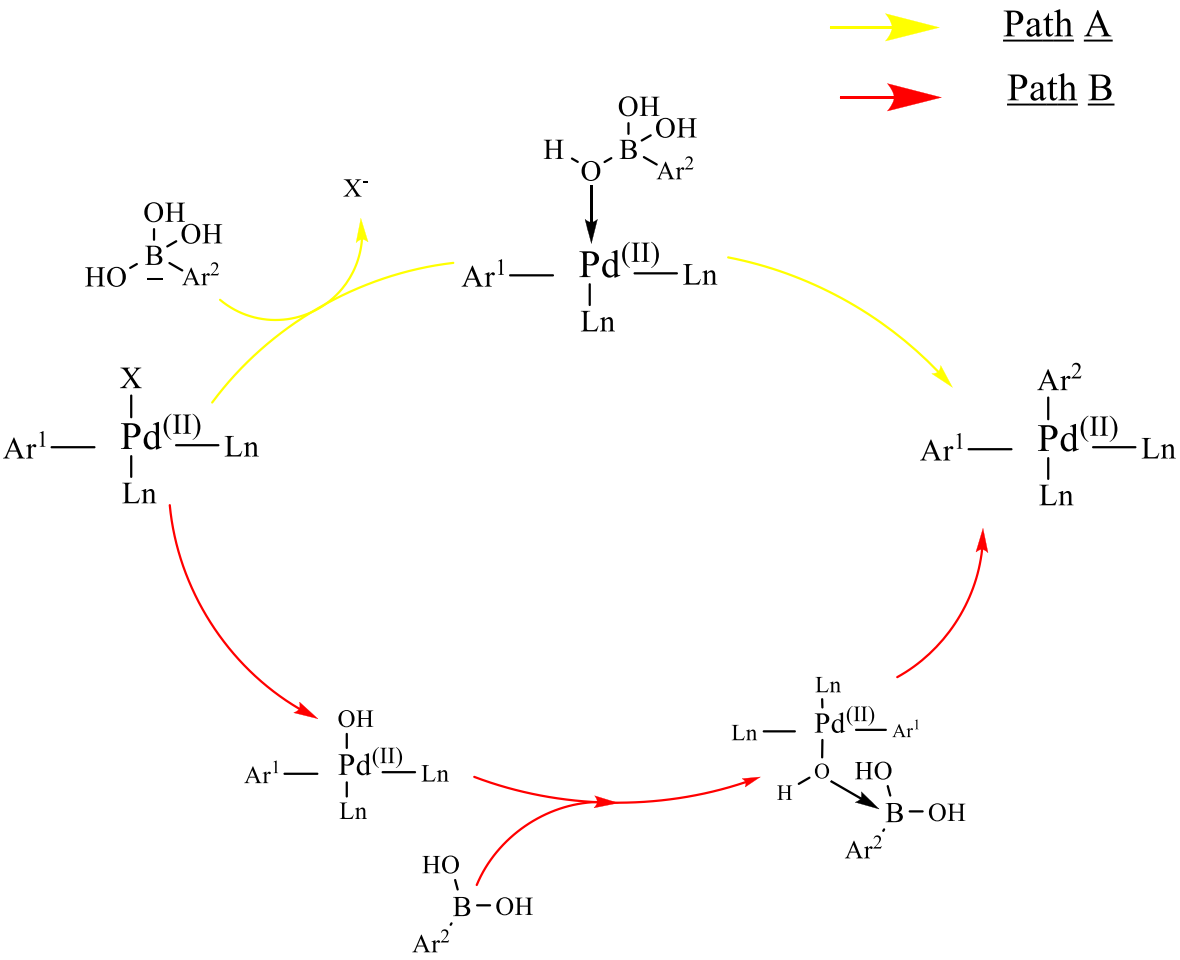

Figure 38 Shows two proposed actions of base in the transmetallation step in Suzuki cross coupling. Path A shows a hydroxylation of the boronic acid coupling partner and subsequent coordination of this molecule to the palladium centre. Path B shows the substitution of X on the initial oxidative addition product with OH which in turn reacts with the boron from the boronic acid.

Reductive elimination is in essence a reverse of oxidative addition, in which a bond is created between two metal (palladium) bound anionic ligands (Ar^1 and Ar^2 in **Fig 40**) causing a reduction in formal oxidation state of the metal by 2, in this case palladium (II) to palladium

(0) resulting in the reformation of the catalyst. In order for the biaryl product to be eliminated the Ar^1 and Ar^2 groups must both be coordinated *cis* to each other therefore *trans* coordinated complexes will isomerise to this preferred configuration. The tetravalent 16-electron palladium species generated by transmetallation eliminates from its square planar complex unassisted followed by formation of the Ar^1-Ar^2 sigma bond yielding the desired coupled product.

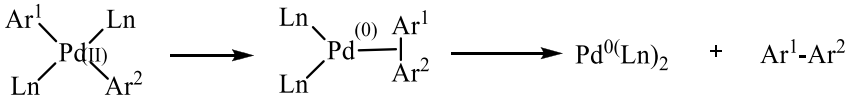

Scheme 39 Scheme showing the reductive elimination of a tetra-substituted Pd $^{(II)}$ intermediate to form a biaryl product and regenerate the Pd $^{(0)}$ catalyst.

It has been reported that some reactions can have a slow transmetallation step, in which case formation of a T- shaped 14- electron intermediate through the dissociation of a ligand can enhance the process **(Fig 41)**. It is believed that through a further rearrangement to a Y shaped species accelerated reductive elimination can occur (Espinet and Echavarren 2004). Addition of an extra ligand to this complex forms the common 18 electron species that allows elimination of the Ar^1-Ar^2 biaryl product.

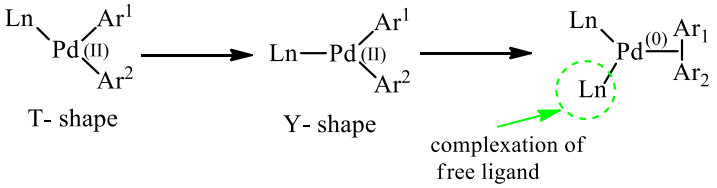

Scheme 40 Scheme showing the rearrangement of a Pd(II) intermediate from a T-shape to a Y-shape to allow the complexation of a free ligand to allow reductive elimination.

Pinacol boronate esters

The popularity of boronate esters in Suzuki coupling has increased dramatically over the past 10 years. Boronic acids can reversibly react with diols to form stable boronic esters that can release the active acid *in situ*. Boronic esters are more stable to air and chromatography, making them easier to store, purify and characterise than boronic acids. Another attractive feature is alternative routes of synthesis that avoid lithium- halogen exchange/ directed ortho metallation. These include Miyuara borylation (Ishiyama, Murata, & Miyaura, 1995), a palladium catalysed reaction with Bis(pinacolato)diboron (B_2Pin_2) and Musada borylation (Murata, Watanabe, & Masuda, 1997) that uses pinacol borane directly **(Fig 42)**

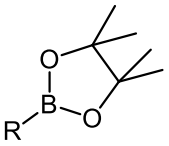

Boronate ester moiety

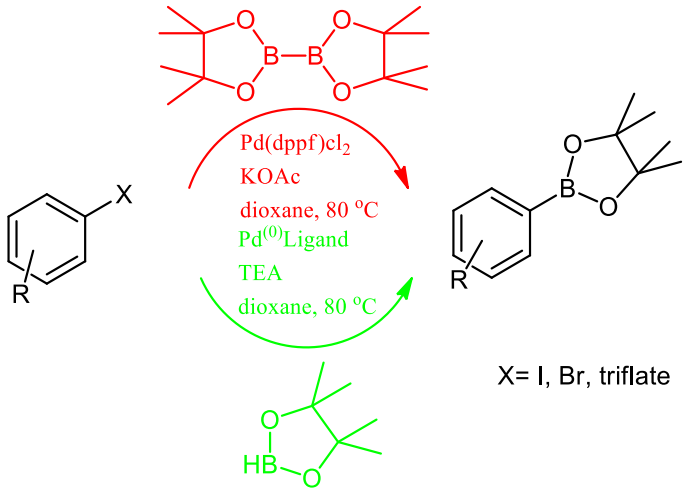

Scheme 41 Scheme showing 2 routes to boronate esters. Miyuara borylation (Red) uses B_2Pin_2 with the $Pd(dppf)Cl_2$. Masuda borylation (Green) utilises pinacol borane with various phosphine based ligands.

The mechanism for Masuda type borylation was much disputed until Lam (Lam *et al*. 2010), using Density Functional Theory (DFT), calculation elucidated the correct pathway.

Fig 43 shows that the oxidative insertion step remains the same for both mechanisms. Lam proved through calculation that the original idea that triethylamine deprotonates pinacol borane isn't possible due to the hydridic tendency of B-H bonds. Lam's transmetallation stage involves ionisation of the oxidative addition product to generate a 14 electron aryl palladium carbonation that subsequently reacts with pinacol borane through a sigma bond metathesis regenerating $Ln_2Pd(0)$ and forming the borylated aromatic product

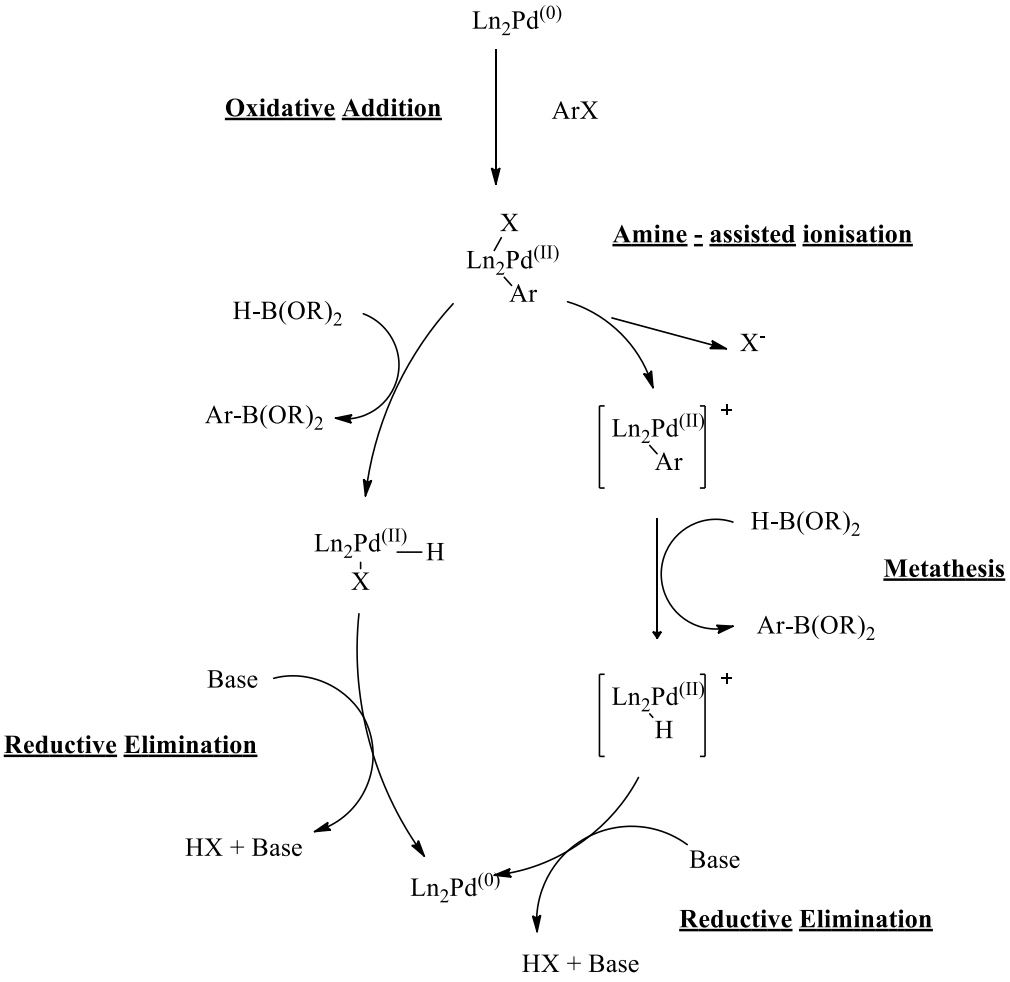

Scheme 42 Scheme showing both the original proposed Masuda mechanism (Left) and the correctly elucidated Lam mechanism (right), with a newly discovered Ionisation / metathesis process.

Buchwald ligands

Until the late 90s catalytic systems used for Suzuki type coupling featured predominantly triarylphosphine ligands. Around this time focus changed to more bulky, electron rich phosphine type ligands mostly created by Buchwald's group at MIT. These ligands can dramatically improve the selectivity and efficiency of C-C (Martin and Buchwald. 2007), (Denmark and Kallemeyn. 2006), C-N (Biscoe *et al*. 2007) and C-O (Anderson *et al*. 2006) coupling reactions

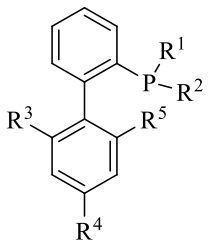

Ligand	R^1	R^2	R^3	R^4	R^5
MePhos	Cyclohexyl	Cyclohexyl	Me	H	H
DavePhos	Cyclohexyl	Cyclohexyl	$N(Me)_2$	H	H
CyJohnPhos	Cyclohexyl	Cyclohexyl	H	H	H
JohnPhos	*t*-Butyl	*t*-Butyl	H	H	H
SPhos	Cyclohexyl	Cyclohexyl	OMe	H	OMe
XPhos	Cyclohexyl	Cyclohexyl	O *i*-Pr	O *i*-Pr	O *i*-Pr
RuPhos	Cyclohexyl	Cyclohexyl	O *i*-Pr	H	O *i*-Pr

Table 43 Diagram showing the general structure of Buchwald ligands and a table showing the appropriate substitutions for each ligand.

These compounds **(Fig 44)** are easily prepared in a one-pot procedure involving the addition of an aromatic Grignard reagent to a benzyne intermediate (generated *in situ*) and the subsequent intermediate is trapped with a substituted chlorophosphine on a 10 kg scale **(Fig 45)** (Kaye *et al*. 2001).

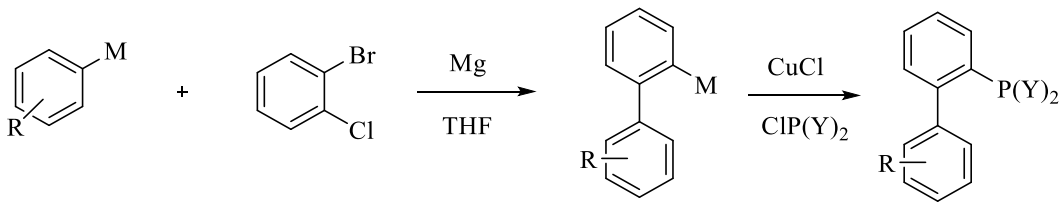

R = alkyl, aryl substitiutions
M = Li , MgX
Y = alkyl, aryl substitiutions

Scheme 44 Scheme showing the general method used for synthesizing Buchwald ligands.

The popularity of these ligands can be attributed to the fact that they are: air stable, crystalline solids, thermally stable, operationally simple to use and commercially available. **Fig 46** summarizes the role of the structural features of this ligand series.

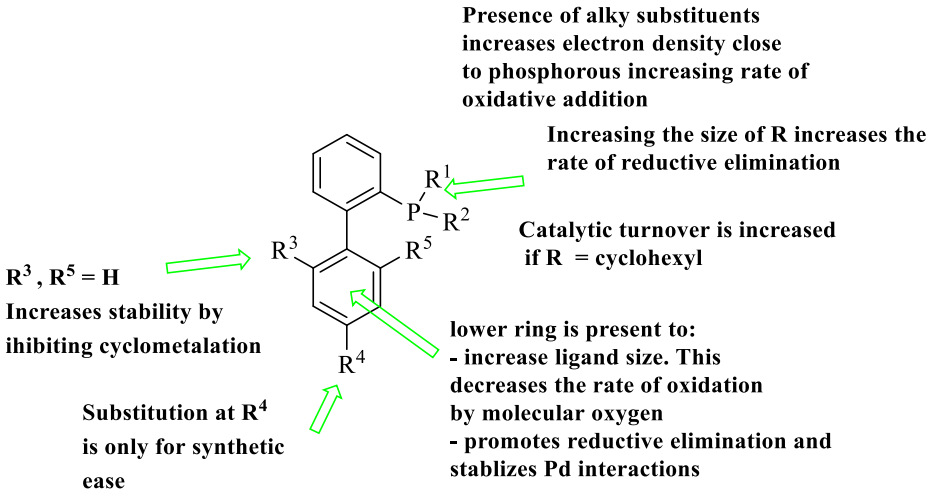

Figure 45 General diagram showing the function of each substituent and the effect than changing these groups has.

The combination of steric and electronic properties can be fine tuned to enhance the rates at each step of the catalytic cycle giving the catalytic species formed their excellent activities.

With specific reference to sterically hindered biaryls, Wolfe (Wolfe *et al.* 1999) reported success in the synthesis of tri-ortho substituted biaryls using both DavePhos and CyJohnPhos catalysed Suzuki reactions in excellent yields.

Bauduoin's (Joncour *et al*. 2006) group has developed Suzuki conditions for the synthesis of tri-ortho substituted biaryl molecules that are structural hybrids of NAC / Steganacin featuring the desired trimethoxy A ring motif (**Fig 47**). The group screened a series of ligands and bases, determining that either S-Phos or DavePhos in combination with barium hydroxide worked best in dioxane at 100 ^{o}C in moderate yield (55%). This catalytic system was also reported for the synthesis of a biaryl precursor (**48)** to steganacin (Baudoin *et al*. 2003) from an aryl halide **(46)** and protected trimethoxy aromatic boronate ester **(47)**

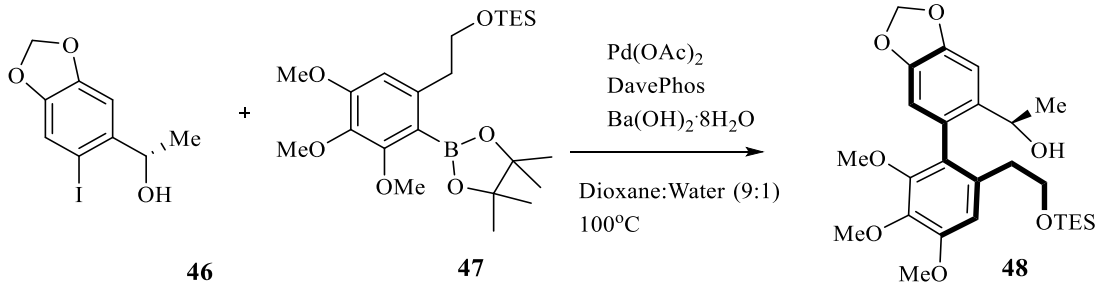

Scheme 46 Scheme showing the Pd/ Phosphine catalysed coupling reaction utilised in Baudoin's synthesis of Steganacin.

***N*-Heterocyclic carbenes (NHC)**

A carbene is a compound of neutral charge that contains a divalent carbon with a 6 electron valence shell. Typically the lack of a full electron octet makes free carbenes unstable and until the late 1980s they were viewed as reaction intermediates unable to be isolated. This changed with the seminal work by Bertrand (Igau *et al*. 1988) who published the first isolatable carbene (**Fig 48, (49)**), stabilised by adjacent silicon and phosphorus atoms.

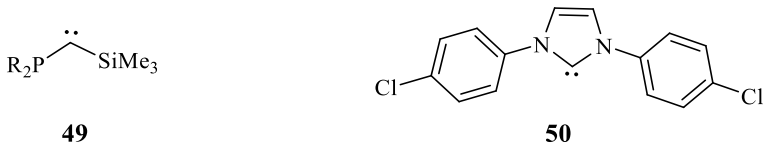

Figure 47 scheme showing both Bertrand's (49) and Arduengo's (50) carbenes.

Following this Arduengo (Arduengo *et al*. 1991) reported the first nitrogen heterocycle carbene **(50)**. This compound was easily prepared and isolated This discovery started a rapid growth in the area of carbene metal complexation resulting in vast libraries of NHC compounds that proved excellent ligands for transition metal catalysis.

There has been a rapid growth in the use of N-heterocyclic carbenes (NHC) as ancillary ligands in transition metal catalysis. In particular, in the area of palladium catalysed coupling reactions as an alternative for phosphine ligands. Reasons for this include a more facile, less expensive synthesis that doesn't require air free preparation and produces non-toxic by-products. Phosphine ligands can also suffer from degradation of the P-C bond at higher temperatures resulting in catalytic deactivation.

These nucleophilic NHCs are neutral ligands that can donate 2 electrons without π – back bonding making them more effective donors than bulky phosphine groups meaning that they are more stable from ligand dissociation from the palladium centre (Huang *et al*. 1999).

The use of NHCs as ligands for Suzuki type cross coupling has been reported (Huang *et al*. 1999), (Organ *et al*. 2009). Ozdemir reported high yields and substrate versatility from a series of tetrahydropyrimidinium NHCs for both Suzuki cross coupling and direct arylation of benzaldehydes (Ozdemir *et al*. 2005a). The group chose 6 membered rings over 5-membered ring geometry as they have a stronger *ortho* donating capability.

Discussion of results

Previous work on dibenzo[c,e]oxepine compounds by Edwards (Edwards *et al*. 2011) utilized Ullmann coupling to synthesise (**Fig 49)** a series of compounds similar to our target molecules. This method was initially used to synthesise the central biaryl precursor **(56)** for a series of fluoro dibenzo[c,e]oxepine derivatives.

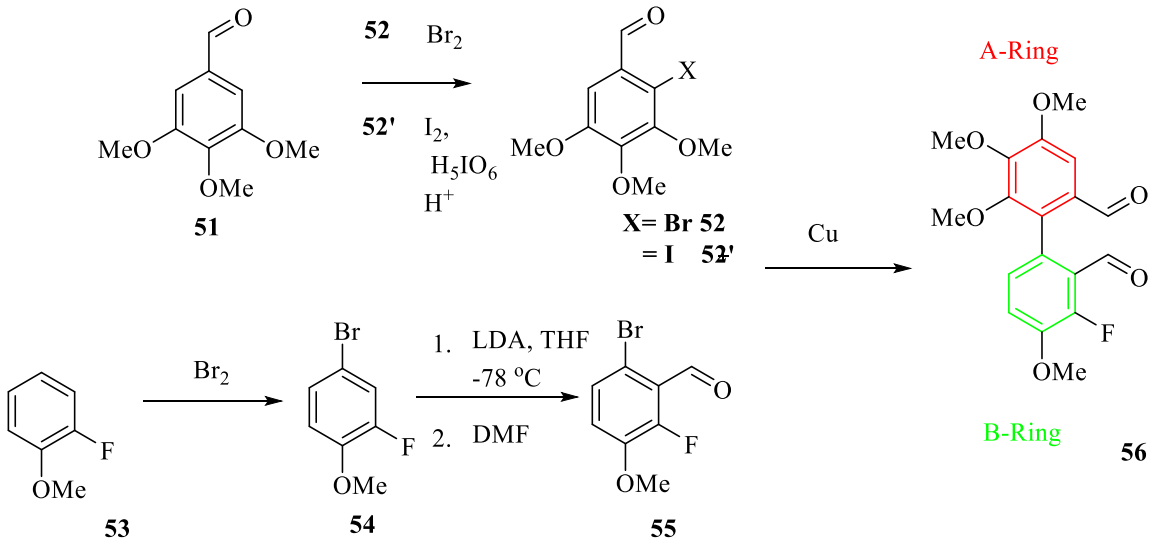

Scheme 48 Reaction scheme showing the synthesis of precursor (56) via Ullmann coupling and preparation of two brominated benzaldehydes (52 and 55) from commercially available starting material

The A ring coupling partner 2-bromo 3,4,5-trimethoxybenzaldehyde **(52)** was prepared in good yield (68%) by the dropwise addition of bromine to 3,4,5-trimethoxybenzaldehyde **(51)** in chloroform. **(52')** was also made from **(51)** via periodic acid catalysed iodination (83%). Synthesis of the B ring coupling partner, 6-bromo 2-fluoro 3-methoxybenzaldehyde **(55)** was produced in 2 steps from 2-fluoroanisole **(53)**. Bromination of 2-fluoroanisole generated **(54)** (84.3%). Formylation of this compound proceeded in moderate yield (57%) via directed ortho metallation of the 2 position by the fluoro group.

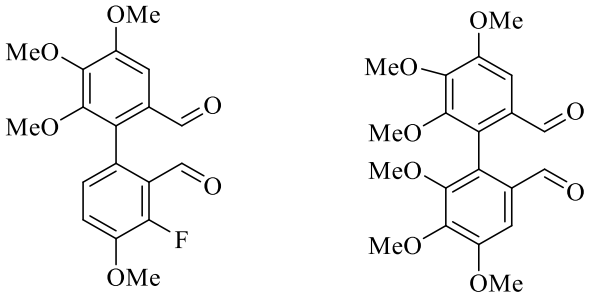

56 **57**

Figure 49 Diagram showing both hetero (56) and homo (57) coupled products from the Ullmann reaction.

The Ullmann coupling was attempted using conditions suggested by Edwards (Edwards *et al*. 2011) giving the desired heterocoupled dialdehyde compound **(56**) in poor yield (22%) along with a mixture of homocoupled **(57)** product (55%) and 3,4,5-trimethoxybenzaldehyde **(51)**. Overall the reaction required 3 eq of 2-bromo 3,4,5-trimethoxybenzaldehyde **(52)** starting material and 10 eq of copper. Changing the coupling partner from bromide to the more reactive 2-iodo 3,4,5-trimethoxybenzaldehyde (**56)** had negligible effect on the reaction outcome.

Ziegler-Ullmann coupling was utilized in an attempt to improve the yield of the desired biaryl **(56).** Both aldehyde coupling partners **(52', 55)** required protection in the form of benzylimine groups. The imine moieties also function as directing groups for Ziegler coupling.

Preparation of the imines **(58, 59)** was achieved in two easy steps from the aryl halides **(52' and 55)**. The conversion of the 2-iodo 3,4,5-trimethoxybenzaldehyde **(52')** to the imine **(59)** was achieved in quantitative yield by reaction of benzaldehyde **(52')** with benzylamine and *para*-toluenesulfonic acid under Dean Stark conditions. Formation of the (E)-N-(6-bromo 2-fluoro 3-methoxybenzylidene) cyclohexylimine **(58)** was first attempted using this method with poor results (17% yield). The reaction was tried at room temperature in methanol and gave a significant increase in yield **(**67%**).** Synthesis of the cuprous iodotriethyl phosphite

complex $CuI{\cdot}P(OEt)_3$ was achieved in one step in good yield (67%) from the reaction of cuprous iodide and triethyl phophite. Lithiation of (*E*)-*N*-(6-bromo 2-fluoro 3-methoxybenzylidene)cyclohexylimine was followed by transmetallation with $CuI{\cdot}P(OEt)_3$ and addition of (*Z*)-*N*-(2-iodo 3,4,5-trimethoxybenzylidene)cyclohexylamine. Treatment with with acid removed the cyclohexylimine groups to afford the desired dialdehyde (**56**) in moderate yield (50%)

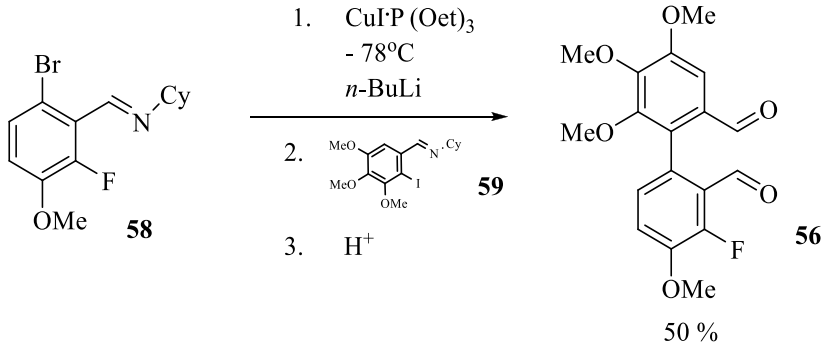

Scheme 50 Scheme showing the Ziegler modified Ullmann coupling of cyclohexylimine functionalised aromatic halides to for a central precursor for oxepine analogues

The Zeigler-Ullmann coupling gave the highest overall yield for the formation of the biaryl dialdehyde (**56**). The work up and purification was much more simple compared to the Ullmann reaction and gave an improved yield of the desired product and reduced yield of homocoupled product.

A limitation to Ullmann Ziegler coupling is the requirement of 1 directing auxiliary in the ortho position to the halide on each coupling partner. Various alternatives to cyclohexylimine have been reported including diethylamine, oxazoline, acetals (Broady *et al*. 2007) and thioacetal but all ultimately are removed to give an ortho benzylic carbonyl (aldehyde or ketone) on each ring. This is unsuitable for the synthesis of biaryl[b,d]oxepines for which alternative routes were investigated.

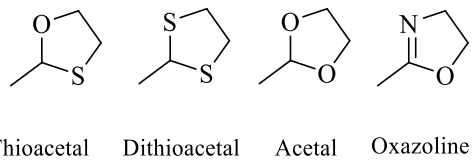

Figure 51 scheme showing a series of 5 membered hetero cyclic protection direction groups for Ziegler coupling

Previous work on these compounds has focused on disconnecting these structures either at the biaryl bond (Oxidative coupling (Sawyer and Macdonald. 1988), Stille/Peir coupling (Edwards *et al*. 2011) or the central ring tether (Aldol reaction (Besong *et al*. 2008)).

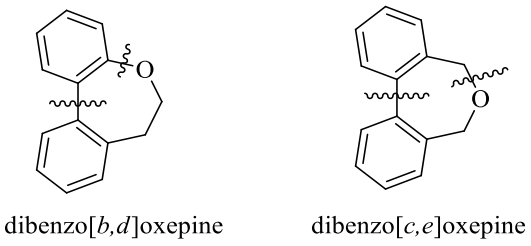

Figure 52 Diagram showing the pints of disconnection investigated for both [*b,d*] and [*c,e*] oxepines

Initial investigations focused on disconnecting at the heteroatom-containing tether first with the rationale that a universal method for both [*b,d*] and [*c,e*] oxepines could be established that involved shared biaryl precursors to improve efficiency (**Fig 53**).

An obvious starting point for this was palladium catalysed cross-coupling, Suzuki –Miyaura cross-coupling (Miyaura *et al*. 1979) was choosen due to its robustness and high functional group tolerance. This involves the palladium catalysed coupling of an aryl/alkyl halide with an aryl/alkyl boronic acid. Numerous examples and reviews have been published reporting high yields and excellent functional group tolerance along with an ever growing selection of ligand / catalyst systems.

Results: Synthesis of coupling precursors

The Suzuki coupling was the obvious choice as its use has been widely reported for biaryl coupling (Heravi and Hashemi. 2012), (Wójtowicz-Rajchel and Koroniak. 2012). Acetal protection of the aldehyde (**52)** giving (**60**) required was required before formation of the boronic acid **(61)** was attempted (**Fig 54**). This was attempted with both the classical ethylene glycol, Dean Stark method and a recent method using triethyl orthoformate (Molander and Ellis. 2007).

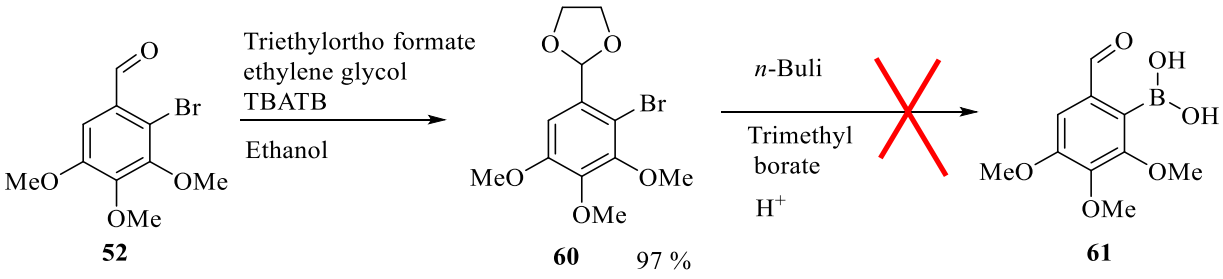

Scheme 53 Reaction scheme showing an acetal protection of an aldehyde followed by a failed attempt at synthesising a boronic acid through lithium halogen exchange followed by electrophile quench (trimethly boronate ester)

As the trimethoxy motif is common to all of the desired analogues 6-formyl-2,3,4-trimethoxyphenylboronic acid **(61)** was chosen as a starting point for synthesis of a common precursor. Synthesis of this has already been described in the literature (Besong *et al*. 2008) in two steps from 3,4,5-Trimethoxybenzaldehyde as a precursor to (–)-N-acetylcolchinol **(29)**. The 3,4,5-Trimethoxybenzaldehyde **(51)** was brominated in the 2-position and the aldehyde subsequently protected as a 1,3 acetal. Attempted boronic acid formation via lithium halogen exchange **(Fig 55)** followed by acetal deprotection failed to afford the desired product. The reaction was also attempted with fresh *t*-BuLi, distilled trimethylborate ester and increased equivalency of *t*-BuLi but to no avail. Increasing lithiation time and temperature (-40 ^{o}C) had no effect as did the addition of the lithiation promoting agent TMEDA. The reaction was attempted in diethyl ether and TBDME All of the mentioned methods produced only 3,4,5-trimethoxybenzaldehyde **(51)**. This indicated that the lithiated

species was being formed and protonated or the boronic acid was forming and protodeborating. With this in mind, the reaction was attempted again with the solution of the electrophile in THF added dropwise for a slower addition, this again only produced the 3,4,5-trimethoxybenzaldehyde **(51)** starting material. Different electrophiles were also employed via canula addition (tri-n-butylborate and tri-isopropyl borate) with no success.

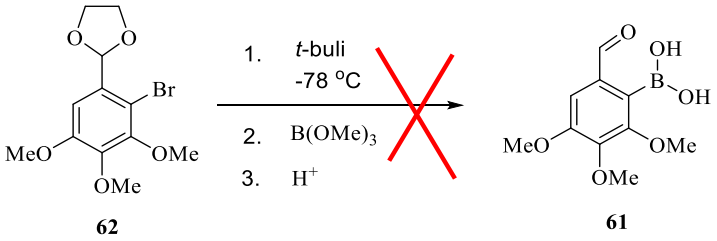

Scheme 54 Scheme showing the attempted formation of a boronic acid through lithium halogen exchange.

Attempted Stille coupling

Besong (Besong *et al*. 2008) also reported the synthesis of 3,4,5-trimethoxy-2-(tributylstannyl)benzaldehyde (**63**) for use in Stille coupling, again using lithium-halogen exchange but quenching the organolithium with tributyltin chloride (**Fig 56)**. However, in our hands this only produced dehalogenated product **(51)**. Labruére reported the palladium catalysed direct stannylation of 2-bromo 3,4,5-trimethoxybenzaldehyde (**52)** using $Pd(PPh_3)_4$ with hexa-n-butylditin in refluxing toluene (Labruére *et al*. 2012) This was attempted, successfully affording the desired stannane **(63)** in high yield (72%).

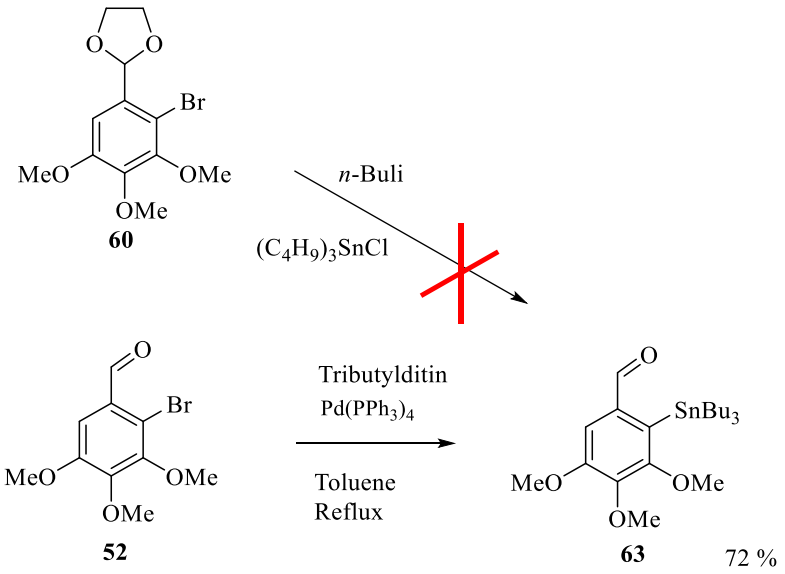

Scheme 55 Reaction scheme showing the successful Pd catalysed stannylation of (52) to generate the desired stannane (63)

Attempts to form biaryl (**96**) using the method described by Besong did not work in our hands giving less than 10% yield of desired biaryl. **Fig 57** summarises the unsuccessful efforts to optimise the cross coupling of the stannane with 6-bromo 2-fluoro 3-methoxybenzaldehyde **(53)** by trialling different catalysts and conditions.

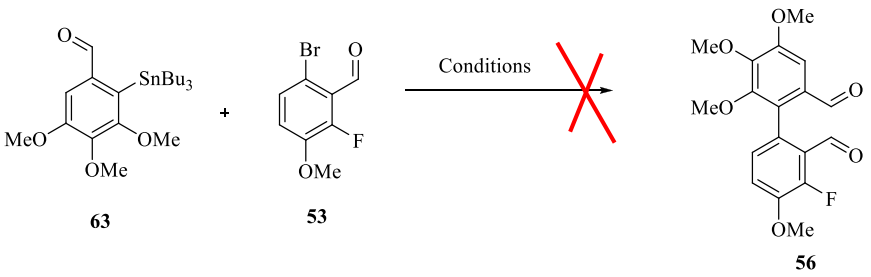

Pd Catalyst	Ligand	Additive 1	Additive 2	Solvent	Temp (^{o}C)	Yield (%)
$Pd(PPh_3)_4$		CuI		DMA	50	-
		CuI	CsF	DMF	100	-
	PPh_3	CuI	CsF	DMF	100	< 10
	PPh_3	CuI	CsF	DMF	120	-
$Pd(dba)_2$		CuI		Dioxane	80	-
		CuI		Dioxane	80	-
$PdCl_2$	P-*t*Bu_3	CuI	CsF	DMA	50	-
	P-*t*Bu_3	CuI	CsF	DMF	50	-
	P-*t*Bu_3	CuI	CsF	DMF	80	< 10
	P-*t*Bu_3	CuI	CsF	DMF	100	-
$Pd(OAc)_2$	DABCO		KF	Dioxane	80	-
	DABCO		KF	Dioxane	100	-

Table 56 Reaction scheme showing the attempted synthesis of dialdehyde **(56)** via Stille coupling and a table summarising the various catalytic systems, bases and conditions trialled.

Baudoin (Baudoin *et al*. 2002) developed a Musada type borylation of this type of electron rich aromatic ring. This method was used to synthesise two trimethoxybenzyl alcohol derivatives with different hydroxyl protecting groups to further investigate Suzuki coupling.

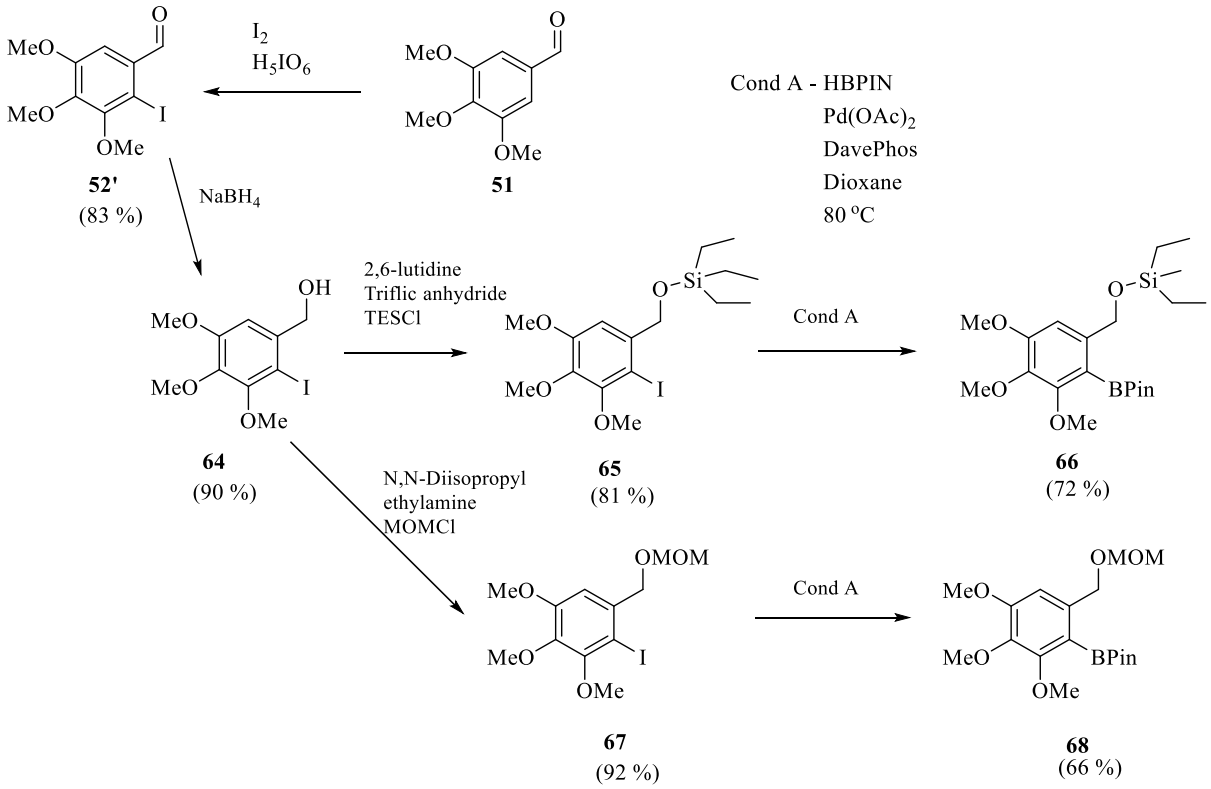

Scheme 57 Scheme showing the synthesis of both silyl and MOM protected benzyl coupling partners for Suzuki coupling.

Iodination of 3,4,5-trimethoxybenzaldehyde **(51)** occurred in excellent yield (83%) using iodine and periodic acid to give **(52').** Reduction with sodium borohydride in methanol afforded the benzyl alcohol **(64)** in excellent yield (90%). Triethylsilyl **(65)** and methoxyl methyl **(67)** protection groups were added in excellent yield (81% and 92% respectively) through base catalysed S_N2 reaction with TES triflate and methoxymethyl chloride respectively. Subsequent borylation of the protected iodides occurred in good yield giving TES **(66)** and MOM **(68)** protected pinacol boranes (72% and 66% respectively).

Results: Attempted Suzuki coupling

Suzuki coupling was attempted on both MOM and TES protected borylated A ring precursor with benzaldehyde **70**, **Fig 59** summarises the conditions used and the halide coupling partner trialled. Overall the only suggestion of formation of **(71)** occurred when the reaction of (**68**) was carried out in refluxing toluene. Adding more catalyst did not improve the yield, changing solvent to DMF and increasing reaction temperature to 150 ^{o}C also resulted in no reaction

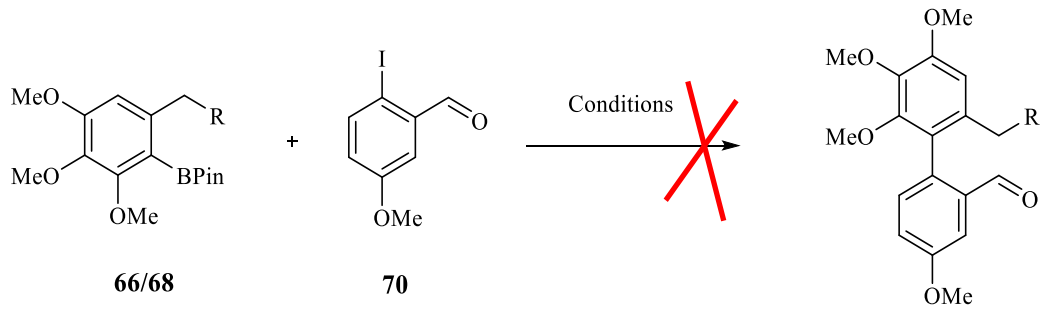

66/68 **70** **71**

.

Pd Catalyst	catalyst	Additive	Solvent	Temp (^{o}C)	Yield (%)
(**68**)	$Pd(PPh_3)_4$		EtOH	80	-
(**68**)		LiCl	EtOH	80	-
(**68**)		LiCl	DME	80	-
(**68**)		LiCl	Toluene	120	< 10
(**68**)			DMF	150	-
(**66**)	$Pd(dba)_2$		EtOH	80	-
(**66**)		LiCl	EtOH	80	-
(**66**)		LiCl	DME	80	-
(**66**)		LiCl	Toluene	120	-
(**66**)		LiCl	DMF	150	-

Table 58 Scheme showing the attempted palladium catalysed Suzuki coupling of a trisubstituted biaryl and a table showing the reagents and conditions trialled

Results: Attempted phosphine catalysed Suzuki reaction

Direct reduction of the commercially available 3,4,5-trimethoxyphenylacetic acid **(72)** with $LiAlH_4$ was low yielding (30%) but conversion of the acid to methyl ester **(73)** was high yielding (79%). Reduction to the alcohol **(74)** was acheived in good yield (75%). This compound was iodinated **(75)** in good yield (74%). Both Methoxyl methyl **(76)** and triethylsilyl (TES) **(78)** protection groups were added in excellent yield through base assisted S_N2 reaction with TES triflate and methoxymethyl chloride (90% and 87% respectively).

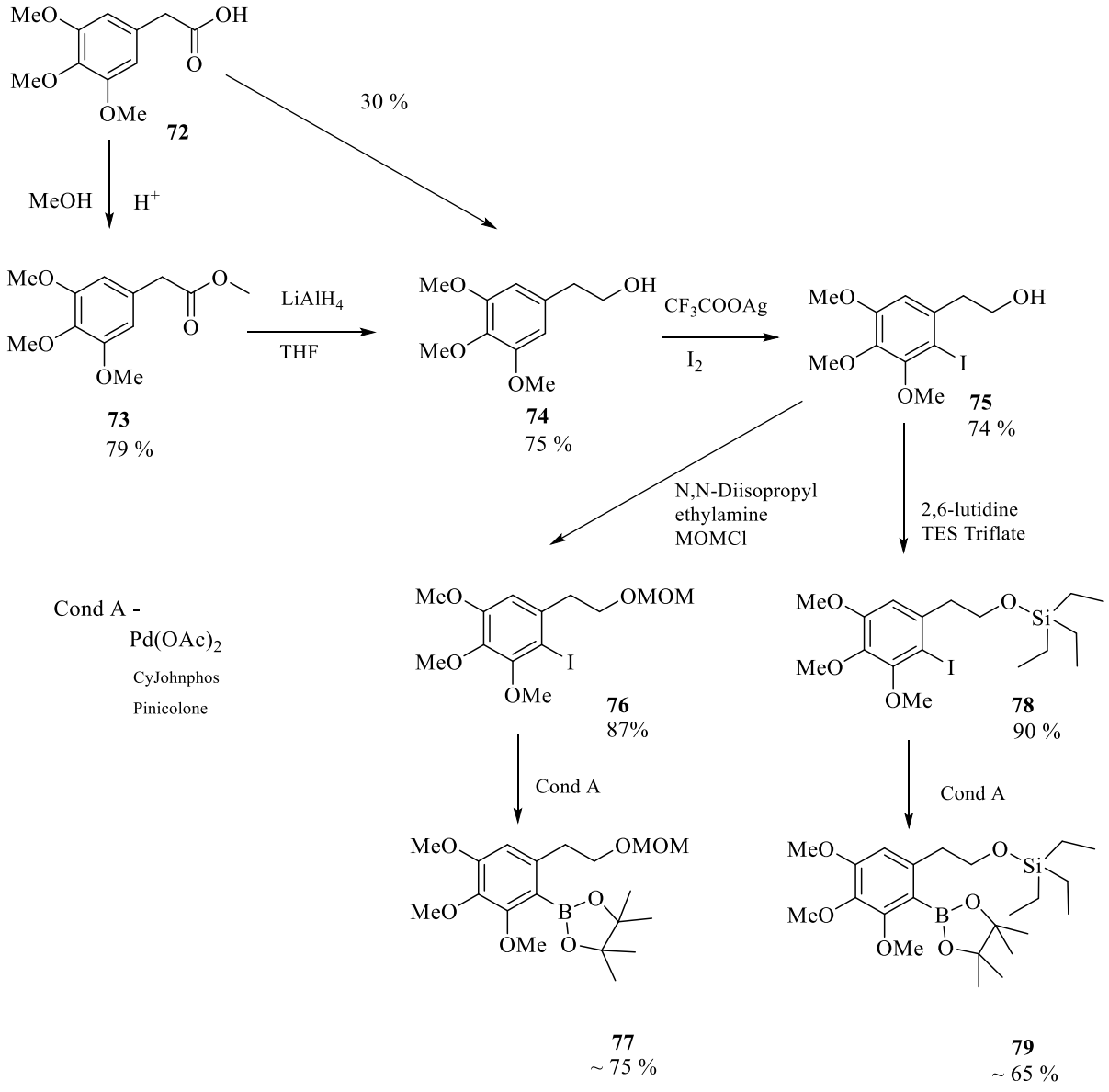

Figure 59 Scheme showing the synthesis of both MOM **(77)** and Silyl **(79)** protected phenyl ethanol coupling partners for Suzuki coupling.

Borylation was first attempted with the TES protected compound **(78)** giving the product as an inseparable mixture of the desired boronate with deiodinated starting material (3:1, approximately 65% determined by ^{1}H NMR). The MOM **(77)** protected iodide was synthesised and borylated in high yield (75%). Several unsuccessful attempts **(Fig 61)** were made to couple aromatic halides **(81)** to both of the borylated **(80)** products using the DavePhos **(83)** / $Pd(OAc)_2$ system described by Baudoin (Colombel *et al*. 2010) in an attempt to form the trisubstituted biaryl **(82)**. Again in all cases deiodinated starting material was recovered indicating that oxidative addition of palladium is occurring at the C-I site suggesting that the reaction is failing at either the transmetallation or reductive elimination stages.

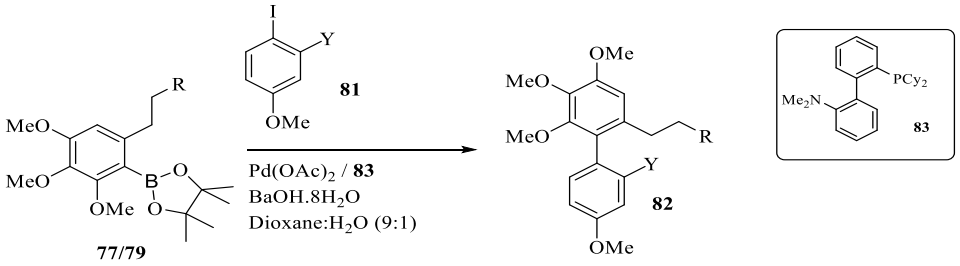

R	Y	Yield %
OMOM	CHO	NR
OMOM	C(=O)Me	< 10
OMOM	OMOM	NR
OMOM	OBn	< 10
OTES	CHO	NR
OTES	C(=O)Me	< 10
OTES	OMOM	NR
OTES	OBn	NR

Table 60 Scheme showing the attempted formation of trisubstituted biaryl via Baudoin's conditions and a table indicating the substituents on each ring (R and Y). A TLC analysis was performed after 6 hours and the concentration of $Pd(OAc)_2$ and DavePhos tripled.

Attempted Suzuki coupling using a Pd/ N-heterocyclic carbene (NHC) catalytic system

As an alternative to phosphine ligands, an N-heterocyclic carbene (NHC) was also synthesised **(Fig 62)** and trialled as a catalytic system for biaryl coupling. The NHC precursor chosen was a tetrahydropyridinium salt **(87)** described by Ozdemir (Özdemir *et al*. 2005b) as a ligand for palladium catalyzed Suzuki coupling. This compound was synthesised in 3 steps from mesitaldehyde **(scheme 62)**

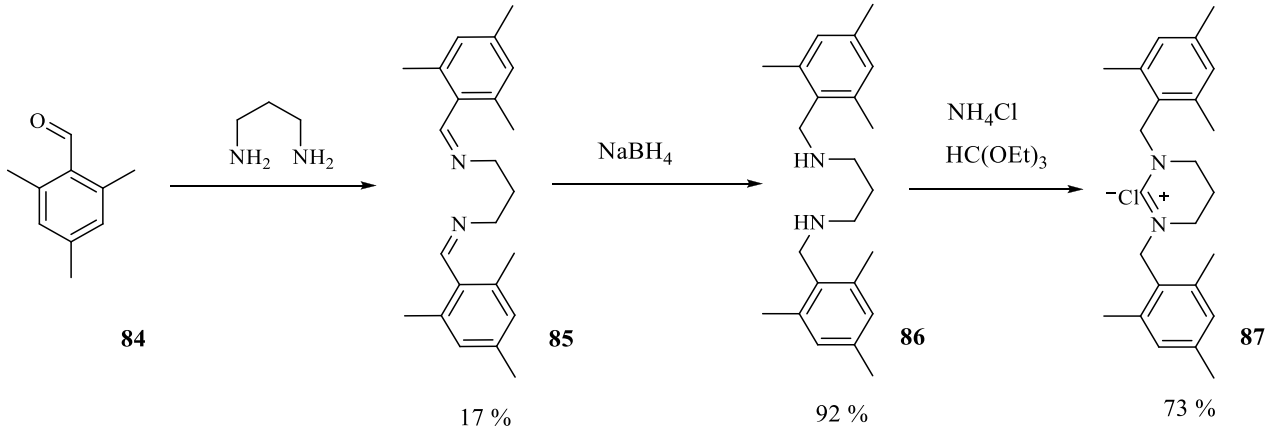

Scheme 61 Scheme showing the synthesis of the tetrahydropyridinium salt ligand (87) from mestitaldehyde (84).

The first step involved the formation of a diimine **(85)** and was poor yielding (17%). $NaBH_4$ reduction of this diamine occurred in excellent yield (92%) to give secondary diamine **(86)** followed by formation of the chloride salt **(87)** (72%) in high purity by melting point.

Suzuki coupling was attempted between the (**88**) **(Fig 63, 68)** and the iodide coupling partner (**70**)using the $Pd(OAc)_2$ / **87** catalyst system under the conditions described by Ozdemir. This was unsuccessful, producing a mixture of dehalogenated and deborated starting materials. Increasing the temperature and catalytic loading failed to give the desired biaryl.

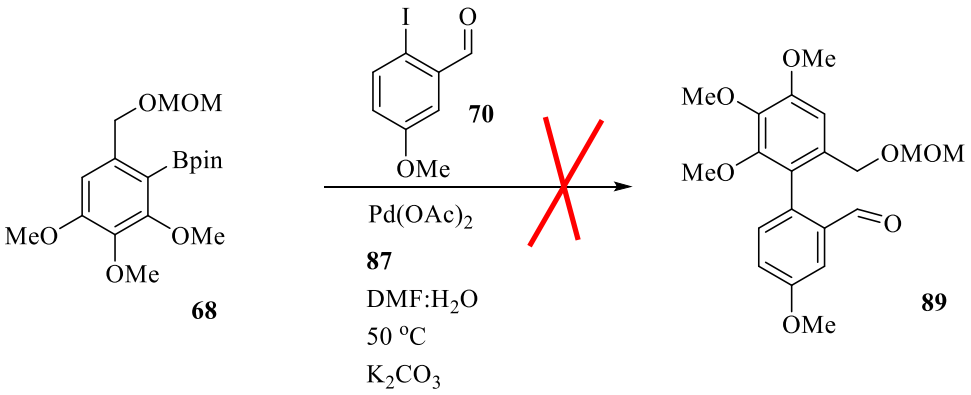

Scheme 62 Scheme showing the attempted formation of a trisubstituted biaryl **(89)** via a Pd/carbene catalysed Suzuki coupling.

Changing the halide coupling partner to 4-bromoanisole under the conditions described by Ozdemir **(scheme 63)** gave excellent conversion to the desired product (90%), again indicating that steric hindrance was the limiting factor when an *ortho* substitution is present on the B-ring coupling partner.

Attempt to form biaryl using Pd/ NHC catalysed direct arylation

Ozdemir also reported the use of this Pd/NHC system to catalyse the direct arylation of electron rich benzaldehydes (Özdemir *et al*. 2005b). This was replicated in our hands resulting in successful direct functionalisation of the 2 position of 3,4,5-trimethoxybenzaldehyde **(51)** with 4 –iodoanisole **(91)**. This proceeded in high yield, affording the biaryl product o**(Fig 64)** (91%). We also attempted the direct functionalisation of 3,4,5-trimethoxybenzaldehyde **(51)** with 6-iodo 3-methoxybenzaldehyde **(70)** (**Fig 64**). This was unsuccessful generating only 3,4,5-trimethoxybenzaldehyde and dehalogenated starting material.

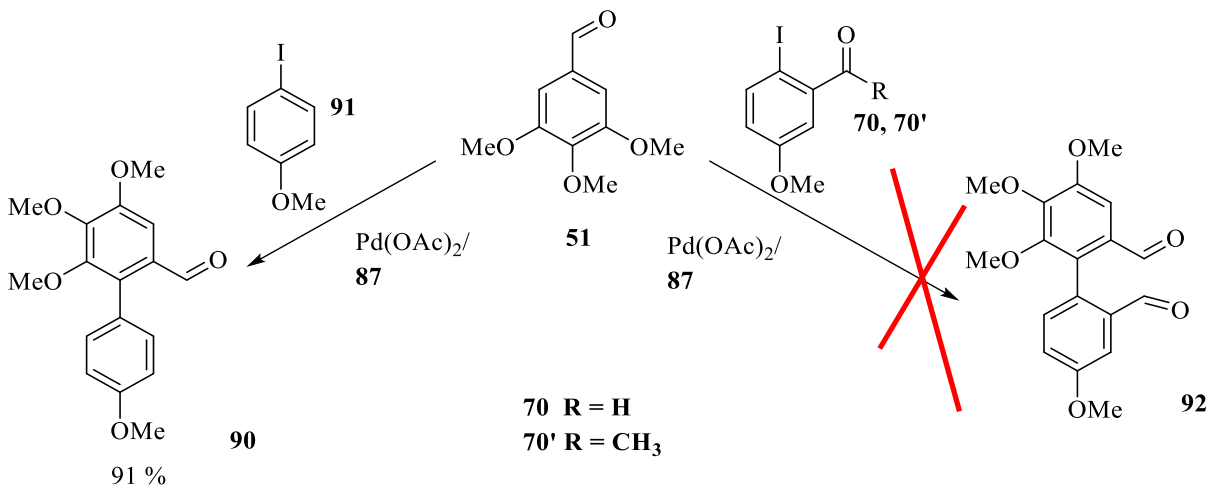

Scheme 63 Scheme showing both the successful formation of a disubstitiuted biaryl (left) and unsuccessful formation of a trisubstituted biaryl (Right) through Pd/carbene catalysed direct arylation.

The reaction was also attempted with 2-iodobenzaldehyde (**70**) and 2-iodoacetophenone (**70'**) but in both cases a mixture of starting material and deiodinated starting material where produced suggesting that oxidative addition at least occurred. So far, attempts have been unsuccessful in the synthesis of the required tri -substituted biaryl precursor **(92)**.

Investigation into the effects of changing groups ortho to the coupling carbons

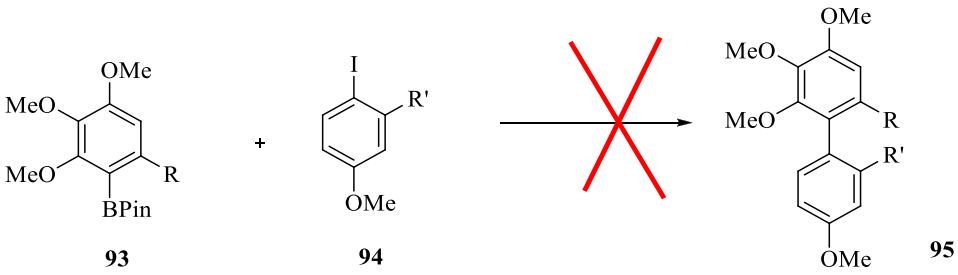

R		R^1	Conditions A Yield (%)	Conditions B Yield (%)	Conditions C Yield (%)
CHO	**70**	CHO	NR	NR	NR
CHO	**71**	C(=O)Me	< 10	NR	NR
CHO	**105**	CH_2 OMOM	NR	NR	NR
CHO	**112**	OBn	NR	NR	NR
CHO		H	88	92	90
OMOM	**70**	CHO	NR	NR	NR
OMOM	**71**	C(=O)Me	NR	NR	NR
OMOM	**105**	CH_2 OMOM	NR	NR	NR
OMOM	**112**	OBn	NR	NR	NR
OMOM		H	67	61	52

Table 64 Diagram showing a general scheme for a Suzuki reaction and a complementary table that shows the various R and R^1 substituents. Conditions A ($Pd(PPh_3)_4$, Na_2CO_3, DME 80 ^oC sealed tube). Conditions B ($Pd(OAc)_2$, DavePhos, $Ba(OH)_2 \cdot 8 H_2O$, Dioxane/H_2O, 100 ^oC), Conditions C ($Pd(OAc)_2$, **87**, K_2CO_3, DMF/H_2O, 50 ^oC).

Various types of palladium catalysed cross-coupling have been attempted to no avail. Several methods have been attempted and have either failed or produced tiny amounts of desired product (<10%) that did not improve through optimisation. Various combinations of the groups *ortho* to the coupling moieties (Boronate ester on A ring **(93)**, iodide on B-ring **(94)** have been trialled **(Fig 65).** On every occasion the only successful coupling occured when the *ortho* group to the halide is hydrogen, further confirming steric hindrance as being a problem. In all cases, deiodinated starting material was recovered indicating that oxidative addition had occurred. Switching the halide group to the A- ring and vice versa for the boronate B-ring had no effect on reaction success, ruling out protodeboronation due to the

electron donating trimethoxy moiety. Sneickus' group encountered this issue with steric hindrance during the total synthesis of the natural product Gymnopusin (Wang *et al*. 2012). The compounds required the formation of a tri-substituted biaryl **(Fig 66)** with a similar substitution pattern to our desired precursor.

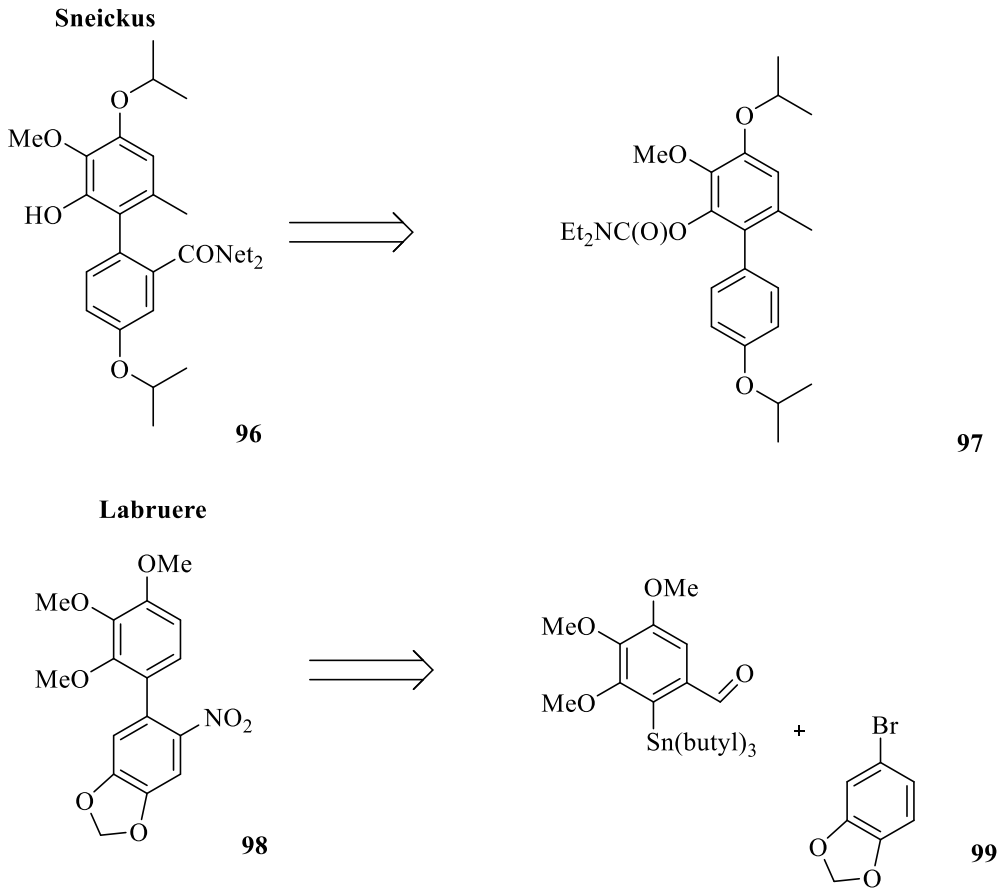

Scheme 65 Scheme shows two examples of alternative retrosynthetic routes to trisubstituted biaryls due to failed cross coupling.

The group attempted several Suzuki conditions to form the biaryl directly but abandoned this method due to the low yields caused by steric hindrance and electron donating nature of the substituents. An alternative route was utilised that involved formation of a di-substituted biaryl followed by a rearrangement. Labruere (Labruere *et al*. 2012) reported a similar problem when dealing with tri-substituted biaryls. The original route was attempted but the Stille coupling failed, fortunately the electron donating substituents on **(99)** allowed for regiospecific nitration to give the desired product **(98).**

A Friedel Crafts approach

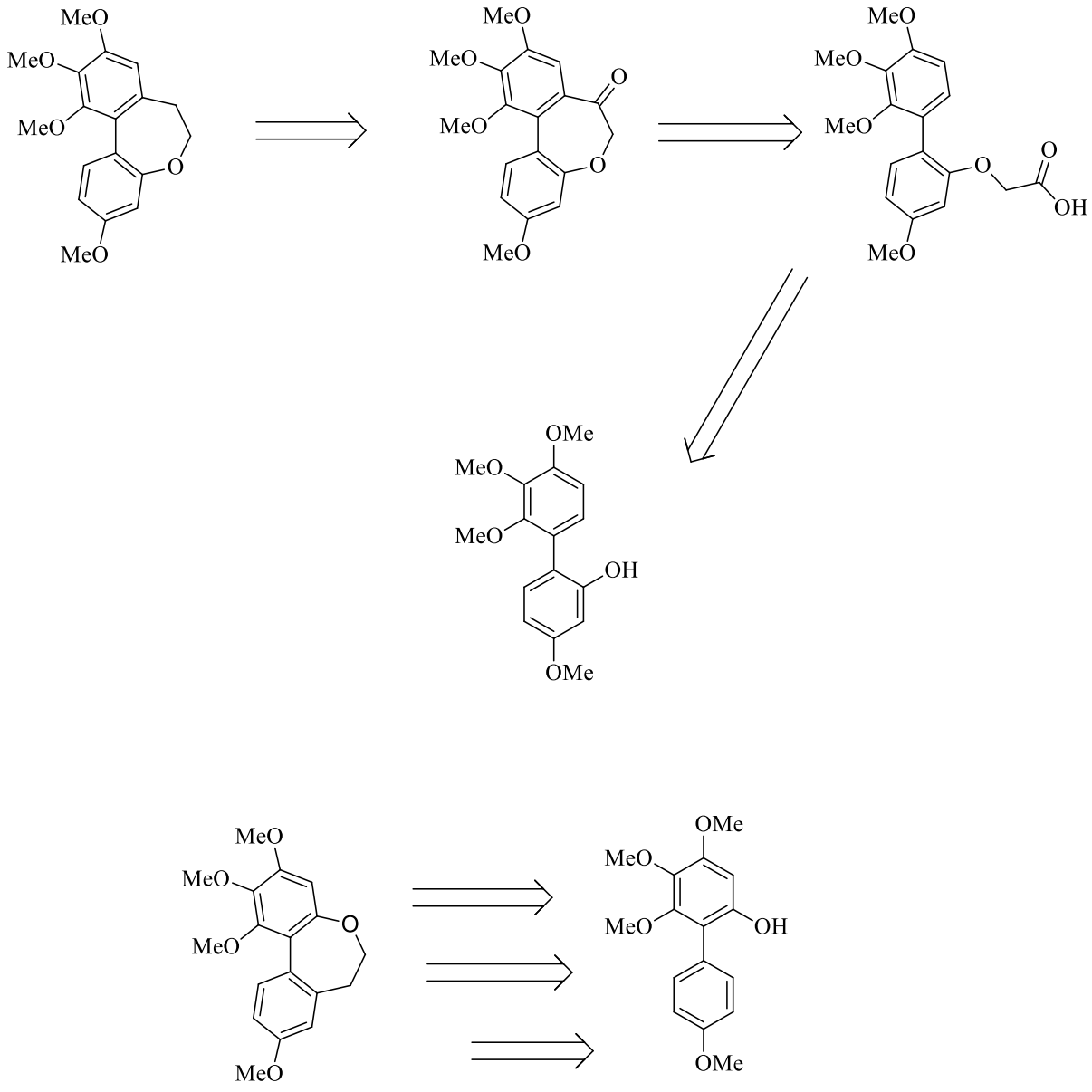

Scheme 66 Retrosynthetic route to [*b*,*d*] oxepines utilizing an intramolecular Friedel Crafts ring closure

As directly preparing a tri-substituted biaryl directly through cross coupling has proven unsuccessful due to steric hindrance a different approach was attempted. Having shown that disubstitiuted biaryl can be formed in excellent yield, this was chosen as a starting point for oxepine construction. The retrosynthesis (**Scheme 67)** shows that a Friedel Crafts acylation ring closure is the key step to form the oxygen containing central ring. This route is exclusively for [*b,d*] oxepines and the electron donating groups present on both the A and C rings should allow for sufficient selectivity in a Friedel Crafts electrophilic ring closure.

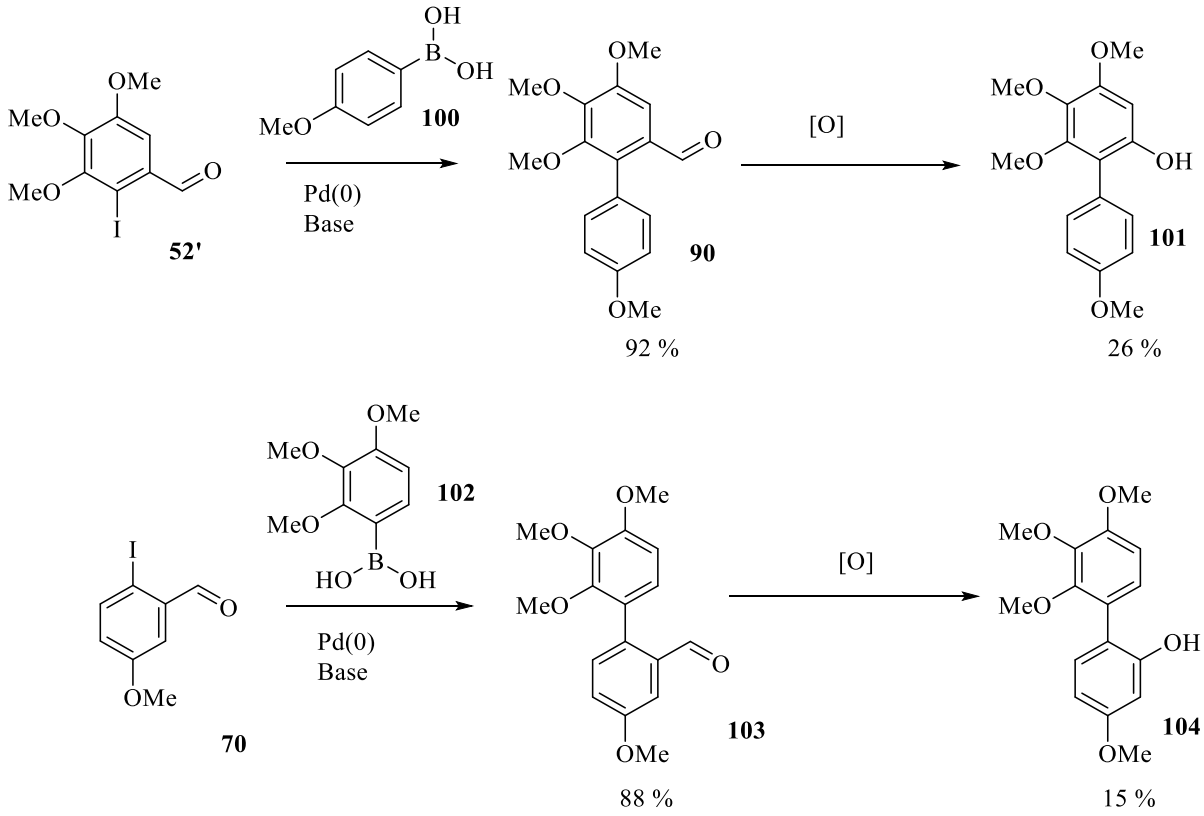

Scheme 67 Scheme showing the synthesis of both a-ring and b ring phenol precursors in 2 steps via a Suzuki reaction and Dakin oxidation.

Initially aldehydes were chosen to generate appropriate starting phenols **(101, 104)** using Dakin/ Baeyer Villiger chemistry **(Scheme 68)**. Both biaryl aldehydes **(90, 103)** were synthesised with via Suzuki coupling in excellent yields**.** Both acid and base-catalysed Dakin reactions were attempted with H_2O_2 giving poor yields. A boric acid / H_2O_2 system has been reported to increase yield in the oxidation of benzaldehydes to phenols (Roy *et al*. 1999), so

this was also attempted and also gave disappointingly low yields. Using *m*-CPBA followed by base hydrolysis, again gave poor yields as did urea/ H_2O_2 (Varma and Naicker. 1999). An attempt was made to oxidise the aromatic benzaldehydes **(Fig 69)** to phenols before Suzuki coupling. Again the desired phenol **(105)** was formed in poor yield (14%) with the major component being an aromatic formate **(106)**. Several attempts to hydrolyse this formate failed even using hot concentrated base (NaOH (50%). As direct Suzuki coupling of 2-iodo 5-methoxyphenol with 2,3,4-trimethoxyphenylboronic acid proceeded in low yield (24%), a series of phenol protecting groups were considered.

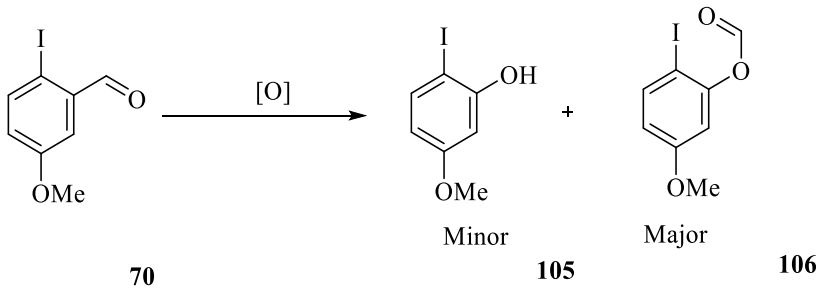

Scheme 68 Scheme showing the attempted Dakin oxidation of benzaldehyde (70) to generate the desired phenol (105) in poor yield and unwanted formate (106) as the major product.

Synthesis of 2-iodo 5-methoxyphenol **(107)** by direct iodination of 3-methoxyphenol **(105)** has been described in the literature. The method described by Das (Das *et al*. 2007) using molecular iodine in acetonitrile with catalytic ceric ammonium nitrate produced a complex mixture of iodinated aromatics with approximately 15% (by crude ^{1}H NMR) of the desired product in our hands unlike the 85% reported. Using silver trifluoroacetate **(Fig 70)** in chloroform gave (**107)** an unimpressive yield of 32%. An optimized yield of 68% was achieved using silver nitrate with a slow canula addition of iodine in chloroform (0.1 g /500 mL) over 24 hrs.

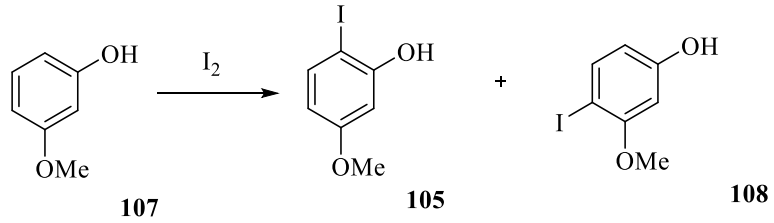

Scheme 69 Scheme showing the iodination of 3- methoxyphenol generating 6-iodo 3-methoxyphenol as the major regiomer (68%) and 4-iodo 3-methoxyphenol

Alkylation of 2-iodo 5-methoxyphenol **(105)** with methyl bromoacetate resulted in the desired acid **(109)** in excellent yield **(**76%**)**. An attempt to couple 2,3,4-trimethoxyphenylboronic acid **(102)** directly with **(109)** generated **(110)** in disappointing yield (<10%) **(Scheme 71)**.

Increasing the amount of catalyst and increasing reaction time did not improve the yield of **(110)**. The reaction was also unsuccessfully attempted at 150 ^{o}C in DMF.

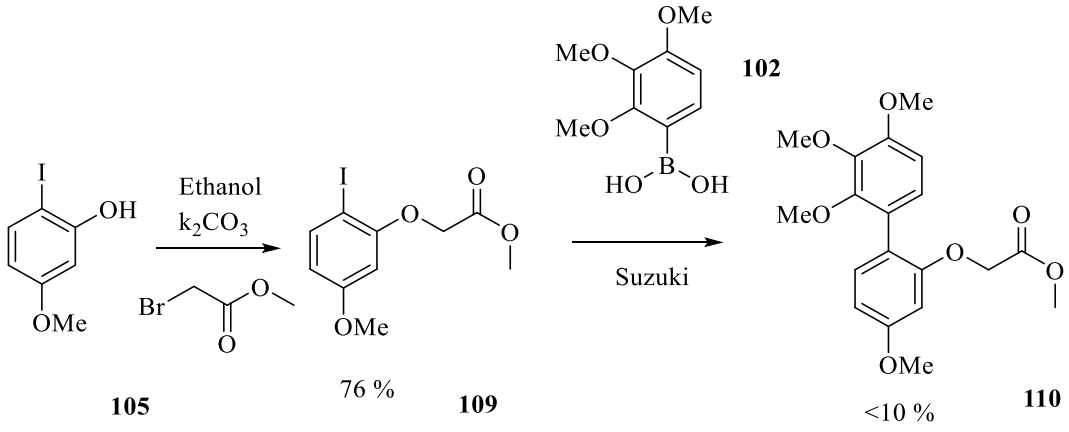

Scheme 70 Scheme showing the alkylation of phenol **(105)** to form acid **(109**). Reaction of this compound with boronic acid **(102)** was unsuccessful.

2-Iodo-5-methoxyphenol **(105)** was protected with a MOM group through base catalysed nucleophilic substitution using Hunigs base and MOMCl in DCM in excellent yield (91%) **(Scheme 92)**. Suzuki coupling of this compound with 2,3,4-trimethoxyphenylboronic acid **(102)** was unsuccessful. Alkylation of 2-iodo 5-methoxyphenol **(105)** with benzyl bromide succeeded in moderate yield (43%), but a Mitsunobu reaction with benzyl alcohol gave a clean conversion to the desired benzyl protected phenol **(112)** in excellent yield (86%)

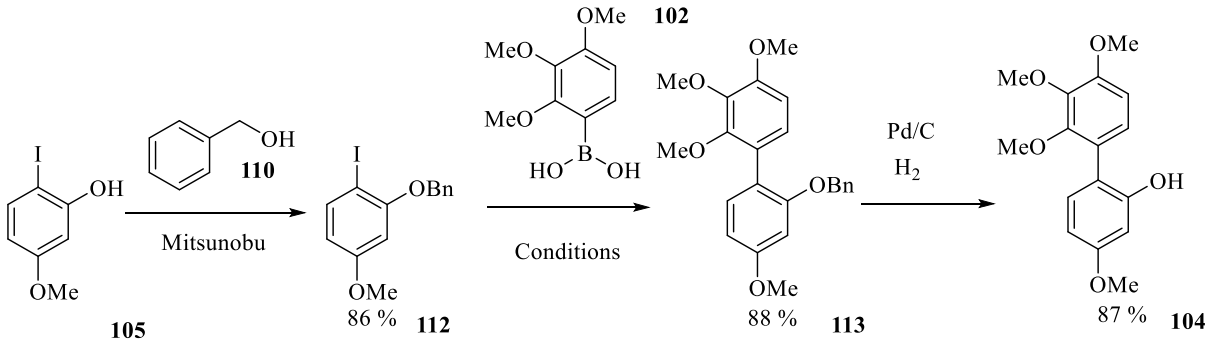

Figure 71 Scheme showing the Mitsunobu reaction between phenol, and benzyl alcohol to generate **(112).** Suzuki coupling of this compound with boronic acid **(102)** and subsequent palladium catalysed hydrogenation to give the desired phenol **(104).**

The subsequent Suzuki coupling of (**112**) with 2,3,4-trimethoxybenzeneboronic acid (**102**) proceeded to generate **(113)** in excellent yield (88%). The benzyl protecting group was removed via palladium catalysed hydrogenation in excellent yield (87%) to give the desired biaryl phenol **(104).** The isomer of this phenol was also required **(101).** The synthesis is described in **Fig 73.**

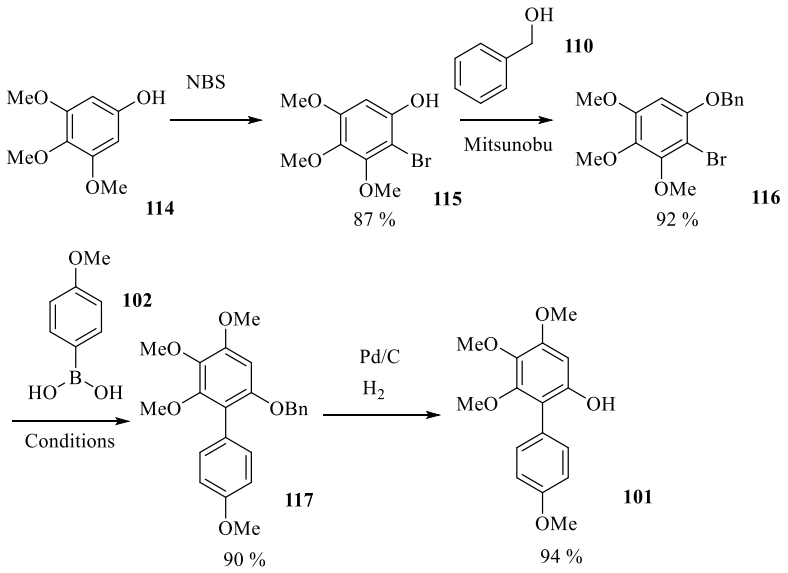

Scheme 72 Reaction scheme showing the preparation of coumpounds **(101** and **(116). (115)** through the bromination of phenol **(114)** with NBS. A Mitsunobu reaction of the product **(115)** with benzyl alcohol **(110)** produced coupling partner **(116).** A Suzuki coupling of this compound **(116)** with boronic acid **(102)** using general proceedure 1 generated benzylated biaryl **(117),** hydrogenation of this compound generated the desired phenol **(101)** in excellent yield.

Bromination of 3,4,5-trimethoxyphenol **(114)** using NBS proceeded in excellent yield (87%) following a procedure described in the literature (Jinno *et al*. 1999). Benzylation of the

phenol **(115)** was best achieved through Mitsunobu reaction with benzyl alcohol **(110)** in excellent yield (92%**)**. Suzuki coupling of this bromide **(116)** with 4-methoxybenzeneboronic acid **(102)** generated the desired biaryl **(117)** in excellent yield (90%) Removal of benzyl protection via Pd catalysed hydrogenation generated the desired phenol **(101)** in excellent yield (94%). Attempts to directly synthesise the required acid **(118)** from this phenol **(101)** with potassium carbonate and 2-bromoacetic acid in methanol was low yielding (25%) and attempts to improve this by changing solvents failed. Using bromoacetic acid methyl ester in ethanol followed by a basic work up gave the desired acid in high yield (85%) (**Fig 74)**. The Friedel Crafts ring closure proceeded in good yield (73%**)** using a mixture of trifluoroacetic acid and trifluoroacetic anhydride (50:50) to generate oxepin-7(6 H)-one **(119)**.

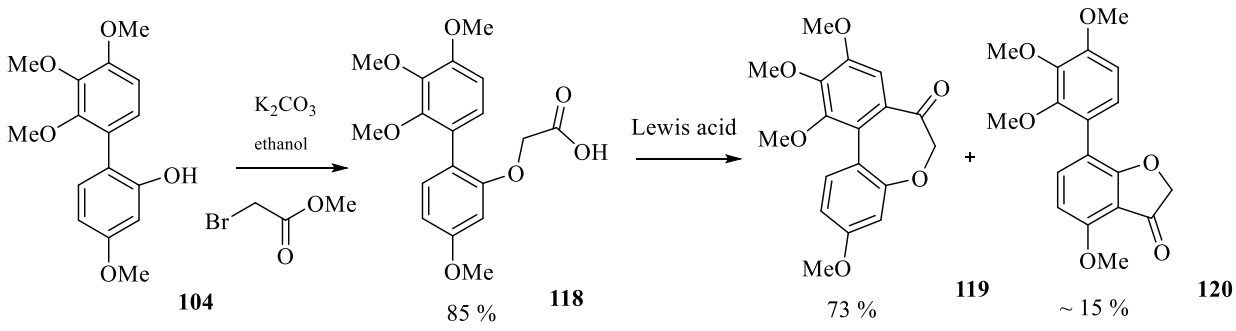

Scheme 73 Scheme showing the alkylation of phenol (104) with 2-bromoacetate followed by acidic work up to generate acid (118). Intramolecular Friedel Crafts of this compound generated dibenzo[*b*,*d*]oxepin-one in good yield with (120) as a minor product.

Attempts to improve the yield of desired oxepin-7(6 H)-one **(119)** and reduce the presence of the benzofuran-2(3*H*)-one side product **(120)** were attempted. Changing the Lewis acid ($TiCl_4$, $BF_3{\cdot}(OEt)_3$ and $AlCl_3$) resulted in overall lower yields for the reaction.

Lewis acid	Time (H)	% yield of **119**	% yield **120**
TFA/TFAA 50:50	24	73	15
TFA/TFAA 75:25	36	60	15
TFA/TFAA 25:75	36	51	10
TFA	36	27	-
TFAA	36	-	-

Table 74 Table showing the conditions attempted to optimise the formation of **(119)** and reduce the formation of impurity **(120)**

Alkylation of the phenol **(101)** with bromoacetic acid methyl ester in ethanol followed by a basic work up gave the desired acid **(121)** in high yield (74%) (**Scheme 76)**. Friedel Crafts ring closure again generated oxepin-7(6 H)-one **(122)** in high yield (75%**)** and this was easily separated from the benzofuranone **(123)** side product.

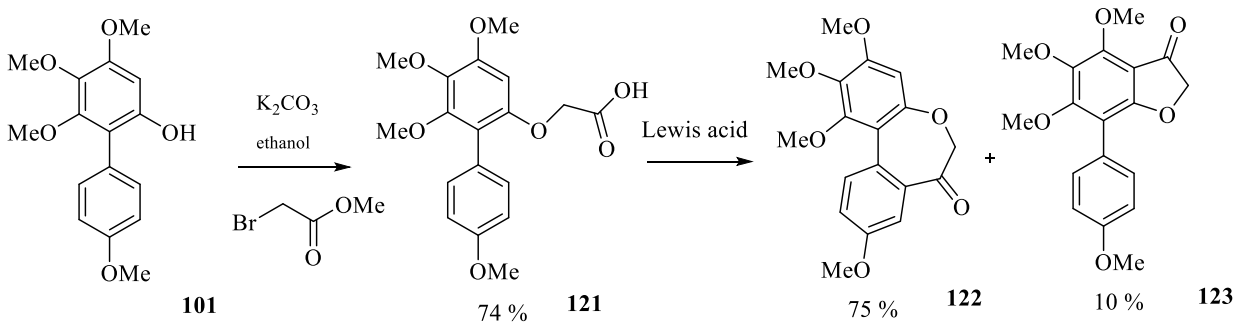

Scheme 75 Scheme showing the alkylation of phenol **(101)** with 2-bromoacetate followed by acidic work up to generate acid **(121).** Intramolecular Friedel Crafts of this compound generated dibenzo[b,d]oxepin-one in good yield with **(123)** as a minor product.

Conclusion

The substitution pattern of the methoxy groups on these molecules (**Fig 77)** supply appropriate directing effects for intramolecular Friedel Crafts ring closure. This is true if the acid is located on either ring. In both cases **(74, 76)** a small amount of unwanted indanone side product **(120, 123)** was produced but was easily removed by chromatography. The ketone moiety on the ring closed products **(119, 122)** can serve as a useful functionality for further derivation or can be removed via reduction. A potential issue with the robustness of the method is outlined in **Fig 77.** If the ring closure was attempted on a molecule **(124)** with a substitution *meta* to the biaryl carbon on the B-ring**,** depending on the directing nature of the substituent a mixture of regiomers **(125, 126)** will form. The ratio of compounds will depend on the directing ability of R.

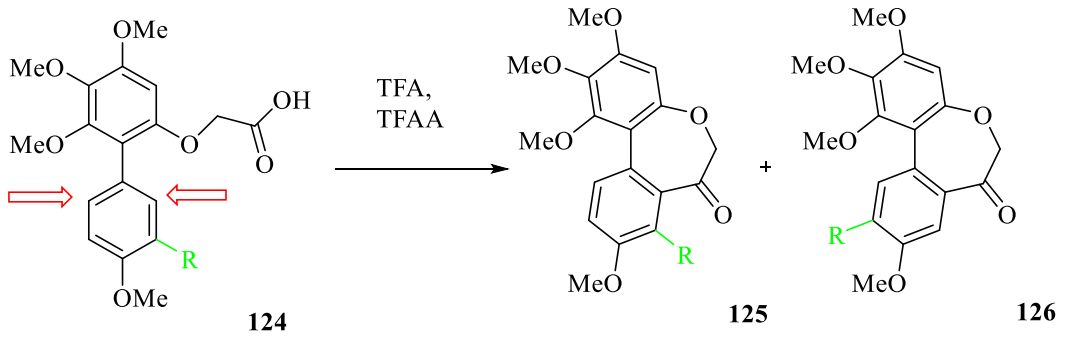

Figure 76 A diagram showing potential issues of regioselectivity when using an intramolecular Friedel Crafts ring closure on an unsymmetrical ring (124). The red arrows indicate the sites of reaction.

Chapter 3: Attempted development of an intramolecular ring closure method

Introduction

Attempts were also made to synthesise oxepines through different routes in which the final step was the formation of the dihedral biaryl bond. Disconnecting the molecule at this bond has the advantage of being thermodynamically favoured and having fewer steps. The disadvantage is the lack of a common precursor in the preparation of a library of compounds.

Edwards (Edwards *et al*. 2011) used an intramolecular CuCl oxidative coupling **(Scheme 78)** first described by Piers (Piers *et al* 2000) to synthesise a series of dibenzo[*c,e*]oxepine colchicine binding analogues **(128)** from distannylated precursor (**127)**. This method required two steps involving toxic stannane reagents, and gave poor to moderate yields.

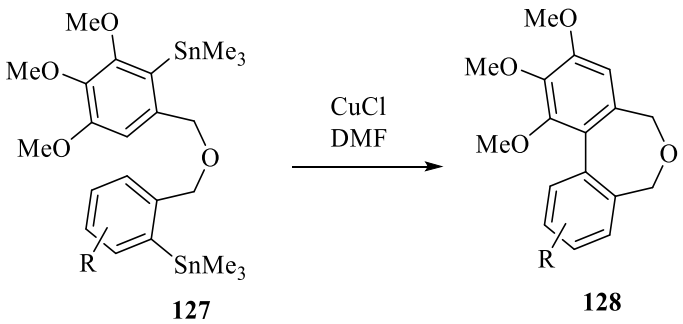

127 **128**

Scheme 77 Reaction scheme showing the copper chloride catalysed intramolecular ring closure of a distannane (127).

Due to the previously mentioned lack of success with Ullmann coupling an intramolecular version wasn't attempted. Miyano reported an Ullmann coupling method that utilised tethers in trying to control atropisomerism of bridged biaryls, again this suffered from low yields. If a sterically hindered bond was formed and would require an extra step (Miyano *et al*. 1984).

Intramolecular oxidative coupling

Intramolecular phenolic oxidative coupling is a key process in several natural product biosynthetic pathways, not least in the biosynthesis of colchicine (Maier and Zenk. 1997). This has been an area of great interest as the process allows the formation of carbon-carbon bonds without the necessity of installing coupling functionalities such as halogens or boronic acids/stannanes and can proceed without transition metal catalysis. Initial research into the process involved highly toxic heavy metal oxidants such as thallium or vanadium complexes ($VOCl_3$, VOF_3). Thallium(III) trifluoroacetate (TTFA) was in fact utilised **(Scheme 79)** as an oxidant in the phenolic oxidative coupling stage in synthesis of racemic NAC **(29)** (Sawyer and Macdonald. 1988). Several other metal oxidants including $FeCl_3$ and $Pb(OAc)_4$ were also trialled.

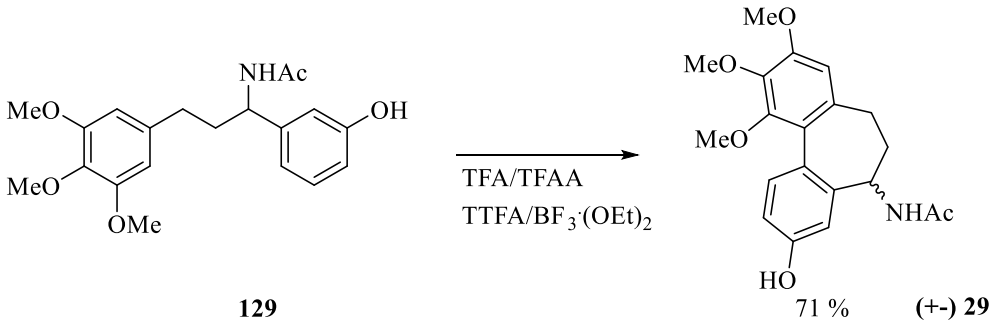

Scheme 78 Reaction scheme showing an intramolecular phenolic oxidative coupling ring closure used in the synthesis of racemic NAC (130) from phenol precursor (129).

The seminal work of Kita (Kita *et al* 1996) in the mid 1990s involved the development of PIFA (Phenyliodine bis(trifluoroacetate) **(131)**, a metal - free hypervalent iodine (III) species for Lewis acid activated oxidative coupling reactions. The group also reported the first non-phenolic oxidative coupling reaction using a non –metal oxidant. Besong (Besong *et al* 2008) reported the asymmetric synthesis of S-(-)-NAC **(29)** via phenolic oxidative coupling. The group directly compared oxidants. PIFA **(131)** offered a better yield (50% over 30%) and

required much lower equivalency of $BF_3{\cdot}(OEt)_2$ (1.5 eq reduced from 35 eq) compared to TTFA as a solvent.

Both suggested mechanisms for phenolic **(Fig 80)** and non-phenolic **(Fig 81)** oxidative coupling resulted in a similar charged pseudo diquinone species that re-aromatised through resonance stabilisation to yield products.

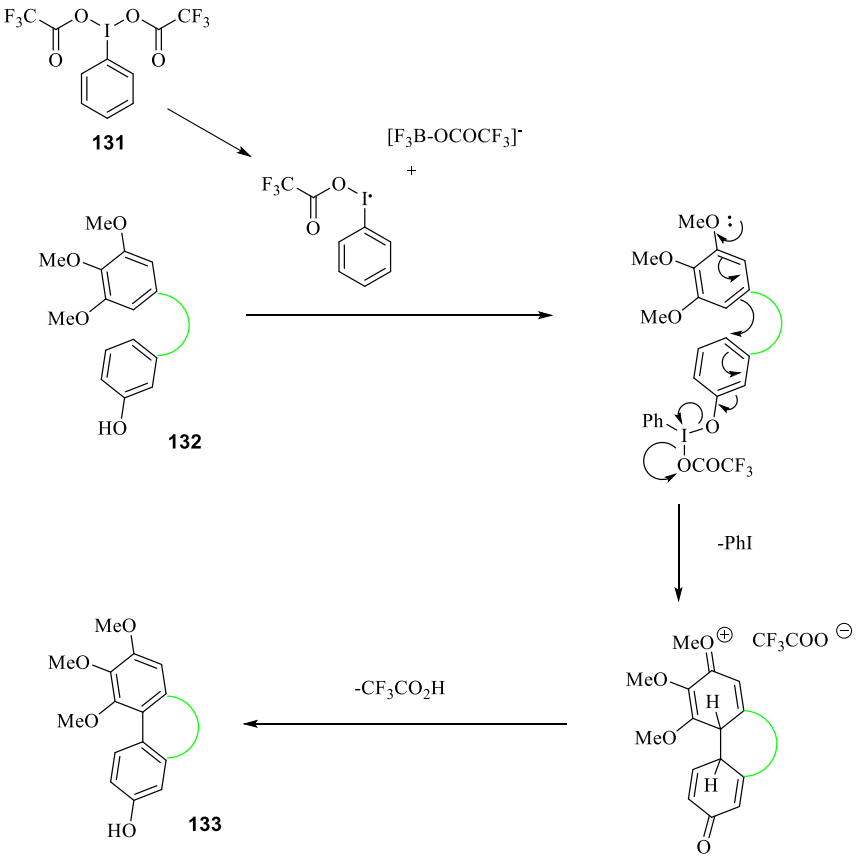

Scheme 79 Scheme showing the proposed mechanism of Lewis acid catalysed intramolecular phenolic oxidative coupling with PIFA **(131)** used as an oxidant to convert a tethered phenol **(132)** to a ring closed product **(133).**

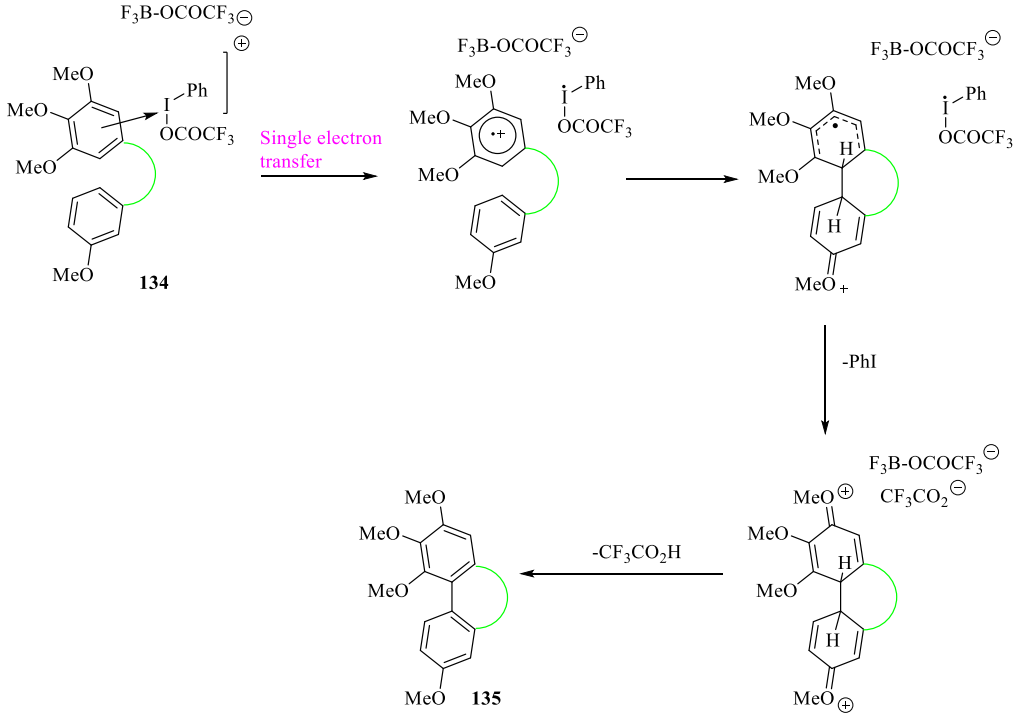

Scheme 80 A reaction scheme showing the proposed mechanism for a Lewis acid catalysed non-phenolic oxidative coupling reaction involving single electron transfer, converting **(134)** to **(135)**

Results

This process was attempted in the synthesis of dibenzo[b,d]oxepines. The B-ring precursors (**Fig 82 (138), (139))** were synthesised in one pot from 2-fluoroanisole **(136)** (63%). Directed *ortho* metallation with *n*-BuLi followed by quenching with triiospropyl borate generated boronic acid **(137)** and addition of hydrogen peroxide and acetic acid gave the phenol **(139)** via an oxidative cleavage. The boronic acid wasn't isolated. Both ether precursors **(141**, **142)** for oxidative coupling were formed using Mitsunobu chemistry in good yield.

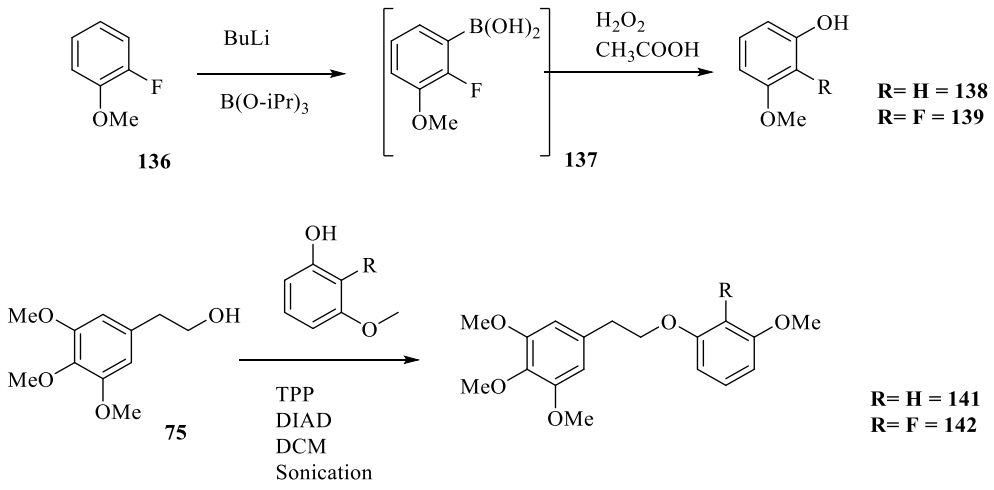

Scheme 81 Scheme showing the synthesis of phenol **(139)** from 2-fluoroanisole **(136).** Also featured is the formation of ethers **(141, 142)** from Mitsunobu coupling of appropriate phenol **(138, 139)** with alcohol **(75).**

In our hands non-phenolic oxidative coupling was unsuccessful. Several conditions were attempted **(Fig 83)** using both PIFA and TTFA as oxidant. Following the Kita procedure (Kita *et al*. 1996) with compound **(141)** gave approximately 5% (By H^1 NMR) of the desired product **(143)** in a complex mixture. Changing temperature or oxidant resulted in quantitative recovery of starting material. With compound **(142)**, again a multi component mixture was produced with no evidence of (**144)**. This may be due to in an imbalance in electro potentials between rings with initial formation of cation intermediates followed by the reforming of

starting material through resonance stabilisation. This could also be due to the position of the ether leading to a competing intermediate ortho to the b-ring methoxy.

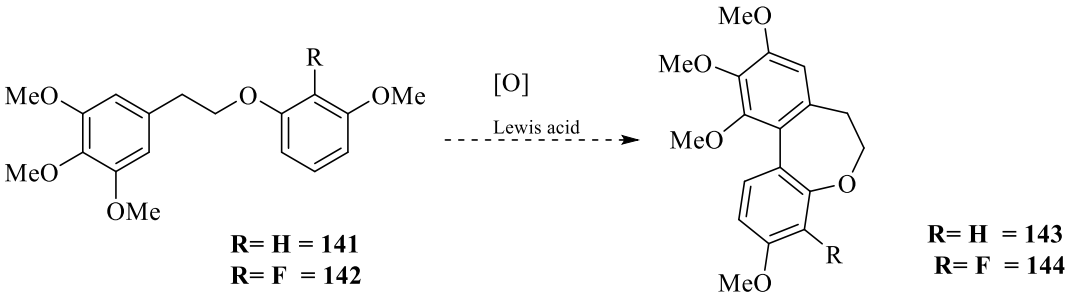

R= H = 141
R= F = 142

R= H = 143
R= F = 144

R	[O]	Solvent	Temp (^{o}C)	Yield %
H	PIFA	$BF_3{\cdot}(OEt)_2$	-40	< 10
			-78	NR
			0	NR
		TFA/TFAA	-40	< 10
			-78	NR
	TTFA	$BF_3{\cdot}(OEt)_2$	-40	NR
			0	NR
F	PIFA	$BF_3{\cdot}(OEt)_2$	-40	< 5
			-78	NR
			0	NR
		TFA/TFAA	-40	< 5
			0	NR
	TTFA	$BF_3{\cdot}(OEt)_2$	-40	NR
			0	NR

Table 82 Scheme showing the attempted non-phenolic intramolecular oxidative coupling reaction on **(141,142)** to form oxepines **143** and **144.** The table shows all of the oxidants, Lewis acids trialled at various temperatures.

Direct arylation

Since the early 2000s there has been shift in research away from traditional cross coupling and heterocyclic chemistry towards C-H functionalisation in general but in particular for the formation of biaryl compounds (Deprez *et al*. 2006), (Lane and Sames. 2004), (Kakiuchi *et al*. 2003).

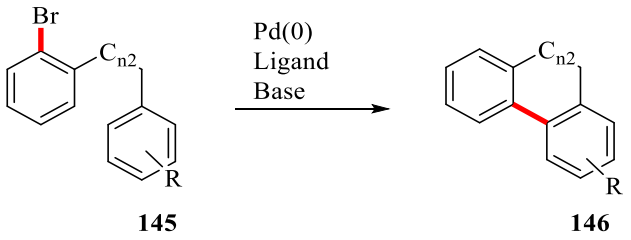

145 **146**

Scheme 83 Diagram showing a general reaction scheme for a palladium catalysed intramolecular arylation. The red bond in halide (145) is the site of palladation. The red line in (146) shows the newly formed biaryl C-C bond.

Palladium catalysed arylation **(Fig 84)** of (hetero) aromatic compounds is a more direct route than classical cross coupling as it requires fewer steps and in the case intramolecular reactions is thermodynamically favoured. This area of direct arylation is of great interest. The only limit seems to be predicting regioselectivity and substrate suitability. This of course comes from understanding of mechanism, of which progress is being made. Several mechanisms have been suggested but two have received the most support. Electrophilic aromatic substitution (SEAr) and concerted metallation deprotonation (CMD) and in both mechanisms oxidative addition occurs at the halide moiety. In SEAr the palladated aryl halide attacks pi-nucleophilic aromatics. (**Fig 85)** In CMD the proton at the desired site of reaction is made acidic by the formation of a palladacycle and abstracted followed by elimination of palladium.

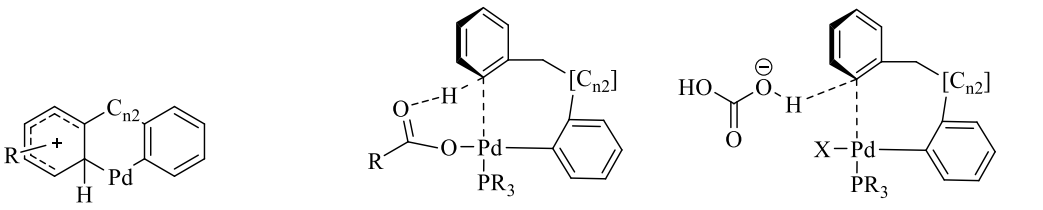

Proposed SEAr transition

Pivalate(R = CMe_3)/ Acetate (R = CH_3) assisted palladation

Fagnou

Carbonate assisted Palladation

Maseras

Figure 84 Diagram showing proposed transitions for SEAr, both Fagnou and Maseras' CMD palladium species.

There have been several mechanistic studies on CMD with most groups in agreement that carboxylate type bases have a critical role, the question of base/metal interaction still remains unanswered (García-Cuadrado *et al*. 2007). The SEAr pathway has all but been debunked in favour of CMD due

to instances of arylation reactions occurring without any directing groups present. (Lapointe and Fagnou. 2010).

A ring Palladation

Initial attempts at direct arylation were focused on forming the palladacycle on the trimethoxy A ring **Scheme 86)**. The coupling precursors **(148, 149)** were synthesised in good yield from the reaction of 2-iodo 3,4,5-trimethoxyphenylethanol **(75)** and the relevant phenol (**138 =** 92%, **139 =** 91%)

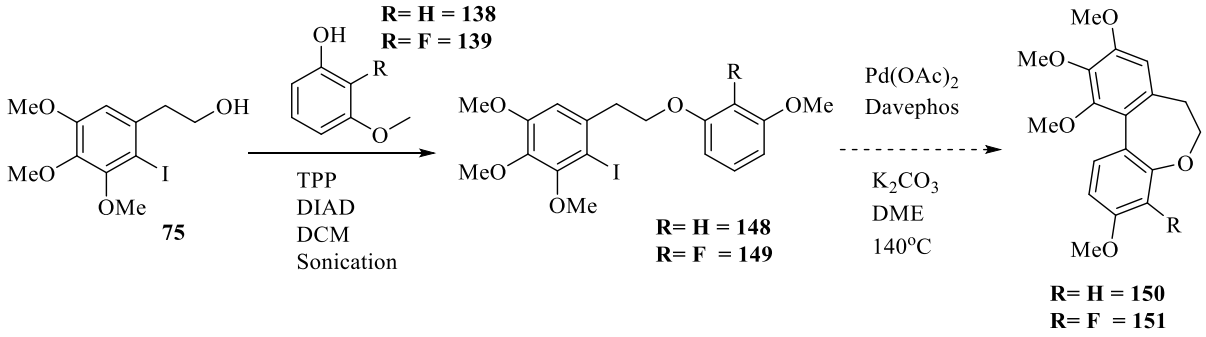

Scheme 85 Scheme showing the attempted formation of a dibenzo[*b*,*d*]oxepine **(150, 151)** via intramolecular arylation. Precursors **(148, 149)** were synthesised via a Mitsunobu reaction between **(75)** and **138 or 139**)

Using the catalytic system described by Fagnou (Campeau *et al*. 2004), several attempts were made to achieve ring closure, all unsuccessful. The deiodinated starting material was recovered, suggesting that oxidative addition of palladium to the carbon - halide bond had occurred. In the case of the fluorinated precursor **(149)**, the major product was again the deiodinated starting material accompanied by a small amount of defluorinated material. Reducing the temperature to 80 ^{o}C resulted in a mixture of starting material and deiodinated material. The proto deiodination is most likely due to the heavily electron donating nature of the trimethoxy motif.

B ring Palladation

Phenol **(152)** was successfully prepared in good yield (71%) by the $AgNO_2$ catalysed iodination of 2-fluoro 3-methoxyphenol **(139)**. The desired precursors for ring closure **(153, 154)** were produced in good yield by reacting the phenols **(110 or 152)** with 3,4,5-trimethoxyphenylethanol**(74)** via a Mitsunobu reaction (**153** = 77%, **154 =** F 86%) (**Fig 87)**.

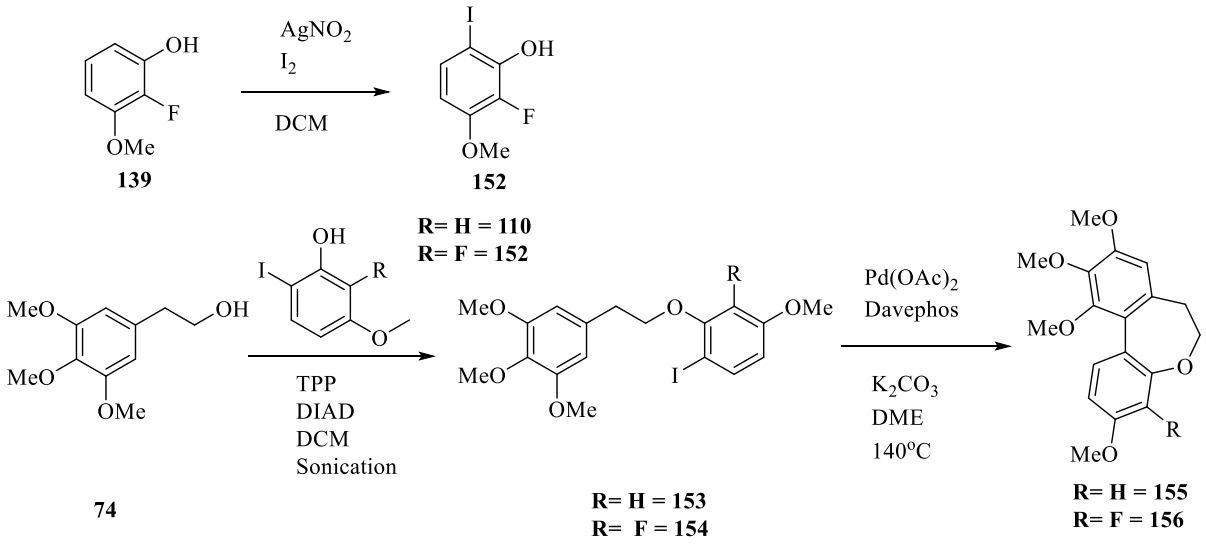

Scheme 86 Scheme showing the iodination of phenol **(139).** The iodinated phenol **(152)** produced and phenol **(110)** were both coupled with phenyl ethanol **(74)** to generate arylation precursors **(153)** and **(154)** respectively. Arylation of **(153)** gave oxepine **(155).** Arylation of **(154)** was unsuccessful in generating dehalogenated starting material **(141, 142)**.

The arylation reaction proceeded in moderate yield (~ 55% by H^1 NMR) under the standard Fagnou conditions with precursor **(153).** The crude material consisted of an unseparable mixture of the desired product and deiodinated starting material. The ring closure was attempted using the fluoro precursor **(154)** again, this was unsuccessful giving a mixture of deiodinated starting material and the ring closed product (by H^1 NMR)

Chapter 4: Synthesis of Dibenzo[*c*,*e*]oxepine analogues

Synthesis of Fluoro analogues of [*c,e*]oxepines

The fluoro analogues were all synthesised from the common biaryl precursor **(56)** due to the ease of access via the dehydrative cyclisation of diol **(157)** to form oxepine and the nucleophilic ring closure of dibomo compound **(159)** to form the various hetrocyclic analogues as described by Edwards (Edwards *et al* 2011).

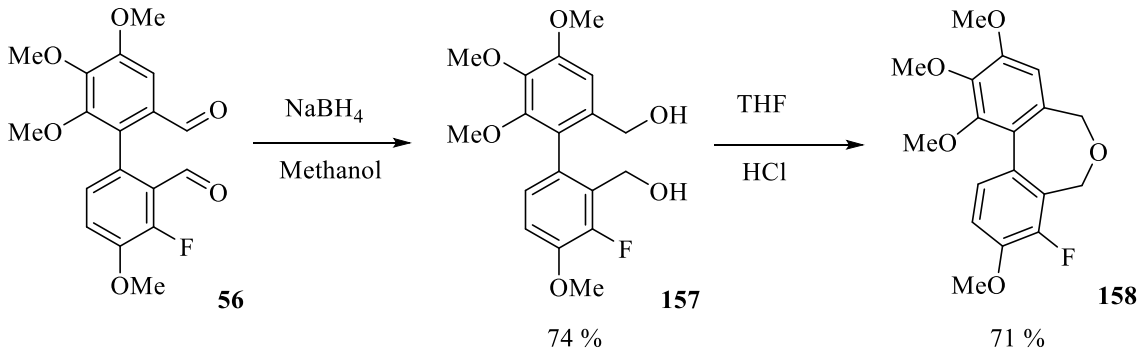

Scheme 87 Scheme showing the synthesis of an oxepine analogue **(158)** from the reduction of dialdehyde **(56)** followed by acid catalysed ring closure of benzylic diol **(157)**

The dialdehyde **(56)** was first reduced to (3-fluoro 4,4',5',6'-tetramethoxy-[1,1'-iphenyl]-2,2'-diyl)dimethanol **(157)** using sodium borohydride in good yield (74%) (Scheme 88). Dibenzo[c,e]oxepine **(158)** was formed in one step from the diol **(157)** by acid catalysed ring closure. This occurred in good yield (71%).

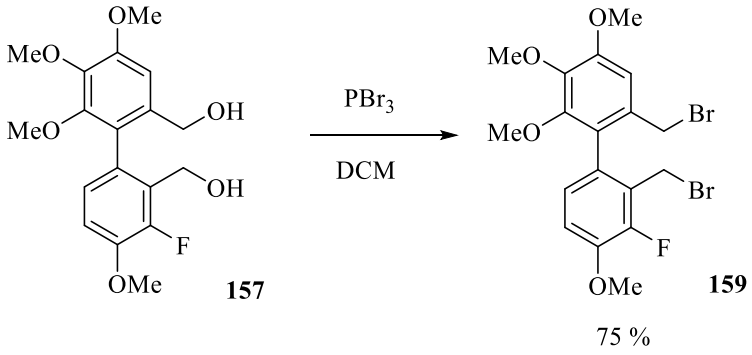

Scheme 88 Reaction scheme showing the dibromination of biaryl diol (157) to generate (159)

The remaining nitrogen and sulphur containing analogues were synthesised from the dibromo precursor. This was produced **(159)** in good yield (75%) from the dibromination of diol (**Fig 89)**. Formation of the 8-fluoro 1,2,3,9-tetramethoxy-5,7-dihydrodibenzo[c,e]thiepine **(160)** occurred in excellent yield (94%) from the reaction of the dibrominated species **(159)** with sodium sulfide.

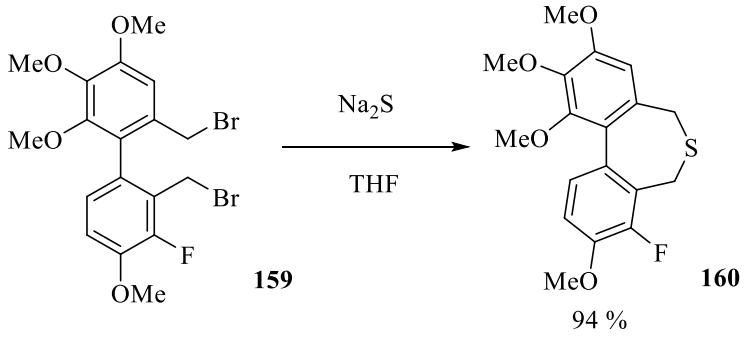

Scheme 89 Scheme showing the fomation of a thiepene **(160)** through nucleophilic ring closure of **(159).**

Oxidation of the thiepine product **(160)** using m-CPBA gave a mixture of 8-fluoro 1,2,3,9-tetramethoxy-5,7-dihydrodibenzo[c,e]thiepine oxide (32%) **(161)** and dioxide (48%) **(162)** respectively **(Fig 91)** that were easily separated via column chromtography.

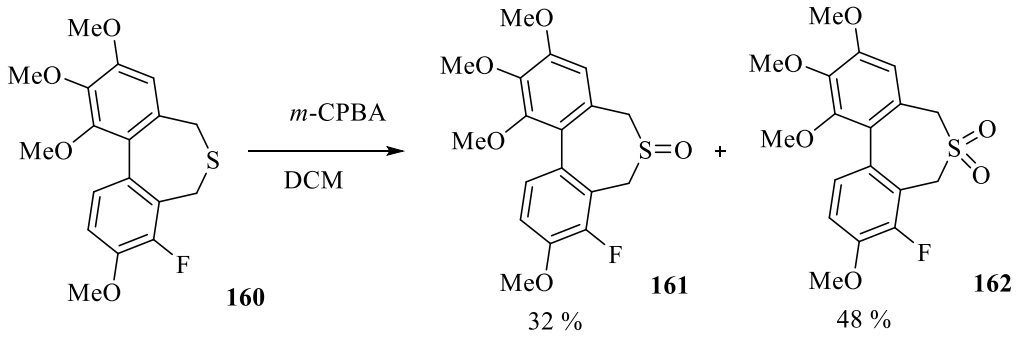

Scheme 90 scheme showing the *m*-CPBA induced oxidation of thiepine **(160)** to form both sulfone **(161)** and sulfoxide **(162)** analogues

The synthesis of 8-fluoro 1,2,3,9-tetramethoxy-6,7-dihydro 5 H-dibenzo[c,e]azepine **(164)** was attempted by multiple routes. The reaction of the dibromo biaryl precursor **(159)** with methanolic ammonia was unsuccessful, failing to yield product **(164)**. **Fig 92** shows the attempts to form the *N*-formyl derivative **(163)** from formic acid catalysed reaction of

formamide with dialdehyde **(56)** followed by hydrolysis to amine **(164).** This approach was also unsuccessful, resulting in decomposition of the molecule.

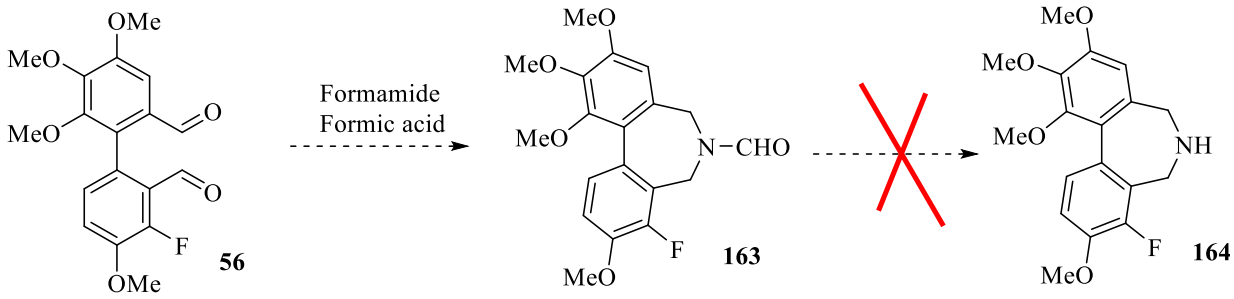

Scheme 91 Scheme showing an attempted formation of azepine **(164)** from dialdehyde **(56)** via a ring closing formylation reaction followed by acid catalysed cleavage of *N*-formyl species **(163).**

The reaction of 2',6-bis(bromomethyl)-3'-fluoro 2,3,4,4'-tetramethoxybiphenyl **(159)** with benzylamine afforded the N-benzylated azepine **(165)** product in good yield (67%) (**Fig 93**). The many attempts to remove the benzyl group from the compound via palladium catalyzed hydrogenation are summarised in table **(Fig 94)**. Increasing the amount of C/Pd had no effect. The reaction was also attempted with Pearlman's catalyst (20% $Pd(OH)_2$), this again gave quantitative return of starting material.

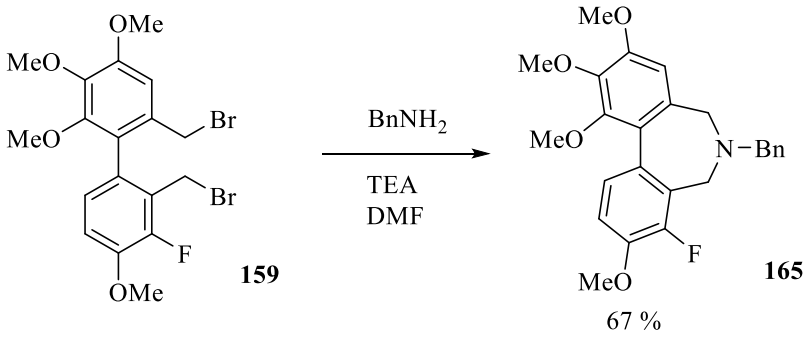

Scheme 92 Scheme showing the formation of *N*-benzyl azepine **(165)** via reaction of benzylamine with dibromo biaryl **(159).**

Methanol (%)	HCl (%)	Temperature (^{o}C)	Pressure (atm)	Yield (%)
0	100	100	1	NR
0	100	100	1	NR
90	10	0	4	NR
75	25	0	4	NR
50	50	0	4	NR

Table 93 Table showing the conditions attempted for the unsuccessful debenzylation of **(165)** via Pd catalysed hydrogenation

Synthesis of hydroxyl analogues

The synthesis of the biaryl precursor **(36)** for the hydroxyl analogues was achieved through Ullmann coupling as formation of the required imine for Ziegler coupling was low yielding.

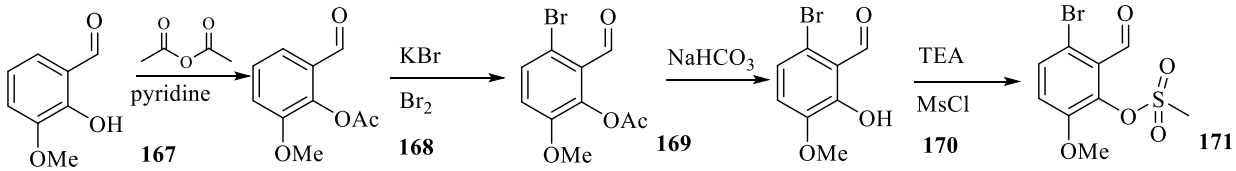

Scheme 94 Scheme showing the synthesis of Ullmann precursor **(167)** from **(171).**

Synthesis of the B-ring precursor 6-bromo 2-methanesulfonyl-3-methoxybenzaldehyde **(171)** was produced in four steps from *ortho* vanilin **(Fig 95, 167)**. The phenol group from (**167)** needed to be protected to direct the bromination to the 6 position. This was achieved in moderate yield (63%) by reaction with acetic anhydride in pyridine at room temperature to give **(168)**. Bromination was achieved using KBr and Br_2 in water to give the crude product

(169). Ttreatment with $NaHCO_3$ gave the deacetylated phenol **(170) w**hich was subsequently mesylated to give the target **(171)** in excellent yield (79%) (**Scheme 96**).

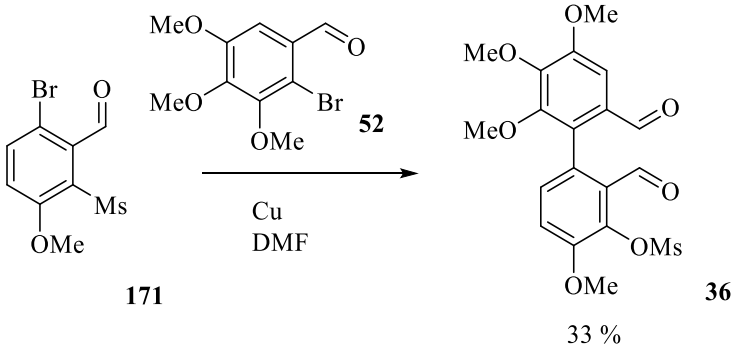

Scheme 95 Scheme showing the formation of mesylated biaryl dialdehyde **(36)** via copper catalysed Ullmann coupling of benzaldehydes **(171)** and **(52).**

The Ullmann coupling proceeded in poor yield (33%). The dialdehyde produced **(36)** was reduced to the diol **(172)** using sodium borohydride in excellent yield (82%) and reaction with PBr_3 gave the dibrominated component **(173)** in excellent yield (90%) (**Scheme 97**).

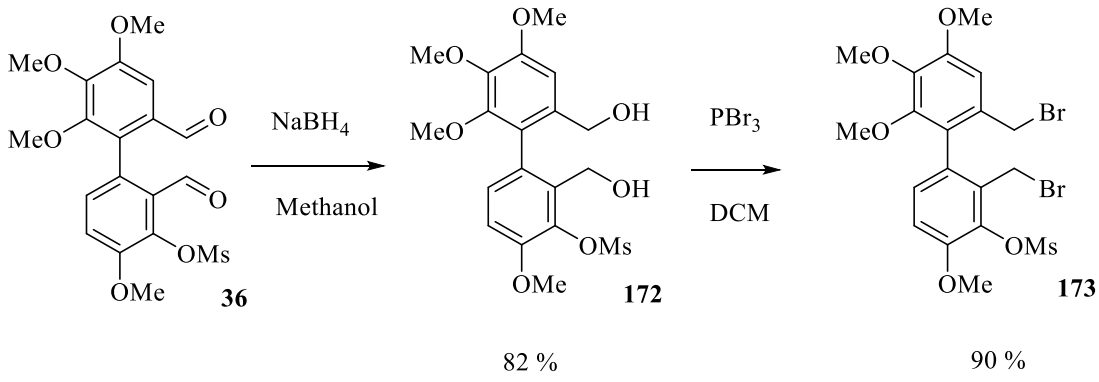

Scheme 96 Scheme showing the synthesis of a dibrominated intermediate **(173)** from the reduction of dialdehyde **(36)** followed by PBr_3 induced bromination of benzylic diol **(172)**

The ring closure of the dibromo compound **(173)** with sodium sulphide was attempted in refluxing water/methanol **(Fig 98)**. This produced a complex mixture. No reaction occurred at room temperature after 3 days. Under sonication, the reaction proceeded to give the desired thiepene **(175)** in poor yield (26%).

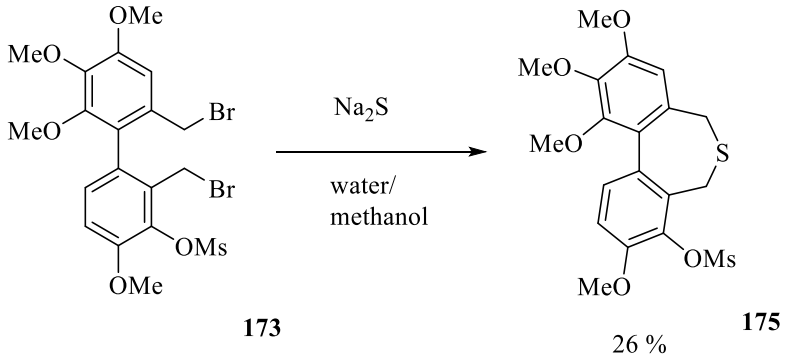

Scheme 97 Scheme showing the formation of thiepine analogue **(175)** from dibrominated species **(173)**

Attempts to remove the mesyl group from the thiepene **(Fig 99)** were unsuccessful resulting in degradation of the product in to complex even at room temperature. The reaction was repeated at room temperature. After 4 hours degradation had occurred. Attempts to oxidise the mesylated thiepene **(175)** to sulfoxide **(177)** and sulphone **(178)** with *m*-CPBA also resulted in degradation (**Scheme 99**).

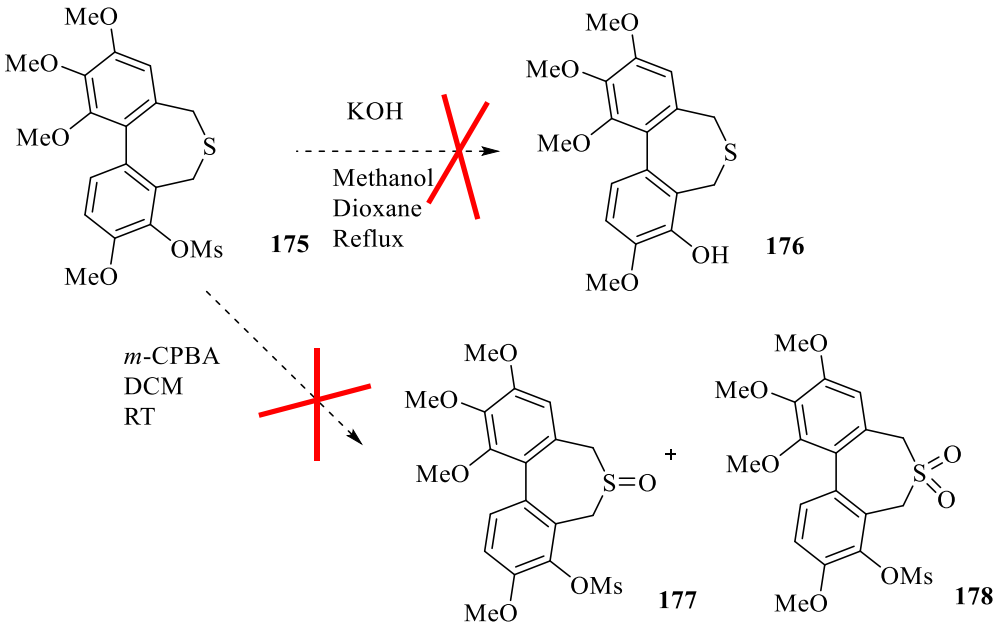

Scheme 98 Scheme showing the failed attempt to deprotect **(175)** to generate phenol (176). The failed oxidation of **(175)** to both thiepene oxide **(177)** and dioxide **(178)** is also described.

Synthesis of biaryl analogues

McNulty (McNulty *et al*. 2015) recently reported low µM from a simplified NAC/Combretastatin hybrid **(31)** with a similar methoxy substitution to Edward's (Edwards *et al*. 2011) oxepine analogues and CA-4 **(Fig 100).**

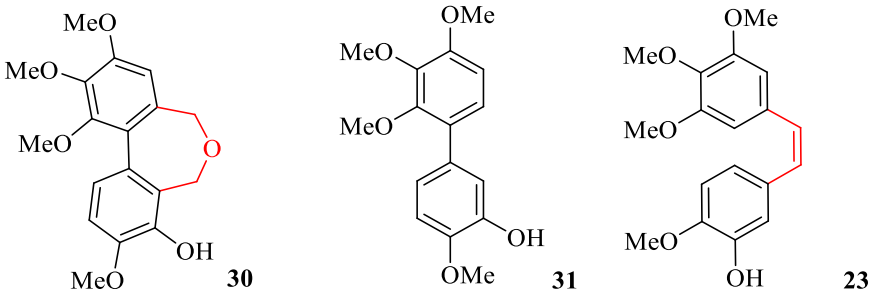

Figure 99 Diagram showing the similarities between Edwards Oxepine **(30)**, Mc Nulty's NAC/ Combretastatin hybrid **(31)** and CA-4 **(23)**

Based on McNulty's suggested pharmacophore (**31),** we synthesized and tested a simplified series of biaryls without a central heterocyclic ring. The molecules are analogous to dibenzoxepines and CA-4. They were also tested to further explore the colchicine pharmacophore.

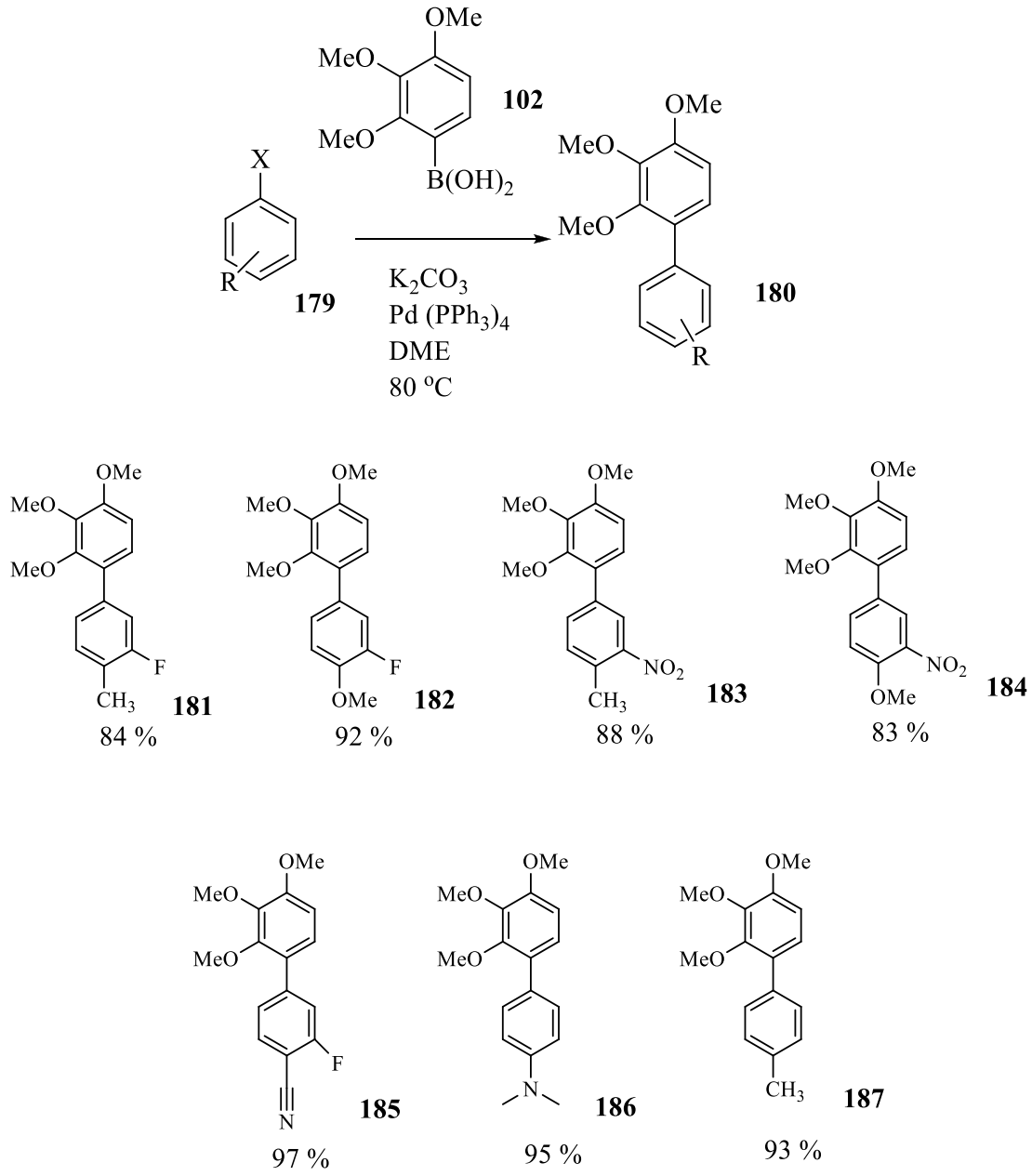

Figure 100 Diagram showing a general reaction scheme for the Suzuki coupling of aryl halides (179) with boronic acid (102). Molecules (181 to 187) show the series of simplified analogues synthesised for biological evaluation.

These compounds were synthesised via Suzuki coupling of the appropriate aryl halide (Br or I) with 2,3,4-trimethoxybenzeneboronic acid **(102)**. All reactions proceeded in excellent yield.

Chapter 5: Biological testing and results

Aim

The standard assays used to evaluate the *in vitro* biological activity of tubulin binding vascular targeting agents are the MTT (3-(4,5-dimethylthiazol-2-yl)-2,5-diphenyltetrazolium bromide) assay and tubulin binding assay. Combretastatin A-4 **(23)** was used as a standard so that the data obtained for tested compounds could be compared with that of existing antivascular compounds in the literature. All of the compounds synthesised will were tested using both the MTT and microtubule assembly assays.

Introduction

Introduction: MTT assay

The library of synthesized target compounds was screened first using the MTT assay. This measures a targets ability to inhibit cell growth. For this assay, the K562 (human chronic myelogenous leukaemia) cell line was used as it is widely reported (Edwards *et al*. 2011; Gaukroger *et al*. 2003a; McNulty *et al*. 2015) in the literature for screening anti-cancer compounds.

In the standard procedure the candidate compound was diluted in DMSO to a sub molar range (commonly 5 µM, 500 nM and 50 nM) and appropriate cells diluted to required concentration (usually 3000 cells/mL) in 10% Feotal Calf Serum (FCS) in RPMI (Roswell Park Memorial Institute) media. The drug in solution was added to cell solution causing a 1000 fold dilution in drug concentration. A series of 1:1 dilutions were carried out to give in total seven drug concentrations. A control consisting of the media without the drug was prepared to allow the validation of any growth inhibition observed in treated cells. The dosed cells were then incubated for 5 days at 37 ^{o}C in a 5% carbon dioxide in air atmosphere.

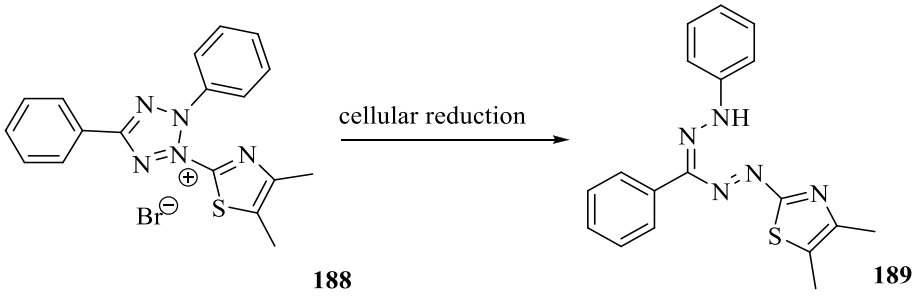

188 189

Scheme 101 A scheme showing the reduction of MTT **(188)** to its corresponding formazan **(189).**

After the incubation period, a solution of MTT (3-(4,5-dimethoxythiazol-2-yl)-2,5-diphenyltetrazolium bromide **(188)** in Phosphate-buffered serum (PBS) was added to each well and the plate incubated for a further 3 hours. The assay is colourimetric in that the yellow MTT reagent is biochemically reduced to a purple formazan **(189)** precipitate by the mitochondrial succinate dehydrogenase enzyme present in living cells **(Fig 102)**.

After the 3 hours the precipitate was removed from the medium and redissolved in DMSO. The extent of cell growth is directly proportional to the intensity of colour, which was determined by measuring the optical density of the solutions using a UV/Vis spectrometer (λ-540 nm). The measured intensity of the control sample is representative of zero cell growth inhibition or 100% growth. Since the control was not treated with drug, this can be compared against the intensities for the cells treated with drug - this allows the determination of cell growth inhibition. As the degree of cell growth inhibition is determined for a range of concentrations for the tested compound, a graph of percentage growth inhibition versus concentration can be plotted.

MTT data is usually presented as an IC_{50} value in the literature. This is the drug concentration which inhibits cell growth by 50%.

Introduction: Tubulin extraction

Tubulin was obtained using a standard extraction procedure involving a two stage polymerisation/depolymerisation method (Williams and Lee. 1982)**.** Tubulin is a dynamic protein that assembles in the presence of GTP at 37 ^{o}C to form microtubules and disassembles when cooled below this temperature or in the presence of Ca^{2+} ions to tubulin heterodimers. This dynamic property is exploited by cycling the crude protein mix through cycles of assembly/disassembly collecting sequentially purified tubulin.

The most readily available source of tubulin is the mammalian brain and nervous system. Cows are the most obvious choice as they have the highest level of tubulin and are farmed for their meat. Unfortunately issues surrounding CJD regulation have all but banned the use of bovine tubulin and when extracted from sheep, the protein has been found to lose its functional activity during storage. For our studies porcine tubulin was used. Roughly 30 brains were acquired and transported in ice to avoid protein degradation. The brains were washed and blended in a buffer giving a slurry that was subjected to centrifugation at 4 ^{o}C to remove cellular debris. After the supernatant layer was removed, addition of GTP followed by incubation at 37 ^{o}C caused polymerisation of the tubulin subunits into microtubules.

Centrifugation of these microtubules at 37 ^{o}C formed pellets that were suspended in fresh buffer. Cooling this solution to 4 ^{o}C again caused depolymerisation of the microtubules into α,β-tubulin dimers.

After further centrifugation the tubulin-containing supernatant was removed and incubated at 37 ^{o}C with GTP again inducing formation of microtubules. The resulting pellet was once again acquired by centrifugation and subsequently homogenised in buffer to give a solution rich in protein. This liquid was added dropwise to liquid nitrogen yielding beads of purified tubulin that were stored in at -80 ^{o}C until required.

Introduction: Microtubule functional assay

The tubulin functional assay was performed to find out if the extracted tubulin dimers were above the concentration required to form microtubules. This requires the optical density of the microtubules to be greater than that of the unpolymerised tubulin. Samples consisted of tubulin, 2-(N-morpholino)ethanesulfonic acid (MES buffer) and GTP prepared in a quartz cuvette at 0 ^{o}C. As the GTP initiates polymerisation of tubulin, it was added in last to prevent any premature tubulin assembly before the experiment began. The cuvettes were placed in the spectrophotometer and heated to 37 ^{o}C. As the temperature increases, so should tubulin polymerization, causing an increase in optical density.

The change in optical density can be monitored and recorded using a spectrophotometer. Control experiments containing identical samples as before without GTP were also performed to rule out other temperature-dependant effects.

Introduction: Quantification of protein

The tubulin concentration in the purified protein solution was determined by the standard spectroscopic methods used by Williams (Williams and Lee. 1982). Guanidine hydrochloride was added to the solution and the absorbance value at 275 nm measured. This induces denaturation of tubulin, exposing the polypeptide chains so that the absorbance can be measured and the molar extinction coefficient and concentration can be calculated.

Introduction: Microtubule Assembly Assay

This assay measures a target compound's ability to inhibit microtubule formation through tubulin assembly. The assay bears similarity to the functional assay differing in that compound being tested is added before the GTP. The overall stock concentration for all tested compounds was chosen to be 10 μM. The samples were analysed in the spectrophotometer as before at 37 ^{o}C. If the optical density for the drug containing sample was less than 50% of the control the experiment was repeated at sequentially decreasing drug concentrations until the IC_{50} could be calculated.

Results and discussion

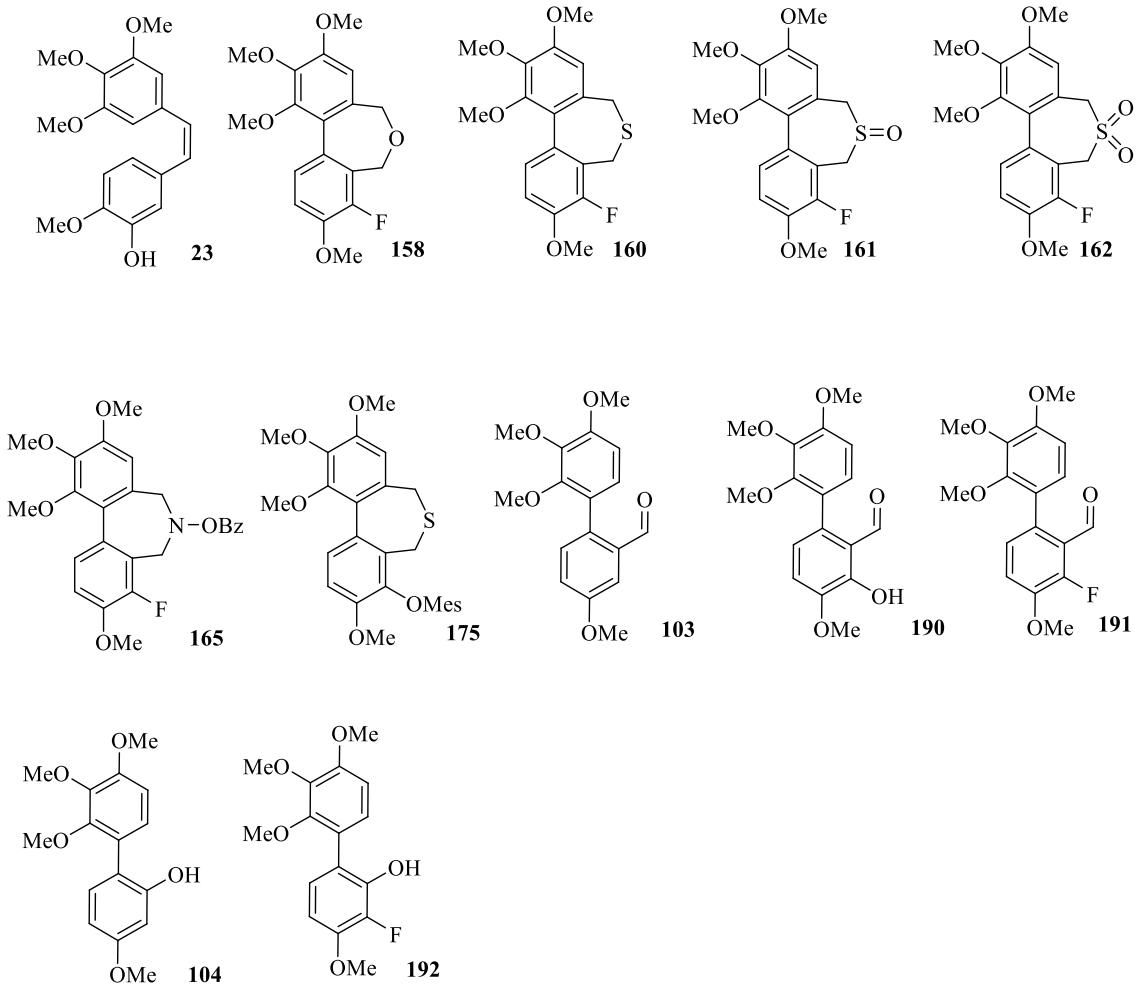

Figure 102 Scheme showing a series of tubulin binding agents that were tested for cytotoxicity.

These compounds **(Fig 103)** have all been subjected to the MTT assay using K562 cells. The results are summarised in **Fig 104.**

Compound	**K562** **IC_{50} (µM)**
23	0.00053
103	>500
104	>500
151	>500
158	0.060
160	>500
162	>500
165	>500
175	>500
190	>500
191	>500
192	>500

Table 103 Table showing the IC_{50} values in µM for all of the compounds tested with the MTT assay against K562 myelogenous leukaemia cells compared to CA-4 as a standard.

From the compounds screened one entry was carried on for the tubulin binding assay. Compound (**158)** is highly cytotoxic with an IC_{50} value in the low nanomolar range (60 nM).

Compound	Microtubule assembly assay (μM)
23	1.3
158	1.2
160	>10
151	>10
162	>10
165	>10
175	>10
103	>10
190	>10
191	>10
104	>10
192	>10

Table 104 Table showing the IC_{50} values in μM for the compounds tested with the tubulin binding assay compared to CA-4 as a standard.

Discussion

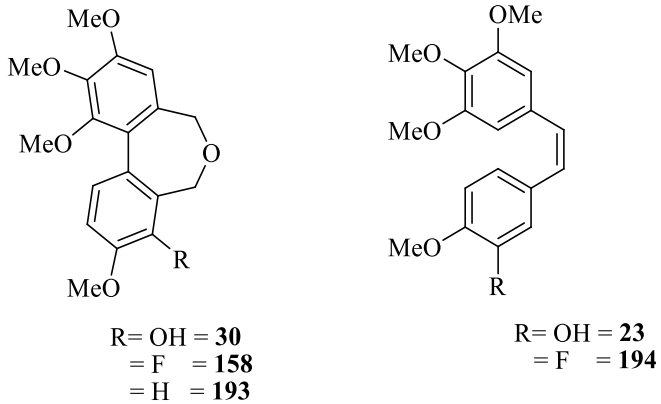

R= OH = **30**
= F = **158**
= H = **193**

R= OH = **23**
= F = **194**

Figure 105 Scheme showing the basic structure of dibenz[*c*,*e*]oxepines and combretastatin A4 .

The most active compound was **(158)** in both MTT (K562, 60 nM) assay and MA (1.2 µM). This is slightly less active than the hydroxyl analogue **(30)** (MTT k562- 44 nM, MA – 1.0 µM) reported by Edwards. Interestingly this activity profile occurs with CA-4 **(23)** and its fluoro analogue **(194).** Replacing the phenol group on **(30)** with a fluorine group **(158)** in the oxepine series **(fig 105)** results in a slightly lower inhibitory activity in the MTT assay (0.001 to 0.01 µM) but an increase in MA inhibition (0.175 µM to 0.085 µM). The difference in cytotoxicity may be due to the extra degree of rotational freedom in CA-4 opposed to the oxepine analogues. This is due to the oxepine compounds being conformationally restricted by both the tethered heteroatom containing B ring and the dihedral biaryl bond. The oxepine where R = H **(193)** also exhibits significant cytotoxicity (130 nM) (Edwards *et al*. 2011).

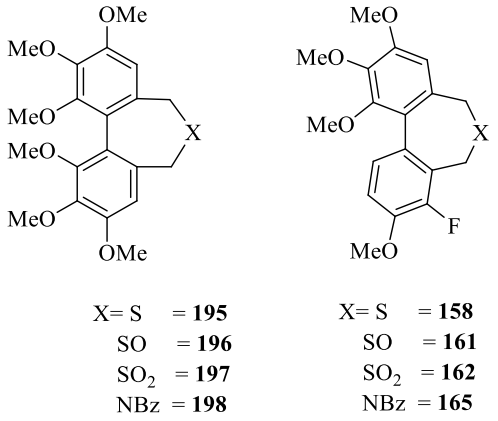

Figure 106 Diagram showing the two series of biaryl compounds with a central 7-membered heterocyclic ring where X is various heteroatom groups Listed. The symmetrical series (left) was published by Edwards **(Edwards *et al*. 2011)**and is analogous to the unsymmetrical fluorinated series

Compounds **(195 - 198)** were also reported by Edwards (Edwards *et al*. 2011). They all had poor activity (MTT - IC_{50} > 500 µM, MA- IC_{50} > 10 µM). The fluorinated dibenzo[*c,e*]oxepines series (**158, 161, 162, 65)** of compounds were synthesised with a pseudo-combretastatin lower ring in an attempt to induce activity and test the effect of heteroatom substitution on the 7 membered central ring (**Fig 107)**. All of the compounds were inactive in both MTT and MA assays.

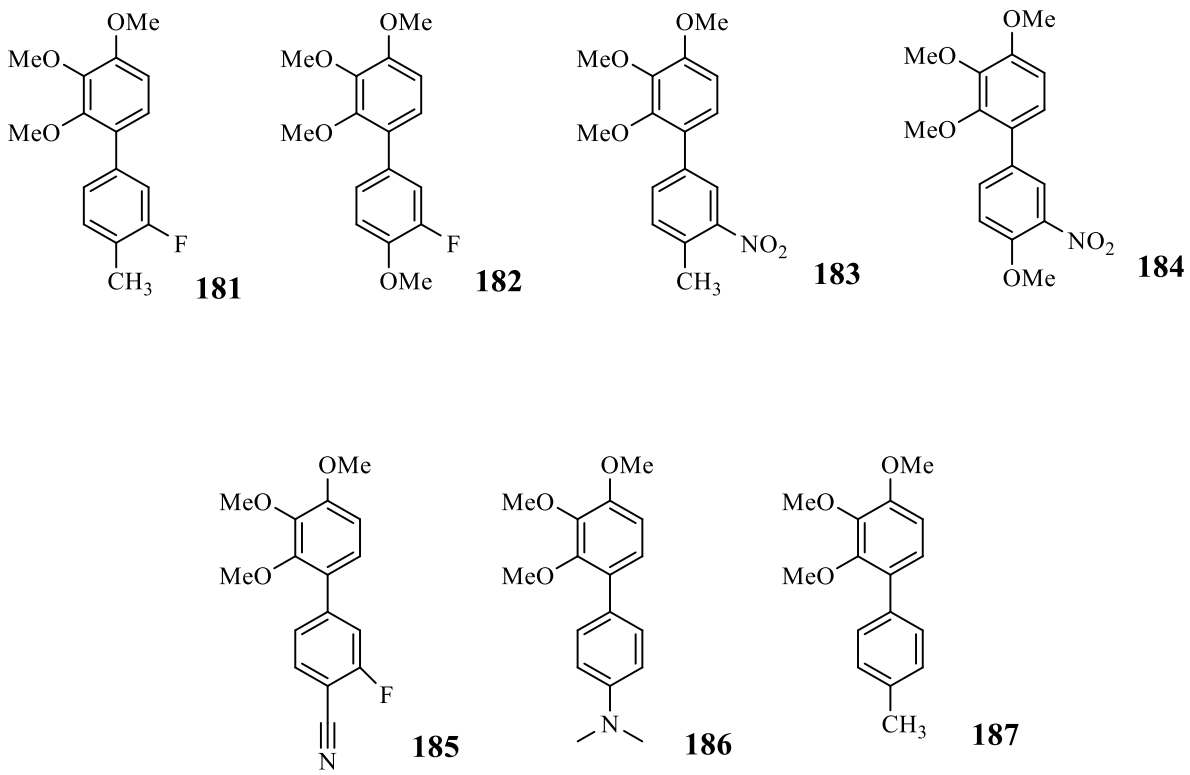

Figure 107 Diagram showing a series of simplified biaryl combretastatin analogues that were for cytotoxicity

All of these compounds (**Fig 108)** have all been subjected to the MTT assay tested on A2780 cells, compounds with IC_{50} values less than 10 µM were subjected to further testing with SAOS-2 and K562 cell lines (**Table 109**).

Compound	A2780 IC_{50} (µM)
23	0.0037
181	60.24
182	2.15
183	3.73
184	35.91
185	58.56
186	47.53
187	78.24

Table 108 Table showing the IC_{50} values in for a the compounds that were tested with the MTT assay against A2780 human ovarian cancer cells compared to CA-4 as a standard

Compounds **182** and **183** were selected for further testing on SAOS-2 and K562 cell lines (**Table 110**)

Compound	SAOS-2 IC_{50} (µM)	K562 IC_{50} (µM)
23	0.007	0.004
182	5.95	1.75
183	11.21	2.32

Table 109 Table showing the IC_{50} values for the compounds subjected to MTT testing on both K562 and SAOS-2 cell ines compared to CA-4 as a standard

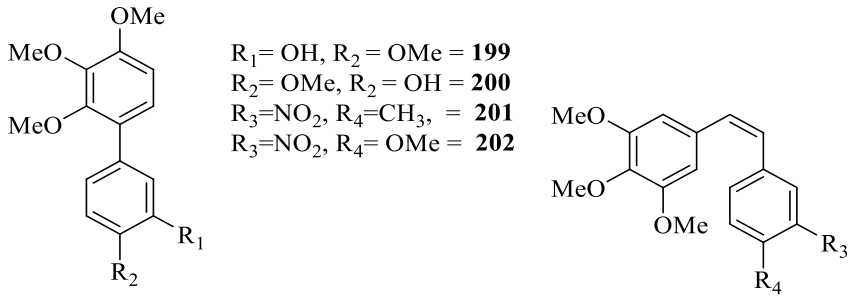

Figure 110 Diagram showing a general structure for both Cis CA4 analogues (R_3, R_4) and simplified biaryl analogues (R_1 and R_2)

For this simplified series of biaryls all of the B-rings were chosen as analogues of known active combretastatins (**111**). McNulty (McNulty *et al*. 2015) reported µM activity from the simplified CA-4 **(199-** IC_{50} = 5.43 µM, MTT SAOS-2 cells) and its regio isomer **(200 -** IC_{50} = 1.77 µM, MTT SAOS-2 cells). Replacing the OH in **(199)** with fluorine (**182**) causes a slight loss in cytotoxicity (5.43 to 5.72 µM). Making this substitution on the [*c,e*], oxepine (**Fig 105, 30, 158**) and CA-4 (**23, 194)** also causes a small reduction in activity (MTT K562 IC_{50} -44 to 60 nM and 1.0 to 10 nM respectively). The nitro containing compound **(183)** was also active in the low micromolar range (MTT -11.21 µM, MA - 2.32 µM). Interestingly when the methyl group is replaced by a methoxy **(184**) the compound is rendered inactive. This pattern of activity also occurs in CA-4 analogues. Changing the methoxy group in **(202)** to a methyl group **(201)** shows increased cytotoxicity (MTT on A2780, IC_{50} - 49 to 6.5 µM).

Biological experimental

Cell culture

A2780 and K562 cell lines were cultured in RPMI 1640 medium supplemented with 2 mM L-Glutamine and 1 0% (v/v) FBS (LabTech, UK). SAOS-2 cell line was cultured in Mc Coy's 5A medium (LabTech, UK) supplemented with 2mM L-Glutamine and 15% (v/v) FBS. Penicillin/Streptomycin (LabTech, UK) was added into media for MTT assay (1 mL per 100 mL of complete medium).

All cell lines were grown at 37˚C and 5% CO_2 in T25 cell culture flasks (Fisher, UK).

Experimental: MTT assay

All cell lines were grown to approximately 70-80% confluence before seeding into 96-well plates. For adherent cells flat bottomed 96-well plates were used and for suspension cells U-bottomed 96-well plates were used (Greiner Bio one, UK). Adherent cells were trypsinised as usual and re-suspended in complete growth medium. Suspension cells were centrifuged (1500 rpm for 5 min) and the cell pellet was re-suspended in complete growth medium. Next cells were counted with the use of haemocytometer slide (LabTech, UK). Cell viability tests were performed with the use of Trypan blue (0.4%) (Fluka, UK). Seeding density was as follows: for K562 2 x 10^3, for A2780: 3 x 10^3 and for SAOS-2: 1 x 10^4 viable cells per well in 100 µL of complete growth medium. After seeding the cells were incubated for 24 hr at 37 ^oC with 5% CO_2 before addition of 100 µL of media with an appropriate concentration of the tested compound.

The stock solutions of the compounds were prepared in DMSO (Fisher, UK) at around 20 mM concentration. Before MTT treatment combretastatin A-4 (CA-4) was further diluted in phosphate buffer saline (PBS) (Fisher, UK). The final concentration of DMSO in each of the wells was less than 0.2% (v/v) for each drug concentration. CA-4 was used as a control compound. Drug concentrations were prepared in 15 mL centrifuged tubes with a double final concentration (as to dose the cells, of drug solution (100 µL) was added to the well, each well already containing medium (100 µL) from the previous day) by serial dilution technique. The dosing was done in triplicate per drug concentration. Each plate had two triplicates of tested compound and one triplicate of a control compound. The cells were incubated for 72 hr at 37 ^{o}C with 5% CO_2.

After this period of time MTT ((3-[4,5-dimethylthiazol-2-yl]-2,5- diphenyltetrazolium bromide; thiazolyl blue), (50 µL) (Alfa Aesar, UK) solution (3 mg/mL in PBS) was added to each well. The plates were incubated for 3 h. Next the liquid above the created formazan crystals was aspirated. Then DMSO (200 µL per well) was added and the absorbances were read at 540 nm and at 690 nm as a reference (blank) wavelength on an MultiScan Ascent 384 microplate reader (Thermo Labsystems, UK). The average absorbance from triplicate experiments was obtained by subtraction of the blank readings from 540 nm readings. The mean absorbances were used for calculation of the percentage cell survival. Absorbance of negative control (cells growing in medium with no drug addition) was assumed as 100% cell survival.

Experimental: Quantification of extracted tubulin

Sample	Absorbance (λ = 275) nM
1	0.171
2	0.145
3	0.150
Average	0.155

Table 111 Table showing the measured absorbance (nM) for the purified tubulin solution.

$$\text{Tubulin concentration} = \frac{\text{Average absorbance at } \lambda = 275 \text{ X } 40}{\text{Extinction coefficient (mL/mg/cm)}}$$

$$= \frac{0.155 \text{ X } 40}{1.03}$$

$$= 6.03 \text{ mg/mL}$$

Experimental: Microtubule assembly assay

All samples were prepared at 0 ^{o}C in quartz cells. To each was added (in order): pH 6.6 Mes buffer (740 µL Mes (1 M)), 0.5 mM $MgCl_2$, 0.1 mM EGTA), drug compound (10 µL in DMSO (1 mM)), tubulin 150 µL, (1 in 4 dilution in Mes from neat) and finally GTP (100 µL, 100 mM). After thoroughly mixing and carefully drying the exterior of each cuvette they were placed in a UV-Vis (Varian Cary 1) that was preheated to 37 ^{o}C. A control cuvette containing DMSO (10 µL) in place of the drug compound was also used. The absorbance at 350 nM was measured for 20 minutes and the results compared with the control to assess relative change in optical density. If tubulin assembly for a compound was less than 50% of the control, the process was repeated at lower concentrations (at increments from 1 mM) of the candidate compound to determine the activity.

Chemistry Experimental

Solvents and reagents

Both dry THF and dry diethyl ether were obtained by distillation over sodium/benzophenone under argon as required. Dry DCM was prepared by storage in a sealed flask over activated 3Å molecular sieves.

Chromatography

Flash chromatography (Still *et al* 1978) was carried out using silica gel (Fluka 60 220-440 mesh 35-70 μm).

TLC chromatography was carried out on pre-coated silica plates (0.2 mm, 60 F_{254}) and observed using a UV lamp (254 nm).

^{1}H NMR

These spectra were obtained using a Bruker AC-400 MHz NMR machine for which $CDCl_3$ was used as the solvent (unless stated otherwise). Chemical shifts (δ_H) values are displayed in parts per million (ppm).

^{13}C NMR

These spectra were obtained using the above instrument at 100 MHz with $CDCl_3$ used as the solvent (unless stated otherwise). Chemical shifts (δ_C) are quoted in parts per million (ppm).

Infra Red

These sprectra were obtained on a Bruker vector 22 Diamond ATR. Absorbances of compounds of interest are reported as wave numbers (cm^{-1}).

Melting point

Melting points (M.p.) were recorded using a Gallenkamp melting point apparatus and were not corrected with standards

General Methods

General procedure 1

To a flask containing aryl iodide/bromide (1 eq), aryl boronic acid (1.3 - 1.5 eq), LiCl (2.95 eq) in dioxane (1 mL / mmol) was added aq Na_2CO_3 (2 M, 4 eq) and the solution degassed for 20 min and an argon atmosphere established. $Pd(PPh_3)_4$ (5 mol %) was added and the reaction heated at 80 ^oC. After 8 hr the reaction was cooled, filtered through celite®, washed with brine, dried with magnesium sulphate and concentrated *in vacuo*. The crude material was purified by column chromatography (silica gel, hexane - ethyl acetate)

General procedure 2

To a flask containing aryl bromide/iodide (1.7 mmol, 1 eq), arylboronic acid (1.9 mmol, 1.1 eq), tetra-*n*-butyl ammonium bromide (TBAB) (1.7 mmol, 1 eq) and K_2CO_3 (4.4 mmol, 2.5 eq) was added degassed water (4 mL) and the solution degassed with argon for 20 min. A reflux condenser was attached, $Pd(OAc)_2$ (0.2 mmol, 0.1 eq) added and the reaction mixture heated to 80 ^oC for 2 hr under an argon atmosphere. The reaction mixture was cooled to room temp, extracted with dichloromethane (2 X 10 mL), the organic layer was filtered through a plug of celite® (~1 g) and washed through with dichloromethane (2 X 20 mL). After drying with anhydrous magnesium sulphate the solution was concentrated under vacuum and purified by column chromatography (silica gel, hexane - ethyl acetate).

General procedure 3

To a round bottom flask with a quickfit neck containing a solution of *O*-benzyl ether (g, 1 eq) in methanol (2 mL/ *g*) was added 10% palladium on activated carbon (0.1 eq). A septum was added, the flask purged with hydrogen for 1 min and a hydrogen filled balloon attached to maintain pressure. After 2 hr stirring the solution was filtered through celite®, washed with dichloromethane (40 mL), concentrated *in vacuo* and purified by column chromatography (silica gel, hexane - ethyl acetate).

General procedure 4

To a round bottom flask with a quickfit neck containing a solution of *O*-benzyl ether (x, 1 eq) in methanol (2 mL/*g*) was added Pearlman's catalyst (0.2 eq). A septum was added, the flask purged with hydrogen for 1 min and a hydrogen filled balloon attached to maintain pressure. After 2 hr stirring the solution was filtered through celite®, washed with dichloromethane (40 mL), concentrated *in vacuo* and purified by column chromatography (silica gel, hexane - ethyl acetate).

General procedure 5

To a solution of phenyl/hydroxyl compound (g, 1 eq) in dichloromethane (2 mL/*g*) at 0 ^{o}was added *N*,*N*-diisopropylethylamine (2.2 eq). After 10 min at this temperature MOMCl (1.5 eq) was added dropwise and the reaction allowed to stir for 2 hours warming to room temp. The reaction was cooled to 0 ^{o}sat. aq NH_4Cl (10 mL/*g*) was added dropwise. The contents of the flask were separated and the aqueous phase was extracted twice with dichloromethane (2 X 10 mL/*g*). The organic extracts were then combined and washed with water (10 mL/ *g*), brine (10 mL/*g*), dried with anhydrous sodium sulphate, concentrated *in vacuo* and purified by column chromatography (silica gel, hexane - ethyl acetate).

General procedure 6

To a solution of alcohol (g, 1 eq) in dichloromethane (2 mL/*g*) under argon at 0 ^{o}2,6-lutidine (1.5 eq) was added followed by the dropwise addition of triethylsilyltrifluoromethane sulfonate (1.2 eq). The reaction mixture was stirred at 0 ^{o}C for 30 min and quenched with sat. aq $NaHCO_3$ (10 mL/*x*). The aqueous layer was extracted with dichloromethane (2 X 20 mL/*x g*), the combined organic extracts dried with magnesium sulphate, concentrated *in vacuo* and purified by column chromatography.

General procedure 7

Dry dioxane (2 mL/*g*) was a added to a screw cap vial containing aryl halide (*x*, 1 eq) palladium (II) acetate (0.2 eq) and 2-(dicyclohexylphosphino)biphenyl (0.4 eq) and the solution was degassed with argon for 20 min. Triethylamine (3 eq) was added dropwise followed by pinacol borane (2 eq) and the vessel backfilled with argon, sealed and heated at 80 ^{o}C for 1 hr. After cooling, sat. aq NH_4Cl (15 mL/*g*) was added dropwise followed by extraction with dichloromethane (2 X 10 mL/*x g*) drying with anhydrous magnesium sulphate and concentration *in vacuo*. The crude product was purified by column chromatography (silica gel, hexane - ethyl acetate).

3-(methanesulfonyl)-4,4',5',6'-tetramethoxybiphenyl-2,2'-dicarbaldehyde (36)

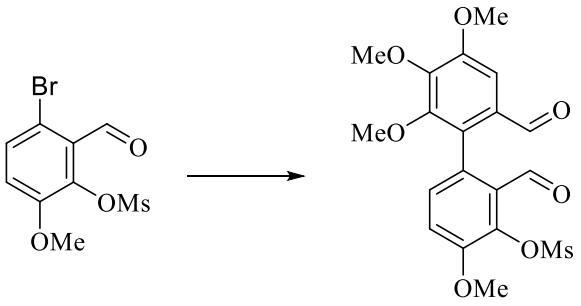

35 **36**

To a refluxing suspension of copper powder (0.65 g, 10 mmol, 1 eq) in dry DMF (2 mL), a solution of 3-bromo 2-formyl-6-methoxyphenyl methanesulfonate **(35)** (0.30 g, 0.10 mmol, 1 eq) and 2-bromo 3,4,5-trimethoxybenzaldehyde **(52)** (0.40 g, 0.15 mmol, 1.5 eq) in DMF (2 mL) was added dropwise. Another equivalent of 2-bromo-3,4,5-trimethoxybenzaldehyde in DMF (2 mL) was added after 2 hrs and the mixture allowed to stir at reflux for a further 1 hr. The reaction mixture was allowed to cool, was passed through a plug of celite® and concentrated *in vacuo*. The crude biaryl mixture was dissolved in diethyl ether (30 mL) and washed with water (4 X 20 mL), brine (50 mL), dried with anhydrous magnesium sulphate and concentrated *in vacuo*. The residue was purified by column chromatography (silica gel, petroleum ether - ethyl acetate, 9:1 to 1:1) to yield an orange semi-solid. Recystallisation from ethyl acetate gave the title compound **(36)** as red solid (0.14 g, 33%), m.p. 128 - 129 ^{o}C (Lit - 129 ^{o}C), TLC petroleum ether - ethyl acetate, 1:1, Rf = 0.23. The hexamethoxy homocoupled dialdehyde described by Edwards was also produced but not isolated.

^{1}H (400 MHz, $CDCl_3$) δ ppm: 10.20 (1H, s, CHO), 9.65 (1H, s, CHO), 7.38 (1H, s, Ar-H), 7.29 (1H, d, *J* = 8.5 Hz, Ar-H: *p*-OMs), 7.18 (1H, d, *J* = 8.5 Hz, Ar-H: *m*-OMes), 4.05 (3H, s, OMe), 4.01 (6 H, s, 2 X OMe), 3.59 (3H, s, OMe), 3.44 (3H, s, $SOOCH_3$)

Spectral and physical data for this compound were in accordance with the literature (Edwards *et al*. 2011).

2-Bromo 3,4,5-trimethoxybenzaldehyde (52)

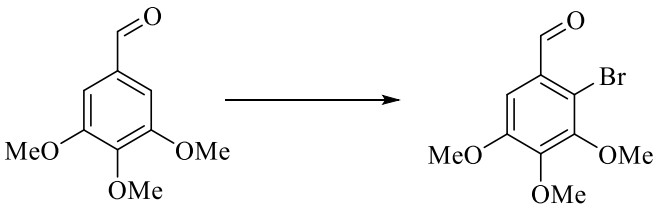

51 **52**

Bromine (4.7 mL, 9.2 mmol, 1 eq) was added dropwise to a stirring, refluxing solution of 3,4,5-trimethoxybenzaldehyde (17 g, 13.8 mmol, 1.5 eq) in chloroform (100 mL) and refluxed over night. The reaction mixture was allowed to cool followed by washing with water (100 mL), sat. aq $NaHCO_3$ (100 mL) and drying with anhydrous sodium sulphate, filtered and concentrated *in vacuo*. The crude orange oil produced crystallised on standing and purification by column chromatography (800 g silica gel, hexane - ethyl acetate, 8:1 to 6:1) gave the title compound as a pale yellow crystalline solid (16.3 g, 68%). M.p. 69 - 70 ^{o}C (Lit - 70 ^{o}C), TLC petroleum ether - ethyl acetate, 1:1, Rf = 0.29

^{1}H (400 MHz, $CDCl_3$) δ ppm: 10.42 (1H, s, CHO), 7.23 (1H, s, Ar-H), 4.02 (3H, s, OMe), 3.96 (3H, s, OMe), 3.95 (3H, s, OMe)

Spectral and physical data for this compound were in accordance with the literature (Edwards *et al*. 2011).

2-Iodo 3,4,5-trimethoxybenzaldehyde (52')

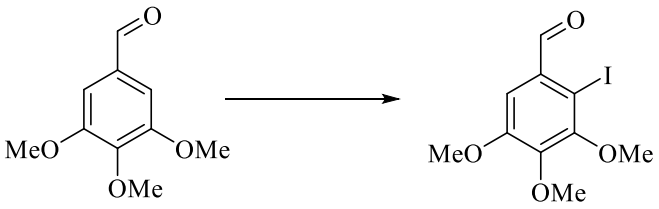

51 **52'**

To a solution of 3,4,5-trimethoxybenzaldehyde **(51)** (29.40 g, 150 mmol, 1 eq) in acetic acid: water: conc. H_2SO_4 (100/10/3, 700 mL) was added iodine (16.00 g, 63 mmol, 0.42 eq) followed by periodic acid (7.50 g, 33 mmol, 0.22 eq) and the reaction vessel warmed until homogeneity was achieved. The solution was heated to 65 ^oC for 4 hr with a rubber septum and balloon attached to the flask to retain vapours. After cooling to room temperature, solid sat. aq $Na_2S_2O_5$ (200 mL) was added resulting in the solution turning black, water (1 L) was added and the cream precipitate collected by filtration, washed with water and recrystallized from ethanol (100 mL) to yield the title compound **(52')** as a cream coloured solid (40 g, 83%), m.p. 67 -69 ^oC (Lit - 67 ^oC), TLC petroleum ether - ethyl acetate, 1:1, Rf = 0.21

^{1}H (400 MHz, $CDCl_3$) δ ppm: 10.05 (1H, s, CHO), 7.32 (1H, s, Ar-H), 3.95 (3H, s, OMe), 3.88 (3H, s, OMe), 3.86 (3H, s, OMe)

Spectral and physical data for this compound were in accordance with the literature (Nicolaus *et al*. 2009).

4-Bromo 2-fluoro 1-methoxybenzene (54)

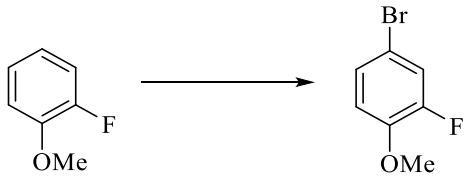

53 **54**

To a stirring, refluxing solution of 2-fluoroanisole **(53)** (73.82 g, 582 mmol, 1 eq) in chloroform (200 mL), bromine (45.3 mL, 877 mmol, 1.5 eq) was added dropwise and the reaction mixture was heated at reflux over night. After cooling, the reaction mixture was washed with water (100 mL), brine (100 mL), dried with anhydrous sodium sulphate and filtered. The solution was concentrated *in vacuo* to yield the title compound **(54)** as a brown liquid (101.25 g, 84.3%), TLC petroleum ether - ethyl acetate, 1:1, Rf = 0.28

^{1}H (400 MHz, $CDCl_3$) δ ppm: 7.15-6.98 (2H, m, Ar-H), 6.71 (1H, t, *J* = 8.95 Hz, Ar-H : *o* OMe), 3.75 (3H, s, OMe)

Spectral and physical data for this compound were in accordance with the literature (Kelly. 1984).

6-Bromo 2-fluoro 3-methoxybenzaldehyde (55)

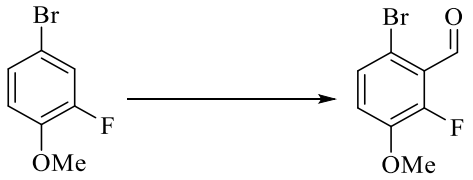

54 **55**

To a argon purged flask containing diisopropylamine (9.1 mL, 64.4 mmol, 1.3 eq), anhydrous THF (100 mL) was added and the temperature reduced to -78 ^{o}C. n-BuLi (50 mL, 1.6 M in hexane, 69.4 mmol, 1.4 eq) was added dropwise and the temperature increased to 0 ^{o}C for 30 mins. The temperature was reduced to -78 ^{o}C and 4-bromo 2-fluoro 1-methoxybenzene **(54)** (10 g, 49.6 mmol, 1 eq) in THF (50 mL) was added and the mixture stirred for 1 hr. DMF (10 mL, 99.2 mmol, 2 eq) and the reaction mixture was warmed to room temperature and stirred at room temperature for 1 hr. The reaction was quenched with sat. aq NH_4Cl solution (10 ml), and extracted with ethyl acetate (2x50 mL). The organic phase was washed with water (100 mL), brine (100 mL), dried with anhydrous sodium sulphate, filtered and concentrated *in vacuo*. This yielded a dark red oil that crystallized on standing to give an orange solid. Recrystallisation (5:1 hexane: ethyl acetate) gave the title compound **(55)** as an orange solid (8.2 g, 71%). M.p. 81 - 82 ^{o}C (Lit - 82 ^{o}C), TLC petroleum ether - ethyl acetate, 1:1, Rf = 0.24

^{1}H (400 MHz, $CDCl_3$) δ ppm: 10.12 (1H, s, CHO), 7.21 (1H, dd, *J* = 1.89, 8.88 Hz, Ar-H : *p*-F), 7.13 (1H, t, *J* = 8.72 Hz, Ar-H : *m*-F), 3.82 (3H, s, OMe)

Spectral and physical data for this compound were in accordance with the literature (Jarnagin and Akama. 2011).

3-Fluoro 4,4',5',6'-tetramethoxy-[1,1'-biphenyl]-2,2'-dicarbaldehyde (56)

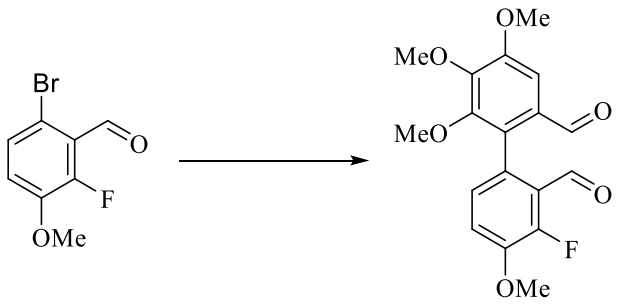

55 **56**

Anhydrous DMF (150 mL) was added to an argon-purged flask containing 2-bromo-3,4,5-trimethoxybenzaldehyde **(52)** (6.31g, 22.98 mmol, 1 eq), 2-bromo 5-methoxy-6-fluorobenzaldehyde **(55)** (5.35 g, 22.98 mmol, 1 eq) and powdered copper (14.61 g, 229.8 mmol, 10 eq). The mixture was heated at 170 ^{o}C overnight. The mixture was cooled, diluted with ethyl acetate (100 mL) and washed through a plug of celite® (50 g) with water (100 mL). The organic layer was washed with brine (100 mL) and concentrated *in vacuo*. The crude brown oil produced was purified using 3 bouts of column chromatography (9:1, 1:1 and 3:7 hexane : ethyl acetate respectively) to give the title compound **(56)** as a white solid (1.76 g, 22%) M.p 161 ^{o}C TLC petroleum ether - ethyl acetate, 1:1, Rf = 0.25

^{1}H (400 MHz, $CDCl_3$) δ ppm: 10.14 (1H, s, CHO), 9.52 (1H, s, CHO), 7.27 (1H, s, Ar-H), 7.15 (1H, t, *J* = 8.22 Ar-H : *m*-F), 6.92 (1H, dd, *J* = 1.45, 8.32 Hz Ar-H : *p*-F), 3.92 (3H, s, OMe), 3.90 (3H, s, OMe), 3.89 (3H, s, OMe), 3.51 (3H, s, OMe)

^{13}C δppm: 190.1 (CHO), 187.9 *(d, J* = 7.31 Hz, CHO), 155.5-150.8 (*bd, J* = 247.92 Hz, c-F), 153.6 (Ar-OMe), 150.8(OMe), 148.2 (d, *J* = 2.07 Hz, Ar-OMe:*o* CF), 148.1 (Ar-OMe), 147.2 (Ar), 130.4 (Ar), 128.3 (d, *J* = 4.48 Hz, Ar-H) 126.3 (Ar), 124.3 (d, *J* = 3.92 Hz, Ar-H). 117 (d, *J* = 3.61 Hz, Ar), 105.7 (Ar-H), 61.1(OMe), 60.8 (OMe), 56.5 (OMe), 56.1 (OMe)

***Amax cm^{-1}*:** 2947, 2793, 2710, 1745, 1711, 1616, 1487, 1414, 1367, 1326, 1272, 1131, 1110, 1026, 871

(E)-N-(6-bromo 2-fluoro 3-methoxybenzylidene)cyclohexanamine (58)

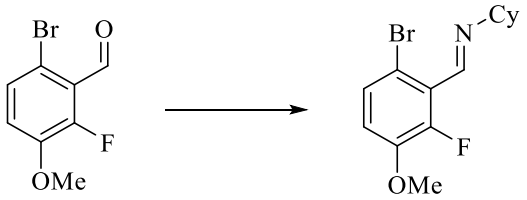

55 **58**

To a flask containing 6-bromo 2-fluoro 3-methoxybenzaldehyde **(55)** (4.0 g, 17.2 mmol, 1 eq) in methanol (20 mL), cyclohexylamine (1.70 g, 17.2 mmol, 1 eq) was added and the solution stirred at room temperature for 4 hr. The precipitate recovered by filtration and washing several times with methanol. The crude solid was recrystallized from methanol and dried to yield title compound **(58)** (3.60 g, 67%) as a white solid. M.p. 162 – 163 ^{o}C (Lit – 162 ^{o}C), TLC petroleum ether - ethyl acetate, 1:1, Rf = 0.26

^{1}H (400 MHz, $CDCl_3$) δ ppm: 8.31(1H, s, HC=NCy), 7.22 (1H, dd, *J* = 9.11, 2.27 Hz, Ar-H : *p*-F), 6.77 (1H, t, *J* = 8.47 Hz, Ar-H), 3.80 (3H, s, OCH_3), 3.22- 3.17 (1H, m, C-H), 1.79-170 (4 H, m, 2 x CH_2), 1.59- 1.48 (6 H, m, 3 x CH_2)

Spectral and physical data for this compound were in accordance with the literature (Ziegler *et al*. 1980).

2-Iodo 3,4,5-trimethoxybenzaldehyde cyclohexylimine (59)

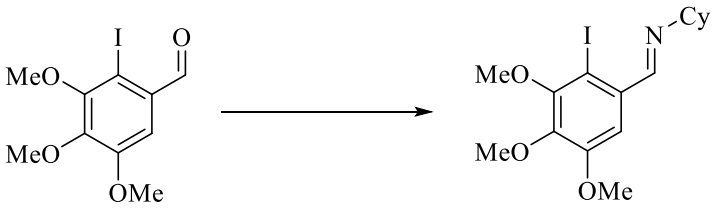

52' **59**

A solution of 2-iodo 3,4,5-trimethoxybenzaldehyde **(52')** (6.13 g, 19 mmol, 1 eq) and cyclohexylamine (2.18 mL, 19 mmol, 1 eq) in anhydrous toluene (50 mL) was heated at 120 °C under argon in a standard Dean Stark apparatus for 4 h. Dichloromethane (40 mL) was added to aid solvent removal and the reaction mixture concentrated *in vacuo*. This yielded the title compound **(59)** as brown oil (7.76 g, 100%), TLC petroleum ether - ethyl acetate, 1:1, Rf = 0.21

^{1}H (400 MHz, $CDCl_3$) δ ppm: 9.98 (1H, s, N=CH), 7.28 (1H, s, Ar-H), 3.90 (3H, s, OCH_3), 3.85 (3H, s, OCH_3), 3.84 (3H, s, OCH_3), 3.21-3.16 (1H, m, C-H : =N-$CH(CH)_2$, 1.78- 1.69 (4 H, m, 2 x CH_2), 1.60- 1.49 (6 H, m, 3 x CH_2)

Spectral and physical data for this compound were in accordance with the literature (Broady *et al*. 2007).

2-(2-Bromo 3,4,5-trimethoxyphenyl)-1,3-dioxolane (60)

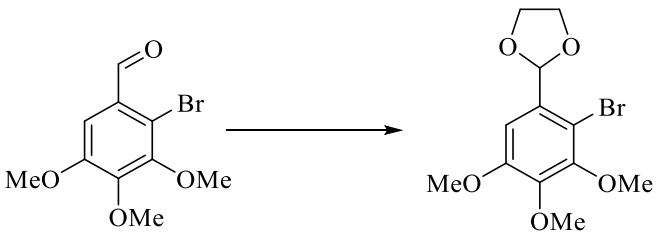

52 **60**

To a flask containing 2-bromo 3,4,5-trimethoxybenzaldehyde **(52)** (0.74 g, 2.6 mmol, 1 eq) absolute ethanol (10 mL) was added. Triethylorthoformate (0.52 mL, 3.2 mmol, 1.2 eq), ethylene glycol (1.00 mL, 11 mmol, 4 eq) and Tetrabutylammoniumtribromide (0.08 g, 0.01 mmol, 6 mol %) were also added and the reaction mixture allowed to stir at room temperature for 30 minutes. The reaction mixture was concentrated *in vacuo*. This was followed by extraction with ethyl acetate (10 mL) and washing with sat. aq $NaHCO_3$ (10 ml). After this the solution was dried with anhydrous sodium sulfate filtered and concentrated *in vacuo* to yield the crude oil product. Column chromatography (20 g silica gel, hexane - ethyl acetate, 1:1) produced the purified title compound **(60)** as a light brown oil that solidified on standing (0.84 g, 87%), m.p. 39 ^{o}C (Lit - 39 ^{o}C), TLC petroleum ether - ethyl acetate, 1:1, Rf = 0.24

^{1}H (400 MHz, $CDCl_3$) δ ppm: 7.01 (1H, s Ar-H), 5.72 (1H, s, C-H : Ar-CH), 4.22- 4.15 (2H, m, CH_2) 4.02- 3.97 (2H, m, CH_2), 3.83 (3H, s, CH_3), 3.74 (3H, s, OMe), 3.65 (3H, s, OMe)

Spectral and physical data for this compound were in accordance with the literature (Besong *et al*. 2008).

2-(Tributylstannyl)-3,4,5-trimethoxybenzaldehyde (63)

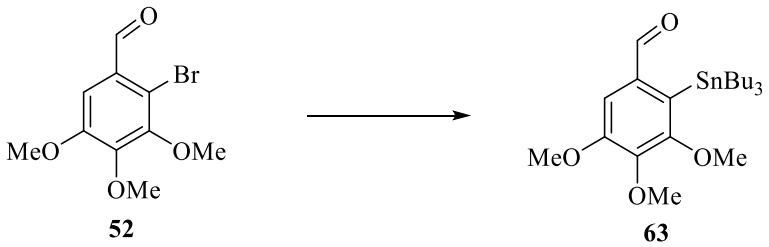

To a flask containing 2-bromo 3,4,5-trimethoxybenzaldehyde **(52)** (0.371 g, 1.3 mmol, 1 eq) in toluene (15 mL), hexabutylditin (0.905 g, 1.6 mmol, 1.2 eq) was added and the solution degassed with argon for 10 min. $Pd(PPh_3)_4$ (0.750 g, 0.65 mmol, 0.5 eq) was added and the reaction mixture heated at refluxed under argon for 48 hrs. After cooling the solvent was removed *in vacuo* and the crude mixture was purified by column chromatography (10 g silica gel, hexane - ethyl acetate, 11:1) to give the title compound **(63)** as a colourless oil. (4.54 g, 74%), TLC petroleum ether - ethyl acetate, 1:1, Rf = 0.20

^{1}H (400 MHz, $CDCl_3$) δ ppm: 9.82 (1H, s, CHO), 7.27 (1H, s, Ar-H), 3.92 (3H, s, OMe), 3.89 (3H, s, OMe), 3.88 (3H, s, OMe), 1.71 - 1.25 (18 H, m, 3 X Sn-$CH_2CH_2CH_2$-), 0.89 (9 H, t, *J* = 7.21 Hz, 3 X butyl: CH_3)

Spectral and physical data for this compound were in accordance with the literature (Labruere *et al*. 2012)

(2-Iodo 3,4,5-trimethoxyphenyl)methanol (64)

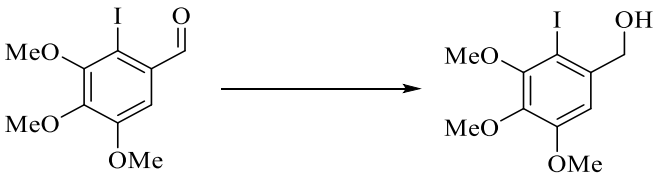

52' **64**

To a solution of 2-iodo 3,4,5-trimethoxybenzaldehyde **(52')** (1.00 g, 3.1 mmol, 1 eq) in methanol (5 mL) at 0 ^{o}C $NaBH_4$ (0.18 g, 4.6 mmol, 1.5 eq) was added in portions over 5 min. After 1 hr water (5 mL) was added dropwise and the reaction mixture extracted with dichloromethane (2 X 10 mL). The organic phase was washed with sat. aq $NaHCO_3$ (10 mL), water (10 mL), brine (10 mL), dried with anhydrous magneisium sulphate and concentrated *in vacuo*. The crude product was further purified by column chromatography (10 g silica gel, hexane - ethyl acetate, 8:2) to yield the title product **(64)** as a white low melting solid (0.910 g, 90%), m.p 53-54 ^{o}C (Lit – 53 - 54 ^{o}C), TLC petroleum ether - ethyl acetate, 1:1, Rf = 0.23

^{1}H (400 MHz, $CDCl_3$) δ ppm: 6.87 (1H, s, Ar-H), 5.15 (2H, s, Ar-CH_2), 3.82 (3H, s, OMe), 3.81 (6 H, s, 2 X OMe), 3.01 (1H, s, OH)

Spectral and physical data for this compound were in accordance with the literature (Ruiz *et al*. 2005).

1-Iodo 6-triethylsilyloxymethyl-2,3,4-trimethoxybenzene (65)

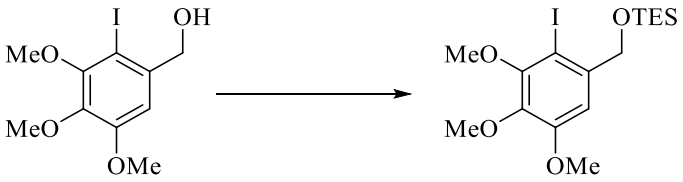

64 **65**

General procedure 6

The crude product was further purified by column chromatography (10 g silica gel, hexane - ethyl acetate, 8:2) to yield the title product **(65)** as a colourless oil (0.295 g, 81%), TLC petroleum ether - ethyl acetate, 1:1, Rf = 0.21

^{1}H (400 MHz, $CDCl_3$) δ ppm: 7.05 (1H, s, Ar-H), 4.63 (2H, s, CH_2), 3.88 (3H, s, OMe), 3.86 (3H, s, OMe), 3.84 (3H, s, OMe), 1.01 (9 H, t, *J* = 7.81 Hz, TES: 3 X CH_3), 0.70 (6 H, q, *J* = 7.81 Hz, TES: 3 X CH_2)

Spectral and physical data for this compound were in accordance with the literature (Baudoin *et al*. 2003).

Triethyl(3,4,5-trimethoxy-2-(4,4,5,5-tetramethyl-1,3,2-dioxaborolan-2-)benzyloxy)silane

(66)

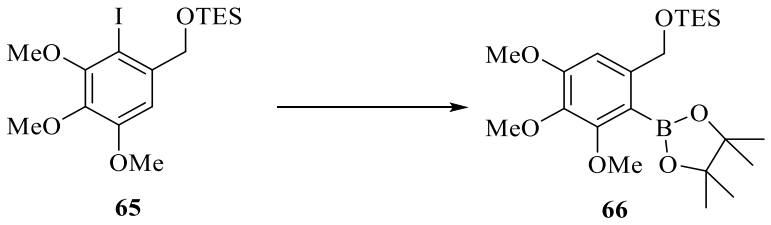

65 **66**

General procedure 7

The crude product was further purified by column chromatography (10 g silica gel, hexane - ethyl acetate, 11:1) to yield the title product as a colourless oil **(66)** (0.230 g, 72%), TLC petroleum ether - ethyl acetate, 1:1, Rf = 0.28

^{1}H (400 MHz, $CDCl_3$) δ ppm: 6.94 (1H, s, Ar-H), 4.77 (2H, s, Ar-CH_2) 3.88 (3H, s, OMe), 3.87 (3H, s, OMe), 3.85 (3H, s, OMe), 1.38 (12H, s, BPIN: 4 X CH_3) 0.99 (9 H, t, *J* = 7.97 Hz, TES: 3 X CH_3), 0.64 (6 H, q, *J* = 7.97 Hz, TES: 3 X CH_2)

Spectral and physical data for this compound were in accordance with the literature (Baudoin *et al*. 2003).

2-Iodo 3,4,5-trimethoxy-1-((methoxymethoxy)methyl)benzene (67)

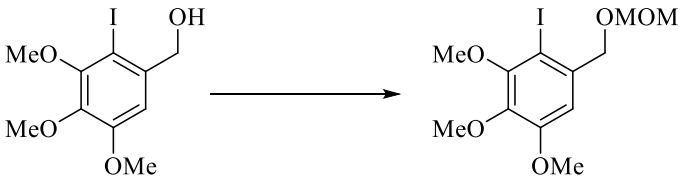

64 **67**

General procedure 5

The crude product was further purified by column chromatography (10 g silica gel, hexane - ethyl acetate, 7:3) to yield the title product as a colourless oil **(67)** (0.300 g, 92%), TLC petroleum ether - ethyl acetate, 1:1, Rf = 0.28

^{1}H (400 MHz, $CDCl_3$) δ ppm: 6.64 (1H, s, Ar-H), 4.57 (2H, s, O CH_2OMe), 4.57 (2H, s, $ArCH_2$- O), 3.80 (3H, s, OMe), 3.79 (3H, s, OMe), 3.78 (3H, s, OMe), 3.66 (3H, s, OMe)

Spectral and physical data for this compound were in accordance with the literature (Baudoin *et al*. 2003).

4,4,5,5-Tetramethyl-2-(2,3,4-trimethoxy-6-((methoxymethoxy)methyl)phenyl)-1,3,2-dioxaborolane (68)

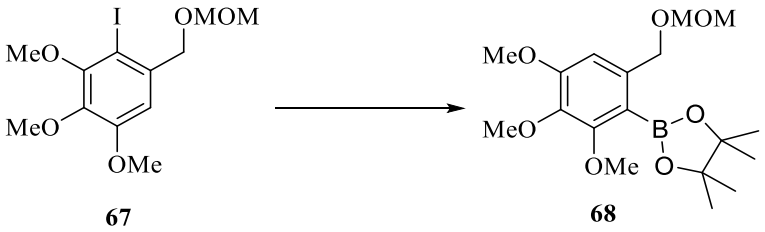

67 **68**

General procedure 7

(10 g silica gel, hexane - ethyl acetate, 9:1) to yield a brown oil (0.710 g, ~ 66%) as a 3:1 inseparable mixture of the product **(68)** and dehalogenated starting material (by NMR), TLC petroleum ether - ethyl acetate, 1:1, Rf = 0.23

^{1}H (400 MHz, $CDCl_3$) δ ppm: 6.63 (1H, s, Ar-H), 4.59 (2H, s, O CH_2-OMe), 4.51, (2H, s, Ar-CH_2-OMOM), 3.80 (3H, s, OMe), 3.79 (3H, s, OMe), 3.77 (3H, s, OMe), 3.63 (3H, s, OMe), 1.31 (12H, s, BPIN)

Spectral and physical data for this compound were in accordance with the literature (Baudoin *et al*. 2003).

2-Iodo 5-methoxybenzaldehyde (70)

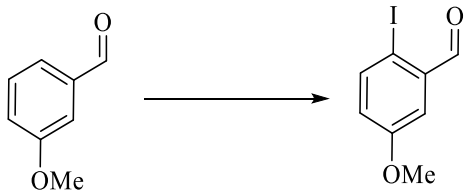

69 **70**

To a solution of 3-methoxybenzaldehyde **(69)** (6.38 g, 46 mmol, 1 eq) in glacial acetic acid: water: conc. H_2SO_4 (100/10/3, 350 mL) was added iodine (5.00 g, 20 mmol, 0.42 eq) followed by periodic acid (2.35 g, 10 mmol, 0.22 eq) and the reaction vessel warmed until homogeneity was achieved. The solution was heated to 65 ^oC for 4 hr with a rubber septum and balloon attached to the flask to retain vapours. After cooling to room temperature sat. aq $Na_2S_2O_5$ (75 mL) was added resulting in the solution turning black, water (400 mL) was added and the cream precipitate collected by filtration, washed with water and recrystallized from ethanol (40 mL) to yield the title compound **(70)** as a cream coloured solid (12.26 g, 83%), m.p 112-113 ^oC (Lit – 112 ^oC), TLC petroleum ether - ethyl acetate, 1:1, Rf = 0.23

^{1}H (400 MHz, $CDCl_3$) δ ppm: 10.98 (1H, s, CHO), 7.78 (1H, d, *J* = 8.5 Hz, Ar-H : *o* CHO), 7.40 (1H, d, *J* = 3.2 Hz, Ar-H : *p*-CHO), 6.98 (1H, dd, *J* = 2.7, 8.3 Hz, Ar-H : *o* I), 3.58 (H, s, OMe)

Spectral and physical data for this compound were in accordance with the literature (Leboeuf *et al*. 2013).

Methyl 2-(3,4,5-trimethoxyphenyl)acetate (73)

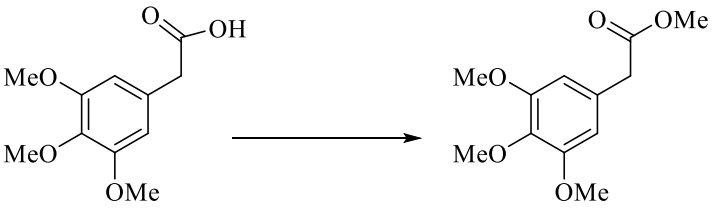

72 **73**

To a round bottom flask containing 2-(3,4,5-trimethoxyphenyl)acetic acid **(72)** (10 g, 44.2 mmol, 1 eq) in methanol (50 mL), H_2SO_4 (5 drops) was added and the reaction mixture stirred at 80 ^oC for 4 hrs. The reaction was allowed to cool followed by the addition of sat. aq $NaHCO_3$ (5 mL). The mixture was extracted with ethyl acetate (2X100 mL) and the organic extracts washed with water (100 mL), dried with anhydrous sodium sulphate, filtered and concentrated *in vacuo* to give the title compound **(73)** as yellow oil (10.16 g, 96%), TLC petroleum ether - ethyl acetate, 1:1, Rf = 0.25

^{1}H (400 MHz, $CDCl_3$) δ ppm: 6.81 (2H, s, Ar-H), 3.8, (6 H, s, OMe), 3.75, (3H, s, OMe), 3.61 (3H, s, $COCH_3$), 3.49 (2H, s, CH_2)

Spectral and physical data for this compound were in accordance with the literature (Sober *et al*. 1981).

2-(3,4,5-Trimethoxyphenyl)ethanol (74)

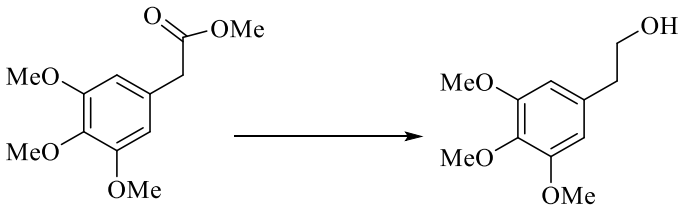

73 **74**

To a solution of methyl 2-(3,4,5-trimethoxyphenyl)acetate **(73)** (7.4 g, 31.0 mmol, 1 eq) and dry THF (75 mL) stirring at 0 ^{o}C under argon, $LiAlH_4$ (1.53 g, 40.3 mmol, 1.3 eq) was added. After 1 hr the reaction was quenched with ethyl acetate (10 mL) and the reaction mixture filtered under vacuum. The filtrate was concentrated *in vacuo* and purified by column chromatography (200 g silica gel, hexane - ethyl acetate, 7:3). The title compound **(74)** was obtained as yellow oil (4.93, 75%), TLC petroleum ether - ethyl acetate, 1:1, Rf = 0.26

^{1}H (400 MHz, $CDCl_3$) δ ppm: 6.92 (2H, s, Ar-H), 3.79, (6 H, s, OMe), 3.76, (3H, s, OMe), 3.74 (2H, t, *J* = 6.53 Hz, CH_2OH), 2.74 (2H, t, *J* = 6.53 Hz, Ar-CH_2), 2.80 (1 H. bs, OH)

Spectral and physical data for this compound were in accordance with the literature (Soderquist *et al*. 2006).

2-(2-Iodo 3,4,5-trimethoxyphenyl)ethanol (75)

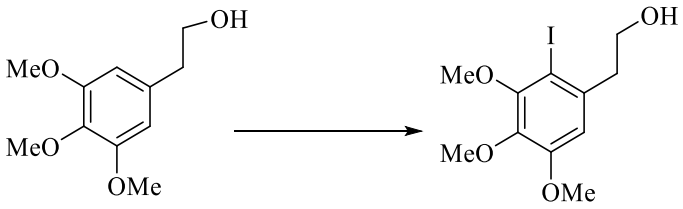

74 **75**

To a flask containing 2-(3,4,5-trimethoxyphenyl)ethanol **(74)** (5.1 g, 24.0 mmol, 1 eq) and silver trifluoroacetate (6.36 g, 28.8 mmol, 1.2 eq) in chloroform (20 mL), a solution of iodine (6.4 g, 25.2 mmol, 1.05 eq) in chloroform (130 mL) was added dropwise and the mixture allowed to stir for 20 min. The reaction mixture was filtered through celite®, concentrated *in vacuo* and purified by column chromatography (200 g silica gel, petroleum ether - ethyl acetate, 1:1) to yield the title **(75)** compound as a pale yellow solid (6.52 g, 80%), m.p. 68 ^{o}C (Lit – 68-69 ^{o}C), TLC petroleum ether - ethyl acetate, 1:1, Rf = 0.30

^{1}H (400 MHz, $CDCl_3$) δ ppm: 6.82 (1H, s, Ar-H), 3.8 (6 H, s, OMe), 3.78 (3H, s, OMe), 3.75 (2H, t, *J* = 7.21 Hz, CH_2OH), 2.95 (2H, t, *J* = 7.21 Hz, CH_2), 1.41 (1H, s, OH)

Spectral and physical data for this compound were in accordance with the literature (Joncour *et al*. 2006).

2-Iodo 3,4,5-trimethoxy-1-(2-(methoxymethoxy)ethyl)benzene (76)

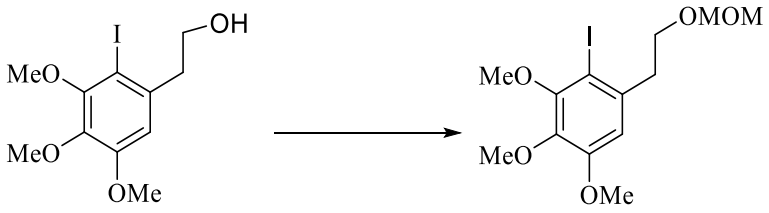

75 **76**

General procedure 5

The crude product was further purified by column chromatography (10 g silica gel, hexane - ethyl acetate, 8:2) to yield the title product **(76)** as a colourless oil (0.201 g, 87%), TLC petroleum ether - ethyl acetate, 1:1, Rf = 0.21

^{1}H (400 MHz, $CDCl_3$) δ ppm: 6.65 (1H, s, Ar-H), 4.59 (2H, s, O CH_2-OMe), 3.79 (3H, s, OMe), 3.78 (3H, s, OMe), 3.77 (3H, s, OMe), 3.66, (2H, t, *J* = 7.44 Hz, CH_2-OMOM), 3.26 (3H, s, OMe), 2.97 (2H, t, *J* = 7.44 Hz, Ar-CH_2)

Spectral and physical data for this compound were in accordance with the literature (Joncour *et al*. 2008)

4,4,5,5-Tetramethyl-2-(2,3,4-trimethoxy-6-(2-(methoxymethoxy)ethyl)phenyl)-1,3,2-dioxaborolane (77)

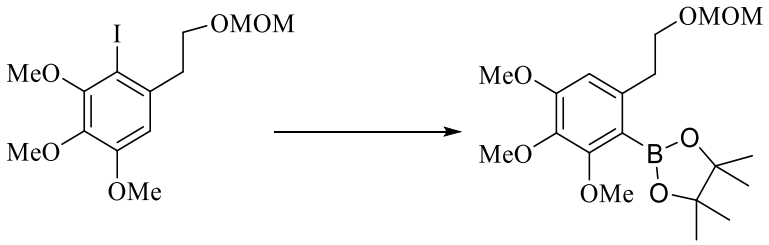

76 **77**

General procedure 6

The crude product was further purified by column chromatography (10 g silica gel, toluene - ethyl acetate, 100:1) to yield the title product **(77)** (3:1 mixture with dehalogenated starting material (0.130 g, ~75% by ^{1}HNMR), TLC petroleum ether - ethyl acetate, 1:1, Rf = 0.23

^{1}H (400 MHz, $CDCl_3$) δ ppm: 6.47 (1H, s, Ar-H), 4.55 (2H, s, O CH_2-OMe), 3.78 (3H, s, OMe), 3.77 (3H, s, OMe), 3.75 (3H, s, OMe), 3.63, (2H, t, *J* = 7.38 Hz, CH_2-OMOM), 3.25 (3H, s, OMe), 2.83 (2H, t, *J* = 7.38 Hz, Ar-CH_2), 1.31 (12H, s, BPIN)

Spectral and physical data for this compound were in accordance with the literature (Joncour *et al*. 2007).

Triethyl(2-iodo 3,4,5-trimethoxyphenethoxy)silane (78)

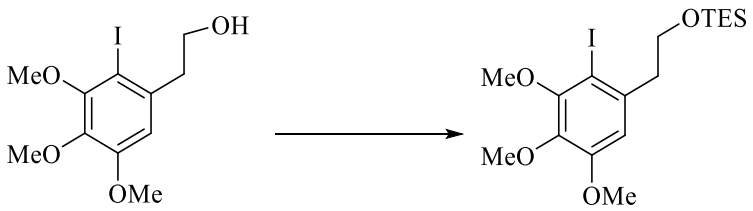

75 **78**

General procedure 6

The crude product was further purified by column chromatography (10 g silica gel, hexane - ethyl acetate, 8:2) to yield the title product **(78)** as colourless oil (0.312 g, 90%). TLC petroleum ether - ethyl acetate, 1:1, Rf = 0.26

^{1}H (400 MHz, $CDCl_3$) δ ppm: 6.71 (1H, s, Ar-H), 3.89 (3H, s, OMe), 3.85 (3H, s, OMe), 3.84 (3H, s, OMe), 3.80 (2H, t, *J* = 7.29 Hz, Ar-CH_2), 2.99 (2H, t, *J* = 7.29 Hz, CH_2-OTES), 0.93 (9 H, t, *J* = 8.19 Hz, TES: 3 X CH_3), 0.57 (6 H, q, *J* = 8.19 Hz, TES: 3 X CH_2)

Spectral and physical data for this compound were in accordance with the literature (Joncour *et al*. 2007).

Triethyl(3,4,5-trimethoxy-2-(4,4,5,5-tetramethyl-1,3,2-dioxaborolan-2-yl)phenethoxy)silane (79)

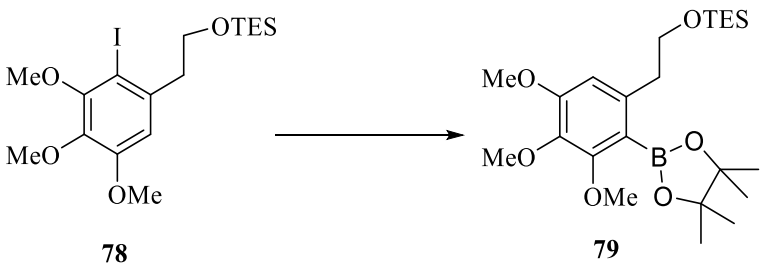

78 **79**

General procedure 7

The crude product was further purified by column chromatography (10 g silica gel, toluene-ethyl acetate, 100:1) to yield the title product **(79)** as an inseparable 3:1 mixture with dehalogenated starting material (0.130 g, ~65% by ^{1}H NMR). TLC petroleum ether - ethyl acetate, 1:1, Rf = 0.14 (spot has faint tail)

^{1}H (400 MHz, $CDCl_3$) δ ppm: 6.56 (1H, s, Ar-H), 3.87 (3H, s, OMe), 3.84 (3H, s, OMe), 3.83 (3H, s, OMe), 3.76 (2H, t, *J* = 7.29 Hz, Ar-CH_2), 2.84 (2H, t, *J* = 7.29 Hz, CH_2-OTES), 1.38 (12H, s, BPIN: 4 X CH_3) 0.93 (9 H, t, *J* = 7.85 Hz, TES: 3 X CH_3), 0.56 (6 H, q, *J* = 7.85 Hz, TES: 3 X CH_2)

Spectral and physical data for this compound were in accordance with the literature (Joncour *et al*. 2007).

(N^3E)-N^1,N^3-bis(2,4,6-trimethylbenzylidene)propane-1,3-diamine (85)

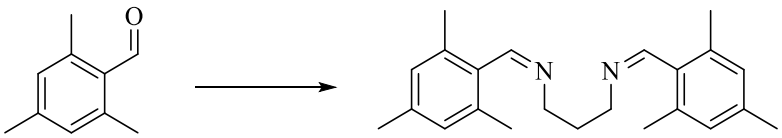

84 **85**

To a stirred solution of metsitaldehyde **(84)** (5.0 g, 33.73 mmol, 1 eq) in methanol (10 mL) 1,3-diaminopropane (1.42 mL, 16.87 mmol, 0.5 eq) was added and the mixture stirred overnight. The reaction mixture was filtered and the solid dried.. Mp 156 ^{o}C (Lit - 156 ^{o}C), TLC dichloromethane - methanol, 95:5, Rf = 0.09

^{1}H (400 MHz, $CDCl_3$) δ ppm: 6.91 (4 H, s, ArH), 6.34 (2H, s, 2 x HC=N), 3.84 (4 H, t, *J* = 7.21 Hz, 2 x N-CH_2), 2.42 (12H, s, 4 x CH_3), 2.31 (6 H, s, 2 x CH_3), 2.13 (2H, t, *J* = 7.2 Hz, $CH_2(CH_2)_2$)

Spectral and physical data for this compound were in accordance with the literature (Özdemir *et al*. 2005b).

N^1,N^3-Bis(2,4,6-trimethylbenzyl)propane-1,3-diamine (86)

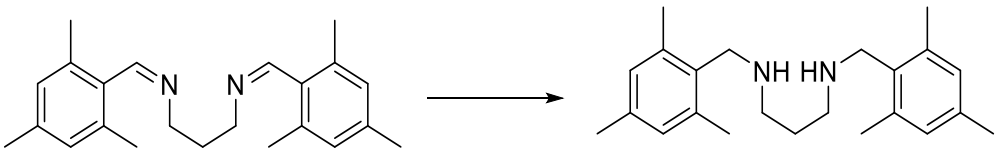

85 **86**

To a suspension of (N^3E)-N^1,N^3-bis(2,4,6-trimethylbenzylidene)propane-1,3-diamine **(85)** (1.87 g, 5.53 mmol, 1 eq) in methanol (10 mL), $NaBH_4$ (0.32 g, 8.38 mmol, 2.5 eq) was added in portions over 30 mins and after another 30 mins water (50 mL) was added. The mixture was extracted with ethyl acetate (2x50 mL), dried with anhydrous magnesium sulphate, filtered and concentrated *in vacuo* to give the title compound **(86)** as a yellow oil (1.72 g, 92%), TLC dichloromethane - methanol, 1:1, Rf = 0.02

^{1}H (400 MHz, $CDCl_3$) δ ppm: 6.83 (4 H, s Ar-H), 3.74 (4 H, s, 2 XAr-CH_2-N), 2.72 (4 H, t, *J* = 8.40 Hz, C-H) 2.4 (12H, s, CH_3), 2.32 (6 H, s, CH_3), 1.62 (2H, t, *J* = 8.40 Hz, $CH_2(CH_2)_2$)

Spectral and physical data for this compound were in accordance with the literature (Özdemir *et al*. 2005b).

1,3-Bis(2,4,6-trimethoxybenzyl)-3,4,5,6-tetrahydropyrimidinium chloride (87)

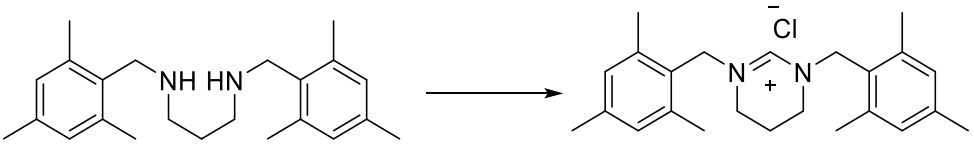

86 **87**

N^1,N^3-bis(2,4,6-trimethylbenzyl)propane-1,3-diamine **(86)** (1.72, 5.1 mmol, 1 eq), NH_4Cl (0.27 g, 5.1 mmol, 1 eq) triethylorthoformate (25 mL) in ethyl acetate (50 mL) were heated in a distillation apparatus until no more ethyl acetate was distilled. The mixture was cooled, the solid product collected by filtration and washed with diethyl ether to yield the title compound as white crystals **(87)** (1.43 g, 73%). M.p. 232 ^oC (Lit - 232 ^oC), TLC petroleum ether - ethyl acetate, 1:1, Rf = 0.02

^{1}H (400 MHz, $CDCl_3$) δ ppm: 7.81 (4 H, s, Ar-H), 6.05 (4 H, s, CH_2), 4.45 (4 H, s, CH_2), 3.70 (12H, s, CH_3), 3.75 (6 H, s, CH_3), 3.33 (4 H, t, J = 5.19 Hz, 2 X N-CH_2), 1.96- 1.91 (2H, m, J = 5.19 Hz, $CH_2(CH_2)_2$)

Spectral and physical data for this compound were in accordance with the literature (Yasar *et al*. 2008).

4,4',5,6-Tetramethoxybiphenyl-2-carbaldehyde (90)

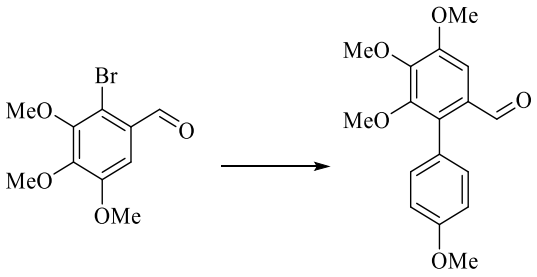

52 **90**

General procedure 2

The title compound was purified by column chromatography (10 g silica gel, hexane - ethyl acetate, 9:1) to yield the title compound as a white solid **(90)** (0.710 g, 92%) m.p. 90 ^{o}C (Lit - 90 ^{o}C), TLC petroleum ether - ethyl acetate, 1:1, Rf = 0.23

^{1}H (400 MHz, $CDCl_3$) δ ppm: 9.65 (1H, s, CHO), 7.30 (1H, s, Ar-H), 7.22 (2H, d, *J* = 8.9 Hz, Ar-H : *m*-OMe), 6.94 (2H, d, *J* = 8.3 Hz, Ar-H : *o* OMe), 3.98 (3H, s, OMe), 3.96 (3H, s, OMe), 3.86 (3H, s, OMe), 3.56 (3H, s, OMe)

Spectral and physical data for this compound were in accordance with the literature (Özdemir *et al*. 2005b)

4,4',5,6-Tetramethoxybiphenyl-2-ol (101)

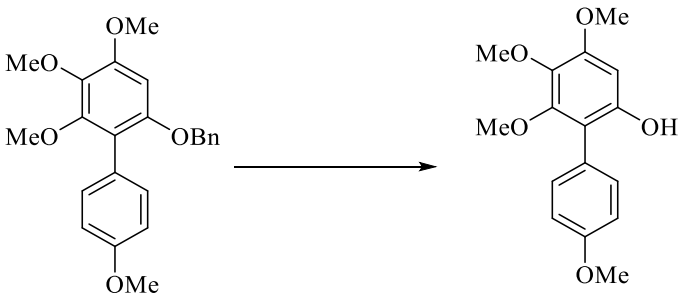

117 **101**

See general procedure 3

product was purified by column chromatography (10 g silica gel, hexane - ethyl acetate, 7:3) to yield the title compound as a white solid **(101)** that was recrystallised from 5:1 hexane : ethyl acetate (0.063 g, 94%), m.p. 109 -110 ^{o}C (Lit - 110 ^{o}C), TLC petroleum ether - ethyl acetate, 1:1, Rf = 0.10

^{1}H (400 MHz, $CDCl_3$) δ ppm: 7.30 (2H, d, *J* = 8.62 Hz, Ar-H), 7.04 (2H, d, *J* = 8.62 Hz, Ar-H : *m*-OMe), 6.40 (1H, s, Ar-H: *o* OH), 4.93 (1H, s, OH), 3.89 (3H, s, OMe), 3.88 (3H, s, OMe), 3.86 (3H, s, OMe), 3.65 (3H, s, OMe)

Spectral and physical data for this compound were in accordance with the literature (Jinno *et al*. 1999).

2',3',4,4'-Tetramethoxybiphenyl-2-carbaldehyde (103)

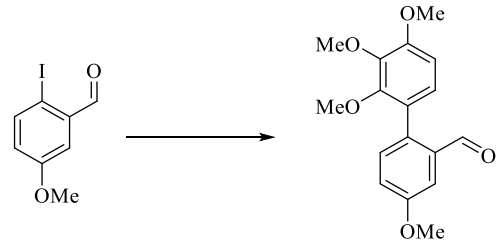

70 **103**

General procedure 1

The title compound was purified by column chromatography (10 g silica gel, hexane - ethyl acetate, 8:2) to yield the title compound as a yellow solid **(103)** (0.710 g, 88%) m.p. 103 - 104 ^{o}C (Lit - 104 ^{o}C), TLC petroleum ether - ethyl acetate, 1:1, Rf = 0.31

^{1}H (400 MHz, $CDCl_3$) δ ppm: 9.82 (1H, s, CHO), 7.52 (2H, d, *J* = 2.71 Hz, ArH : *o* CHO), 7.31 (1H, d, *J* = 8.41 Hz, ArH : *o* 3' OMe), 7.22 (1H, dd, *J* = 3.01, 9.41 Hz, Ar-H : *m*-CHO), 6.97 (1H, d, *J* = 8.41 Hz, Ar-H : : *m*- 3' OMe) 6.78 (1H, d, *J* = 8.63 Hz, Ar-H), 3.94, (3H, s, OMe), 3.92 (3H, s, OMe), 3.56 (3H, s, OMe)

Spectral and physical data for this compound were in accordance with the literature (Mamane *et al*. 2004).

2',3',4,4'-Tetramethoxybiphenyl-2-ol (104)

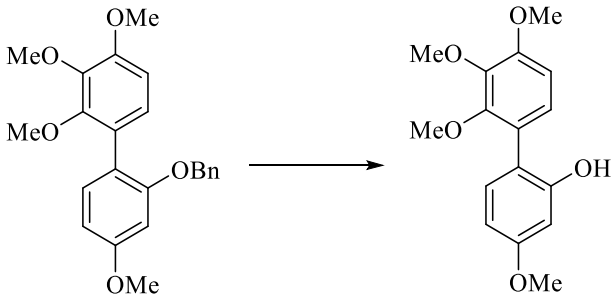

113 **101**

General procedure 3

product was purified by column chromatography (10 g silica gel, hexane - ethyl acetate, 7:3) to yield the title compound as an white solid that was recrystallised from 5:1 hexane : ethyl acetate (0.30 g, 87%). M.p. 109 - 108 ^{o}C (Lit - 108 ^{o}C), TLC petroleum ether - ethyl acetate, 1:1, Rf = 0.09

^{1}H (400 MHz, $CDCl_3$) δ ppm: 7.18 (1 H d, *J* = 8.32 Hz, Ar-H), 7.10 (1H, bs, OH), 6.98 (1H, d, *J* = 8.83 Hz, Ar-H : *o* 4 OMe), 6.81 (1H, d, *J* = 8.83 Hz, Ar-H : *m*- 4 OMe), 6.62 (1H, d, *J* = 2.62 Hz, ar-H *o* OH), 6.58 (1H, dd, *J* = 2.62, 8.68 Hz, Ar-H : *m*-OH) 3.94 (1H, s, OMe), 3.91 (1H, s, OMe), 3.82 (1H, s, OMe); 3.73 (1H, s, OMe)

Spectral and physical data for this compound were in accordance with the literature (Kang *et al*. 1990).

2-Iodo 5-methoxyphenol (105)

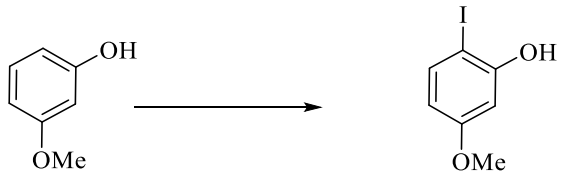

107 **105**

To a flask containing 3-methoxyphenol **(107)** (1.2 g, 9 mmol, 1 eq) and silver trifluoroacetate (2.2 g, 9 mmol, 1 eq) in chloroform (10 mL) was added via canula a solution of iodine (2.54 g, 11 mmol, 1.1 eq) in chloroform (700 mL) over 4 hr. The reaction mixture was filtered through a plug of celite® and concentrated *in vacuo*. The product was purified by column chromatography (10 g silica gel, hexane - ethyl acetate, 9:1) to give a crude solid that was recyrstallized from methanol to yield the title compound **(105)** (1.68 g, 74%) as a white powder. Melting range 71-72 ^{o}C (Lit - 72 ^{o}C), TLC petroleum ether - ethyl acetate, 1:1, Rf = 0.19

^{1}H (400 MHz, $CDCl_3$) δ ppm: 11.72 (1H, s, OH), 7.43 (1H, d, *J* = 8.5 Hz, Ar-H : *p*- OH), 6.79 (1H, d, *J* = 2.4 Hz, Ar-H : *o* OH), 6.73 (1H, dd, *J* = 2.7, 8.29 Hz Ar-H : *m*- OH), 3.58 (H, s, OMe)

Spectral and physical data for this compound were in accordance with the literature (Dirr *et al*. 2008).

2-Iodo 5-methoxyphenyl benzoate (112)

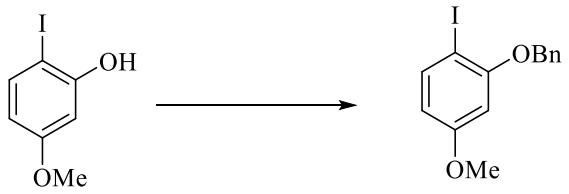

105 **112**

To a solution of 2-iodo 5-methoxyphenol **(105)** (2.00 g, 7.90 mmol, 1 eq) in dry THF (1 mL) was added triphenylphosphine (2.31 g, 8.8 mmol, 1.1 eq), benzyl alcohol (0.911 mL, 8.8 mmol, 1.1 eq) and the mixture sonicated for 10 min. Diisopropyl azodicarboxylate (DIAD) (1.75 mL, 8.8 mmol, 1.1 eq) was then added dropwise and the reaction mixture sonicated for 1 hr. The viscous mixture was concentrated *in vacuo* and the crude product was purified by column chromatography (10 g silica gel, hexane - ethyl acetate, 9:1) to yield the title product **(112)** (2.22 g, 81%) as a colourless oil, TLC petroleum ether - ethyl acetate, 1:1, Rf = 0.23

^{1}H (400 MHz, $CDCl_3$) δ ppm: 7.67 (1H, d, *J* = 8.7, Ar-H), 7.53- 7.48 (2H, m, Ar-H), 7.42-7.38 (2H, m, Ar-H), 7.35- 7.32 (1H, m, Ar-H), 6.50 (1H, d, *J* = 2.61 Hz, Ar-H : *o* OBn), 6.36 (1H, dd, *J* = 2.6, 8.6 Hz, Ar-H : *m*- OBn), 5.15 (2H, s, CH_2), 3.79 (3H, s, OMe)

Spectral and physical data for this compound were in accordance with the literature (Dirr *et al*. 2008).

2'-(Benzyloxy)-2,3,4,4'-tetramethoxybiphenyl (113)

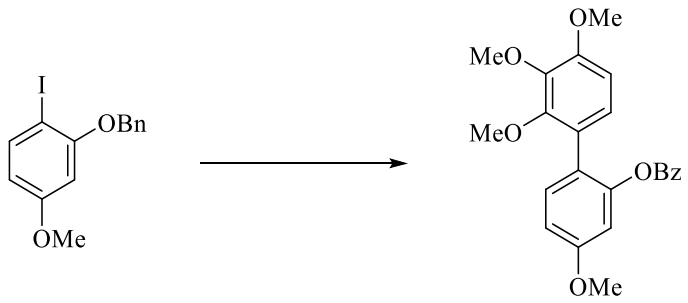

112 **113**

General procedure 1

The title compound was purified by column chromatography (10 g silica gel, hexane - ethyl acetate, 9:1) to yield the title compound as an amber oil **(113)** (0.96 g, 88%), TLC petroleum ether - ethyl acetate, 1:1, Rf = 0.24

^{1}H (400 MHz, $CDCl_3$) δ ppm: 7.46 (1H, d, *J* = 2.97 Hz, Ar-H: *o* OBn), 7.27- 7.22 (4 H, m, 4 X Ar-H: OBn), 7.09 (1H, dd, *J* = 8.31, 2.93 Hz, Ar-H: *o* 4'OMe), 7.05- 7.01 (2H, m, Ar-H), 6.92 (1H, d, *J* = 8.57 Hz, Ar-H: *o* 4'OMe), 6.69 (1H, d, *J* = 8.57 Hz, Ar-H), 5.15 (2H, s, CH_2: OBn), 3.90 (3H, s, OMe), 3.89 (3H, s, OMe), 3.77 (3H, s, OMe), 3.5 (3H, s, OMe)

^{13}C δppm: 168.15 (Ar-OMe), 158.45 (Ar-OMe), 153.1 (Ar-OMe), 151.0 (Ar-OMe), 142.0 (Ar), 135.6 (Ar), 132.6 (Ar), 132.3(Ar-H), 130.7(Ar-H), 128.2 (2Ar-H), 127.8 (Ar), 127.7 (2Ar-H), 124.1(Ar-H), 117.5(Ar-H), 114.5(Ar-H), 107.0(Ar-H), 66.7 (CH_2: OBn),60.8 (OMe), 60.4 (OMe), 55.9 (OMe), 55.5 (OMe)

***Amax cm*$^{-1}$:** 2894, 2831, 1485, 1451, 1434, 1394, 1281, 1273, 1103, 984, 821, 780, 694

2-Bromo 3,4,5-trimethoxyphenol (115)

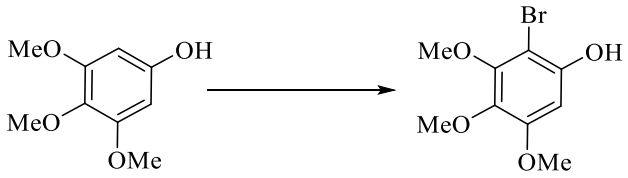

114 **115**

To a solution of 3,4,5-trimethoxyphenol **(114)** (0.20 g, 1 mmol, 1 eq) in THF (10 mL) at 0 ^{o}C N-Bromosuccinimide (NBS) (0.23 g, 1 mmol, 1 eq) was added and the reaction mixture stirred 1 hr, poured into ice water (10 mL) and extracted with ethyl acetate (2 X 10 mL). The organic layers were washed with sat. aq $NaHCO_3$ (10 mL), water (10 mL), dried with anhydrous magnesium sulphate, filtered and concentrated *in vacuo*. The crude product was further purified by column chromatography (10 g silica gel, hexane - ethyl acetate, 8:2) to yield the title product **(115)** (0.286 g, 87%) as a brown oil, TLC petroleum ether - ethyl acetate, 1:1, Rf = 0.17

^{1}H (400 MHz, $CDCl_3$) δ ppm: 6.46 (s, 1H, Ar-H), 5.50 (s, 1H, OH), 3.93 (s, 3H, OMe), 3.85 (s, 3H, OMe), 3.83 (s, 3H, OMe)

Spectral and physical data for this compound were in accordance with the literature (Jinno *et al*. 1999).

2-Bromo 3,4,5-trimethoxyphenyl benzyl ether (116)

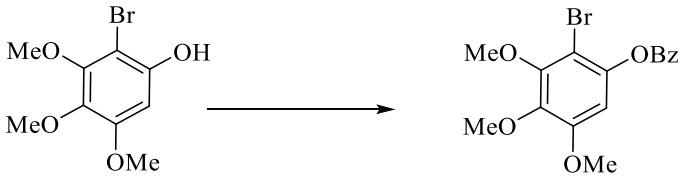

115 **116**

To a concentrated solution of 2-bromo -3,4,5-trimethoxyphenol **(115)** (0.160 g, 6 mmol, 1 eq) in dichloromethane (1 mL) was added triphenylphosphine (0.175 g, 7 mmol, 1.1 eq), benzyl alcohol (0.065 mL, 6 mmol, 0.95 eq) and sonicated for 10 min. Diisopropyl azodicarboxylate (DIAD) (0.135 mL, 7 mmol, 1.1 eq) was then added dropwise and the solution sonicated for 1 hr. The viscous mixture was concentrated *in vacuo* and the crude product was purified by column chromatography (10 g silica gel, hexane - ethyl acetate, 8:2) to yield the title product **(116)** (0.190 g, 90%) as a colourless oil, TLC petroleum ether - ethyl acetate, 1:1, Rf = 0.23

^{1}H (400 MHz, $CDCl_3$) δ ppm: 7.51- 7.47 (2H, m, Ar-H), 7.42- 7.38 (2H, m, Ar-H), 7.35-7.29 (1H, m, Ar-H), 6.44 (s, 1H, Ar-H), 5.14 (s, 2H, CH_2), 3.94 (s, 3H, OMe), 3.85 (s, 3H, OMe), 3.83 (s, 3H, OMe)

Spectral and physical data for this compound were in accordance with the literature (Jinno *et al*. 1999).

4,4',5,6-Tetramethoxybiphenyl-2-yl benzoate (117)

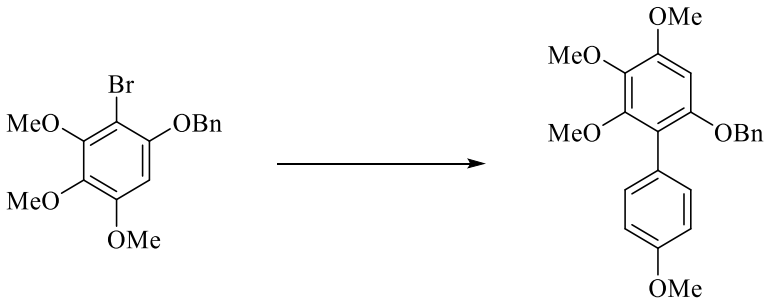

116 **117**

See general method 2

1-(Benzyloxy)-2-bromo 3,4,5-trimethoxybenzene **(116)** (0.07g, 0.2 mmol, 1 eq) was purified by column chromatography (hexane - ethyl acetate, 9:1) to yield the title compound **(117)** (0.063 g, 90%) as an amber oil. TLC petroleum ether - ethyl acetate, 1:1, Rf = 0.21

^{1}H (400 MHz, $CDCl_3$) δ ppm: 7.29 (2H, d, *J* = 8.61 Hz, Ar-H : *m*- 4'OMe), 7.24- 7.17 (3H, m, Ar-H: OBn), 7.18- 7.11 (2H, m, Ar-H : OBn) 7.05 (2H, d, *J* = 8.61 Hz, Ar-H : *o* 4'OMe), 6.44 (1H, s, Ar-H), 4.85 (2H, s, CH_2), 3.89 (3H, s, OMe), 3.88 (3H, s, OMe), 3.86 (3H, s, OMe), 3.65 (3H, s, OMe)

^{13}C δppm: 168.15 (Ar-OMe), 158.45 (Ar-OMe), 153.1 (Ar-OMe), 151.0 (Ar-OMe), 142.0 (Ar), 135.6 (Ar), 132.6 (Ar), 132.3(Ar-H), 130.7(Ar-H), 128.2 (2Ar-H), 127.8 (Ar), 127.7 (2Ar-H), 124.1(Ar-H), 117.5(Ar-H), 114.5(Ar-H), 107.0(Ar-H), 66.7 (CH_2: OBn),60.8 (OMe), 60.4 (OMe), 55.9 (OMe), 55.5 (OMe)

***Amax cm^{-1}*:** 2894, 2831, 1485, 1451, 1434, 1394, 1281, 1273, 1103, 984, 821, 780, 694

2-(2',3',4,4'-Tetramethoxybiphenyl-2-yloxy)acetic acid (118)

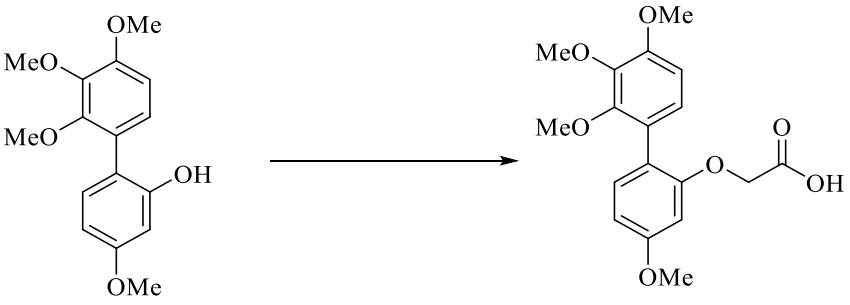

104 **118**

To a solution of 2',3',4,4'-tetramethoxybiphenyl-2-ol **(104)** (0.30 g, 1 mmol, 1 eq) in ethanol (10 mL) was added K_2CO_3 (0.285 g, 2.12mmol, 2 eq) and bromo acetate (0.300 mL, 3 mmol, 3 eq) and the reaction mixture heated at 80 ^oC for 4 hr. The mixture was cooled and concentrated under vacuum. A solution of 2M NaOH (50 mL) was added and stirred for 1 hr. The suspension was acidified to pH 1 using conc HCl , extracted with dichloromethane (2 X 50 mL) and the organic layer washed with water (50 mL), dried with anhydrous magnesium sulphate, filtered and concentrated *in vacuo*. The crude product was recrystallised from methanol to yield the product as a white powder **(118)** (0.310 g, 89%) M.p 129 ^oC. TLC petroleum ether - ethyl acetate, 1:1, Rf = 0.03 (As smear)

^{1}H (400 MHz, $CDCl_3$) δ ppm: 8.88 (1H, s, COOH), 7.12 (1H, d, *J* = 8.41 Ar-H : *m*- 4 OMe), 6.87 (1H, d, *J* = 8.5 Ar-H: *o* Ar-O CH_2), 6.73 (1H, d, *J* = 8.41 Ar-H : *o* 4 OMe), 6.56 (1H, dd, *J* = 2.42, 8.41 Hz, Ar-H : *m*- 4'OMe), 6.39 (1H, d, *J* = 2.31 Ar-H : *o* Ar-O CH_2), 4.56 (2H, s, Ar-H : O CH_2-), 3.85 (3H, s, OMe), 3.82 (3H, s, OMe), 3.76 (3H, s, OMe), 3.58 (3H, s, OMe)

^{13}C δppm: 178.1 (COOH), 162.1 (Ar-OMe), 154.5 (Ar-OMe), 153.2 (Ar-OMe), 152.4 (Ar-OMe), 142.2(Ar), 134.3 (Ar-H), 132.2 (Ar), 125.2 (Ar), 118.8 (Ar), 115.4 (22 X Ar-H), 94.3 (Ar), 71.2 (*o* CH_2), 61.4 (OMe), 60.3 (OMe), 59.2 (OMe), 56.1 (OMe)

***Amax cm^{-1}*:** 3309, 2872, 2743, 1617, 1481, 1465, 1344, 1310, 1293, 1115, 1094, 932, 892

3,9,10,11-Tetramethoxydibenzo[b,d]oxepin-7(6 H)-one (119)

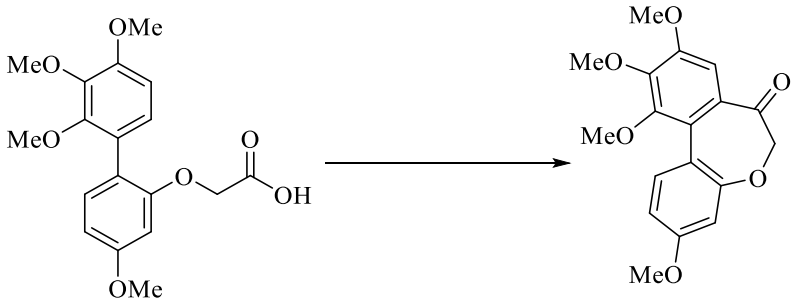

118 **119**

2-(2',3',4,4'-Tetramethoxybiphenyl-2-yloxy)acetic acid **(118)** (0.110 g, 0. 35 mmol, 1 eq) was dissolved in a 50:50 trifluoroacetic acid /trifluoroacetic acid anhydride (5 mL) and stirred overnight. The solvent was evaporated and the resulting material was dissolved in dichloromethane (10 mL). The organic layer was washed with sat. aq $NaHCO_3$ (10 mL), water (10 mL), brine (10 mL), dried with anhydrous magnesium sulphate, filtered and concentrated *in vacuo*. The mixture was purified by column chromatography (10 g silica gel, hexane - ethyl acetate, 8:2) to yield the title compound **(119)** as red crystals (0.076 g, 73%), m.p. 139 $^{o\,C\,TLC}$ petroleum ether - ethyl acetate, 1:1, Rf = 0.22

^{1}H (400 MHz, $CDCl_3$) δ ppm:7.58 (1H, d, *J* = 8.50 Hz, Ar-H : *o* 4' OMe), 7.07 (1H, s, Ar-H: *o* 4 OMe), 6.75 (1H, dd, *J* = 2.47 Hz, Ar-H : *m* – O CH_2C), 6.69 (1H, d, *J* = 2,47 Hz, Ar-H: *o* – O CH_2C), 4.67 (2H, s : -O CH_2), 3.92 (3H, s, OMe), 3.87(3H, s, OMe), 3.78 (OMe), 3.53 (3H, s, OMe)

^{13}C δppm: 200.4 (C=O), 162.7 (Ar-OMe), 158.8 (Ar-OMe), 155.2 (Ar-OMe), 148.7 (Ar-OMe), 140.3 (Ar), 134.4 (Ar), 131.6 (Ar), 115.7 (Ar-H), 107.8(Ar), 105.1 (Ar-H), 104.5 (Ar-H), 99.4 (Ar-H), 71.8 (CH_2: Ar-CH_2), 65.8 (OMe), 63.1 (OMe), 59.2 (OMe), 57.8 (OMe)

***Λmax cm*$^{-1}$:** 2905, 2852, 1710 1617, 1481, 1465, 1412, 1270, 1243, 1171, 1143, 1047

2-(4,4',5,6-Tetramethoxybiphenyl-2-yloxy)acetic acid (121)

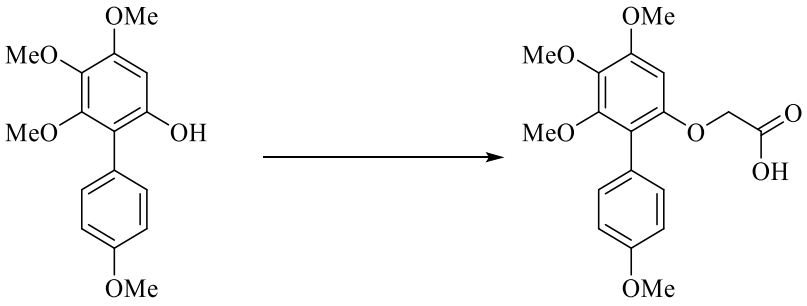

101 **121**

To a solution of 4,4',5,6-tetramethoxybiphenyl-2-ol **(101)** (0.05, 0.17 mmol, 1 eq) in ethanol (10 mL) was added K_2CO_3 (0.07 g, 0.51 mmol, 3 eq) and bromo acetate (0.035 mL, 0.34 mmol, 2 eq) and the reaction mixture heated at 80 ^oC for 4 hr. The mixture was cooled and concentrated *in vacuo*. A solution of 2M NaOH (50 mL) was added and the mixture and stirred for 1 hr. The suspension was acidified to ph 1 with conc. HCl, extracted with dichloromethane (2 X 50 mL) and the organic layer washed with water (50 mL), dried with anhydrous magnesium sulphate, filtered and concentrated *in vacuo*. The crude was recrystallised from methanol to yield the product as a white powder **(121)** (0.045 g, 76%), m.p 135 ^{o}C, TLC petroleum ether - ethyl acetate, 1:1, Rf = 0.08 (smear)

^{1}H (400 MHz, $CDCl_3$) δ ppm: 8.21-7.44 (1H, broad s, OH), 7.32 (2H, d, *J* = 8.21, Ar-H : *o* 4' OMe), 6.95 (2H, d, *J* = 8.21, Ar-H : *o* 4' OMe), 6.35 (1H, s, Ar-H : *o* 4 OMe), 4.43 (2H, s, CH_2 : Ar-O CH_2), 3.87 (3H, s, OMe), 3.86 (3H, s, OMe), 3.84 (3H, s, OMe), 3.60 (3H, s, OMe)

^{13}C δppm: 172.8 (COOH), 158.6 (Ar-OMe), 152.6 (Ar-OMe), 152.6 (Ar-OMe), 151.1(Ar-OMe), 138.2(Ar), 131.7 (22 X Ar-H), 125.2 (Ar), 118.8 (Ar), 113.5 (22 X Ar-H), 95.9 (Ar), 66.8 (*o* CH_2), 61.1(OMe), 60.9 (OMe), 56.2 (OMe), 55.2 (OMe)

***Amax cm*$^{-1}$:** 3222, 2905, 2865, 1710 1617, 1481, 1465, 1347, 1310, 1253, 1204, 1143, 934

1,2,3,9-Tetramethoxydibenzo[b,d]oxepin-7(6 H)-one (22)

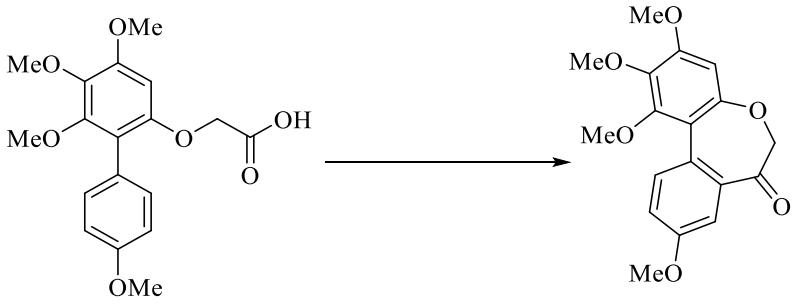

121 **122**

2-(4,4',5,6-Tetramethoxybiphenyl-2-yloxy) **(121)** (0.115 g, 0.33 mmol, 1 eq) was dissolved in a 50:50 mixture of trifluoroacetic acid /trifluoroacetic acid anhydride (5 mL) and stirred overnight. The solvent was evaporated and the resulting material was dissolved in dichloromethane (10 mL). The organic layer was washed with sat. aq $NaHCO_3$ (10 mL), water (10 mL), brine (10 mL), dried with anhydrous magnesium sulphate, filtered and concentrated *in vacuo*. The mixture was purified by column chromatography (10 g silica gel, hexane - ethyl acetate, 8:2) to yield the title compound **(122)** as red crystals (0.082 g, 75%), m.p. 123 ^{o} C, TLC petroleum ether - ethyl acetate, 1:1, Rf = 0.25

^{1}H (400 MHz, $CDCl_3$) δ ppm: 7.60 (1H, d, *J* = 8.50 Hz, Ar-H: *p*- O CH_2), 7.21 (1H, d, *J* = 2.92 Hz, Ar-H : *o* O CH_2), 7.08 (1H, dd, *J* = 8.11, 2.47 Hz, Ar-H : *m*- O CH_2), 6.51 (1H, s, Ar-H: *o* 4 OMe), 4.69 (2H, s : Ar-O CH_2), 3.82 (9 H, s, 3 X OMe), 3.53(3H, s, OMe)

^{13}C δppm: 203.2 (C=O), 162.3 (Ar-OMe), 159.1 (Ar-OMe), 153.1 (Ar-OMe), 149.4 (Ar-OMe), 139.1 (Ar), 136.6 (Ar), 134.2 (Ar), 107.1(Ar), 106.2 (22 X Ar-H), 100.0 (Ar-H), 98.2 (Ar-H), 74.1 (CH_2: Ar-CH_2), 64.8 (OMe), 60.1 (22 X OMe), 55.5 (OMe)

***λmax cm*$^{-1}$:** 2879, 2852, 1695, 1513, 1473, 1398, 1267, 1243, 1171, 1145, 1100, 865

2-Fluoro 3-methoxyphenol (139)

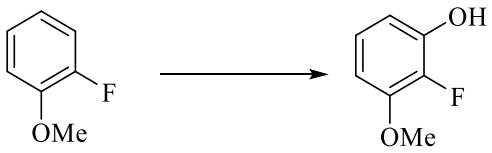

136 **139**

To a purged flask containing 2-fluoroanisole **(136)** (0.76 mL, 6.76 mmol, 1 eq) and pentamethyldiethylenetriamine (1.69 mL, 8.11 mmol, 1.2 eq) in dry THF at -78^{o}n-BuLi (5.07 mL, 1.6 M in hexanes,1.2 eq) was added followed by stirring for 3 hrs. Trimethyl borate ester

(0.92 mL, 8.11 mmol, 1.2 eq) was added dropwise and the reaction was allowed to warm to room temperature and stirred for 1 hr. This was followed by the slow addition of glacial acetic acid (0.5 mL, 8.73 mmol, 1.3 eq), then 35% hydrogen peroxide (0.85 mL, 7.5 mmol, 1.1 eq). Water (20 mL) was added and the reaction was extracted with ethyl acetate (3X50 mL), dried with anhydrous magnesium sulphate, filtered and concentrated *in vacuo* to give a crude product. This was purified by column chromatography (200 g silica gel, petroleum ether - ethyl acetate, 9:1) to yield the title compound as a dark green oil **(139)** (0.61 g, 63%), TLC petroleum ether - ethyl acetate, 1:1, Rf = 0.14

^{1}H (400 MHz, $CDCl_3$) δ ppm: 6.95- 6.89(1H, m, ArH), 6.64- 6.59 (1H, m, ArH), 6.54- 6.49 (1H, m, ArH), 5.19 (1H, b s, OH), 3.81 (3H, s, OMe)

Spectral and physical data for this compound were in accordance with the literature (Pirrung and Park. 2000).

1,2,3-Trimethoxy-5-(2-(3-methoxyphenoxy)ethyl)benzene (141)

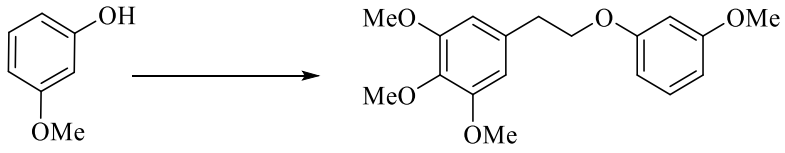

140 **141**

To a concentrated solution of 3,4,5-trimethoxyphenylethanol **(140)** (0.255 g, 1.2 mmol, 1 eq) in dry THF (1 mL) was added triphenylphosphine (0.377 g, 1.4 mmol, 1.2 eq), 3-methoxyphenol (0.360 mL, 1.4 mmol, 1.2 eq) and the mixture sonicated for 10 min. Diisopropyl azodicarboxylate (0.285 mL, 1.2 mmol, 1 eq) was then added dropwise and the reaction mixture sonicated for 1 hr. The viscous mixture was concentrated *in vacuo* and the crude product was purified by column chromatography (10 g silica gel, hexane - ethyl acetate, 9:1) to yield the title product **(141)** (0.410 g, 92%) as a colourless oil, TLC petroleum ether - ethyl acetate, 1:1, Rf = 0.24

^{1}H (400 MHz, $CDCl_3$) □ **400 M**7.23- 7.19 (1H, m, Ar-H), 6.55 (1H, d, *J* = 2.4, Ar-H : *o* Ar-O CH_2, *o* OMe), 6.53 (2H, s, Ar-H : *o* 1, 3 OMe), 6.52 (1H, d, *J* = 8.21 Hz, Ar-H), 6.49-6.42 (1H, m, Ar-H), 4.18 (2H, t, *J* = 7.11 Hz, Ar-O CH_2), 3.88 (6 H, s, OMe), 3.86 (3H, s, OMe), 3.81 (3H, s, OMe), 3.06 (2H, t, *J* = 7.11 Hz, Ar-CH_2)

^{13}C δppm: 160.9 (Ar-OMe), 160.0 (Ar-OMe), 153.2 (2 X Ar-OMe), 136.6 (Ar), 134.0 (Ar), 129.9 (Ar), 106.8 (Ar), 106.3 (22 X Ar-H: o $ArCH_2$), 105.9 (Ar-H). 101.1(Ar-H), 68.7(Ar-O CH_2), 60.8 (OMe), 56.1 (22 X OMe) 55.2 (OMe), 36.1(Ar-CH_2)

***λmax cm*$^{-1}$:** 2887, 2871, 1474, 1458, 1423, 1370, 1266, 1242, 1214, 1038, 932, 899

5-(2-(2-Fluoro 3-methoxyphenoxy)ethyl)-1,2,3-trimethoxybenzene (142)

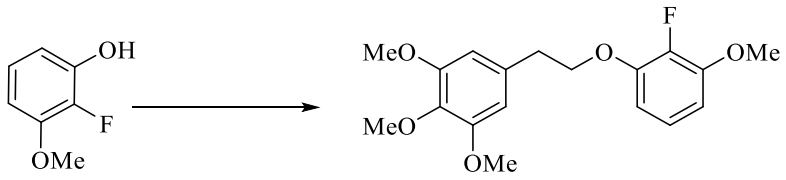

139 **142**

To a solution of 3, 4, 5-trimethoxyphenylethanol **(139)** (0.15 g, 1.2 mmol, 1 eq) in dry THF (1 mL) was added triphenylphosphine (0.377 g, 1.4 mmol, 1.2 eq)2-fluoro 3-methoxyphenol (0.360 mL, 1.4 mmol, 1.2 eq) and the mixture sonicated for 10 min. Diisopropyl azodicarboxylate (0.285 mL, 1.2 mmol, 1 eq) was then added dropwise and the reaction mixture sonicated for 1 hr. The viscous mixture was concentrated *in vacuo* and the crude product was purified by column chromatography (10 g silica gel, hexane - ethyl acetate, 9:1) to yield the title product **(142)** (0.370 g, 81%) as a colourless oil, TLC petroleum ether - ethyl acetate, 1:1, Rf = 0.28

^{1}H (400 MHz, $CDCl_3$) δ ppm: 6.86- 6.82 (1H, m, Ar-H), 6.55- 6.51 (1H, m, Ar-H), 6.61 (2H, s, Ar-H), 6.45-6.41 (1H, m, Ar-H), 4.20 (2H, t, *J* = 7.11 Hz, Ar-O CH_2), 3.91 (6 H, s, 2 X OMe), 3.86 (3H, s, OMe), 3.81 (3H, s, OMe), 3.06 (2H, t, *J* = 7.11 Hz, Ar-CH_2)

^{13}C δppm: 160.9 (Ar-OMe), 160.4-157.9 (bd, *J* = 243.99 Hz, C-F), 160.0 *(d,* J = 12.51 Hz, Ar-OMe; *o* CF), 153.2 (2 X Ar-OMe), 135.3 (Ar), 134.0 (Ar), 112.5 (d J = 4.28 Hz, Ar), 110.4 (22 X Ar-H: o $ArCH_2$), 105.9 (Ar-H). 103.2 (Ar-H), 69.2 (Ar-O CH_2), 61.7 (OMe), 56.3 (22 X OMe) 55.2 (OMe), 39.8 (Ar-CH_2)

***Amax cm^{-1}*:** 2905, 2861, 1491, 1465, 1432, 1310, 1261, 1243, 1211, 1030, 935, 895, 760

2-Fluoro 6-iodo 3-methoxyphenol (152)

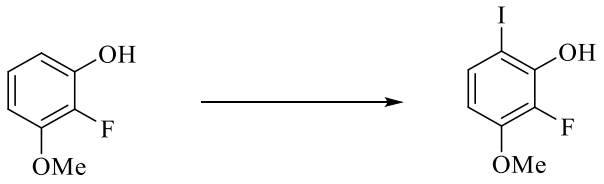

139 **152**

To a flask containing 2-fluoro 3-methoxyphenol **(139)** (1.00 g, 7 mmol, 1 eq) and silver trifluoroacetate (1.71 g, 7.7 mmol, 1 eq) in chloroform (10 mL) was added via cannula a solution of iodine (1.78 g, 7 mmol, 1 eq) in chloroform (700 mL) over 4 hr. The reaction mixture was filtered through a plug of celite® and concentrated *in vacuo*. The product was purified by column chromatography (10 g silica gel, hexane - ethyl acetate, 9:1) to give a crude soild that was recyrstallized from chloroform to yield the title compound **(152)** (1.35 g, 71%) as a yellow powder. Melting range 91-92 ^{o}C (Lit - 92 ^{o}C), TLC petroleum ether - ethyl acetate, 1:1, Rf = 0.12

^{1}H (400 MHz, $CDCl_3$) δ ppm: 7.37 (1H, dd, *J* = 2.41, 9.12 Hz, Ar-H : *p*- F), 6.41 (1H, t, *J* = 8.9 Hz, Ar-H : *p*- F), 4.72 (1H, s, Ar-OH), 3.89 (3H, s, OMe)

Spectral and physical data for this compound were in accordance with the literature (Nakasato *et al*. 2006)

5-(2-(2-Iodo 5-methoxyphenoxy)ethyl)-1,2,3-trimethoxybenzene (153)

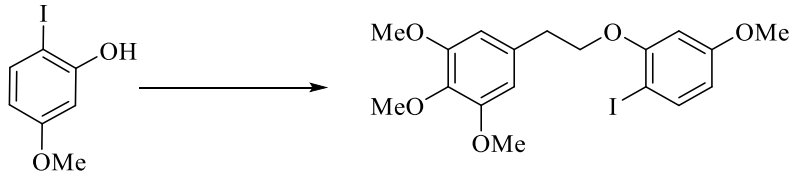

105 **153**

To a concentrated solution of 2-iodo 3,4,5-trimethoxyphenylethanol **(105)** (0.25 g, 1.2 mmol, 1 eq) in dry THF (1 mL) was added triphenylphosphine (0.377 g, 1.4 mmol, 1.2 eq), 2-iodo 5-methoxyphenol (0.36 mL, 1.4 mmol, 1.2 eq) and sonicated for 10 min. Diisopropyl azodicarboxylate (0.28 mL, 1.2 mmol, 1 eq) was then added dropwise and the reaction mixture sonicated for 1 hr. The viscous mixture was concentrated *in vacuo* and the crude product was purified by column chromatography (10 g silica gel, hexane - ethyl acetate, 9:1) to yield the title product **(153)** (0.413 g, 77%) as a colourless oil, TLC petroleum ether - ethyl acetate, 1:1, Rf = 0.23

^{1}H (400 MHz, $CDCl_3$) δ ppm: 7.63 (1H, d, *J* = 8.6 Hz, Ar-H), 6.61 (2H, s, Ar-H : *o* 1, 3 OMe), 6.39 (1H, d, *J* = 2.6 Hz, Ar-H : *o* Ar-O CH_2, *o* OMe), 6.33 (1H, dd, *J* = 2.7, 8.6 Hz, Ar-H : *m*- I), 4.19 (2H, t, *J* = 6.41 Hz, Ar-CH_2), 3.89 (6 H, s, OMe), 3.84 (3H, s, OMe), 3.78 (6 H, s, OMe), 3.11 (2H, t, *J* = 6.41 Hz, O CH_2)

^{13}C δppm: 161.2 (Ar-OMe), 158.1 (Ar-OMe), 153.1 (2Ar-OMe), 139.1 (Ar), 136.6 (Ar), 134.2 (Ar), 107.1(Ar), 106.2 (22 X Ar-H), 100.0 (Ar-H), 75.2 (Ar-H), 69.9 (CH_2-OAr), 60.8 (OMe), 56.2 (22 X OMe), 55.5 (OMe), 36.1(CH_2: Ar-CH_2)

***Λmax cm^{-1}*:** 2831, 2791, 1501, 1465, 1412, 1399, 1261, 1243, 1211, 1132, 932, 833

2-Fluoro 4-iodo 1-methoxy-3-(3,4,5-trimethoxyphenethoxy)benzene (154)

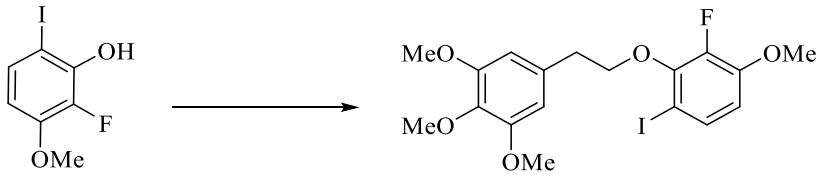

152 **154**

To a solution of 3,4,5-trimethoxyphenylethanol **(152)** (0.25 g, 1.2 mmol, 1 eq) in dry THF (1 mL) was added triphenylphosphine (0.377 g, 1.4 mmol, 1.2 eq), 6-fluoro-2-iodo 5-methoxyphenol (0.360mL, 1.4 mmol, 1.2 eq) and sonicated for 10 min. Diisopropyl azodicarboxylate (0.285 mL, 1.2 mmol, 1 eq) was then added dropwise and the reaction mixture sonicated for 1 hr. The viscous mixture was concentrated under reduced pressure and the crude product was purified by column chromatography (10 g silica gel, hexane - ethyl acetate, 9:1) to yield the title product **(154)** (0.413 g, 86%) as a colourless oil, TLC petroleum ether - ethyl acetate, 1:1, Rf = 0.27

^{1} H (400 MHz, $CDCl_3$) δ ppm: 7.35 (1H, dd, *J* = 8.91, 2.3 Hz, Ar-H : *p*- F), 6.47 (2H, s, Ar-H : *o* 1, 3 OMe), 6.44 (1H, t, *J* = 8.71 Hz, Ar-H : *m*- F), 4.25 (2H, t, *J* = 7.12 Hz, Ar-CH_2), 3.81(6 H, s, 2 X OMe), 3.79 (3H, s, OMe), 3.75 (3H, s, OMe), 3.05 (2H, t, *J* = 7.12 Hz, Ar-O CH_2)

^{13}C δppm: 160.9 (Ar-OMe), 160.4-157.9 (bd, *J* = 246.67 Hz, C-F), 160.0 *(d,* J = 12.51 Hz, Ar-Ome; *o* CF), 153.2 (2 X Ar-OMe), 135.3 (Ar), 134.0 (Ar), 112.5 (d J = 4.28 Hz, Ar), 110.4 (22 X Ar-H: o $ArCH_2$), 105.9 (Ar-H). 103.2(Ar-H), 69.2(Ar-O CH_2), 61.7 (OMe), 56.3 (22 X OMe) 55.2 (OMe), 39.8 (Ar-CH_2)

***λmax cm^{-1}*:** 2912, 2831, 1608, 1517, 1494, 1465, 1412, 1399, 1258, 1222, 1135, 1132, 932, 847

3-Fluoro 4,4',5',6'-tetramethoxy-[1,1'-biphenyl]-2,2'-diyl)dimethanol (157)

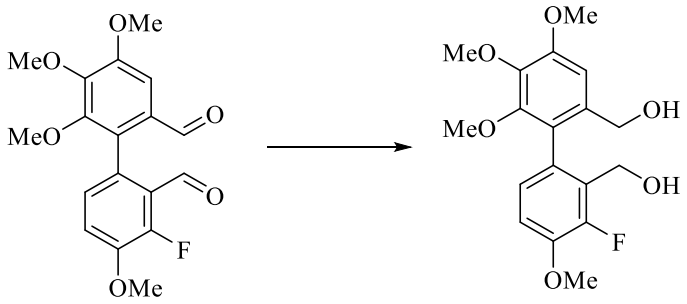

56 **157**

Sodium borohydride (0.20 g, 3.6 mmol, 4 eq) was added in portions to a flask containing the crude dialdehyde **(56)** (0.32 g, 0.91 mmol, 1 eq) in methanol (5 mL) over a 1 hour period at 0 ^{o}C. Water (5 mL) was added to vessel and the reaction mixture was extracted with ethyl acetate (2 x 10 mL). The organic phase was washed with 1M HCl (10 mL), dried with anhydrous sodium sulphate, filtered and concentrated *in vacuo*. The crude diol was purified by column chromatography (10 g silica gel, hexane - ethyl acetate, 1:1) to give a mixture title compound **(157)** and an unknown impurity that did not separate with further chromatography (0.24 g, ~75%), TLC petroleum ether - ethyl acetate, 1:1, Rf = 0.12. The mixture was carried on to the next step without further purification.

^{1}H (400 MHz, $CDCl_3$) δ ppm: 6.9 (1H, t, *J* = 8.71 Hz, Ar-H : *m*- F), 6.84- 6.80 (3H, m, Ar-H), 4.5 (1H, dd, *J* = 1.89, 11.58 Hz, CHOH), 4.25- 4.16 (3H, m, CHOH, CH_2OH), 3.8 (3H, s, OMe), 3.5 (3H, s, OMe), 3.2, (3H, s, OMe), 2.7(2H, s, 2 OH)

8-Fluoro 1,2,3,9-tetramethoxy-5,7-dihydrodibenzo[c,e]oxepine (158)

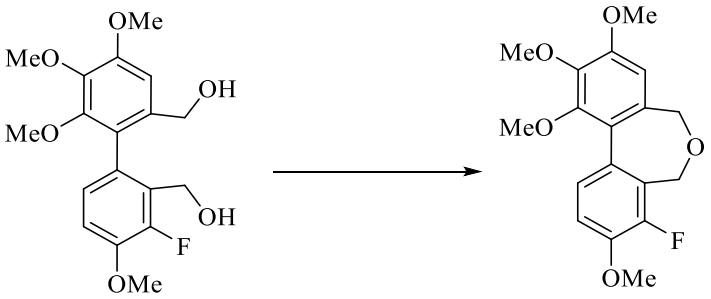

157 **158**

To a flask containing (3-fluoro 4,4',5',6'-tetramethoxybiphenyl-2,2'-diyl)dimethanol **(157)** (0.190 g, 0.5 mmol, 1 eq), and THF (2 mL), conc HCl (2 mL) was added and the reaction mixture was heated at refluxed overnight. Water was added (10 mL) and the mixture was extracted with ethyl acetate (10 mL), dried with anhydrous sodium sulphate, filtered and concentrated *in vacuo*. Recrystallization with ethyl acetate yielded the title compound **(158)** (0.125 g, 71%) as a white crystalline solid, m.p. 151 ^{o}C, TLC petroleum ether - ethyl acetate, 1:1, Rf = 0.28

^{1}H (400 MHz, $CDCl_3$) δ ppm: 7.3 (1H, dd, *J* = 1.52, 7.36 Hz, Ar-H : *p*- F), 7.1 (1H, t, *J* = 8.39 Hz, Ar-H : *m*- F), 6.7(1H, s, Ar-H), 4.8 (1H, s, C-H), 4.2 (1H, s, C-H), 3.5 (1H, s, C-H), 3.4 (1H, s, C-H), 3.2 (3H, s, OMe), 3.0 (3H, s, OMe), 2.8 (3H, s, OMe)

^{13}C δ ppm: 152.1 (Ar-OMe), 150.3-147.8 (bd, *J* = 243.99 Hz, c-F), 149.6 (Ar-OMe), 145.6 (d, *J* = 12.54 Hz, ar-OMe *o* C-F), 129.9 (Ar), 129.3 *(d,* 2.3 Hz, Ar), 124.5 *(d,* 1.90 Hz, Ar), 124.0 (d J = 4.28 Hz, Ar), 122.0 (d, *J* = 14.21 Hz, Ar), 111.6 (d, *J* = 2.30 Hz, C-H: *m* -CF), 107.8 (C-H), 66.8 (CH_2), 60.1 (OMe), 59.8 (OMe), 57.6 (d, *J* = 5.95 Hz, CH_2, *o* C-F), 55.8 (OMe)

***λmax cm*$^{-1}$:** 2912, 2831, 1608, 1517, 1494, 1465, 1412, 1399, 1258, 1222, 1135, 1158, 1034

2',6-Bis(bromomethyl)-3'-fluoro 2,3,4,4'-tetramethoxy-1,1'-biphenyl (159)

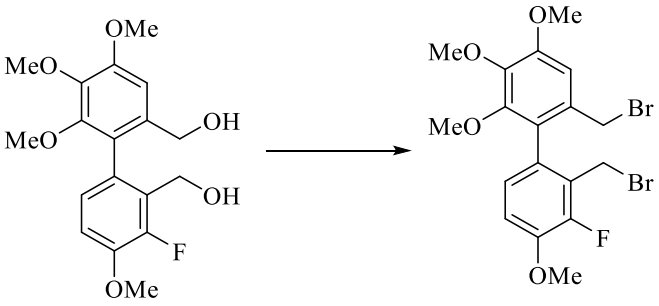

157 **159**

To a flask containing (3-fluoro 4,4',5',6'-tetramethoxy-[1,1'-biphenyl]-2,2'-diyl)dimethanol **(157)** (0.50 g, 1.4 mmol, 1.0 eq) in dichloromethane (5 mL), phosphorous tribromide (0.3 mL, 3.1 mmol, 2.2 eq) was added dropwise at 0 ^{o}C. After 1 hr the reaction mixture was allowed to warm to room temperature and stir overnight. The temperature was lowered to 0 ^{o}C and water (10 mL) was slowly added. The aq phase was extracted with dichloromethane (2 x 10 mL), washed with sat. aq $NaHCO_3$ (2 x 10 mL), brine, dried with anhydrous sodium sulphate and concentrated *in vacuo*. The oil produced was further purified by column chromatography (10 g silica gel, hexane - ethyl acetate, 1:1) and recrystallized from ethanol to yield the title compound (159) as a white powder **(159)** (0.49 g, 79%), m.p 145 ^{o}C. TLC petroleum ether - ethyl acetate, 1:1, Rf = 0.16

^{1}H (400 MHz, $CDCl_3$) δ ppm: 7.41 (1H, dd, *J* = 1.05, 7.22 Hz, Ar-H : *p*- F), 6.92 (1H, t, *J* = 8.27 Hz, Ar-H : *m*- F), 6.79 (1H, s, Ar-H : *o* 4 OMe), 4.42 (1H, d, *J* = 9.88 Hz, Ar-CH_2-Br), 4.25 (1H, d, *J* = 10.54 Hz, Ar-CH_2-Br), 4.03 (1H, d, *J* = 10.54 Hz, Ar-CH_2-Br), 4.03 (1H, d, *J* = 10.54 Hz, Ar-CH_2-Br), 3.98 (1H, dd, *J* = 2.66, 10.21 Hz, CH_2Br; *o* CF), 3.88 (3H, s, OMe), 3.86 (3H, s, OMe), 3.84 (3H, s, OMe), 3.53 (3H, s, OMe)

^{13}C δ ppm: 150.3-147.8 (bd, *J* = 243.99 Hz, c-F), 152.1 (Ar-OMe), 149.6 (2 X Ar-OMe), 145.6 (d, *J* = 12.54 Hz, ar-OMe *o* C-F), 129.9 (Ar), 129.3 (d, *J* = 2.3 Hz, Ar), 124.5 (d, *J* = 1.90 Hz Ar), 124.0 (d J = 4.28 Hz, Ar), 122.0 (d, *J* = 14 Hz, Ar), 111.6 (d, *J* = 2.30 Hz, C-H), 107.8 (C-H), 62.1 (OMe), 61.8 (OMe), 57.4 (OMe), 57.1 (OMe) 38.6 (d, *J* = 6.23 Hz, CH_2, *o* C-F), 29.4 (CH_2Br)

***Amax cm^{-1}*:** 2894, 1598, 1481, 1471, 1453, 1369, 1306, 1293, 1124, 1112, 871, 856

8-Fluoro 1,2,3,9-tetramethoxy-5,7-dihydrodibenzo[c,e]thiepine (160)

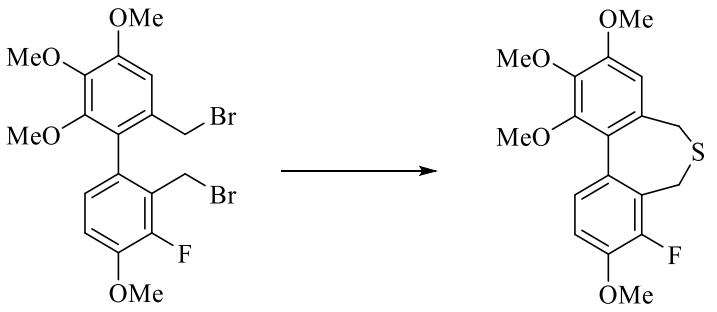

159 **160**

To a solution of 2',6-bis(bromomethyl)-3'-fluoro 2,3,4,4'-tetramethoxy-1,1'-biphenyl **(159)** (0.286 g, 0.6 mmol, 1.0 eq) in methanol/water (20 mL/ 1 mL) sodium sulfide (0.43 g, 1.8 mmol, 3.0 eq) was added and the reaction mixture was heated at reflux overnight. The mixture allowed to cool and the methanol removed *in vacuo*. Water (10 mL) was added and the white solid produced was collected by filtration. The crude product was further purified by column chromatography (10 g silica gel, hexane - ethyl acetate, 1:1) and recrystallized from ethanol to yield the title product **(160)** (0.17 g, 81%). Mp 173 $^{o\,C\,TLC}$ petroleum ether - ethyl acetate, 1:1, Rf = 0.21

^{1}H (400 MHz, Acetone-*d6*) δ ppm: 7.02- 6.98 (2H, m, 2 Ar-H: *p* and *m* to C-F), 6.88 (1H, s, Ar-H : *o* 4 OMe), 3.87 (3H, s, OMe), 3.84 (3H, s, OMe), 3.83 (3H, s, OMe), 3.75 (1H, d, *J* = 12.67 Hz, C-H), 3.53 (3H, s, OMe), 3.33 (1H, d, *J* = 12.67 Hz, C-H), 3.16 (1H, d, *J* = 13.22 Hz, C-H), 3.13 (1H, dd, *J* = 3.41 Hz, 12.61 Hz, C-H)

^{13}C δppm:153.3 (Ar-OMe), 150.8 (Ar-OMe), 150.23-147.8 (bd, *J* = 247.13, Hz, C-F), 146.9 (d, *J* = 12.81 Hz, Ar-OMe:*o CF*), 141.7 (Ar-OMe), 131.8 (Ar), 129.0 (d, *J* = 2.14 Hz, Ar), 125.5 (d, *J* = 4.08 Hz, Ar), 124.6 (d, *J* = 2.08 Hz, Ar-H), 123.7 (d, *J* = 13.3 Hz, Ar)111.6 (d, *J* = 2.14 Hz, Ar-H), 107.3 (Ar-H), 61.1 (OMe), 60.8 (OMe), 56.3 (OMe), 56.0 (OMe), 31.8 (Ar-CH_2), 23.4 (d, *J* = 4.41 Hz, CH-$_2$:*o* CF).

***Λmax cm*$^{-1}$:** 2894, 2831, 1485, 1451, 1434, 139, 1281, 1273, 1103, 984, 821, 780, 694

8-Fluoro 1,2,3,9-tetramethoxy-5,7-dihydrodibenzo[c,e]thiepine oxide and dioxide (161, 162)

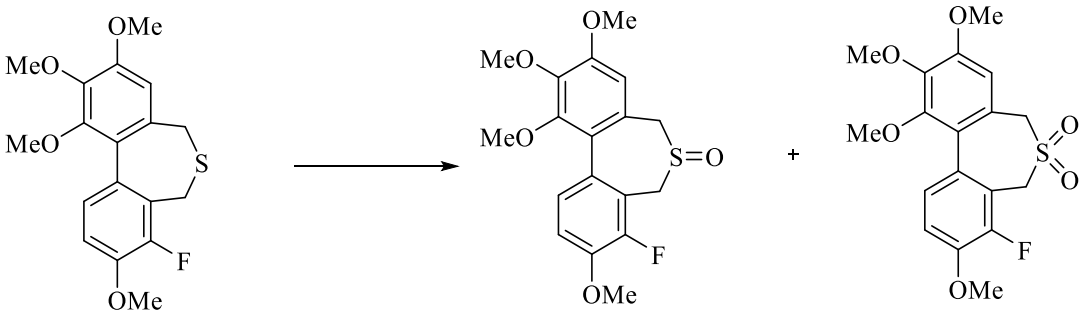

160 **161** **162**

Meta-Chloroperoxybenzoic acid (m-CPBA) (0.06 g, 0.36 mmol, 1 eq) was added to a solution of 2',6-bis(bromomethyl)-3'-fluoro 2,3,4,4'-tetramethoxybiphenyl **(160)** (0.12 g, 0.36 mmol, 1 eq) in acetone (5 mL) and stirred at 0 ^{o}C for 5 hrs. Water (20 mL) was added and the solution warmed to room temperature. The reaction mixture was extracted with ether (3 x 10 mL), dried with anhydrous sodium sulphate, filtered and concentrated *in vacuo*. The crude mixture was dissolved in dichloromethane (10 mL) and washed with 2 M NaOH (10 mL). The organic layer was washed with brine (20 mL), dried with anhydrous magnesium sulphate and concentrated *in vacuo*. Further purification of the crude mixture was achieved by column chromatography (dichloromethane - methanol 9:1) yielding the title compounds. The thiepene oxide **(161)** was recrystallised from methanol (0.04 g, 32%), M.p. 204 ^{o}C. TLC petroleum ether - ethyl acetate, 1:1, Rf = 0.34. Thiepene dioxide **(162)** was recrystallised from ethanol (0.06 g, 48%), m.p. 185 $^{o\,C\,TLC}$ petroleum ether - ethyl acetate, 1:1, Rf = 0.28

Thiepine oxide

^{1}H (400 MHz, $CDCl_3$) δ ppm: 7.02 (1H, dd, *J* = 7.78, 1.54 Hz, Ar-H : *p*- F), 8.62 (1H, t, *J* = 8.62 Hz, Ar-H : *m*- F), 6.59 (1H, s, Ar-H : *o* 4 OMe), 3.87 (3H, s, OMe),3.84 (3H, s, OMe), 3.83 (3H, s, OMe), 3.75 (1H, d, *J* = 12.38 Hz, C-H), 3.53 (3H, s, OMe), 3.33 (1H, d, *J* = 13.32 Hz, C-H), 3.16 (1H, d, *J* = 12.38 Hz, C-H), 3.49 (1H, d, *J* = 13.32 Hz, C-H)

^{13}C δ ppm: 153.3(Ar-OMe), 150.8 (Ar-OMe),150.2-147.8 (bd, *J* = 243.61 Hz, c-F), 146.9 (d, *J* = 12.63 Hz, Ar-OMe: o C-F), 141.8 (Ar-OMe), 129.0 (d, *J* = 2.41 Hz, Ar), 125.6(d, *J* = 3.98 Ar-H: *o* CF), 124.7 (d, *J* = 2.30 Hz, Ar), 11.6 (d, *J* = 2.02 Hz, Ar-H), 107.3 (Ar), 61.1 (OMe), 60.8 (OMe), 56.3, (OMe), 56.1 (OMe), 31.8 (CH_2- A ring), 23.42 (d, *J* = 4.48 Hz, CH_2-*o* C-F)

***Amax cm*$^{-1}$** 2941, 2832, 1618, 1576, 1484, 1455, 1412, 1349, 1238, 1223, 1146, 1118, 1036

Thiepine dioxide

^{1}H (400 MHz, $CDCl_3$) δ ppm: 7.2 (1H, dd, *J* = 1.70, 7.77 Hz, Ar-H : *p*- F), 7.01 (1H, t, *J* = 8.64 Hz, Ar-H : *m*- F), 6.71 (1H, s, Ar-H : *o* 4 OMe), 4.45 (1H, dd, *J* = 2.45, 12.31 Hz, C-H), 3.90 (1H, d, *J* = 14.20 Hz, C-H) 3.91 (3H, s, OMe), 3.87 (3H, s, OMe), 3.86 (3H, s, OMe), 3.81 (1H, dd, *J* = 1.90, 10.93 Hz, C-H), 3.68 (1H, dd, J = 2.45, 12.31 Hz, C-H), 3.58 (3H, s, OMe)

^{13}C δ ppm: 157.2(Ar-OMe), 155.1-151.7 (bd, *J* = 245.22 Hz, C-F), 149.5 (2Ar-OMe),146.9 (d, *J* = 12.63 Hz, Ar-OMe: o C-F), 132.0 (d, *J* = 3.21 Hz, Ar), 129.6 (d, *J* = 4.25Ar-H: *o* CF), 126.1 (d, *J* = 1.92 Hz, Ar), 117.6 (d, *J* = 3.18 Hz, Ar-H), 107.3 (Ar), 61.1 (2OMe), 56.3, (OMe), 56.1 (OMe), 44.2 (CH_2- A ring), 39.3 (d, *J* = 5.2 Hz, CH_2-*o* C-F)

***Amax cm*$^{-1}$** 2955, 2784, 1633, 1554, 1465, 1434, 1390, 1341, 1222, 1190, 1123, 1112, 1059

_N_-Benzyl-8-fluoro 1,2,3,9-tetramethoxy-6,7-dihydro 5 H-dibenzo[c,e]azepine (165)

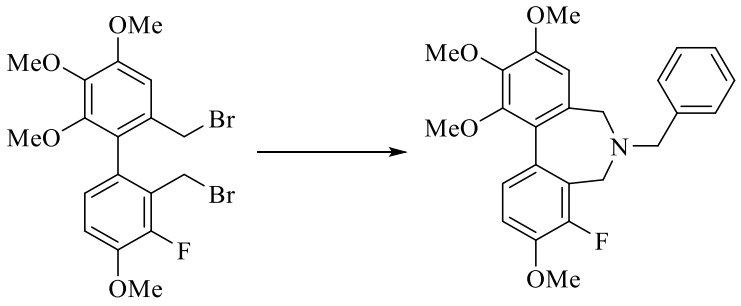

159 **165**

Benzylamine (0.28 mL, 2 mmol, 6 eq) was added to a solution of 2',6-bis(bromomethyl)-3'-fluoro 2,3,4,4'-tetramethoxybiphenyl (0.20 g, 0.42 mmol, 1 eq) in dry DMF (20 mL). Triethylamine (0.35 mL, 2 mmol, 6 eq) was added and the reaction was stired overnight at room temperature. The mixture was extracted with ethyl acetate (2 x 20 mL), the oganic layer washed with water (4 x 100 mL) brine (30 mL), dried with sodium sulphate, filtered and concentrated *in vacuo*. The crude product was further purified by column chromatography (40 g silica gel, hexane - ethyl acetate, 7:3) and recrystallized from ethanol to yield the title product (0.12 g, 67%). Mp 140 $^{o\,C}$ ^{TLC} petroleum ether - ethyl acetate, 1:1, Rf = 0.19

^{1}H (400 MHz, $CDCl_3$) δ ppm:7.41 (2H, d, *J* = 7.31 Ar-H), 7.32- 7.26 (3H, m, ArH), 7.21-7.17 (2H, m, Ar-H), 6.92 (1H, t, *J* = 8.99 Hz, Ar-H : *m*- F), 6.62 (1H, s, Ar-H : *o* 4 OMe), 3.99 (1H, d, *J* = 13.92 Hz, C-H), 3.92 (3H, s, OMe), 3.85 (3H, s, OMe), 3.82 (3H, s, OMe), 3.69 (1H, d, *J* = 13.06 Hz, CH), 3.59 (3H, s, OMe), 3.52 (1H, d, *J* = 13.06 Hz, C-H), 3.44 (1H, d, *J* = 11.76 Hz, C-H, N-Benzyl), 3.11 (1H, dd, *J* = 4.60, 16.31 Hz, C-H (α-N, *o* CF) 2.85 (1H, d, *J* = 11.76 Hz, C-H, N-Benzyl)

^{13}C δ ppm: δ ppm:159.1-156.5(bd, *J* = 251.54 Hz, c-F), 154.2(Ar-OMe), 151.8 (2Ar-OMe), 149.6 (d, *J* = 12.54 Hz, ar-OMe *o* C-F), 136.9(2Ar), 129.3 *(d,* 2.3 Hz, Ar), 128.1 (2Ar), 124.5 (d, *J* = 1.90 Hz Ar), 124.0(d J = 4.28 Hz, Ar), 123.9 (Ar), 122.0(d, *J* = 14 Hz, Ar), 118.3 (Ar-H), 114.2 (Ar),111.6 (d, *J* = 2.30 Hz, C-H), 107.8 (2C-H), 66.8 (CH_2), 60.1 (OMe), 59.8 (OMe), 57.6 (d, *J* = 5.95 Hz, CH_2, *o* C-F), 55.8 (OMe) 48.2 (N-Benzyl)

***Amax cm*$^{-1}$:** 2973, 2824, 1611, 1582, 1515, 1476, 1427, 1337, 1203, 1112, 1045, 732, 682

2-Formyl-6-methoxyphenyl acetate (167)

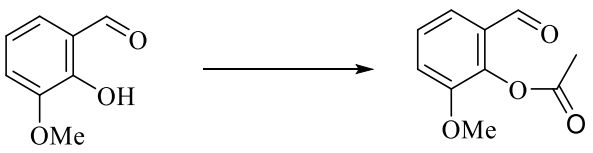

167 **168**

Orthovanillin **(167)** (5.00 g, 32.7 mmol, 1 eq) was dissolved in pyridine (20 mL) and acetic anhydride (3.50 mL, 34 mmol, 1.2 eq) added. The mixture was stirred overnight at room temperature. The contents of the flask where transferred to a solution of HCl (6 M, 30 mL) and stirred for 10 min. The white solid formed was filtered and recrystallized from methanol to yield the title compound **(168)** (4.09 g, 63%) as a salmon coloured solid. M.p. 71 ^{o}C (Lit - 71 ^{o}C), TLC petroleum ether - ethyl acetate, 1:1, Rf = 0.29

^{1}H (400 MHz, $CDCl_3$) δ ppm: 10.12 (1H, s, CHO), 7.38 (1H, dd, *J* = 1.39, 8.0 Hz, Ar-H : *m*- OMe), 7.26 (1H, d, *J* = 8.20 Hz, Ar-H : *m*- OMe), 7.14 (1H, d, *J* = 8.0 Hz, Ar-H : *o* OMe) 3.86 (3H, s, OCH_3), 2.89 (3H, s, CH_3)

Spectral and physical data for this compound were in accordance with the literature (Dark *et al*. 1997).

2-Hydroxy-3-methoxy-6-bromobenzaldehyde (170)

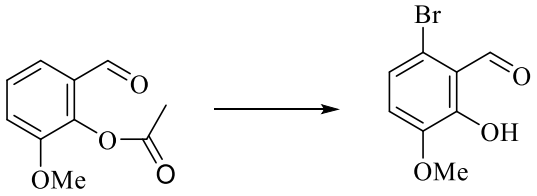

168 **169**

2-formyl-6-methoxyphenyl acetate **(168)** (4.00 g, 21 mmol, 1 eq) was added in small portions to a solution of KBr (7.49 g, 63 mmol, 3 eq) and bromine (1.00 mL, 41 mmol, 2 eq) in water (40.00 mL) over a 1 hr period. The mixture was filtered and the pink solid collected, suspended in 6M HCl (20 mL) and stirred for 3 hrs. The crude solid suspended in sat. aq $NaHCO_3$ (20 mL, 50%) for 24 hrs. The solid collected and recrystallized from methanol to yield yellow crystals **(169)** (3.57 g, 75%), m.p. 121^{o}C (Lit - 121 ^{o}C), TLC petroleum ether - ethyl acetate, 1:1, Rf = 0.19

^{1}H (400 MHz, $CDCl_3$) δ ppm: 12.22 (1H, s, OH), 10.29 (1H, s, CHO), 7.03 (1H, d, *J* = 8.53 Hz, Ar-H : *o* Br), 6.85 (1H, d, *J* = 8.53 Hz, Ar-H : *o* OMe), 3.83 (3H, s, OMe)

Spectral and physical data for this compound were in accordance with the literature (Pettit *et al*. 2000).

3-Bromo 2-formyl-6-methoxyphenyl methanesulfonate (171)

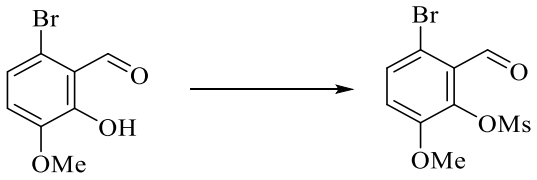

170 **171**

To a solution of 2-hydroxy-3-methoxy-6-bromobenzaldehyde **(170)** (0.275 g, 1.20 mmol, 1 eq) and triethylamine (2 mL, 1.4 mmol, 1.2 eq) in dichloromethane (10 mL) at 0 ^{o}C methanesulfonyl chloride (0.18 mL, 2.4 mmol, 2 eq) was added. The reaction mixture was stirred at first at 0 ^{o}C for 10 min, then room temperature for 30 min until the development of a brown colour. Water (30 mL) was added and the layers separated and the aqueous layer extracted with ethyl acetate (2 X 30 mL). The combined organic phases were washed with brine (30 mL), dried with sodium sulphate, filtered and concentrated *in vacuo* to yield a crude solid. This was purified by column chromatography (silica gel, petroleum ether - ethyl acetate, gradient 9:1 to 1:1) to yield the title compound as a yellow solid **(171)** (0.290 g, 79%), m.p. 95 ^{o}C (Lit - 95 ^{o}C), TLC petroleum ether - ethyl acetate, 1:1, Rf = 0.26

^{1}H (400 MHz, $CDCl_3$) δ ppm: 10.23 (1H, s, CHO), 7.55 (1H, d, *J* = 8.81 Hz, Ar-H : *o* Br), 7.05 (1H, d, *J* = 8.81 Hz, Ar-H : *o* OMe), 3.82 (3H, s, OMe), 2.24 (3H, s, $SOOCH_3$)

Spectral and physical data for this compound were in accordance with the literature (Edwards *et al*. 2011).

2,2'-Bis(hydroxymethyl)-4,4',5',6'-tetramethoxybiphenyl-3-yl methanesulfonate (172)

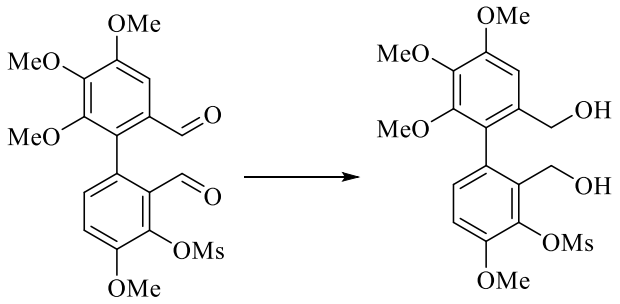

36 **172**

$NaBH_4$ (0.05 g, 0.96 mmol, 4 eq) was added in portions to a flask containing the crude dialdehyde **(36)** (0.10 g, 0.24 mmol, 1 eq) in methanol (10 mL) over a 1 hour period at 0 ^oC. Water (10 mL) was added to vessel and the reaction mixture was extracted with ethyl acetate (2 x 10 mL). The organic phase was washed with 1M HCl (10 mL), dried with anhydrous sodium sulphate, filtered and concentrated *in vacuo*. The crude diol was purified by column chromatography (10 g silica gel, hexane - ethyl acetate, 7:3) to give the purified title compound **(172)** (0.08 g, 82%), m.p 125 ^oC (Lit - 125 ^oC), TLC petroleum ether - ethyl acetate, 1:1, Rf = 0.26

^{1}H (400 MHz, $CDCl_3$) δ ppm: 7.05 (1H, d, *J* = 8.51 Hz, Ar-H : *m*- 4' OMe), 6.99 (1H, d, *J* = 8.51 Hz, Ar-H : *o* 4' OMe), 6.86 (1H, s, Ar-H : *o* 4 OMe), 4.59 (1H, dd, *J* = 4.2, 12.0 Hz, CHOH), 4.18- 4.11 (3H, m, CHOH, CH_2OH), 3.89 (3H, s, OMe), 3.86 (3H, s, OMe), 3.82 (3H, s, OMe), 3.56 (3H, s, OMe), 3.41, (3H, s, $SOOCH_3$), 2.7(2H, s, 2OH)

Spectral and physical data for this compound were in accordance with the literature (Edwards *et al*. 2011).

2,2'-Bis(bromomethyl)-4,4',5',6'-tetramethoxybiphenyl-3-yl methanesulfonate (173)

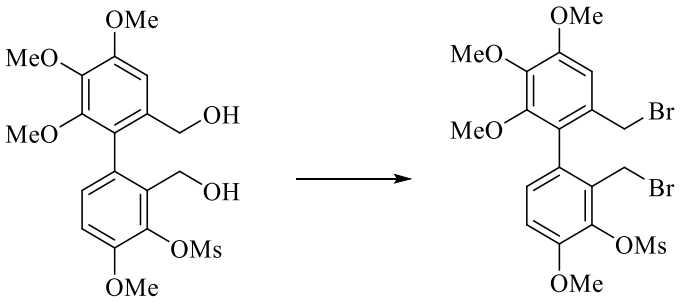

172 **173**

To a flask containing 2,2'-bis(hydroxymethyl)-4,4',5',6'-tetramethoxybiphenyl-3-yl methanesulfonate **(172)** (0.05 g, 0.12 mmol, 1.0 eq) in dichloromethane (5 mL), phosphorous tribromide (0.07 mL, 0.36 mmol, 2.2 eq) in dichloromethane (2 mL) was added dropwise at 0 ^{o}C. After 1 hr the reaction mixture was allowed to warm to room temperature and stir overnight. The temperature was lowered to 0 ^{o}C and water (10 mL) was slowly added. The aq phase was extracted with dichloromethane (2 x 10 mL), the organic layer was washed with sat. aq. $NaHCO_3$ (2 x 10 mL), brine, dried with sodium sulphate, filtered and concentrated *in vacuo*. The solid produced was recrystallized from ethanol to yield the title product **(173)** as a white powder which was used in the next step without further purification (0.06 g, 90%), Mp 152 ^{o}C, TLC petroleum ether - ethyl acetate, 1:1, Rf = 0.22

^{1}H (400 MHz, $CDCl_3$) δ ppm: 7.19 (2H, d, *J* = 8.51 Hz, Ar-H : *m*- 4' OMe), 6.99 (1H, d, *J* = 8.51, Ar-H : *m*- 4' OMe), 6.83 (1H, s, Ar-H : *o* 4 OMe), 4.53 (1H, d, *J* = 10.31 Hz, CH), 4.27 (1H, d, *J* = 10.31 Hz, CH), 4.05 (1H, d, *J* = 10.31 Hz, CH), 3.98 (1H, d, *J* = 10.31 Hz, CH), 3.93 (3H, s, OMe), 3.87 (3H, s, OMe), 3.83 (3H, s, OMe), 3.55 (3H, s, OMe), 3.42 (3H, s, $SOOCH_3$)

^{13}C δppm: 153.5 (Ar-OMe), 151.2 (Ar-OMe), 150.7 (Ar-OMe), 141.6 (Ar) Me;*o* CMes), 136.0 (Ar), 131.6, 131.1, 129.3(2Ar-H)124.6 (Ar), 40.0 SO_2CH_3) 111.1 (Ar-H), 107.2 (Ar-H), 61.1 (OMe), 60.9 (OMe), 56.1(OMe), 56.0 (OMe), 31.7 (CH_2), 25.3 (CH_2)

***Amax cm^{-1}*:** 2947, 1616, 1487, 1414, 1367, 1326, 1272, 1131, 1110, 1026, 871

8-(methanesulfonyl)-1,2,3,9-tetramethoxy-5,7-dihydrodibenzo[c,e]thiepine (175)

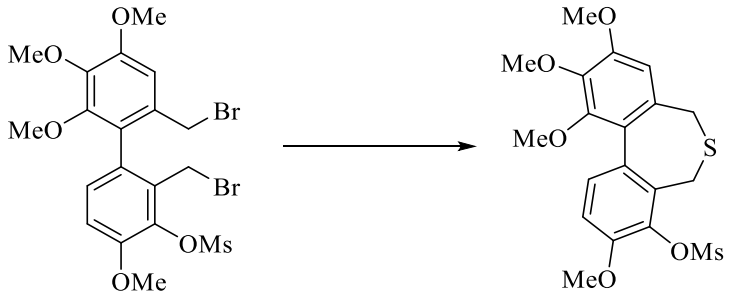

173 **175**

To a solution of 2',6-bis(bromomethyl)-3'-(methanesulfonyl)-2,3,4,4'-tetramethoxybiphenyl **(173)** (0.592g, 0.9 mmol, 1.0 eq) in methanol/water (20:1) sodium sulfide (0.683 g, 2.7 mmol, 3.0 eq) was added and the reaction mixture was heated at reflux overnight. The mixture was allowed to cool and the methanol removed *in vacuo*. Water (10 mL) was added and the white solid produced was collected by filtration. The crude product was further purified by column chromatography (10 g silica gel, hexane - ethyl acetate, 1:1) and recrystallized from ethanol to yield the title product **(175)** (0.121 g, 26%). Mp 141^{o} C TLC petroleum ether - ethyl acetate, 1:1, Rf = 0.30

^{1}H (400 MHz, $CDCl_3$) δ ppm: 7.59 (1H, d, *J* = 8.71 Hz, Ar-H : *m*- 4' OMe), 7.12 (1H, d, *J* = 8.71 Hz, Ar-H : *o* 4' OMe), 6.93 (1H, s, Ar-H : *o* 4 OMe), 4.91 (1H, d, *J* = 11.31 Hz, C-H), 4.61 (1H, d, J = 11.31 Hz, C-H), 4.15 (1H, d, *J* = 11.46 Hz, C-H), 3.99 (3H, s, OMe), 3.96 (3H, s, OMe), 3.92 (3H, s, OMe), 3.88 (1H, d, *J* = 11.46 Hz, C-H), 3.73 (3H, s, OMe), 3.42 (3H, s, S – CH_3).

^{13}C δ ppm:153.8 (Ar-OMe), 151.3 (Ar-OMe), 150.6 (Ar-OMe), 142.8 (Ar-OMe), 137.1 (Ar), 131.0 (Ar), 130.8 (Ar), 130.2 (Ar), 129.0 (Ar-H), 125.4 (Ar-H), 112.3 (Ar-H), 107.6 (Ar-H), 60.9 (2OMe), 60.7 (OMe), (CH_2), 56.1 (OMe), (CH_2), 35.3 (-O Ms)

λmax cm^{-1}: 3020, 1625, 1565, 1475, 1460, 1350, 1270, 1150, 1135, 920, 825

3'-Fluoro 2,3,4-trimethoxy-4'-methylbiphenyl (181)

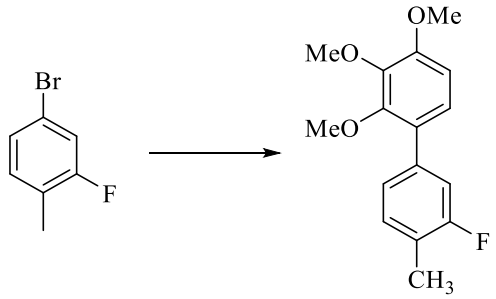

181

General procedure 1

The title compound was purified by column chromatography (10 g silica gel, hexane - ethyl acetate, 9:1) to yield the title compound **(181)** as a colourless oil (0.15 g, 84%). TLC petroleum ether - ethyl acetate, 1:1, Rf = 0.23

^{1}H (400 MHz, $CDCl_3$) δ ppm: 7.27- 7.20 (3H, m, Ar-H), 7.05 (1H, d, *J* = 8.71 Hz Ar-H : *m*-4 OMe), 6.76 (1H, d, *J* = 8.71 Hz, Ar-H : *o* 4 OMe), 3.97 (3H, s, OMe), 3.91 (3H, s, OMe), 3.73 (3H, s, OMe), 2.34 (3H, s, CH_3)

^{13}C δ ppm:162.3 (*bd*, *J* = 246.37 Hz, c-F), 159.9 (Ar-OMe), 153.4 (Ar-OMe), 151.4 (Ar-OMe), 142.8 (Ar) 137.7 (2 Ar), 131.2 (d, *J* = 5.7, Ar), 124.7 (d, *J* = 3.11 Hz, Ar), 123.0 (C,d, Ar), 115.7(d, *J* = 24.3 Hz, ar-H, *o* F),107.5(Ar-H), 60.9 (2OMe), 56.0 (OMe), 14.4(Me)

***Λmax cm*$^{-1}$:** 3071, 1316, 1211, 749, 548

3'-Fluoro 2,3,4,4'-tetramethoxybiphenyl (182)

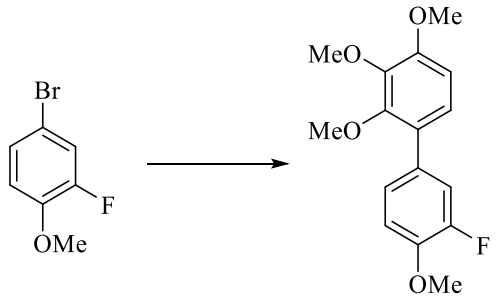

182

General procedure 1

The title compound was purified by column chromatography (10 g silica gel, hexane - ethyl acetate, 9:1) to yield the title compound **(182)** as an amber oil (0.120 g, 92%), TLC petroleum ether - ethyl acetate, 1:1, Rf = 0.29

^{1}H (400 MHz, $CDCl_3$) δ ppm: 7.27(1H, dd, *J* = 2.31, 12.28 Hz, Ar-H), 7.13 (1H, d, *J* = 8.81 Hz, Ar-H), 6.92- 6.88 (2H, m, Ar-H), 6.65 (1H, d, *J* = 8.31 Hz, Ar-H), 3.93 (3H, s, OMe), 3.90 (3H, s, OMe), 3.87 (3H, s, OMe), 3.70 (3H, s, OMe)

^{13}C δ ppm:153.2-150.8, (bd, *J* = 244.91 Hz, C-F), 153.1 (C- OMe),151.3(C- OMe),145.5(C-OMe),142.6(Ar), 131.2(d, *J* = 8.52 Hz, (oMe-*o* F), 127.2(d, *J* = 1.48 Hz, Ar), 124.7 (d, *J* = 3.46, Ar-H), 124.4 (Ar-H), 116.9 (d, *J* = 19.58 Hz, Ar-H *o* CF), 13.0 (d, *J* = 2.17 Hz, Ar-H), 107.5(Ar-H), 61.0 (OMe), 60.8 (OMe), 56.3 (OMe), 56.1 (OMe)

***Amax cm*$^{-1}$:** 3038, 1113, 1008, 810, 776

2,3,4-Trimethoxy-4'-methyl-3'-nitrobiphenyl (183)

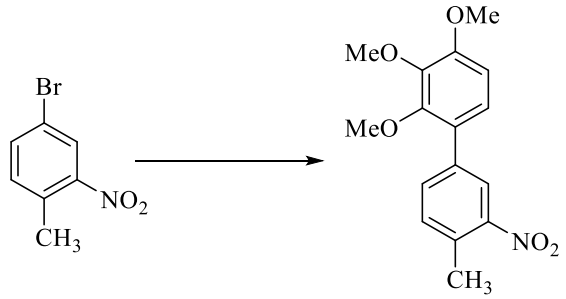

183

General procedure 1

The title compound was purified by column chromatography (10 g silica gel, hexane - ethyl acetate, 9:1) to yield the title compound **(183)** as green crystals (0.210 g, 88%) M.p. 141 ^{o}C, TLC petroleum ether - ethyl acetate, 1:1, Rf = 0.23

^{1}H (400 MHz, $CDCl_3$) δ ppm: 8.16 (1H, d, *J* = 7.69 Hz, Ar-H : *m*- 4 OMe), 7.69 (1H, dd, *J* = 2.41, 8.46 Hz, Ar-H : *o* NO_2), 7.38 (1H, d, *J* = 7.69 Hz, Ar-H : *o* 4 OMe), 7.07 (1H, d, *J* = 8.12 Hz, Ar-H : *m*- CH_3), 6.79 (1H, d, *J* = 8.12 Hz, Ar-H : *m*- CH_3), 3.98 (3H, s, OMe), 3.93 (3H, s, OMe), 3.75 (3H, s, OMe), 2.62 (3H, s, Me)

^{13}C δ ppm:154.9 (Ar-OMe), 151.3 (Ar-OMe), 149.2 (Ar-OMe), 142.7 (ar), 137.3 (ar) 133.7 (Ar), 132.5 (Ar), 131.74 (Ar), 125.9 (2Ar-H), 125.1 (Ar-H), 124.5(C-H, Ar-H), 60.9 (OMe), 60.7 (OMe), 56.1 (OMe), 20.3 (CH_3)

***Amax cm^{-1}* :** 3309, 2931, 1533, 130, 1293, 812, 738, 699

2,3,4,4'-Tetramethoxy-3'-nitrobiphenyl (184)

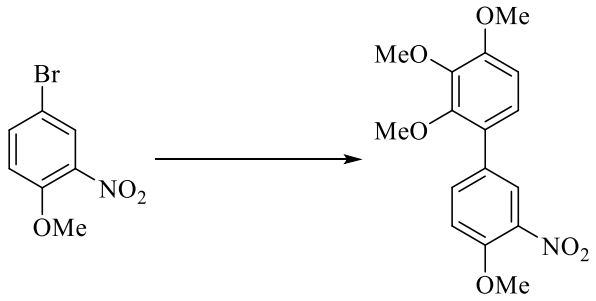

184

General procedure 1

The title compound was purified by column chromatography (10 g silica gel, hexane - ethyl acetate, 8:2) to yield the title compound **(184)** as yellow crystals (0.132, 83%), m.p. 142 ^{o}C, TLC petroleum ether - ethyl acetate, 1:1, Rf = 0.21

^{1}H (400 MHz, $CDCl_3$) δ ppm: 7.95 (1H, d, *J* = 2.31 Hz, Ar-H : *o* NO_2), 7.65 (1H, dd, *J* = 2.32, 8.32 Hz, Ar-H : *p*- NO_2), 7.05 (1H, d, *J* = 8.41 Hz, Ar-H : *m*- 4 OMe), 6.95 (1H, d, *J* = 8.41 Hz, Ar-H : *o* NO_2), 6.68 (1H, d, *J* = 8.41 Hz, Ar-H : *o* 4 OMe), 3.94 (3H, s, OMe), 3.86 (3H, s, OMe), 3.84 (3H, s, OMe),3.64 (3H, s, OMe)

^{13}C δ ppm:153.8 (Ar-OMe),153.5 (Ar-OMe), 151.3 (Ar-OMe), 142.7(Ar), 134.8 (Ar) 130.7 (Ar-H), 126.1(Ar-H), 125.(Ar-H), 124.4 (Ar-H), 113.3 (Ar-H), 107.2 (Ar-H), 61.1(OMe), 61.0 (OMe), 56.6 (OMe), 56.1 (OMe)

***Amax cm^{-1}* :** 3123, 2932, 1516, 1305, 814, 749, 698

2,3,4-Trimethoxy-4'-methylbiphenyl (187)

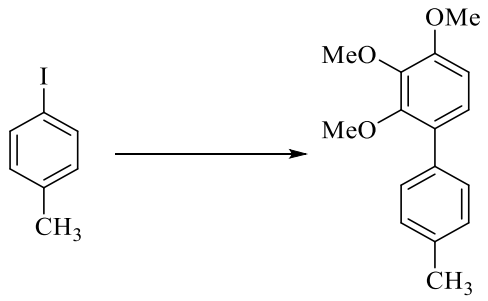

187

General procedure 1

The title compound was purified by column chromatography (10 g silica gel, hexane - ethyl acetate, 10:1) to yield the title compound **(187)** as a colourless oil (0.122 g, 93%), TLC petroleum ether - ethyl acetate, 1:1, Rf = 0.31

^{1}H (400 MHz, $CDCl_3$) δ ppm: 7.21 (2H, d, *J* = 8.12 Hz, Ar-H : *m*- CH_3), 7.10 (2 H d, *J* = 8.12 Hz, Ar-H : *o* CH_3), 6.90 (1H, d, *J* = 8.70 Hz, Ar-H : *m*- 4 OMe), 6.90 (1H, d, *J* = 8.70 Hz, Ar-H : *o* CH_3), 3.83 (3H, s, OMe),3.81 (3H, s, OMe), 3.55 (3H, s, OMe), 2.31 (3H, s, CH_3)

Spectral data was in accordance with the literature (Putta and Ghosh. 2011).

2',3',4'-Trimethoxy-N,N-dimethylbiphenyl-4-amine (186)

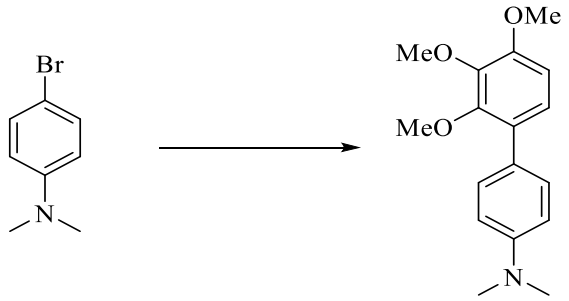

186

General procedure 1

The title compound was purified by column chromatography (10 g silica gel, hexane - ethyl acetate, 9:1) to yield the title compound as a colourless oil (0.130 g, 95%), TLC petroleum ether - ethyl acetate, 1:1, Rf = 0.1

^{1}H (400 MHz, $CDCl_3$) δ ppm: 7.31 (2H, d, *J* = 7.62 Hz, Ar-H), 6.97 (1H, d, *J* = 8.34 Hz, Ar-H), 6.71 (2H, d, *J* = 8.34 Hz, Ar-H), 6.61 (1H, d, *J* = 8.34 Hz, Ar-H), 3.86 (3H, s, OMe), 3.82 (3H, s, OMe), 3.60 (3H, s, OMe), 2.92 (6 H, s, NMe_2)

^{13}C δ ppm:152.5 (Ar-NMe_2), 151.9 (Ar-OMe), 149.5(Ar-OMe), 142.58(Ar-OMe), 129.71(2Ar-H), 128.8(Ar), 126.37(Ar), 124.5(Ar-H), 112.3(2Ar-H), 107.4(Ar-H),61.8 (OMe), 60.7 (OMe), 56.1(OMe), 40.65 ($2NMe_2$)

***Amax cm^{-}*:** 2930, 1532, 1471, 1345, 1139, 736, 718

References

Web page

Ambient-temperature Ullmann reaction: 4,5,4’,5’-tetramethoxy-1,1’-biphemyl-2’2’-dicarboxaldehyde . Available at: http://www.orgsyn.org/demo.aspx?prep=CV8P0586 [Accessed February 12, 2015a].

Taxol® NSC 125973. Microtubule assembly, organization and dynamics in axons and dendrites : Nature Reviews Neuroscience. Available at: http://www.nature.com/nrn/journal/v10/n5/box/nrn2631_BX1.html [Accessed August 19, 2012b].

Image: Available at: http://dtp.nci.nih.gov/timeline/flash/success_stories/S2_taxol.htm [Accessed April 18, 2015c].

The Binding Sites of Microtubule-Stabilizing Agents. Available at: http://ac.els-cdn.com/S1074552113000410/1-s2.0-S1074552113000410-main.pdf?_tid=5c6c104c-92b7-11e4-8fd6-00000aab0f6b&acdnat=1420227875_0fe8d056775e1f06350bbaf7d24a177f [Accessed January 2, 2015e].

http://www.sabiosciences.com/pathwaymagazine/pathways11/ppage6.php [Accessed April 18, 2015c].

Journal

Anderson, K.W. *et al*., 2006. The selective reaction of aryl halides with KOH: synthesis of phenols, aromatic ethers, and benzofurans. *Journal of the American Chemical Society*, 128(33), pp.10694–5.

Arduengo, A.J., Harlow, R.L. & Kline, M., 1991. A stable crystalline carbene. *Journal of the American Chemical Society*, 113(1), pp.361–363.

Aylett, C.H.S., Löwe, J. & Amos, L.A., 2011. Chapter one - New Insights into the Mechanisms of Cytomotive Actin and Tubulin Filaments. In K. W. J. B. T.-I. R. of C. and M. Biology, ed. Academic Press, pp. 1–71.

Bai, R. *et al*., 2000. Mapping the Binding Site of Colchicinoids on {beta}-Tubulin: 2- 2-2-chloroacetyl-2-demethylthiocolchicine covalently reacts predominantly with cysteine 239 and secondarily with cysteine 354. *Journal of Biological Chemistry*, 275(51), pp.40443–40452.

Balamuth, N.J. & Womer, R.B., 2010. Ewing's sarcoma. *The lancet oncology*, 11(2), pp.184–92.

Bassily, M.N. *et al*., 2010. Cancer survival as a function of age at diagnosis: A study of the Surveillance, Epidemiology and End Results database. *Cancer Epidemiology*, 34(6), pp.667–681.

Baudoin, O. *et al*., 2003. A Novel 1,3-Central-to Axial Chirality Induction Approach to Cyclooctadiene Lignans. *Synlett*, 2003(13), pp.2009–2012.

Baudoin, O. *et al*., 2002. Application of the Palladium-Catalyzed Borylation/Suzuki Coupling (BSC) Reaction to the Synthesis of Biologically Active Biaryl Lactams. *The Journal of Organic Chemistry*, 67(4), pp.1199–1207.

Beerepoot, L. V *et al*., 2006. Phase I clinical evaluation of weekly administration of the novel vascular-targeting agent, ZD6126, in patients with solid tumours. *Journal of clinical oncology : official journal of the American Society of Clinical Oncology*, 24(10), pp.1491–8.

Bennett, M.J. *et al*., 2010. Discovery and characterization of the laulimalide-microtubule binding mode by mass shift perturbation mapping. *Chemistry & biology*, 17(7), pp.725–34.

Besong, G. *et al*., 2008. A synthesis of (aR,7S)-(−)-N-acetylcolchinol and its conjugate with a cyclic RGD peptide. *Tetrahedron*, 64(21), pp.4700–4710.

Van der Bilt, A.R.M. *et al*., 2012. Turning promise into progress for antiangiogenic agents in epithelial ovarian cancer. *Critical reviews in oncology/hematology*. 84(2) pp.224-242

Biscoe, M.R., Barder, T.E. & Buchwald, S.L., 2007. Electronic effects on the selectivity of pd-catalyzed C-N bond-forming reactions using biarylphosphine ligands: the competitive roles of amine binding and acidity. *Angewandte Chemie (International ed. in English)*, 46(38), pp.7232–5.

Boyland, E. & Boyland, M.E., 1937. Studies in tissue metabolism: The action of colchicine and B. typhosus extract. *The Biochemical journal*, 31(3), pp.454–60.

Broady, S.D. *et al*., 2007. Asymmetric synthesis of (S)-(−)-N-acetylcolchinol via Ullmann biaryl coupling. *Tetrahedron Letters*, 48(26), pp.4627–4630.

Brun, L. *et al*., 2009. A theory of microtubule catastrophes. *Proceedings of the National Academy of Sciences.* 106(50), pp. 21173-21178

Campeau, L.-C. *et al*., 2004. Biaryl synthesis via direct arylation: establishment of an efficient catalyst for intramolecular processes. *Journal of the American Chemical Society*, 126(30), pp.9186–7.

Casado, A.L. & Espinet, P., 1998. On the Configuration Resulting from Oxidative Addition of RX to Pd(PPh 3) 4 and the Mechanism of the cis -to trans Isomerization of [PdRX(PPh 3) 2] Complexes (R = Aryl, X = Halide) †. *Organometallics*, 17(5), pp.954–959.

Castro, J.S. *et al*., 2010. Heterogeneous and homogeneous nucleation of Taxol^{TM} crystals in aqueous solutions and gels: Effect of tubulin proteins. *Colloids and Surfaces B: Biointerfaces*, 76(1), pp.199–206.

Chaplin, D.J., Pettit, G.R. & Hill, S.A., Anti-vascular approaches to solid tumour therapy: evaluation of combretastatin A4 phosphate. *Anticancer research*, 19(1A), pp.189–95.

Chen, K. *et al*., 2008. Identification of tubulin drug binding sites and prediction of relative differences in binding affinities to tubulin isotypes using digital signal processing. *Journal of molecular graphics & modelling*, 27(4), pp.497–505.

Colombel, V. *et al*., 2010. Synthesis of antimicrotubule dibenzoxepines. *Tetrahedron Letters*, 51(23), pp.3127–3129.

Conde, C. & Caceres, A., 2009. Microtubule assembly, organization and dynamics in axons and dendrites. *Nat Rev Neurosci*, 10(5), pp.319–332.

Cortese, F., Bhattacharyya, B. & Wolff, J., 1977. Podophyllotoxin as a probe for the colchicine binding site of tubulin. *The Journal of biological chemistry*, 252(4), pp.1134–40.

Dark, G.G. *et al*., 1997. Combretastatin A-4, an agent that displays potent and selective toxicity toward tumour vasculature. *Cancer research*, 57(10), pp.1829–34.

Das, B. *et al*., 2007. A mild and simple regioselective iodination of activated aromatics with iodine and catalytic ceric ammonium nitrate. *Tetrahedron Letters*, 48(1), pp.81–83.

Davis, P.D. *et al*., 2002. ZD6126: a novel vascular-targeting agent that causes selective destruction of tumour vasculature. *Cancer research*, 62(24), pp.7247–53.

Dehay, C. & Kennedy, H., 2007. Cell-cycle control and cortical development. *Nature reviews. Neuroscience*, 8(6), pp.438–50.

Denekamp, J., 1982. Endothelial cell proliferation as a novel approach to targeting tumour therapy. *British journal of cancer*, 45(1), pp.136–9.

Deng, Z., Chuaqui, C. & Singh, J., 2004. Structural interaction fingerprint (SIFt): a novel method for analyzing three-dimensional protein-ligand binding interactions. *Journal of medicinal chemistry*, 47(2), pp.337–44.

Denmark, S.E. & Kallemeyn, J.M., 2006. Stereospecific palladium-catalyzed cross-coupling of (E)- and (Z)-alkenylsilanolates with aryl chlorides. *Journal of the American Chemical Society*, 128(50), pp.15958–9.

Deprez, N.R. *et al*., 2006. Room temperature palladium-catalyzed 2-arylation of indoles. *Journal of the American Chemical Society*, 128(15), pp.4972–3.

Dibbens, J. a *et al*., 1999. Hypoxic regulation of vascular endothelial growth factor mRNA stability requires the cooperation of multiple RNA elements. *Molecular biology of the cell*, 10(4), pp.907–19.

Dirr, R., Anthaume, C. & Désaubry, L., 2008. Regioselectivity of fluorine substitution by alkoxides on unsymmetrical difluoroarenes. *Tetrahedron Letters*, 49(31), pp.4588–4590.

Dong, X., Han, Z.C. & Yang, R., 2007. Angiogenesis and antiangiogenic therapy in hematologic malignancies. *Critical reviews in oncology/hematology*, 62(2), pp.105–18.

Dorléans, A. *et al*., 2009. Variations in the colchicine-binding domain provide insight into the structural switch of tubulin. *Proceedings of the National Academy of Sciences of the United States of America*, 106(33), pp.13775–9.

Dupuis-Williams, P. *et al*., 1996. The tubulin gene family of Paramecium: Characterization and expression of the αPT1 and αPT2 genes which code for α-tubulins with unusual C-terminal amino acids, GLY and ALA. *Biology of the Cell*, 87(1–2), pp.83–93.

Edwards, D.J. *et al*., 2011. Tubulin-binding dibenz[c,e]oxepines as colchinol analogues for targeting tumour vasculature. *Organic & biomolecular chemistry*, 9(1), pp.219–31.

Ehrlich, P.F. *et al*., 2006. The value of surgery in directing therapy for patients with Wilms' tumour with pulmonary disease. A report from the National Wilms' Tumour Study Group (National Wilms' Tumour Study 5). *Journal of pediatric surgery*, 41(1), pp.162–7; discussion 162–7.

Eskens, F. a L.M. & Verweij, J., 2006. The clinical toxicity profile of vascular endothelial growth factor (VEGF) and vascular endothelial growth factor receptor (VEGFR) targeting angiogenesis inhibitors; a review. *European journal of cancer (Oxford, England : 1990)*, 42(18), pp.3127–39.

Espinet, P. & Echavarren, A.M., 2004. The mechanisms of the Stille reaction. *Angewandte Chemie (International ed. in English)*, 43(36), pp.4704–34.

Evelhoch, J.L. *et al*., 2004. Magnetic resonance imaging measurements of the response of murine and human tumours to the vascular-targeting agent ZD6126. *Clinical cancer research : an official journal of the American Association for Cancer Research*, 10(11), pp.3650–7.

Fuertes, M. a, Alonso, C. & Pérez, J.M., 2003. Biochemical modulation of Cisplatin mechanisms of action: enhancement of antitumour activity and circumvention of drug resistance. *Chemical reviews*, 103(3), pp.645–62.

Galbraith, S.M. *et al*., Effects of combretastatin A4 phosphate on endothelial cell morphology in vitro and relationship to tumour vascular targeting activity in vivo. *Anticancer research*, 21(1A), pp.93–102.

Galli, U. *et al*., 2015. Design, Synthesis and Biological Evaluation of Combretabenzodiazepines: a Novel Class of Antitubulin Agents. *Journal of medicinal chemistry*.

García-Cuadrado, D. *et al*., 2007. Proton-abstraction mechanism in the palladium-catalyzed intramolecular arylation: substituent effects. *Journal of the American Chemical Society*, 129(21), pp.6880–6.

Gaukroger, K. *et al*., 2003a. Structural requirements for the interaction of combretastatins with tubulin: how important is the trimethoxy unit? *Organic & biomolecular chemistry*, 1(17), pp.3033–7.

Gaukroger, K. *et al*., 2003b. Structural requirements for the interaction of combretastatins with tubulin: how important is the trimethoxy unit?Electronic supplementary information (ESI) available: experimental details. See http://www.rsc.org/suppdata/ob/b3/b306878a/. *Organic & Biomolecular Chemistry*, 1(17), p.3033.

Gee, M.S. *et al*., 2003. Tumour vessel development and maturation impose limits on the effectiveness of anti-vascular therapy. *The American journal of pathology*, 162(1), pp.183–93.

Goertz, D.E. *et al*., 2002. High-frequency Doppler ultrasound monitors the effects of antivascular therapy on tumour blood flow. *Cancer research*, 62(22), pp.6371–5.

Gopie, J.P., Vasen, H.F. a & Tibben, A., 2012. Surveillance for hereditary cancer: Does the benefit outweigh the psychological burden?-A systematic review. *Critical reviews in oncology/hematology*, pp.1–12.

Grosios, K. *et al*., Combination chemotherapy with combretastatin A-4 phosphate and 5-fluorouracil in an experimental murine colon adenocarcinoma. *Anticancer research*, 20(1A), pp.229–33.

Hanahan, D. & Weinberg, R. a, 2011. Hallmarks of cancer: the next generation. *Cell*, 144(5), pp.646–74.

Hatanaka, Y. & Hiyama, T., 1988. Cross-coupling of organosilanes with organic halides mediated by a palladium catalyst and tris(diethylamino)sulfonium difluorotrimethylsilicate. *The Journal of Organic Chemistry*, 53(4), pp.918–920. Available at: http://dx.doi.org/10.1021/jo00239a056

Heravi, M.M. & Hashemi, E., 2012. Recent Applications of the Suzuki Reaction in Total Synthesis. *Tetrahedron*. 68(45), pp. 9145-9178

Hinnen, P. & Eskens, F. a L.M., 2007. Vascular disrupting agents in clinical development. *British Journal of Cancer*, 96(8), pp.1159–1165.

Hollebecque, A., Massard, C. & Soria, J.-C., 2012. Vascular disrupting agents: a delicate balance between efficacy and side effects. *Current opinion in oncology*, 24(3), pp.305–15.

Horwitz, S.B., 1994. Taxol (paclitaxel): mechanisms of action. *Annals of oncology : official journal of the European Society for Medical Oncology / ESMO*, 5 Suppl 6, pp.S3–6.

Huang, J. *et al*., 1999. Stereoelectronic Effects Characterizing Nucleophilic Carbene Ligands Bound to the Cp*RuCl (Cp* = η 5 -C 5 Me 5) Moiety: A Structural and Thermochemical Investigation. *Organometallics*, 18(12), pp.2370–2375.

Igau, A. *et al*., 1988. Analogous.alpha.,.alpha.'-bis-carbenoid, triply bonded species: synthesis of a stable.lambda.3-phosphino carbene-.lambda.5-phosphaacetylene. *Journal of the American Chemical Society*, 110(19), pp.6463–6466.

Ishiyama, T., Murata, M. & Miyaura, N., 1995. Palladium(0)-Catalyzed Cross-Coupling Reaction of Alkoxydiboron with Haloarenes: A Direct Procedure for Arylboronic Esters. *The Journal of Organic Chemistry*, 60(23), pp.7508–7510.

Jinno, S. *et al*., 1999. Total synthesis of a natural antioxidant and structure-activity relationships of related compounds. *Chemical & pharmaceutical bulletin*, 47(9), pp.1276–83.

Joncour, A. *et al*., 2007. Asymmetric synthesis of antimicrotubule biaryl hybrids of allocolchicine and steganacin. *Chemistry (Weinheim an der Bergstrasse, Germany)*, 13(19), pp.5450–65.

Joncour, A. *et al*., 2006. Biaryl axis as a stereochemical relay for the enantioselective synthesis of antimicrotubule agents. *Angewandte Chemie (International ed. in English)*, 45(25), pp.4149–52.

Joncour, A. *et al*., 2008. Synthesis of anti-microtubule biaryls and preliminary evaluation as vascular-disrupting agents. *ChemMedChem*, 3(11), pp.1731–9.

Jordan, M.A. *et al*., 1993. Mechanism of mitotic block and inhibition of cell proliferation by taxol at low concentrations. *Proceedings of the National Academy of Sciences*, 90(20), pp.9552–9556.

Jordan, M.A., Thrower, D. & Wilson, L., 1992. Effects of vinblastine, podophyllotoxin and nocodazole on mitotic spindles. Implications for the role of microtubule dynamics in mitosis. *Journal of cell science*, 102 (Pt 3, pp.401–16.

Jordan, M.A. & Wilson, L., 2004. Microtubules as a target for anticancer drugs. *Nature reviews. Cancer*, 4(4), pp.253–65.

Jubb, A.M. *et al*., 2006. Predicting benefit from anti-angiogenic agents in malignancy. *Nature reviews. Cancer*, 6(8), pp.626–35.

Jussila, L. & Alitalo, K., 2002. Vascular growth factors and lymphangiogenesis. *Physiological reviews*, 82(3), pp.673–700.

Kakiuchi, F. *et al*., 2003. A Ruthenium-Catalyzed Reaction of Aromatic Ketones with Arylboronates: A New Method for the Arylation of Aromatic Compounds via C−H Bond Cleavage. *Journal of the American Chemical Society*, 125(7), pp.1698–1699.

Kang, G.J. *et al*., 1990. N-acetylcolchinol O methyl ether and thiocolchicine, potent analogs of colchicine modified in the C ring. Evaluation of the mechanistic basis for their enhanced biological properties. *The Journal of biological chemistry*, 265(18), pp.10255–9.

Kanthou, C. & Tozer, G.M., 2002. The tumour vascular targeting agent combretastatin A-4-phosphate induces reorganization of the actin cytoskeleton and early membrane blebbing in human endothelial cells. *Blood*, 99(6), pp.2060–9.

Kaye, S. *et al*., 2001. The Use of Catalytic Amounts of CuCl and Other Improvements in the Benzyne Route to Biphenyl-Based Phosphine Ligands. *Advanced Synthesis & Catalysis*, 343(8), pp.789–794.

Kelly, S.M., 1984. The synthesis and transition temperatures of benzoate ester derivatives of 2-fluoro 4-hydroxy-and 3-fluoro 4-hydroxybenzonitriles. *Helvetica Chimica Acta*, 67(6), pp.1572–1579.

King, A.O., Okukado, N. & Negishi, E., 1977. Highly general stereo-, regio-, and chemo-selective synthesis of terminal and internal conjugated enynes by the Pd-catalysed reaction of alkynylzinc reagents with alkenyl halides. *Journal of the Chemical Society, Chemical Communications*, (19), p.683

Kita, Y. *et al*., 1996. Non-phenolic oxidative coupling of phenol ether derivatives using phenyliodine(III) bis(trifluoroacetate). *Chemical Communications*, (12), p.1481.

KloM., Li, X.C. & Ghobrial, R.M., RhoA Cytoskeletal Pathway to Transplantation. *Journal of Immunology & Clinical Research*.

Kohler, B. a *et al*., 2011. Annual report to the nation on the status of cancer, 1975-2007, featuring tumours of the brain and other nervous system. *Journal of the National Cancer Institute*, 103(9), pp.714–36.

Konerding, M.A., Fait, E. & Gaumann, A., 2001. 3D microvascular architecture of pre-cancerous lesions and invasive carcinomas of the colon. *British journal of cancer*, 84(10), pp.1354–62.

Krendel, M., Zenke, F.T. & Bokoch, G.M., 2002. Nucleotide exchange factor GEF-H1 mediates cross-talk between microtubules and the actin cytoskeleton. *Nature cell biology*, 4(4), pp.294–301.

Lai, E.Y., Remillard, S.P. & Fulton, C., 1994. A β-tubulin gene of Naegleria encodes a carboxy-terminal tyrosine: Aromatic amino acids are conserved at carboxy termini. *Journal of Molecular Biology*, 235(1), pp.377–388.

Lam, K.C., Marder, T.B. & Lin, Z., 2010. Mechanism of the Palladium-Catalyzed Borylation of Aryl Halides with Pinacolborane. *Organometallics*, 29(7), pp.1849–1857.

Lane, B.S. & Sames, D., 2004. Direct C−H Bond Arylation: Selective Palladium-Catalyzed C2-Arylation of N -Substituted Indoles. *Organic Letters*, 6(17), pp.2897–2900.

Lapointe, D. & Fagnou, K., 2010. Overview of the Mechanistic Work on the Concerted Metallation–Deprotonation Pathway. *Chemistry Letters*, 39(11), pp.1118–1126.

Leboeuf, D., Ciesielski, J. & Frontier, A., 2013. Gold(I)-Catalyzed Iodination of Arenes. *Synlett*, 25(03), pp.399–402.

Lennard, C.M. *et al*., 2001. Intensity of vascular endothelial growth factor expression is associated with increased risk of recurrence and decreased disease-free survival in papillary thyroid cancer. *Surgery*, 129(5), pp.552–8.

Lin, C.M. *et al*., 1989. Antimitotic natural products combretastatin A-4 and combretastatin A-2: studies on the mechanism of their inhibition of the binding of colchicine to tubulin. *Biochemistry*, 28(17), pp.6984–6991.

Loeb, L.A., 2001. Perspectives in Cancer Research A Mutator Phenotype in Cancer 1.,(1), pp.3230–3239.

Lorusso, G. & Rüegg, C., 2012. New insights into the mechanisms of organ-specific breast cancer metastasis. *Seminars in Cancer Biology*, 22(3), pp.226–233.

Lorusso, G. & Rüegg, C., 2008. The tumour microenvironment and its contribution to tumour evolution toward metastasis. *Histochemistry and Cell Biology*, 130(6), pp.1091–1103.

LoRusso, P.M. *et al*., 2008. Phase I clinical evaluation of ZD6126, a novel vascular-targeting agent, in patients with solid tumours. *Investigational new drugs*, 26(2), pp.159–67.

Löwe, J. *et al*., 2001. Refined structure of alpha beta-tubulin at 3.5 A resolution. *Journal of molecular biology*, 313(5), pp.1045–57.

Ludford, R.J., 1948. Factors determining the action of colchicine on tumour growth. *British journal of cancer*, 2(1), pp.75–86.

Ludueña, R.F., 1997. Multiple Forms of Tubulin: Different Gene Products and Covalent Modifications. In K. W. J. B. T.-I. R. of Cytology, ed. Academic Press, pp. 207–275.

Machaca, K., 2011. Ca2+ signaling, genes and the cell cycle. *Cell Calcium*, 49(5), pp.323–330.

Mader, R.M. *et al*., 1997. Transcription and activity of 5-fluorouracil converting enzymes in fluoropyrimidine resistance in colon cancer in vitro. *Biochemical pharmacology*, 54(11), pp.1233–42.

Madhusudan, S. & Ganesan, T.S., 2004. Tyrosine kinase inhibitors in cancer therapy. *Clinical biochemistry*, 37(7), pp.618–35.

Maier, U.H. & Zenk, M.H., 1997. Colchicine is formed by para-para phenol coupling from autumnaline. *Tetrahedron Letters*, 38(42), pp.7357–7360.

Mamane, V., Hannen, P. & Fürstner, A., 2004. Synthesis of phenanthrenes and polycyclic heteroarenes by transition-metal catalyzed cycloisomerization reactions. *Chemistry (Weinheim an der Bergstrasse, Germany)*, 10(18), pp.4556–75.

Martin, R. & Buchwald, S.L., 2007. Pd-catalyzed Kumada-Corriu cross-coupling reactions at low temperatures allow the use of Knochel-type Grignard reagents. *Journal of the American Chemical Society*, 129(13), pp.3844–5.

Matos, K. & Soderquist, J.A., 1998. Alkylboranes in the Suzuki-Miyaura Coupling: Stereochemical and Mechanistic Studies. *The Journal of organic chemistry*, 63(3), pp.461–470.

McGown, A.T. & Fox, B.W., 1989. Structural and biochemical comparison of the anti-mitotic agents colchicine, combretastatin A4 and amphethinile. *Anti-cancer drug design*, 3(4), pp.249–54.

McNulty, J. *et al*., 2015. Antimitotic activity of structurally simplified biaryl analogs of the anticancer agents colchicine and combretastatin A4. *Bioorganic & medicinal chemistry letters*, 25(1), pp.117–21.

Mehta, D.R. *et al*., 2011. Fludarabine and cytarabine in patients with acute myeloid Leukaemia refractory to two different courses of front-line chemotherapy. *Leukaemia research*, 35(7), pp.885–8.

Micheletti, G. *et al*., 2003. Vascular-targeting activity of ZD6126, a novel tubulin-binding agent. *Cancer research*, 63(7), pp.1534–7.

Miyano, S. *et al*., 1984. The asymmetric Ullmann coupling reaction of chiral diol diesters of 1-bromo 2-naphthoic acid and 2-halo 3-nitrobenzoic acids: Highly diastereoselective synthesis of atropisomeric 6,6'-dinitrodiphenic acids. *Bulletin of the Chemical Society of Japan*, 57(7), pp.1943–1947.

Miyaura, N., Yamada, K. & Suzuki, A., 1979. A new stereospecific cross-coupling by the palladium-catalyzed reaction of 1-alkenylboranes with 1-alkenyl or 1-alkynyl halides. *Tetrahedron Letters*, 20(36), pp.3437–3440.

Molander, G.A. & Ellis, N., 2007. Organotrifluoroborates : Protected Boronic Acids That Expand the Versatility of the Suzuki Coupling Reaction Background : Organotrifluoroborates., pp.275–286.

Murata, M., Watanabe, S. & Masuda, Y., 1997. Novel Palladium(0)-Catalyzed Coupling Reaction of Dialkoxyborane with Aryl Halides: Convenient Synthetic Route to Arylboronates. *The Journal of Organic Chemistry*, 62(19), pp.6458–6459.

Nawrotek, A., Knossow, M. & Gigant, B., 2011. The determinants that govern microtubule assembly from the atomic structure of GTP-tubulin. *Journal of molecular biology*, 412(1), pp.35–42.

Nelson, J.A., 1990. Characterization of macrophage subsets regulating murine natural killer cell activity. *Journal of Leukocyte Biology.* 48(5), pp. 382-393

Nelson, T.D. & Meyers, A.I., 1994. The Asymmetric Ullmann Reaction. 2. The Synthesis of Enantiomerically Pure C2-Symmetric Binaphthyls. *The Journal of Organic Chemistry*, 59(9), pp.2655–2658.

Nguyen, T.L. *et al*., 2010. The assembly-inducing laulimalide/peloruside a binding site on tubulin: molecular modeling and biochemical studies with [^{3}H]peloruside A. *Journal of chemical information and modeling*, 50(11), pp.2019–28.

Nicolaou, K.C. *et al*., 1994. Total synthesis of taxol. *Nature*, 367(6464), pp.630–634.

Nicolaus, N. *et al*., 2009. A [2 + 2 + 2]-cycloaddition approach toward 6-oxa-allocolchicinoids with apoptosis-inducing activity. *Organic letters*, 11(2), pp.341–4.

Nogales, E. *et al*., 1995. Structure of tubulin at 6.5 A and location of the taxol-binding site. *Nature*, 375(6530), pp.424–7.

Obasaju, C.K., Cowan, R.A. & Wilkinson, P.M., 1993. Oncology Original Article., pp.203–206.

Ohsumi, K. *et al*., 1998. Novel Combretastatin Analogues Effective against Murine Solid Tumours: Design and Structure−Activity Relationships. *Journal of Medicinal Chemistry*, 41(16), pp.3022–3032.

Oppenheimer, S.B., 2006. Cellular basis of cancer metastasis: A review of fundamentals and new advances. *Acta histochemica*, 108(5), pp.327–34.

Organ, M.G. *et al*., 2009. Pd-PEPPSI-IPent: An Active, Sterically Demanding Cross-Coupling Catalyst and Its Application in the Synthesis of Tetra- Ortho -Substituted Biaryls. *Angewandte Chemie*, 121(13), pp.2419–2423.

Özdemir, I., Demir, S. & Çetinkaya, B., 2005a. Use of tetrahydropyrimidinium salts for highly efficient palladium-catalyzed cross-coupling reactions of aryl bromides and chlorides. *Tetrahedron*, 61(41), pp.9791–9798.

Özdemir, I., Demir, S. & Çetinkaya, B., 2005b. Use of tetrahydropyrimidinium salts for highly efficient palladium-catalyzed cross-coupling reactions of aryl bromides and chlorides. *Tetrahedron*, 61(41), pp.9791–9798.

Padera, T.P. *et al*., 2002. Lymphatic metastasis in the absence of functional intratumour lymphatics. *Science (New York, N.Y.)*, 296(5574), pp.1883–6.

Paine, A.J., 1987. Mechanisms and models for copper mediated nucleophilic aromatic substitution. 2. Single catalytic species from three different oxidation states of copper in an Ullmann synthesis of triarylamines. *Journal of the American Chemical Society*, 109(5), pp.1496–1502.

Pedley, R.B. *et al*., 2001. Eradication of colourectal xenografts by combined radioimmunotherapy and combretastatin a-4 3-O phosphate. *Cancer research*, 61(12), pp.4716–22.

Pera, B. *et al*., 2010. Molecular recognition of peloruside A by microtubules. The C24 primary alcohol is essential for biological activity. *Chembiochem : a European journal of chemical biology*, 11(12), pp.1669–78.

Pettit, G.R. *et al*., 1995. Antineoplastic agents 322. synthesis of combretastatin A-4 prodrugs. *Anti-cancer drug design*, 10(4), pp.299–309.

Pettit, G.R. *et al*., 1998. Antineoplastic agents. 379. Synthesis of phenstatin phosphate. *Journal of medicinal chemistry*, 41(10), pp.1688–95.

Pettit, G.R. *et al*., 2000. Antineoplastic Agents. 443. Synthesis of the Cancer Cell Growth Inhibitor Hydroxyphenstatin and Its Sodium Diphosphate Prodrug. *Journal of Medicinal Chemistry*, 43(14), pp.2731–2737.

Pineda, O. *et al*., 2004. Computational comparison of microtubule-stabilising agents laulimalide and peloruside with taxol and colchicine. *Bioorganic & medicinal chemistry letters*, 14(19), pp.4825–9.

Pirrung, M.C. & Park, K., 2000. Discovery of selective metal-binding peptoids using 19F encoded combinatorial libraries. *Bioorganic & Medicinal Chemistry Letters*, 10(18), pp.2115–2118.

Pommier, Y. *et al*., 2010. DNA topoisomerases and their poisoning by anticancer and antibacterial drugs. *Chemistry & biology*, 17(5), pp.421–33.

Prota, A.E. *et al*., 2013. Molecular mechanism of action of microtubule-stabilizing anticancer agents. *Science (New York, N.Y.)*, 339(6119), pp.587–90.

Putta, C.B. & Ghosh, S., 2011. Palladium Nanoparticles on Amphiphilic Carbon Spheres: A Green Catalyst for Suzuki-Miyaura Reaction. *Advanced Synthesis & Catalysis*, 353(11-12), pp.1889–1896.

Raja, F. a, Hook, J.M. & Ledermann, J. a, 2012. Biomarkers in the development of anti-angiogenic therapies for ovarian cancer. *Cancer treatment reviews*, 38(6), pp.662–72.

Rao, S., Horwitz, S.B. & Ringel, I., 1992. Direct Photoaffinity Labeling of Tubulin With Taxol. *JNCI Journal of the National Cancer Institute*, 84(10), pp.785–788.

Ravelli, R.B.G. *et al*., 2004. Insight into tubulin regulation from a complex with colchicine and a stathmin-like domain. *Nature*, 428(6979), pp.198–202.

Roy, A. *et al*., 1999. Hydrogen Peroxide/Boric Acid: An Efficient System for Oxidation of Aromatic Aldehydes and Ketones to Phenols. *Synthetic Communications*, 29(21), pp.3781–3791.

Ruiz, J. *et al*., 2005. An efficient entry to pyrrolo[1,2-b]isoquinolines and related systems through Parham cyclisation. *Tetrahedron*, 61(13), pp.3311–3324.

Sawyer, J.S. & Macdonald, T.L., 1988. Total Synthesis of (±)-N-Acetylcolchinol. *Tetrahedron Letters*, 29(38), pp.4839–4842.

Sigmond, J. *et al*., 2007. The synergistic interaction of gemcitabine and cytosine arabinoside with the ribonucleotide reductase inhibitor triapine is schedule dependent. *Biochemical pharmacology*, 73(10), pp.1548–57.

Skoufias, D.A. & Wilson, L., 1992. Mechanism of inhibition of microtubule polymerization by colchicine: inhibitory potencies of unliganded colchicine and tubulin-colchicine complexes. *Biochemistry*, 31(3), pp.738–746.

Snyder, J.P. *et al*., 2001. The binding conformation of Taxol in beta-tubulin: a model based on electron crystallographic density. *Proceedings of the National Academy of Sciences of the United States of America*, 98(9), pp.5312–6.

Sober, D.J. *et al*., 1981. Selective and potent.beta.2-adrenoceptor agents within the tetrahydroisoquinoline class: effect of methyl substitution at the benzylic carbon of the 1-(3,4,5-trimethoxybenzyl) group of trimetoquinol. *Journal of Medicinal Chemistry*, 24(8), pp.970–974.

Soderquist, J.A., Kock, I. & Estrella, M.E., 2006. Reductive Cleavage of Acetals and Ketals with 9-Borabicyclo[3.3.1]nonane †. *Organic Process Research & Development*, 10(5), pp.1076–1079.

Stanton, R.A. *et al*., 2011. Drugs that target dynamic microtubules: a new molecular perspective. *Medicinal research reviews*, 31(3), pp.443–81.

Stark, L.M., Lin, X.-F. & Flippin, L.A., 2010. ChemInform Abstract: Total Synthesis of Amaryllidaceae Pyrrolophenanthridinium Alkaloids via the Ziegler-Ullmann Reaction: Tortuosine, Criasbetaine, and Ungeremine. *ChemInform*, 31(36), p.no–no.

Still, W.C., Kahn, M. & Mitra, A., 1978. Rapid chromatographic technique for preparative separations with moderate resolution. *The Journal of Organic Chemistry*, 43(14), pp.2923–2925. Available at: http://dx.doi.org/10.1021/jo00408a041

Stille, J.K. & Lau, K.S.Y., 1977. Mechanisms of oxidative addition of organic halides to Group 8 transition-metal complexes. *Accounts of Chemical Research*, 10(12), pp.434–442.

Sui, H. & Downing, K.H., 2010. Structural basis of inter-protofilament interaction and lateral deformation of microtubules. *Structure (London, England : 1993)*, 18(8), pp.1022–1031.

Tamao, K., Sumitani, K. & Kumada, M., 1972. Selective carbon-carbon bond formation by cross-coupling of Grignard reagents with organic halides. Catalysis by nickel-phosphine complexes. *Journal of the American Chemical Society*, 94(12), pp.4374–4376.

Tanpure, R.P. *et al*., 2013. Synthesis of structurally diverse benzosuberene analogues and their biological evaluation as anti-cancer agents. *Bioorganic & medicinal chemistry*, 21(24), pp.8019–32.

Tulpule, A. *et al*., 2001. Original article Liposomal daunorubicin in the treatment of relapsed or refractory non-Hodgkin ' s lymphoma *., pp.457–462.

Varma, R.S. & Naicker, K.P., 1999. The Urea−Hydrogen Peroxide Complex: Solid-State Oxidative Protocols for Hydroxylated Aldehydes and Ketones (Dakin Reaction), Nitriles, Sulfides, and Nitrogen Heterocycles. *Organic Letters*, 1(2), pp.189–192.

Vaupel, P. *et al*., 1987. Blood flow, oxygen consumption, and tissue oxygenation of human breast cancer xenografts in nude rats. *Cancer research*, 47(13), pp.3496–503.

Vaupel, P. & Hockel, M., 2000. Blood supply, oxygenation status and metabolic micromilieu of breast cancers: characterization and therapeutic relevance. *International journal of oncology*, 17(5), pp.869–79.

Verdier-Pinard, P. *et al*., 2000. Sustained intracellular retention of dolastatin 10 causes its potent antimitotic activity. *Molecular pharmacology*, 57(1), pp.180–7.

Vincent, L. *et al*., 2005. Combretastatin A4 phosphate induces rapid regression of tumour neovessels and growth through interference with vascular endothelial-cadherin signaling. *The Journal of clinical investigation*, 115(11), pp.2992–3006.

Wachsberger, P.R. *et al*., 2005. Effect of the Tumour Vascular-Damaging Agent, ZD6126, on the Radioresponse of U87 Glioblastoma. *Clin. Cancer Res.*, 11(2), pp.835–842.

Wang, X., Fu, J. & Snieckus, V., 2012. Directed Metalation□Cross-Coupling Strategies. Total Syntheses of the Alleged and the Revised Phenanthrene Natural Product Gymnopusin. *Helvetica Chimica Acta*, 95(12), pp.2680–2694.

Weisenberg, R.C., Broisy, G.G. & Taylor, E.W., 1968. Colchicine-binding protein of mammalian brain and its relation to microtubules. *Biochemistry*, 7(12), pp.4466–4479.

Williams, R.C. & Lee, J.C., 1982. *Structural and Contractile Proteins Part B: The Contractile Apparatus and the Cytoskeleton*, Elsevier.

Wójtowicz-Rajchel, H. & Koroniak, H., 2012. Synthesis of 5-fluorovinyl derivatives of pyrimidines via Suzuki–Miyaura coupling and their 1,3-dipolar cycloaddition reactions with nitrones. *Journal of Fluorine Chemistry*, 135, pp.225–230.

Wolfe, J.P. *et al*., 1999. Highly Active Palladium Catalysts for Suzuki Coupling Reactions. *Journal of the American Chemical Society*, 121(41), pp.9550–9561.

Yasar, S. *et al*., 2008. Benzylic Imidazolidinium, 3,4,5,6-Tetrahydropyrimidinium and Benzimidazolium Salts: Applications in Ruthenium-Catalyzed Allylic Substitution Reactions. *European Journal of Organic Chemistry*, 2008(12), pp.2142–2149.

Zefirova, O.N. *et al*., 2011. Synthesis and SAR requirements of adamantane–colchicine conjugates with both microtubule depolymerizing and tubulin clustering activities. *Bioorganic & Medicinal Chemistry*, 19(18), pp.5529–5538.

Ziegler, F.E. *et al*., 1980. The ambient temperature Ullmann reaction and its application to the total synthesis of (.+-.)-steganacin. *Journal of the American Chemical Society*, 102(2), pp.790–798.